uOttawa

L'Université canadienne
Canada's university

FACULTÉ DES ÉTUDES SUPÉRIEURES ET POSTOCTORALES

uOttawa

L'Université canadienne
Canada's university

FACULTY OF GRADUATE AND POSDOCTORAL STUDIES

Nicole Blaquiere
AUTEUR DE LA THÈSE / AUTHOR OF THESIS

M.Sc. (Chemistry)
GRADE / DEGREE

Department of Chemistry
FACULTÉ, ÉCOLE, DÉPARTEMENT / FACULTY, SCHOOL, DEPARTMENT

Part I: The Development and Mechanistic Study of a Biomimetic Decarboxylative Aldol Reaction
Part II: Ruthenium-Catalyzed Dehydrogenation of Ammonia-Boranes

TITRE DE LA THÈSE / TITLE OF THESIS

Dr. K. Fagnou
DIRECTEUR (DIRECTRICE) DE LA THÈSE / THESIS SUPERVISOR

CO-DIRECTEUR (CO-DIRECTRICE) DE LA THÈSE / THESIS CO-SUPERVISOR

EXAMINATEURS (EXAMINATRICES) DE LA THÈSE / THESIS EXAMINERS

Dr. A. Beauchemin

Dr. L. Barriault

Gary W. Slater
Le Doyen de la Faculté des études supérieures et postdoctorales / Dean of the Faculty of Graduate and Postdoctoral Studies

Part I. The Development and Mechanistic Study of a Biomimetic Decarboxylative Aldol Reaction.

Part II. Ruthenium-Catalyzed Dehydrogenation of Ammonia-Boranes.

Nicole Blaquiere

Thesis submitted to the
Faculty of Graduate & Postdoctoral Studies
University of Ottawa
In partial fulfillment of the requirements for the
M.Sc. degree in the
Ottawa-Carleton Chemistry Institute

Your file Votre référence
ISBN: 978-0-494-51635-5
Our file Notre référence
ISBN: 978-0-494-51635-5

"The real voyage of discovery consists not in seeking new landscapes, but in having new eyes."
~ Marcel Proust ~

Some thoughts on research from the man himself...

"If we knew what it was we were doing, it would not be called research, would it?"

"Insanity: doing the same thing over and over again and expecting different results."

~ Albert Einstein ~

Table of Contents

Chapter 5

Chapter 6

List of Schemes

Chapter 1

Chapter 2

Chapter 3

Chapter 4

Chapter 5

Chapter 6

List of Figures

Chapter 2

represent the mean of 3 trials, and error bars represent the standard deviation. Integrations were measured relative to an internal standard (pentachlorobenzene).

Figure 2.12 Relative concentration of MAHO **2.4** (blue), intermediate (green) and β-hydroxyester **2.5** (red) over 12 hours analyzed by ^{1}H NMR in THF-d_8 overlapped with the theoretical curves obtained from the irreversible (dashed lines) and reversible (solid lines) integrated rate equations predicted by COPASI. Data points represent the mean of 3 trials, and error bars represent the standard deviation. Integrations were measured relative to an internal standard (pentachlorobenzene).

Figure 2.13 Relative concentration of MAHO **2.4** (blue), intermediate (green) and β-hydroxyester **2.5** (red) over 12 hours analyzed by ^{1}H NMR in C_6D_6 overlapped with the theoretical curves obtained from the irreversible (dashed lines) and reversible (solid lines) integrated rate equations predicted by COPASI. Data points represent the mean of 3 trials, and error bars represent the standard deviation. Integrations were measured relative to an internal standard (pentachlorobenzene).

Chapter 4

Figure 4.14 Hydrogen Evolution as a function of time and catalyst loading. (A): [AB] = 5.0 M. (B): [x] = 0.025 M.

Figure 4.15 Hydrogen evolution from different AB sources using 0.1 mol % Ru in THF at 50 °C. Solid lines represent dehydrogenation of AB prepared by method A. Dashed lines represent dehydrogenation of AB prepared by method B. Blue = 4.5, Orange = 4.6 and Purple = 4.7.

Figure 4.16 Hydrogen evolved as a function of time and [AB].

Figure 4.17 Hydrogen evolution as a function of time and catalyst loading.

Figure 4.5 Evolution of Hydrogen over time catalyzed by **4.4-4.8** and **4.12** at room temperature or 50 °C. Precatalysts were deprotonated with 30 equivalents KO*t*Bu prior to use.

Figure 4.6 Rate of hydrogen evolution from AB catalyzed by different catalytic species **4.10, 4.13, 4.14** and **4.15**.

Figure 4.7 Evolution of hydrogen from a 1:1 AB:MeAB mixture as a function of time. Control A was run in the absence of catalyst and base, and control B was run in the absence of catalyst.

Figure 4.8 Evolution of hydrogen from a 35:65 AB:MeAB mixture as a function of time and concentration.

Figure 4.9 Hydrogen evolution from MeAB as a function of time and catalyst loading. [MeAB] = 1.0 M.

Figure 4.10 Evolution of the second equivalent of hydrogen from MeAB as a function of time and concentration. [Ru] = 0.5 mol %, 50 °C.

Figure 4.11 Evolution of the first equivalent of hydrogen from MeAB as a function of time and concentration. [Ru] = 0.5 mol %, 50 °C.

Chapter 5

Chapter 6

List of Tables

Chapter 2

Chapter 4

List of Abbreviations

A	Acid
ACP	Acyl Carrier Protein
Ar	Aryl
Asn	asparagine
B	base
BINOL	1,1'-bi(2-naphthol)
Bn	benzyl
cat.	catalyst
CoA	coenzyme A
Cp	cyclopentadienyl
d	doublet
dba	dibenzylidene acetone
DCE	1,2-dichloroethane
DMF	*N,N*-dimethylformamide
DMSO	dimethylsulfoxide
DMTC	5,5-dimethylthiazolidinium-4-carboxylate
dr	diastereomeric ratio
E	enzyme
ee	enantiomeric excess
Et	Ethyl
equiv.	equivalents
Glu	glutamate
Gly	glycine
h	hour

His	histidine
HPLC	High Performance Liquid Chromatography
HRMS	high resolution mass spectroscopy
Hz	hertz
*i*Pr	*iso*-propyl
IR	infrared
KS	Keto Synthase
L.A.	Lewis Acid
LLB	lanthanum-lithium-BINOL
Lys	lysine
m	multiplet
M	molarity
MAHT	malonic acid half thioester
MeMAHT	methyl malonic acid half thioester
MAHO	malonic acid half oxyester
MeCN	acetonitrile
Me	methyl
mol	moles
MS	molecular sieves
NMR	nuclear magnetic resonance
OTf	Triflate
Ph	phenyl
PhMe	toluene
PPE	ethyl polyphosphate
ppm	parts per million
Pro	proline
q	quartet

rt	room temperature
s	singlet
Ser	serine
*t*Bu	*tert*-butyl
Tf	trifluoromethanesulfonate
THF	tetrahydrofuran
Thr	threonine
TLC	thin layer chromatography
TMS	trimethylsilyl
Ts	para-toluene sulfonyl
°C	degrees Celcius

Abstract

Part I. The Development and Mechanistic Study of a Biomimetic Decarboxylative Aldol Reaction.

A reaction has been developed in which malonic acid half thioesters (MAHTs) and malonic acid half oxyesters (MAHOs) are shown to undergo decarboxylative nucleophilic addition reactions with ketone and aldehyde electrophiles under exceptionally mild conditions. In the presence of Et_3N at room temperature in THF, various nucleophile and electrophile analogues form β-hydroxyester and thioester products in moderate to good yields.

It is also demonstrated spectroscopically that these decarboxylative aldol reactions proceed through a post-addition, pre-decarboxylation intermediate. The formation of this intermediate is shown to be reversible using both experimental and kinetic means of analysis. The rate constants for intermediate formation and decomposition to product in various solvents have been calculated using two different models and calculation methods.

Part II. Ruthenium-Catalyzed Dehydrogenation of Ammonia-Boranes.

The dehydrogenation of ammonia-borane (AB) and methylammonia-borane (MeAB) is shown to be catalyzed by several Ru-amido complexes. Up to one equivalent H_2 (1.0 system wt %) is released from AB by as little as 0.03 mol % Ru within 5 minutes, and up to two equivalents H_2 (3.0 system wt %) are released from MeAB with 0.5 mol % Ru in under 10 minutes at room temperature, the first equivalent emerging within 10 seconds. Also, a mixture of AB/MeAB yields up to 3.6 system wt % H_2 within 1 hour with 0.1 mol % Ru. Several catalytic analogues were synthesized to evaluate the active species the catalytic cycle, and computational studies were performed to elucidate the mechanism of dehydrogenation of AB. Finally, it was shown that alkylamine-boranes can serve as a source of H_2 in the Ru-catalyzed reduction of ketones and imines.

Acknowledgements

Firstly I would like to thank my supervisor, Keith Fagnou, for the opportunity to work and learn in his lab for the last 4 years. Keith, it has been a real pleasure working for someone so enthusiastic and passionate about what they do. Also, a supervisor who checks back every few minutes on the progress of a TLC and is willing to bet a beer on the outcome is rare, but awesome, to come across.

Of the many workers of the 'Fagnou Factory', the original grad student, Marc, gets first thanks. Marc, no matter what the undergrads say, you've been an amazing teacher and an even better friend. Those of us lucky enough to have you around can always take comfort that you're the guy who will really do anything for his friends... including endless years of designatedly driving around intoxicated grad students.

Of course many thanks go to the other original members of the crew, who will probably never get to read this: LC, you love chemistry way too much, and that is a good thing for the rest of us with endless questions about how to do anything. A guy who can go from talking about the complexities of a total synthesis to the regularity of his... well... you know, with equal enthusiasm, gets a thumbs up in my books. Mathieu, you've always had an encouraging word when things got difficult, and I'm sure your new little girl will appreciate that in the future! Mélissa, you are genuinely one of the nicest people I know, and you also make the most hilarious English mistakes ever, which makes you even cooler. JP, despite your terrible taste in music, you are an amazing chemist and someone with a consistently optimistic attitude that we can all learn from. Val, you taught me a lot, and I always enjoyed our coffee runs for some daily gossip.

Enter the era of D-Ross and the San Capris... Dave, you are one of those rare guys who can girl-talk, shamelessly state his love for girly music and chick flicks, discuss yesterday's yogalates class, order a skim chai latte, and still maintain total guy-ness. You are also undoubtedly the funniest drunk I have ever met and will ever meet. Ever.

Megan and Sophie... I could never have guessed that I would become so close to fellow lab-mates, but you girls totally rocked my world, despite your annoying love of hockey. In the words of the great Mariah Carey, 'you'll always be a part of me'... if for nothing else,

introducing me to the wonderful world of over-priced shoes. But seriously. Sophie, you are seriously one of the smartest people I know, and I can't wait to see where you end up in the future. You are also an amazing confidante, gossip-sharer, and friend. The summer of 2006, some might call it the summer of Nicophie, was a memorable one, with conversations so girly they drove Keith away from our fumehood area. Dr. Megan, master of *ze escrime*, I'm so glad we got to travel together and have a little more precious time before we went our separate ways! Chemistry friend, shopping friend, yoga friend, and just friend, it's been great! Dan Shore: Simpsons expert, history teacher, all around good person. Whoever ends up in the same lab as you is very lucky, you are a wonderful person to have around.

Laurence, you are the most unintentionally hilarious person I know. I'm glad you joined the downstairs lab for a while, because you are great to talk to and have a refreshing attitude on everything. Mégan, if I had to describe you in 4 words, it would be 'super nice' and 'great hair'. Your constant smile can brighten any bad chemistry day! Élisia and David, you guys are an awesome couple and always are willing to help and share new music. Chris, your intensity and focus are something to be admired, and I really wish I got to hear you play guitar! Derek, a fellow east coaster with some of the most offensive/hilarious jokes I've heard, and Malcolm, you are an incredibly honest person with a strangely intricate knowledge of Ottawa keggers.

Postdoc love... Dan Black, you always had good advice and extra beer; a good labmate indeed. Ben, the perfect example of someone who works hard and plays hard, you really have helped hold the lab together. I've enjoyed exchanging music with you!

Newbies... you seem like great additions to the lab and you will almost certainly love the time you spend here!

Of course all of the professors who have taught me at Ottawa U, you have all contributed to my decision to pursue this field and I thank you for that! Also Glenn Facey, who has been incredibly patient with teaching me all of the weird NMR experiments that no one ever does, as well as the Mass Spec guys, who fondly know me as 'Hydrogen Girl'.

Finally all the family and friends, who have hung around for the ups and downs of grad school, I really have appreciated your support.

Chapter 1

Introduction

1.1 Aldol Reactions as C-C bond forming strategy

One of the most well known carbon-carbon bond forming strategies in organic chemistry is without a doubt the aldol reaction, in which two carbonyl-containing compounds self or cross-react to form β-hydroxy ketones, a familiar motif in many natural products. Several research groups have focused their efforts on countering the problems associated with the chemo-, regio- and stereoselectivity inherent to the classical aldol reaction.[1] Problems such as self-condensation and selectivity in the presence of two enolizable compounds often result in low yields and product mixtures. In the presence of a base, the substrate with the lowest pKa will form an enolate which will then act as the nucleophile, or donor, in the aldol reaction. When the reaction of a donor with a higher pK_a (e.g. esters) is desired, additional steps must be taken which normally involve the formation of an enolate equivalent prior to the addition of an electrophile to the reaction mixture.[2] By reacting the donor carbonyl compound with a stoichiometric amount of strong base, one can form the metal enolate which can then react with the aldehyde or ketone acceptor (scheme 1.1).[3] These strongly basic conditions can limit the scope of substrates amenable to this transformation.

Scheme 1.1 **General aldol reaction under basic conditions.**

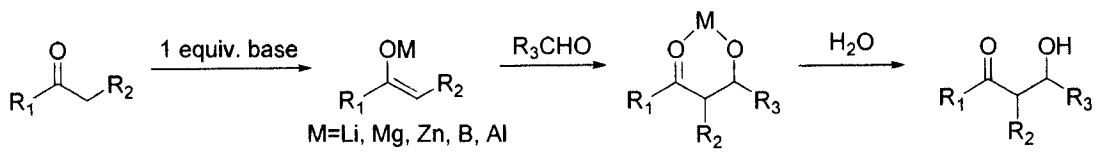

1.1 **1.2** **1.3** **1.4**

[1] Palomo, C.; Oiarbide, M.; Garcia, J. M. *Chem. Soc. Rev.*, **2004**, *33*, 65.
[2] Nelson, S. G. *Tetrahedron: Asymmetry*, **1998**, *9*, 357.
[3] Mukaiyama, T. *Org. React.*, **1998**, *28*, 203.

1.1.1: Mukaiyama Aldol Strategy for Ester Nucleophiles

As mentioned above, the reactivity of substrates in the aldol reaction is governed by their relative pK_a's, amongst other factors. This can be especially problematic when one desires to react esters and their derivatives as donor substrates, as they are generally approximately five orders of magnitude less acidic than their ketone counterparts. Perhaps the most commonly used solution for this issue is the formation of a silyl ketene acetal, an isolable enolate equivalent which can react with an electrophile in the presence of a catalytic or sub-stoichiometric amount of Lewis acid.[4] This methodology, originally introduced by Mukaiyama and co-workers, eliminates most problems associated with chemoselectivity and base sensitivity. Many chiral Lewis acidic complexes have been developed with the objective of generating β-hydroxy esters asymmetrically (scheme 1.2).[5,6]

Scheme 1.2 **General Mukaiyama aldol reaction and representative chiral Lewis acid catalysts.**

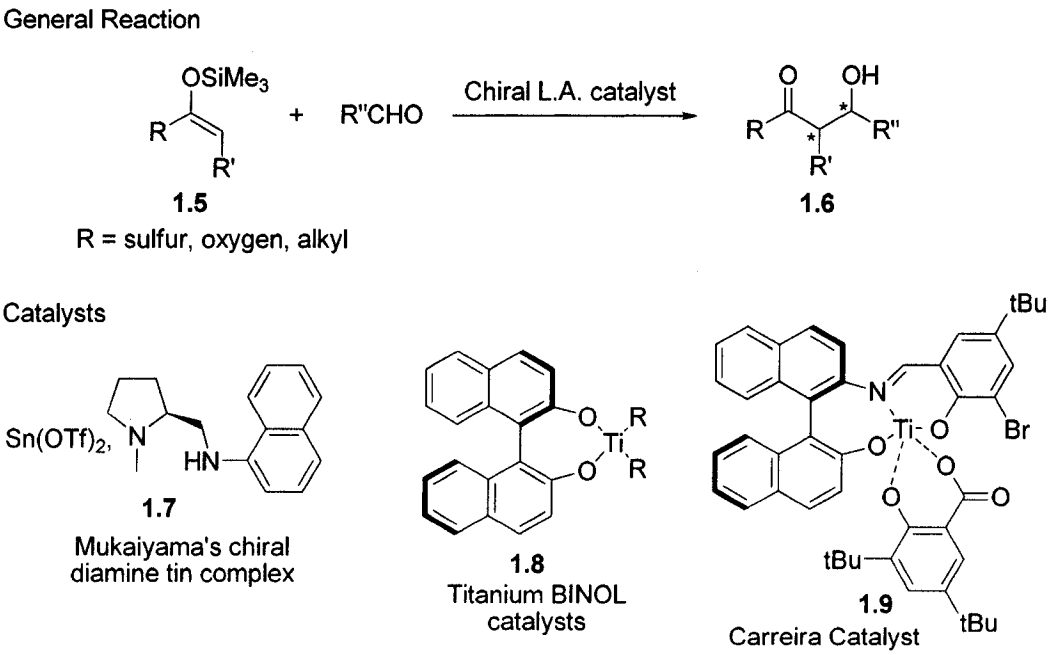

[4] Carreira, E. M. in *Comprehensive Asymmetric Catalysis*, **Vol. 3**, Eds. E. N. Jacobsen, A. Pfaltz and H. Yamamoto, Springer, Heildelberg, **1999**, 997-1065.

[5] Kobayashi, S.; Fujishita Y.; Mukaiyama, T. *Chem. Lett.*, **1990**, 1455.

[6] (a) Mikami, K.; Matsukawa, S. *J. Am. Chem. Soc.*, **1995**, *116*, 8837. (b) Keck, G. E.; Krishnamurthy, D. *J. Am. Chem. Soc.*, **1995**, *117*, 2363. (b) Carreira, E. M.; Singer, R. A.; Lee, W. *J. Am. Chem. Soc.* **1994**, *116*, 8837.

Although extremely useful, this methodology suffers from high catalyst loadings and additional steps in the preparation of substrates. The preparation of silyl ketene acetals requires strong base as well as silicon reagents which end up as stoichiometric amounts of inorganic salts and silicon waste products.

1.1.2: Biomimetic Aldol Reactions

When seeking milder and more efficient reactions, chemists are often inspired from enzymes, nature's 'custom catalysts'. For most metabolic reactions, there is an enzyme designed to generate the single desired product with perfect selectivity. This is an attractive concept for chemists, as nature generally does not make use of protecting groups or wasteful additives.[7] The aqueous reaction media and mild conditions are also desired factors in chemical synthesis. *In vivo* aldol reactions, such as the kind catalyzed by the type I aldolase enzymes, make use of covalently modified intermediates in which one functional group of the substrate is temporarily replaced by a more reactive one. This type of reactivity has been originally mimicked by the Hajos-Parrish-Eder-Sauer-Wiechert reaction, in which proline catalyzes an intramolecular asymmetric aldol reaction.[8] This reactivity was first extended to an intermolecular reaction by List, Lerner and Barbas, who used a proline or proline-derived catalyst which covalently modifies the substrate to form a reactive enamine intermediate. The enamine is then added stereoselectively to an aldehyde, and hydrolysis of the iminium regenerates the ketone functionality (scheme 1.3).[9] MacMillan has also developed a proline-catalyzed reaction for the formation of enantioenriched β-hydroxyaldehydes through the cross-aldol reaction of aldehydes (scheme 1.3).[10] Although these reactions represent a significant advancement in organocatalysis and asymmetric aldol reactions, high catalyst loadings and a large excess of ketone are often necessary in the former

---

[7] Wong, C.-H.; Machajewski, T. D. *Angew. Chem. Int. Ed.* **2000**, *39*, 1352.

[8] (a) Hajos, Z. G.; Parrish, D. R. *J. Org. Chem.* **1974**, *39*, 1615. (b) Eder, U.; Sauer, G.; Wiechert, R. *Angew. Chem. Int. Ed. Eng.* **1971**, *10*, 496.

[9] (a) List, B.; Lerner, R. A.; Barbas III, C. F. *J. Am. Chem. Soc.* **2000**, *122*, 2395 (b) Notz, W.; Tanaka, F.; Barbas III, C. F. *Acc. Chem. Res.*, **2004**, *37*, 580. (b) Sakthivel, K.; Notz, W.; Bui, T.; Barbas III, C. F. *J. Am. Chem. Soc.* **2001**, *123*, 5260.

[10] Northrup, A. B.; MacMillan, D. W. C. *J. Am. Chem. Soc.*, **2002**, *124*, 6798.

examples. The latter requirement often limits the scope of starting materials to acetone and hydroxyacetone which can be used as co-solvents.

Scheme 1.3 **Catalytic aldol reactions mimicking type I aldolase.**

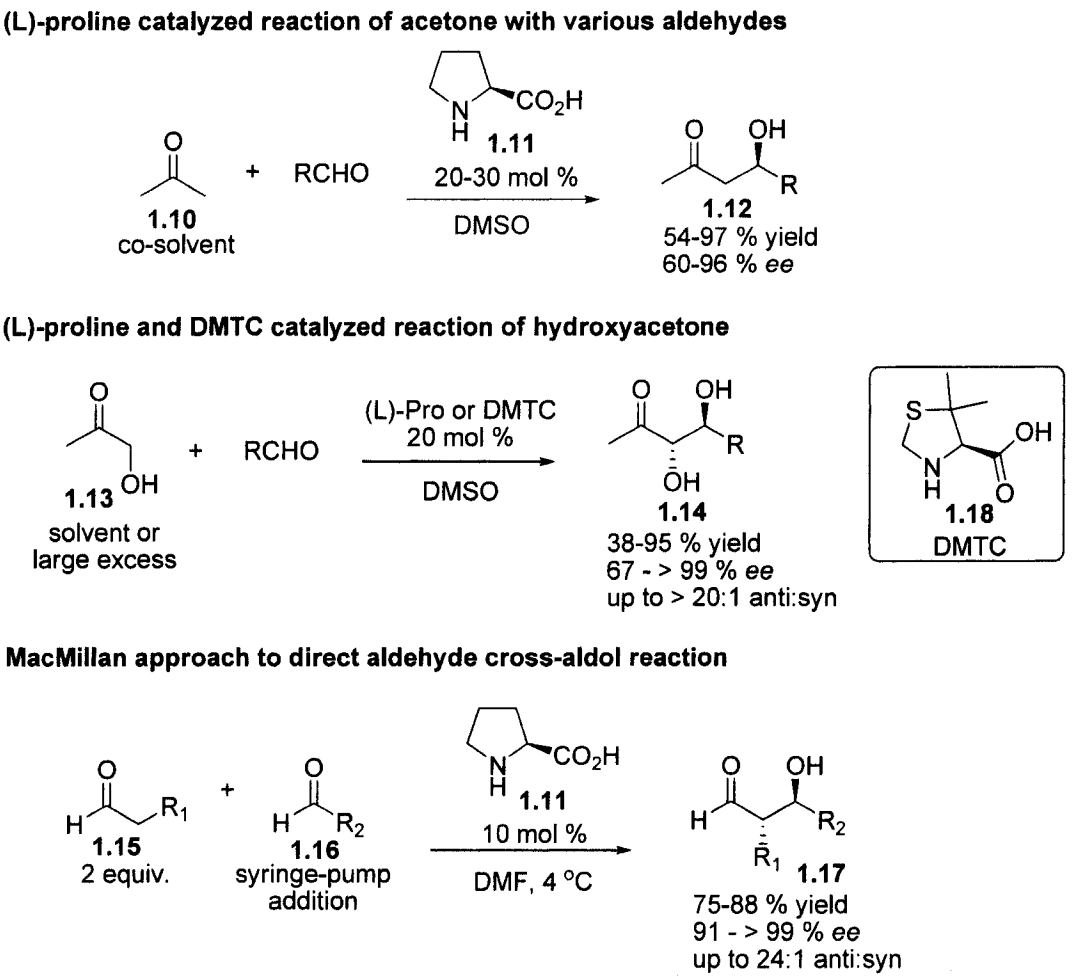

In the case of type II aldolases, there is activation of the electrophilic component of the aldol reaction by coordination to a transition metal co-factor.[7] Trost and coworkers have adopted this concept to develop a bifunctional dinuclear zinc complex which catalyzes the addition of hydroxyacetophenone and acetone to a variety of aldehydes (scheme 1.4).[11] Shibasaki and coworkers have also developed a heterobimetallic catalytic complex, which has a slightly broader scope than the Trost catalyst, but also requires higher catalyst loadings.[12] As opposed to

[11] Trost, B. M.; Ito, H.; Silcoff, E. R. *J. Am. Chem. Soc.* **2001**, *123*, 3367.

[12] Yamada, Y. M. A.; Yoshikawa, N.; Sasai, H.; Shibasaki, M. *Angew. Chem. Int. Ed. Engl.* **1997**, *36*, 1871.

the proline-catalyzed reactions previously described, these transformations are carried out with relatively low catalyst loadings. However, the significantly higher molecular weights of these compounds would still have them account for a considerable portion of the mass of reagents. The recurring problem of excess nucleophile also has yet to be resolved.

Scheme 1.4 **Catalytic aldol reactions mimicking type II aldolase.**

Trost's dinuclear zinc complex

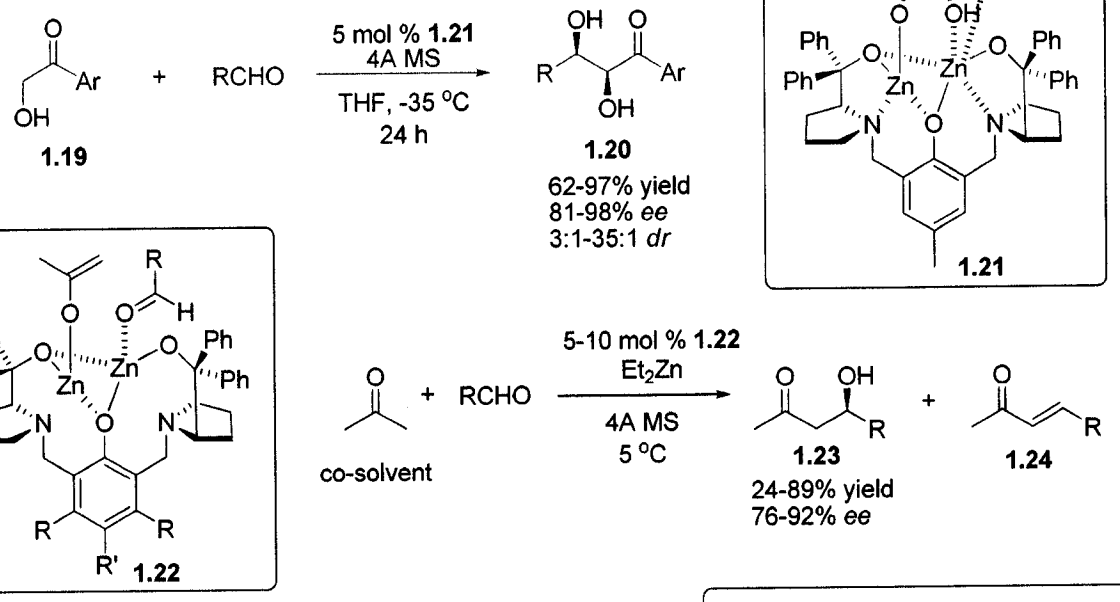

Shibasaki lanthanum catalyst

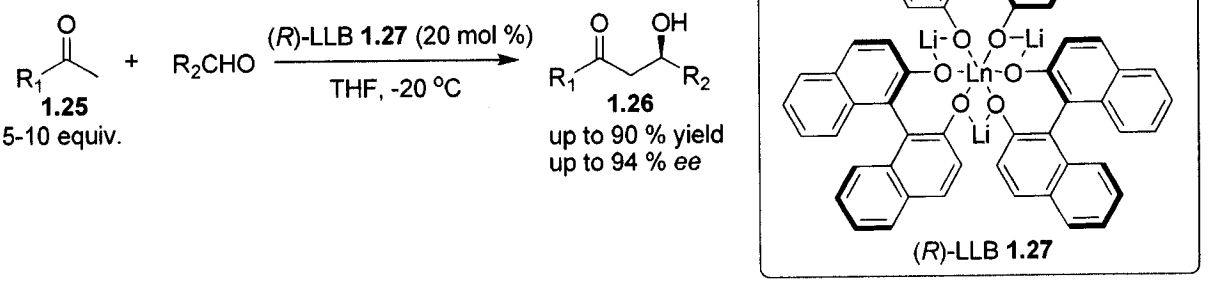

1.2 Decarboxylative Nucleophilic Addition Reactions

1.2.1: Decarboxylative Nucleophilic Additions in Nature

Nature has many strategies for the formation of enolates and these are not limited to aldol reactions. The enzyme responsible for polyketide biosynthesis,[13] fatty acid synthase,[14] employs a decarboxylative Claisen condensation in its chain elongation step. The keto synthase (KS) component of the enzyme complex catalyzes the decarboxylative Claisen-type condensation of a malonyl unit bound to an acyl carrier protein (ACP) with an acyl unit, which is bound to the keto synthase subunit. Both substrates are bound as thioesters to their respective enzymes through cysteine residues (scheme 1.5).

Scheme 1.5 **Decarboxylative Claisen Condensation in Fatty Acid Synthase.**

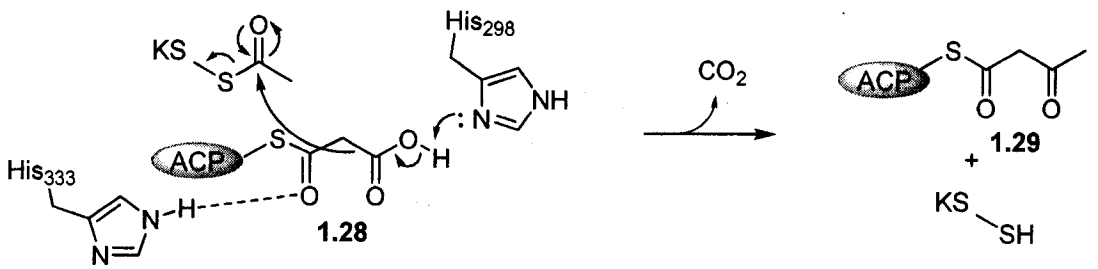

The thioester is more reactive masked as its malonic acid analogue due to the increased acidity of the thioester α-hydrogens. A series of hydrogen-bonding and basic amino acid residues (mainly histidine) in the enzymatic active site enable decarboxylation and addition to an adjacent thioester electrophile, although not necessarily in that order.[15] These malonic acid half thioesters (MAHTs) are characterized as thermodynamically unstable, with a significant entropic driving force for decarboxylation.[16] However, their kinetic stability renders these compounds virtually unreactive until activated by an outside source, such as the active site of the enzyme.

---

[13] For a review on polyketide biosynthesis: Staunton, J.; Weissman, K. J. *Nat. Prod. Rep.* **2001**, *18*, 380.
[14] Maier, T.; Jenni, S.; Ban, N. *Science*, **2006**, *311*, 1258.
[15] McGuire, K. A.; Siggaard-Andersen, M.; Bangera, M. G; Olsen, J. G.; von Wettstein-Knowles, P. *Biochemistry*, **2001**, *40*, 9836.
[16] For a review on sodium ion-translocating decarboxylases: Buckel, W. *Biochem. et Biophys. Acta*, **2001**, *1505*, 15.

Furthermore, the efficiency of the transformation is heightened by the loss of CO_2 as the only by-product, making this a traceless form of activation of thioesters.

1.2.1.1: Mechanistic Insights into Nature's Decarboxylative Nucleophilic Addition Reactions.

Modeling studies of some enzymes in the decarboxylase family suggest that the carboxylate functionality of the malonyl-ACP unit, which hydrogen bonds to a glycine and histidine residue, is oriented orthogonally to the plane of the thioester carbonyl.[17] From a chemist's perspective, this is logical as the σ orbital of the bond to be broken is properly aligned with the π* orbital of the thioester carbonyl. These studies provide an interesting argument against the classical mechanism thought to occur in metal ion-assisted decarboxylations, which involves the formation of a six-membered ring with the metal ion (scheme 1.6).

Scheme 1.6 **Classical model for metal ion-assisted decarboxylation.**

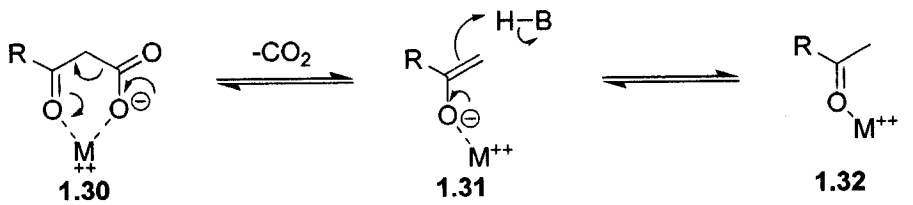

There is some debate in the literature as to the mechanism of this decarboxylative nucleophilic addition, with three distinct mechanistic possibilities being advanced (scheme 1.7). First, decarboxylation and nucleophilic attack may occur in a single concerted step (mechanism 1, scheme 1.7). A stepwise addition, in which decarboxylation occurs first to form a discrete thioester enolate, followed by addition to the acetyl unit has also been postulated (mechanism 2, scheme 1.7). Finally, enolization and addition of the malonyl moiety to the acetyl group could take place prior to decarboxylation (mechanism 3, scheme 1.7). Generally speaking, there is support for both a concerted (mechanism 1) and stepwise decarboxylation-addition mechanism (mechanism 2) in the literature, but neither of these has been explicitly demonstrated experimentally. Arndstadt *et al.* have supported a concerted mechanism and provide evidence

[17] Benning, M. M.; Haller, T.; Gerlt, J. A.; Holden, H. M. *Biochemistry,* **2000**, *39*, 4630.

against mechanism 3 through isotopic labelling experiments.[18] Alternatively, there is some computational evidence for a stepwise decarboxylation-addition mechanism;[19] however, these studies were performed with a simplified model system which may not be representative of the enzymatic active site.

Scheme 1.7 **Possible mechanisms for the decarboxylative Claisen condensation.**

Mechanism 1: Concerted Decarboxylation-Addition

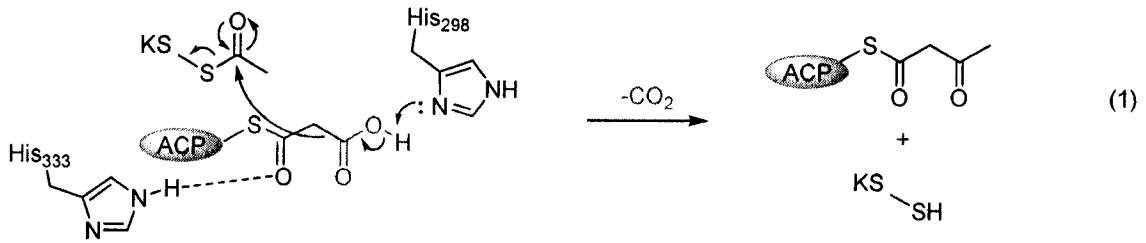

Mechanism 2: Stepwise Decarboxylation-Addition

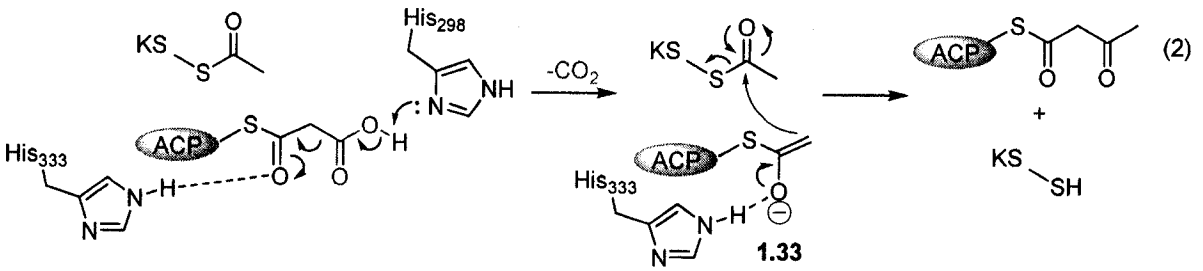

Mechanism 3: Stepwise Addition-Decarboxylation

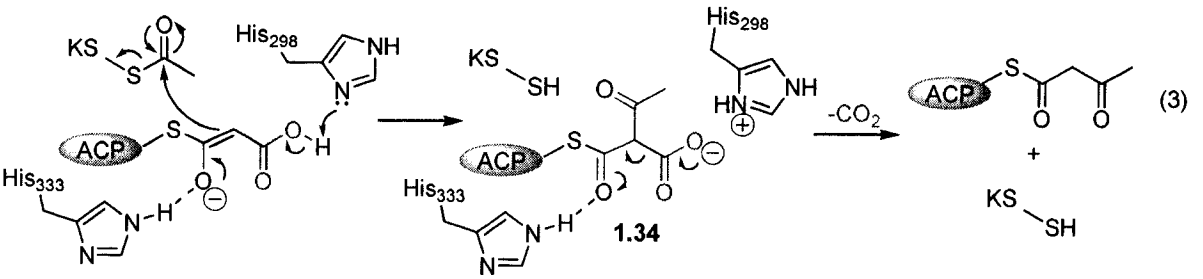

[18] Arnstadt, K. I.; Schindlbeck, G; Lynen, F. *Eur. J. Biochem.* **1975**, *55*, 561.
[19] Dewar, M. J. S.; Dieter, K. M. *Biochemistry*, **1988**, *27*, 3302.

1.2.2: Decarboxylative Claisen Condensation

This enzymatic decarboxylative Claisen condensation has been mimicked synthetically, mainly using cationic metal sources rather than hydrogen-bonding components as the activating species. The first biomimetic intermolecular decarboxylative Claisen condensation was a single example reported by Kobuke and Yoshida[20] in which a malonic acid half *n*-butylthioester was decarboxylatively added to phenyl thioacetate in the presence of magnesium acetate and imidazole to form the β-ketothioester in 60 % yield (scheme 1.8). Despite the moderate yield and long reaction time, this was a proof of concept for the synthetic utility of MAHTs.

Scheme 1.8 **Synthetic decarboxylative Claisen condensation.**

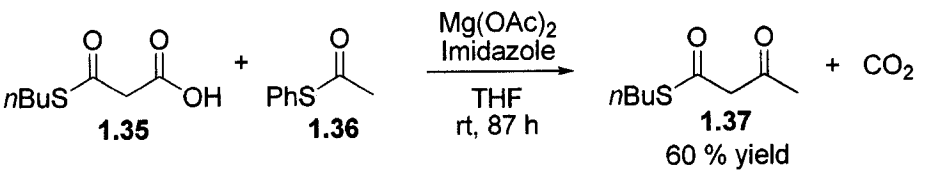

Over 20 years later, the self-condensation of a broader scope of MAHTs was reported using the same conditions as Kobuke and Yoshida.[21] A few other variations on this methodology have been reported, such as modifying the electrophile to an amide instead of a thioester to produce an imidazole rather than thiol leaving group, eliminating the need for an additional base in the reaction.[22]

Generally speaking, synthetic attempts at biomimetic polyketide synthesis and imitation of biosynthetic pathways employing polyketide intermediates have failed; however, there have been reports of successful enzymatic decarboxylative Claisen condensations of malonyl CoA derivatives using polyketide synthase (PKS) enzymes *in vitro*.[23]

---

[20] Kobuke, Y.; Yoshida, J. *Tetrahedron Lett.* **1978**, *4*, 367.
[21] Sakai, N.; Sordé, N.; Matile, S. *Molecules*, **2001**, *6*, 845.
[22] Reetz, M. T.; Maier, W. F.; Schwellnus, K.; Chatziiosifidis, I. *Angew. Chem., Int. Ed. Engl.* **1979**, *18*, 72.
[23] (a) Abe, I.; Abe, T.; Wanibuchi, K.; Noguchi, H. *Org. Lett.* **2006**, *8*, 6063; (b) Abe, I.; Morita, H.; Oguro, S.; Noma, H.; Wanibuchi, K.; Kawahara, N.; Goda, Y.; Noguchi, H.; Kohno, T. *J. Am. Chem. Soc.* **2007**, *129*, 5976; (c) Ryu, Y.; Kim, K.-J.; Roessner, C. A.; Scott, A. I. *Chem. Commun.* **2006**, 1439.

1.2.3 Modifications of the Knoevenagel-Doebner Reaction

A well known example of carboxylic acids as traceless activating groups is the Galat modification of the Knoevenagel-Doebner reaction.[24] By reacting malonic acid half oxyesters (MAHOs) with aromatic aldehydes in the presence of piperidine in refluxing pyridine, the corresponding α,β-unsaturated esters can be obtained in good yields. The same transformation can be carried out with aliphatic aldehydes; however, mixtures of the α,β- and β,γ-unsaturated esters are common (Scheme 1.9). Under the classical conditions for this reaction, the β,γ-isomer tends to predominate. This is thought to occur because of the proposed mechanism in which addition to the aldehyde precedes dehydration and decarboxylation (Scheme 1.9).[25] The dienolate intermediate **1.45** formed is thought to protonate at the more reactive α-position, generating a majority of the less thermodynamically favoured product **1.46**.

Scheme 1.9 **Proposed mechanism for the decarboxylative Knoevenagel-Doebner reaction.**

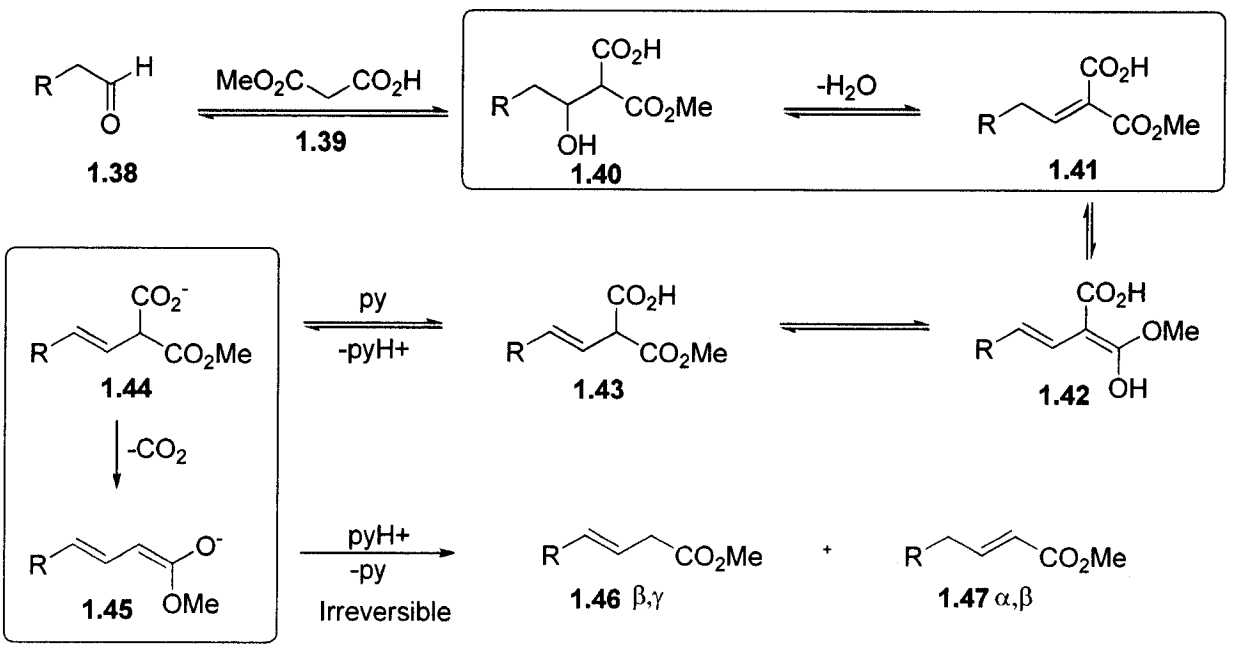

[24] Galat, A. *J. Am. Chem. Soc.* **1946**, *68*, 376.

[25] List, B.; Doehring, A; Hechavarria Fonseca, M. T.; Job, A.; Rios Torres, R. *Tetrahedron*, **2006**, *62*, 476.

List and coworkers developed a modification of this reaction which establishes an equilibrium between the α,β- and β,γ-unsaturated esters using a DMAP catalyst.[25] This allows the formation of the thermodynamically preferred α,β-unsaturated product (scheme 1.10).

Scheme 1.10 **Knoevenagel-Doebner variant favouring the α,β-unsaturated ester.**

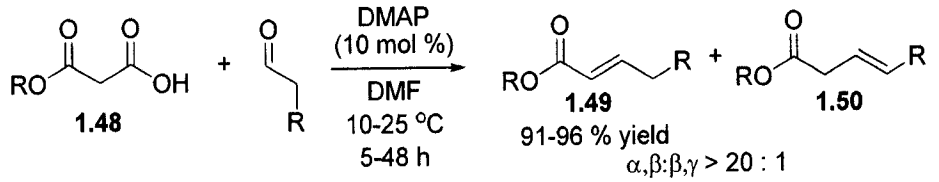

Kinetic studies by Corey have suggested that following the formation of the β-hydroxymalonic acid in decarboxylative condensation reactions (intermediate **1.40**), the polarity of the reaction media should dictate which decarboxylative pathway occurs.[26] Solvents with high dielectric constants should disfavor a concerted decarboxylation-elimination pathway from intermediate **1.40** and instead induce dehydration first, as shown in Scheme 1.9, followed by isomerization to the β,γ-unsaturated malonic acid **1.44**, which then undergoes decarboxylation. Tanaka and coworkers[27] were able to show that the Knoevenagel-Doebner reaction with malonic acid and *p*-nitrobenzaldehyde proceeds through a β-hydroxymalonic acid intermediate similar to intermediate **1.40** (Scheme 1.9) which decarboxylates *prior* to dehydration in the presence of pyridine. The authors isolated this intermediate and re-subjected it to the reaction conditions; the appearance of starting materials in the reaction mixture indicated that the formation of this intermediate is reversible. Kinetic studies by NMR indicated that the decarboxylation step was rate-limiting in this reaction.

A recent publication also describes the Knoevenagel-Doebner condensation between malonic acid half thioesters (MAHTs) and aldehydes using metal catalysis (scheme 1.11).[28] The authors propose that carbon-carbon bond formation leading to the intermediate **1.55** occurs first, followed either by decarboxylation in the presence of copper, such as in the chemistry initially developed by Shair and co-workers (*vide infra*), or by dehydration then decarboxylation in the presence of other metal catalysts (Zn, Mg, Yb).

---

[26] Corey, E. J. *J. Am. Chem. Soc.* **1952**, *74*, 5897

[27] Tanaka, M.; Oota, O.; Hiramatsu, H.; Fujiwara, K. *Bull. Chem. Soc. Jpn.* **1988**, *61*, 2473.

[28] Berrué, F.; Antoniotti, S.; Thomas, O. P.; Amade, P. *Eur. J. Org. Chem.* **2007**, 1743.

Scheme 1.11 **Biomimetic Knoevenagel-Doebner Reaction.**

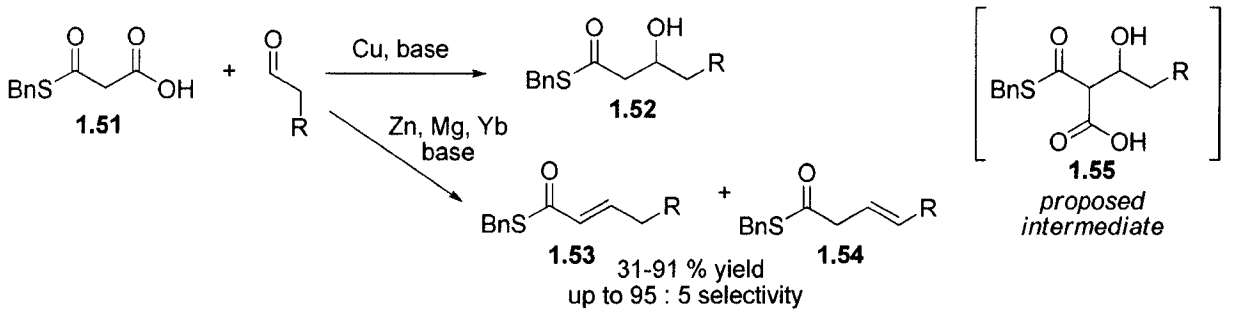

The authors support this explanation with the fact that the MAHT does not decarboxylate in the absence of aldehyde, and that the β-hydroxythioester **1.52** does not dehydrate to form the unsaturated products **1.53** and **1.54** when subjected to the dehydration conditions.

1.2.4. Decarboxylative Nucleophilic Additions Using Malonic Acid Half Thioesters

1.2.4.1. Decarboxylative Aldol Reactions

The first report of a biomimetic decarboxylative aldol reaction was described by Shair and co-workers,[29] wherein malonic acid half thioesters (MAHTs) are reacted with aliphatic and electron-deficient aromatic aldehydes in the presence of catalytic copper and an amine base (Scheme 1.12). The heightened reactivity of the malonyl-derived nucleophiles relative to simple thioesters obviates the need for strong base and harsh conditions used in some crossed-aldol reactions.

Scheme 1.12 **First report of a copper-catalyzed decarboxylative aldol reaction using MAHTs.**

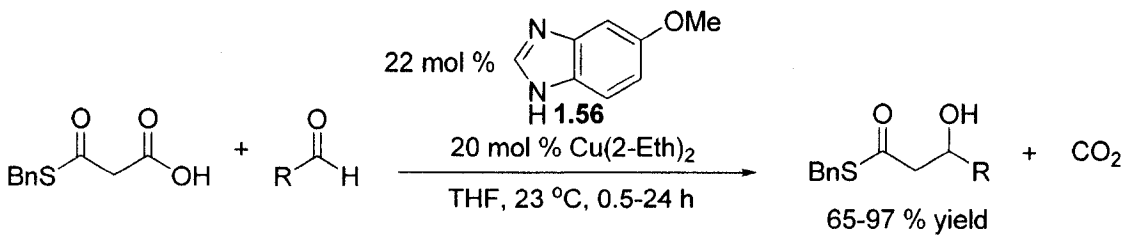

[29] (a) Lalic, G.; Aloise, A. D.; Shair, M. D. *J. Am. Chem. Soc.* **2003**, *125*, 2852. (b) Magdziak, D.; Lalic, G.; Lee, H. M.; Fortner, K. C.; Aloise, A. D.; Shair, M. D. *J. Am. Chem. Soc.* **2005**, *127*, 7284.

The reaction proceeds at room temperature and is stable to air and water; however, relatively high catalyst loadings (20 mol %) and an expensive benzimidazole base are required to maintain good reactivity and catalyst turnover. Decreasing the catalyst loading to 5 mol % requires the use of three equivalents of aldehyde to maintain adequate yields. Aromatic aldehydes are less compatible, unless an electron-withdrawing substituent is present. Importantly, no reactivity was observed using malonic acid half oxyesters (MAHOs) as nucleophiles.

The authors subsequently reported an enantioselective version of this methodology which employs α-methyl-substituted MAHTs (MeMAHT) and a copper (II) Phbox catalyst system (Scheme 1.13).[27b]

Scheme 1.13 **Enantio- and diastereoselective copper-catalyzed decarboxylative aldol reaction.**

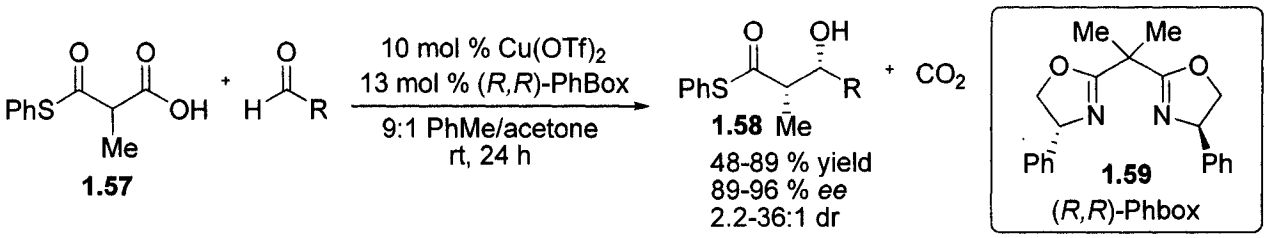

These new conditions are compatible with aldehydes bearing multiple functional groups and result in excellent enantiomeric excesses (≥ 89 % *ee*) and varying diastereomeric ratios (2.2-36:1). A slight excess of oxazolidine ligand with respect to the copper source is necessary for the reaction to occur, most likely due to its role as a base as well as a ligand. Although the mild reaction conditions were conserved, the requirement of a stronger Lewis acid ($Cu(OTf)_2$) compromised the stability of the reaction to air, requiring extensive drying of the catalyst prior to the reaction as well as the need to azeotrope trace water away from the MeMAHTs. Once again, MAHOs and aromatic aldehydes lacking electron-withdrawing substituents, as well as α,β-unsaturated aldehydes, were unreactive in these conditions.

It should be noted that prior to this report, an article by Cozzi and co-workers described an enantioselective decarboxylative aldol reaction between MAHTs and aldehydes using catalytic $Cu(OTf)_2$ and enantiopure bisbenzimidazole ligands (Scheme 1.14).[30]

[30] Orlandi, S.; Benaglia, M.; Cozzi, F. *Tetrahedron Lett.* **2004**, *45*, 1747.

Scheme 1.14 **Decarboxylative aldol reaction using $Cu(OTf)_2$, bisbenzimidazole ligand and base.**

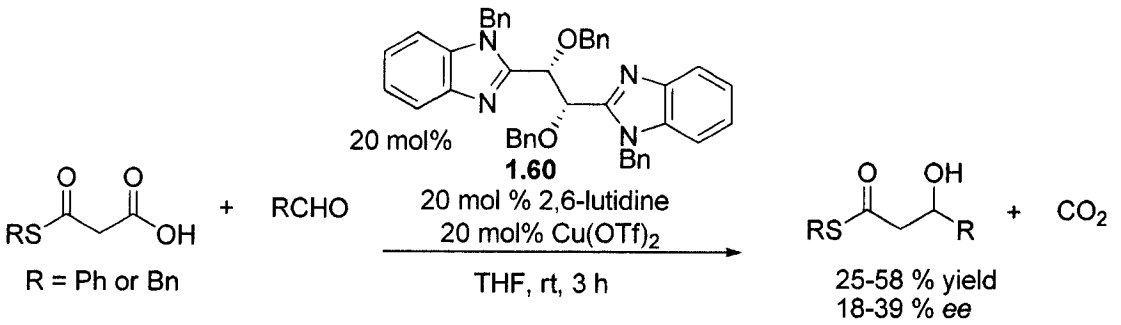

An achiral base was used in addition to the metal and ligand in order to try to improve the poor yields. However, only low to moderate yields and *ee*'s were obtained using this methodology. From our own observations with these types of substrates, it is likely that a significant background reaction is occurring with the achiral base and reactants, explaining the poor *ee*'s observed.

A subsequent report by the Shair group disclosed mechanistic studies investigating the pathway involved in the formation of *β*-hydroxythioesters using their copper-catalyzed methodology.[31] Evidence from several kinetic and isotopic labeling experiments suggested a catalytic cycle involving the reversible formation of a post-addition, pre-decarboxylation type intermediate (Scheme 1.15); however, no direct detection or isolation of this intermediate was reported.

[31] Fortner, K. C.; Shair, M. D. *J. Am. Chem. Soc.* **2007**, *129*, 1032.

Scheme 1.15 **Proposed catalytic cycle for the copper-catalyzed decarboxylative aldol reaction.**

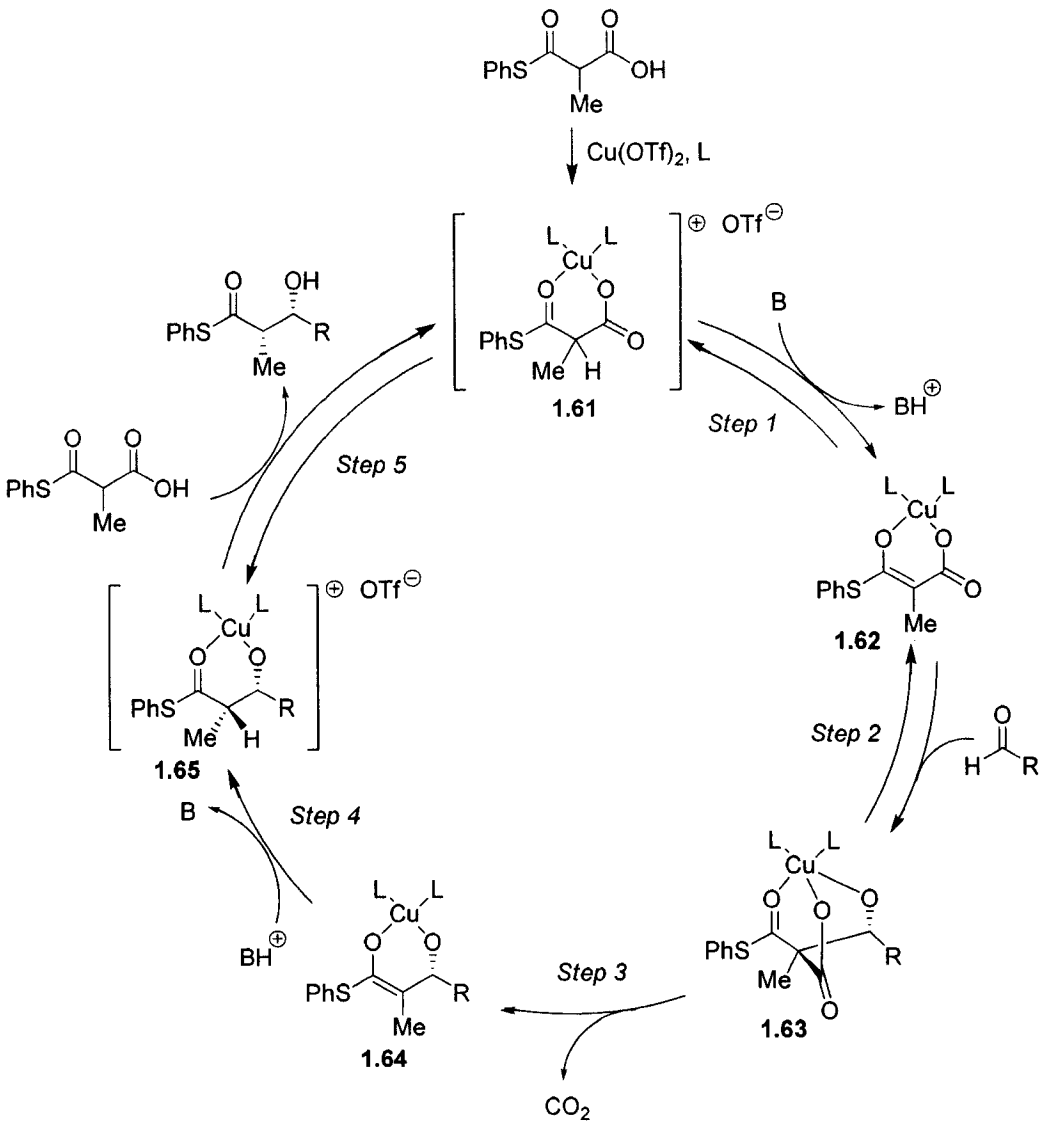

Kinetic ^{1}H NMR studies showed that the reaction was first order in the $Cu(OTf)_2$ – (*R*,*R*)-Phbox – MeMAHT mixture, as well as first order in the aldehyde at concentrations below 0.2 M. At higher concentrations of aldehyde, the rate of enolization of the MeMAHT was found to be partially rate limiting.

Isotopic labeling studies with deuterium-labeled MeMAHT (MeMAHT-D) revealed a negligible kinetic isotope effect of 1.06; however, a reaction run with half MeMAHT and half MeMAHT-D in one pot showed a product ratio of 6:1 H:D at low conversion, indicating that selectivity for the H:D ratio in the product occurs in a non rate-limiting step of the cycle.

^{13}C-Labeled MeMAHTs were also prepared, in which half the solution contained a ^{13}C label at the thioester carbon and half at the carboxylic acid position. An experiment was run in which half the solution consisted of MeMAHT-D, and the other half of MeMAHT-^{13}C (Scheme 1.16). Five minutes into the reaction (< 3 % conversion), 90 % of the reaction mixture was removed and the product was isolated. It was observed that the isotopic labeling in the products was completely scrambled with respect to the original labeling pattern in the starting materials. Upon isolation of the starting materials one minute later, the labeling was not yet scrambled completely, indicating that simple enolization of the MeMAHTs was not responsible for the ration of H:D observed in the products. This implies that another step in the reaction cycle would be responsible for this observation.

Scheme 1.16 **Isotopic labeling studies by Shair and coworkers.**

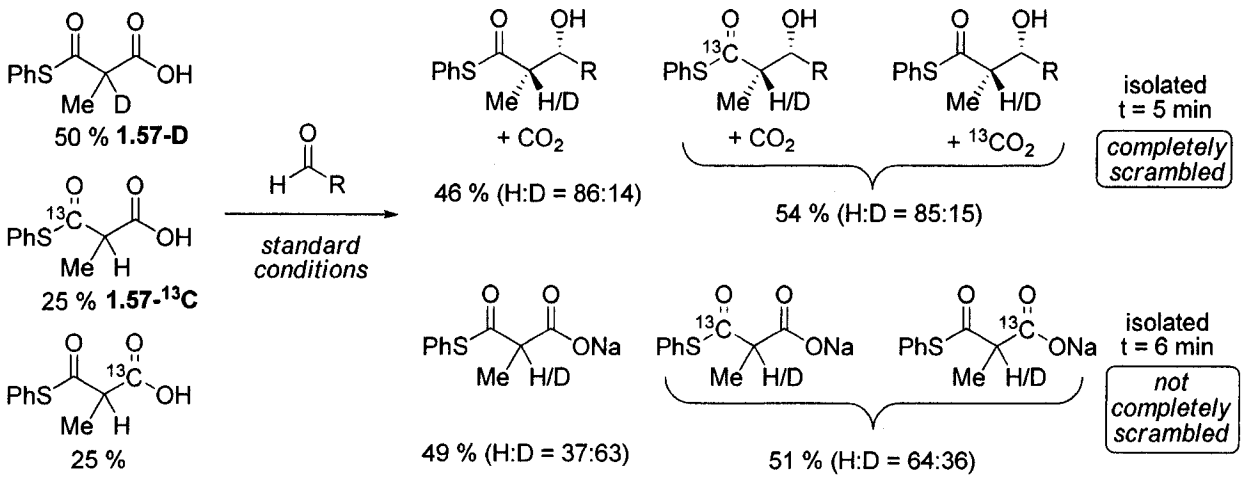

The reaction products were also found to be configurationally stable when re-subjected to the reaction conditions, indicating that enolization of the products is also not responsible for the observed isotopic ratios. These observations are consistent with a mechanism in which the aldehyde is added to the MeMAHT first, at which point decarboxylation follows and protonation occurs giving the observed H:D ratio (steps *2*, *3* and *4*, Scheme 1.15).

In order to investigate the reversibility of the intermediate formation, more isotopic labeling studies were run, this time using only the 1:1 mixture of MeMAHT-^{13}C at the thioester and carboxylate positions (Scheme 1.17). At high conversion, the starting materials were

analyzed for selective depletion of ^{12}C over ^{13}C. A kinetic isotope effect of 1.020 ± 0.002 was observed, which is a significant effect when dealing with carbon isotopes. When comparing an irreversible and reversible formation of the intermediate, one would expect to see a KIE for a reversible intermediate formation but not for the irreversible formation. This is because the step responsible for the KIE is the one in which a bond to the labeled atom in question is being formed or broken; in this case, the decarboxylation step. The first step of the cycle, addition of the aldehyde, would presumably show no KIE since the carboxylate is not directly involved at this point. If this step is irreversible, then depletion of ^{12}C and ^{13}C in the MeMAHTs would be expected to be identical, as the intermediate would at this point be committed to product formation. In a reversible first step, the intermediate has the option of either decarboxylation and product formation, or reversion to starting materials. In this scenario, the MeMAHT-^{12}C would be more likely to proceed with decarboxylation than the MeMAHT-^{13}C, explaining the observed KIE in this experiment.

Scheme 1.17 **Reversibility studies using ^{13}C kinetic isotope effects.**

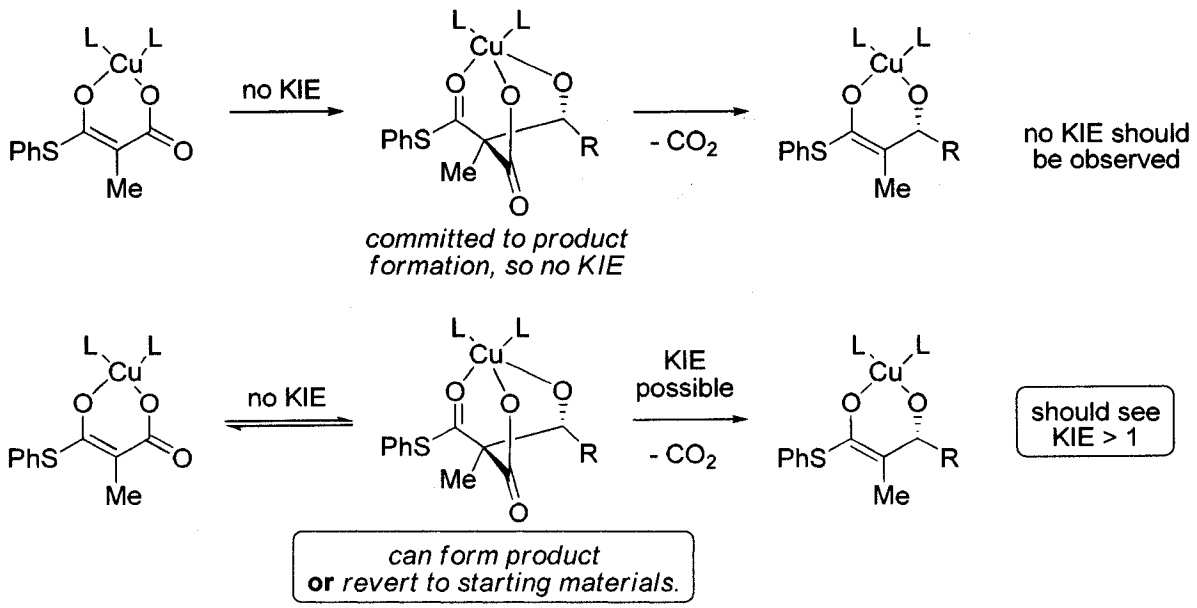

The authors stipulate that decarboxylation only occurs following addition to the aldehyde because of the presence of copper, which chelates the MAHT in a way that holds the carboxylate and thioester moieties coplanar. In this configuration, overlap of the carbon-carbon σ orbital with the thioester π* orbital necessary for decarboxylation is impossible (Scheme 1.18).

However, the α-hydrogen is stereoelectronically aligned for deprotonation, making enolization favourable in this species.

Scheme 1.18 **Proposed coordination of the Cu-ligand complex to the MAHT.**

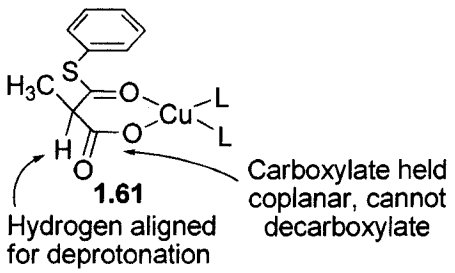

1.2.4.2. Application to imine and nitroolefin electrophiles.

Subsequent to the report of this methodology, decarboxylative Mannich[32] and 1,4-addition[33] reactions with MAHTs were published in which no metals and only a catalytic amount of base were necessary. Ricci and co-workers described the formation of enantioenriched β-amino acid precursors by the decarboxylative addition of MAHTs to *N*-tosyl imines (Scheme 1.19).[30]

Scheme 1.19 **Catalytic decarboxylative addition of MAHTs to *N*-Tosyl imines.**

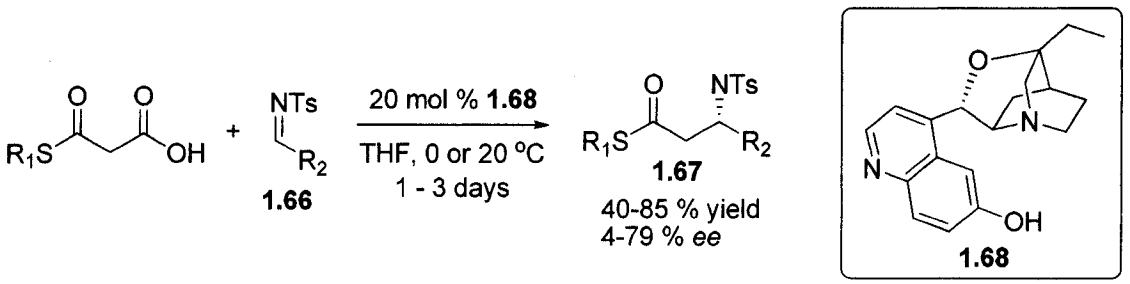

This reaction is catalyzed by cinchona alkaloid analogue **1.68**. The organocatalyst is thought to create a chiral environment through an ionic interaction between the thioester acetate and protonated quinuclidine moieties, as well as hydrogen bonding with the phenolic hydroxyl group on the quinoline moiety (Scheme 1.20).

---

[32] Ricci, A.; Petterson, D.; Bernardi, L.; Fini, F.; Fochi, M.; Perez Herrera, R.; Sgarzani, V. *Adv. Synth. Catal.* **2007**, *349*, 1037.

[33] Lubkoll, J.; Wennemers, H. *Angew. Chem. Int. Ed.* **2007**, *46*, 6841.

Scheme 1.20 **Proposed interaction between the cinchona-derived organocatalyst 1.68 and reactants.**

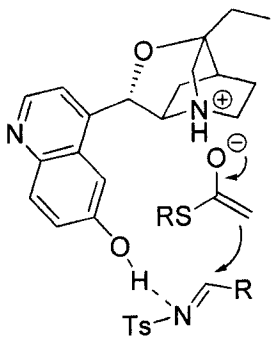

In order to investigate the mechanism of this transformation, the authors prepared analogues of the MAHT starting materials (Scheme 1.21) and tested them under their standard reaction conditions.

Scheme 1.21 **MAHT analogues prepared for mechanistic studies.**

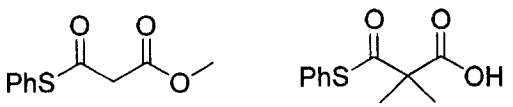

1.69 **1.70**

When MAHT **1.69** was used, very little reactivity was observed and mostly starting materials remained after 24 hours. MAHT **1.70** also showed no addition product and yielded mostly decarboxylated starting material. This was taken as evidence for a stepwise decarboxylation-addition mechanism. Although these findings are compatible with this type of pathway, they do not necessarily disprove a stepwise addition-decarboxylation mechanism. One could explain the low reactivity of **1.69** by a reversible addition of the enolized MAHT to the imine, which reverts mostly to starting materials due to the lack of an irreversible decarboxylation step. MAHT **1.70** could be unreactive due to the lack of an enolizable proton in the α-position, and not necessarily due to sterics as the authors suggest.

It would also be interesting to test the stability of the β-aminothioesters to the reaction conditions. During our own research in this field we noticed the susceptibility of our reaction products to kinetic resolution in the presence of chiral amine bases, including cinchona derivatives. The trends of yields and enantiomeric excesses reported in the scope tables do not necessarily contradict this possibility.

At around the same time, Wennemers and Lubkoll reported the enantioselective 1,4-addition of MAHTs to nitroolefins.[31] In this report, a urea-functionalized cinchona derivative (**1.73**) was used to induce enantioselective formation of γ-nitrothioesters (scheme 1.22).

Scheme 1.22 **Enantioselective organocatalytic decarboxylative 1,4-addition of MAHTs to nitroolefins.**

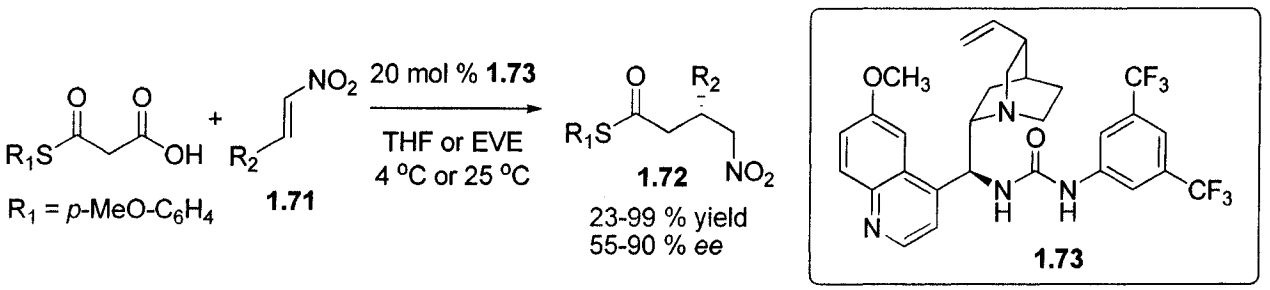

Good yields and moderate *ee*'s (55–67 %) were obtained when using THF as the solvent; however, when using ethyl vinyl ether (EVE) as the reaction medium, the enantioselectivities increased, albeit at the expense of the high yields. It is noted in the references that an increase in *ee* was observed over the course of the reaction in EVE, an observation indicative of possible kinetic resolution of the already moderately enantioenriched products. No mechanistic studies were undertaken to investigate the order of addition and decarboxylation throughout the reaction.

1.3 Project Goals

The aim of this research project was to elucidate and prove the mechanism of the decarboxylative aldol reaction, as well as extending the reactivity to a broader scope of nucleophilic and electrophilic components. More specifically, the analysis of the reaction mechanism would be done through spectroscopic means to identify any intermediates occurring throughout the course of the reaction. The previously unknown reactivity of malonic acid half oxyesters would also be developed and applied to a variety of electrophiles.

Chapter 2

Results and Discussion – Decarboxylative Aldol Reaction

2.1 Reaction Development

2.1.1 Optimization

During initial trials, electron-poor aldehyde and ketone electrophiles were used to encourage the nucleophilic addition of MAHT **2.1** (Scheme 2.1). Ethyl pyruvate **2.2** was chosen as the standard electrophile for optimization and mechanistic studies due to the consistently higher yields and clarity of the ^{1}H NMR spectrum of the reaction mixture (*vide infra*).

Scheme 2.1 **General reaction of MAHT 2.1 and ethyl pyruvate.**

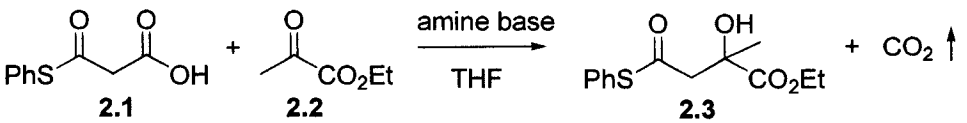

These initial trials were attempted in the absence of copper to facilitate observation by NMR. In contrast to previous reports, it was found that no metal catalysts were necessary for nucleophilic addition to occur. During our work on this methodology, the reports on the organocatalytic addition of MAHTs to imines[30] and nitroolefins[31] were published; however, no reports exist as of yet for the addition of MAHTs to ketones and aldehydes in the absence of metal catalysts. The reaction between MAHT **2.1** and ethyl pyruvate **2.2** proceeded smoothly at room temperature in the presence of one equivalent of Et_3N to afford the β-hydroxythioester **2.3** in 70 % yield in under 3 hours (Table 2.1). Catalytic base also induced decarboxylative addition, with 10 mol % Et_3N resulting in an 86 % yield of product overnight. It was also observed that heat is not necessary, and even detrimental to the reaction, with the best yields being observed at room temperature. This can be attributed to the instability of the β-hydroxythioester product to the basic reaction conditions.

Due to the seemingly facile nature of the reaction, mono-phenylmalonate (MAHO **2.4**), which has not been previously shown to undergo decarboxylative aldol reactions, was also evaluated as

a potential starting reagent. We were pleased to see that over a slightly longer reaction time (4 hours) and otherwise identical conditions, MAHO **2.4** reacted smoothly with ethyl pyruvate (Table 2.1). The reaction can be carried out in the presence of catalytic Et_3N (10 mol %), but for the purposes of our mechanistic studies and reduced reaction times, as well as the low cost of Et_3N, stoichiometric amounts were used in most cases. The reaction was also attempted with excess ethyl pyruvate; however, no significant increase in yield was observed. In all subsequent reactions, equal ratios of MAHT or MAHO to electrophile were used. To rule out the possibility of phenyl acetate reacting with the electrophile through decarboxylation and protonation of the MAHO followed by enolization, a control reaction was run. Phenyl acetate and Et_3N were stirred in the presence of ethyl pyruvate, and no reaction was observed under our standard conditions after several hours.

Table 2.1 **Optimization for MAHT and MAHO starting materials with ethyl pyruvate.**

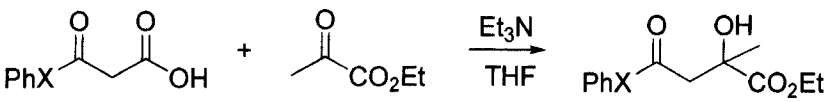

Entry	Et_3N (equiv.)	A:B	Temperature (°C)	X	Yield (%)[a]
1	1.0	1:1	60	S	42
2	1.0	1:1	rt	S	70
3	0.1	1:1	rt	S	86
4	1.0	1:3	50	O	73
5	1.0	1:1	50	O	70
6	1.0	1:1	rt	O	82

[a] Isolated yield. Conditions: MAHT or MAHO (1 equiv.), ethyl pyruvate (1 equiv.), Et_3N (1 equiv.) in THF (0.5 M), room temperature, 2-4 h.

Brief solvent and base scans were performed for optimization purposes (Table 2.2). We found that THF afforded the highest yields in the shortest time span. The type of amine base did not have a significant effect on yields, so Et_3N was used in all subsequent reactions.

Table 2.2 **Solvent and base optimization.**

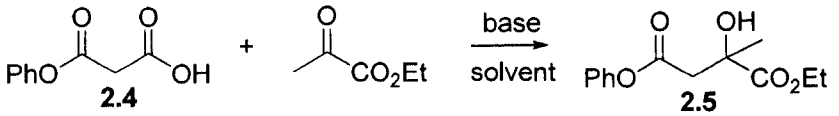

Entry	Solvent	Base	Yield (%)
1	THF	Et_3N	80[a]
2	DMSO	Et_3N	43[b]
3	DCE	Et_3N	32[b]
4	CH_3CN	Et_3N	65[a]
5	PhMe	Et_3N	38[b]
6	EtOH	Et_3N	45[b]
7	Benzene	Et_3N	65[b]
8	THF	Imidazole	73[b]
9	THF	iPr_2NEt	77[a]
10	THF	DMAP	75[b]

[a]Isolated yield. [b]NMR yield. Conditions: MAHO (1 equiv.), ethyl pyruvate (1 equiv.), base (1 equiv.) in solvent (0.5 M), room temperature, 16 h.

2.1.2 Scope

To investigate the scope of this reaction, a variety MAHOs and α-ketoesters were reacted in the presence of stoichiometric Et_3N at room temperature and open to air (Table 2.3).

Table 2.3 **Scope of decarboxylative aldol reaction with MAHOs.**

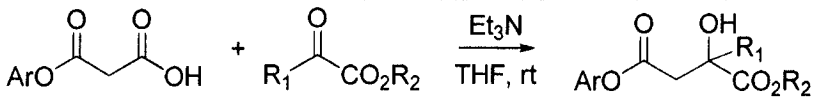

Entry	Ar	R_1	R_2	Yield (%)[a]
1	Ph	Me	Et	82
2	Ph	CF_3	Et	84
3	Ph	Ph	Et	46
4	Ph	H	Et	65
5	Ph	H	*i*Pr	46
6	Ph	Me	Me	47
7	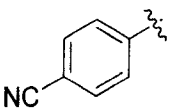	Me	Et	42
8	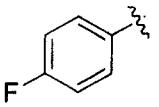	Me	Et	70
9	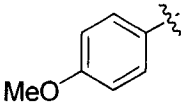	H	Et	70
10	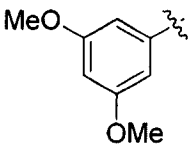	Me	Et	50
11	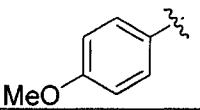	Me	Et	70

[a] Isolated yield. Reactions were run at room temperature for 4 – 16 hours open to air. Conditions: MAHO (1 equiv.), electrophile (1 equiv.), Et_3N (1 equiv.) in THF (0.5 M), room temperature, 4-16 h.

The reaction proceeded best with electron-withdrawing groups on the α-ketoesters (entry 2), and also tolerated bulkier groups in the position α to the carbonyl, albeit in lower yields (entry 3). Aldehydes were also compatible, although yields varied and were mainly moderate to good (entries 4, 5 and 9). Distillation of these aldehydes was found to be vital as they are known to polymerize at room temperature, and often only technical grades are available. Substitution on the aromatic ring of the MAHO with both electron-rich and electron-poor groups also resulted in moderate to good yields, with electron-rich functionalities generally resulting in better conversions (entries 7-11). The lower yield in entry 7 can possibly be attributed to the instability of the product due to the hightened electrophilic nature of the ester. The starting material itself (*p*-cyanophenylmalonic acid half ester) was also difficult to prepare in good yields because of its increased propensity to decarboxylate relative to the other MAHOs. Non-aromatic esters were

generally incompatible with the reaction, with only trace amounts of product being observed with malonic acid half ethyl and half *t*-butyl esters by NMR.

The reaction was found to be less successful with aromatic and aliphatic aldehydes. Benzaldehyde yielded only 13 % of the aldol product, with trace amounts (< 1 %) of the dehydrated product (α,β-unsaturated ester) being observed as well. Aliphatic aldehydes such as dihydrocinnamaldehyde resulted in nearly full conversion of the starting materials but yielded complex mixtures of products. Products isolated from the reaction mixture consisted of the α,β-unsaturated product (~10 % yield), as well as an initially unidentified major product. Spectroscopic studies revealed that a cyclic lactone-type product (**2.9**) resulting from a double addition of the aldehyde was formed, presumably through the mechanism shown below (Scheme 2.2).

Scheme 2.2 **Products observed from reaction of MAHO 2.4 with dihydrocinnemaldehyde.**

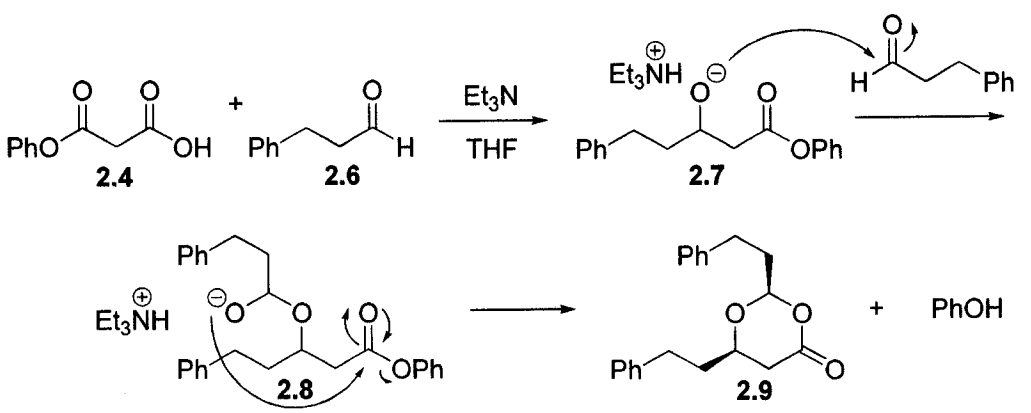

During the course of our scope studies we also attempted the 1,4-addition of MAHO **2.4** to methyl vinyl ketone and cyclohexenone; however, no addition products were observed under our standard conditions and mostly decarboxylated side-products were obtained.

2.1.3 Use of Chiral Bases

Since the decarboxylative aldol reaction of MAHOs could be carried out with catalytic base, we decided to evaluate the effect of chiral amines on product formation. Chiral amino

alcohols, cinchona derivatives and amino acids all resulted in very little or no enantioselectivity in the formation of **2.5** when run in overnight reactions. However, it was observed that if left stirring for a few days, some enantioenriched products were formed. More specifically, when MAHO **2.4** was stirred with ethyl pyruvate and (1*S*,2*R*)-*N*-methylephedrine **2.10** for 3 days, the resulting β-hydroxyester was obtained with 60 % *ee* (Scheme 2.3). A yield was not obtained for this initial hit as the conversion was too low for isolation and the entire crude sample was subjected to HPLC analysis.

Scheme 2.3 **Initial results obtained with (1*S*,2*R*)-*N*-Methylephedrine.**

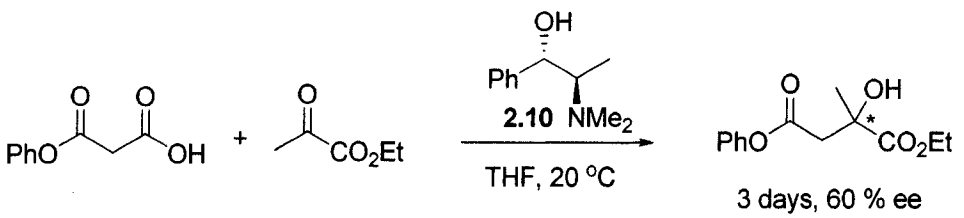

Control reactions with racemic β-hydroxyester in the presence of chiral bases revealed that although there is little or no enantioselectivity in the product forming step of the reaction, the products become gradually enantioenriched over time through kinetic resolution. This project was continued by Sophie Rousseaux and Derek Schipper, who found that the resolution was occurring through a transesterification reaction of the aminoalcohol and phenylester (Scheme 2.4).[34] Derek Schipper optimized the conditions to obtain S factors up to 38, with conversions up to 51 % and *ee*'s up to 89 %.[35]

Scheme 2.4 **Kinetic resolution of β-hydroxyesters with (1*S*,2*R*)-*N*-methylephedrine.**

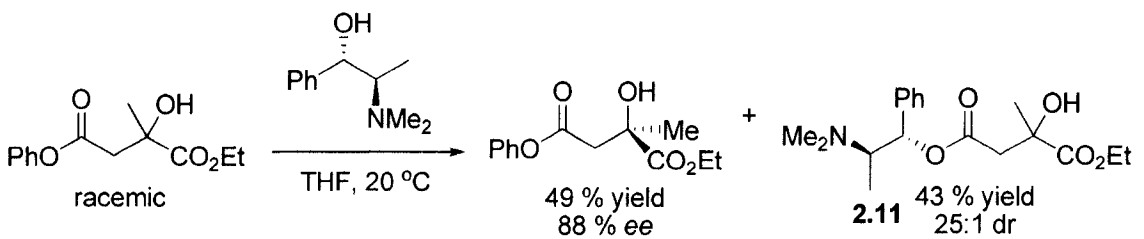

[34] Rousseaux, S. **2007**, Honours thesis: Ottawa, University of Ottawa.
[35] Schipper, D. J.; Rousseaux, S.; Fagnou, K. *Manuscript in preparation.*

2.2 Mechanistic Studies

2.2.1 NMR Analysis and Intermediate Detection

With the goal of elucidating the mechanism for this transformation by ^{1}H NMR analysis, two possible mechanistic pathways were considered (Scheme 2.5). Routes involving either a stepwise decarboxylation followed by addition to the electrophile (Mechanism 1) or addition to the electrophile followed by decarboxylation (Mechanism 2) both contain intermediates potentially observable by NMR (**2.11** or **2.12** and **2.13** or **2.14**).

Scheme 2.5 **Possible mechanisms for the decarboxylative aldol reaction.**

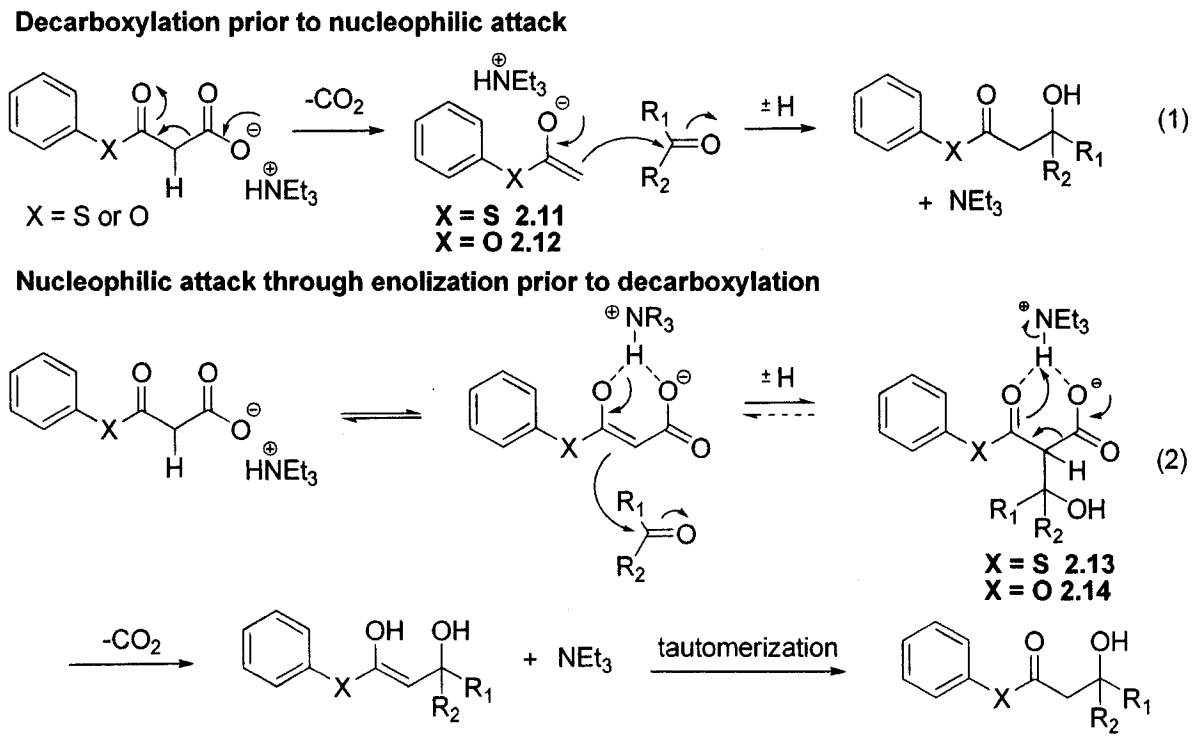

The reaction between MAHT **2.1** and ethyl pyruvate was selected for further analysis due to its high yield and clean ^{1}H NMR reaction spectrum. While scanning the crude spectrum for peaks corresponding to possible intermediates, two singlets at around 4.5 and 4.9 ppm stood out as candidates for the hydrogen in both diastereoisomers of intermediate **2.13** in Mechanism 2 of Scheme 2.5 (Figure 2.1).

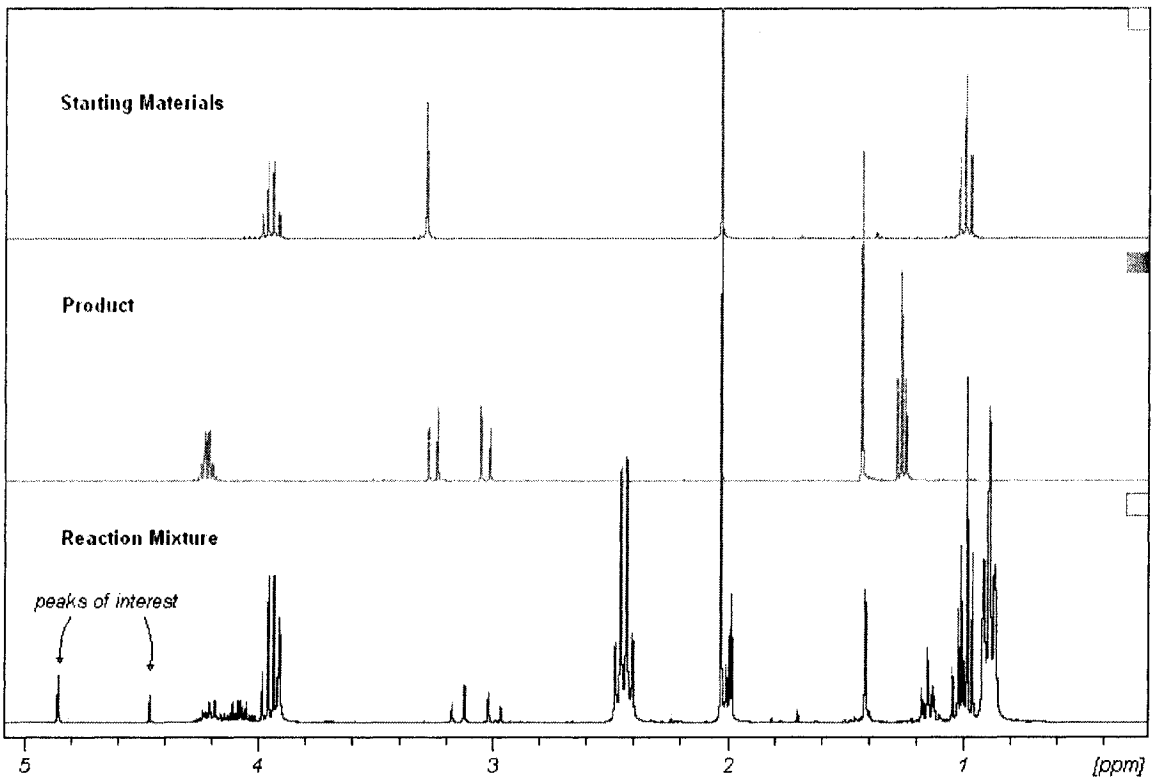

Figure 2.1 **^{1}H NMR spectra of reaction mixture, starting material 2.2 and product 2.3.**

In fact, the relative conversion of starting material, presumed intermediate and product could be clearly followed and quantified by ^{1}H NMR overnight (Figure 2.2).

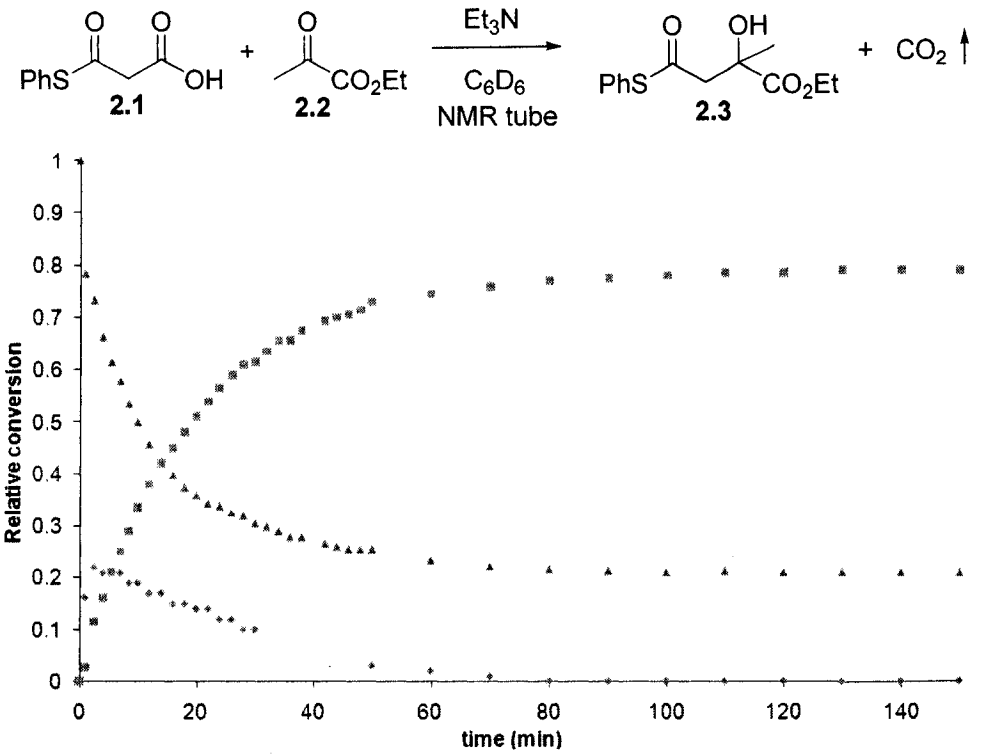

Figure 2.2 **Relative concentration of MAHT 2.1 (blue), intermediate peaks (green) and β-hydroxythioester 2.3 (red). Integrations were measured relative to an internal standard (pentachlorobenzene).**

Deuterated benzene was generally used as the solvent for analysis of the reaction by ^{1}H NMR because of price and availability; however, when trials were run in deuterated THF, the kinetic profile was similar. All attempts to isolate or analyze this postulated intermediate any further failed due to its short lifetime and low overall concentration in the reaction medium. Knowing that the MAHO reacted slower than the MAHT, we decided to follow its reaction with ethyl pyruvate in the hopes of seeing a slower disappearance of intermediate. Analysis of the crude ^{1}H NMR spectrum of MAHO **2.4** reacting with ethyl pyruvate again showed singlets corresponding to the possible diastereomeric intermediates **2.14** (Scheme 2.5). Gratifyingly, in this case, the overall reaction is much slower and there is an accumulation of nearly 80 mol % of the intermediate prior to conversion to products (Figure 2.3).

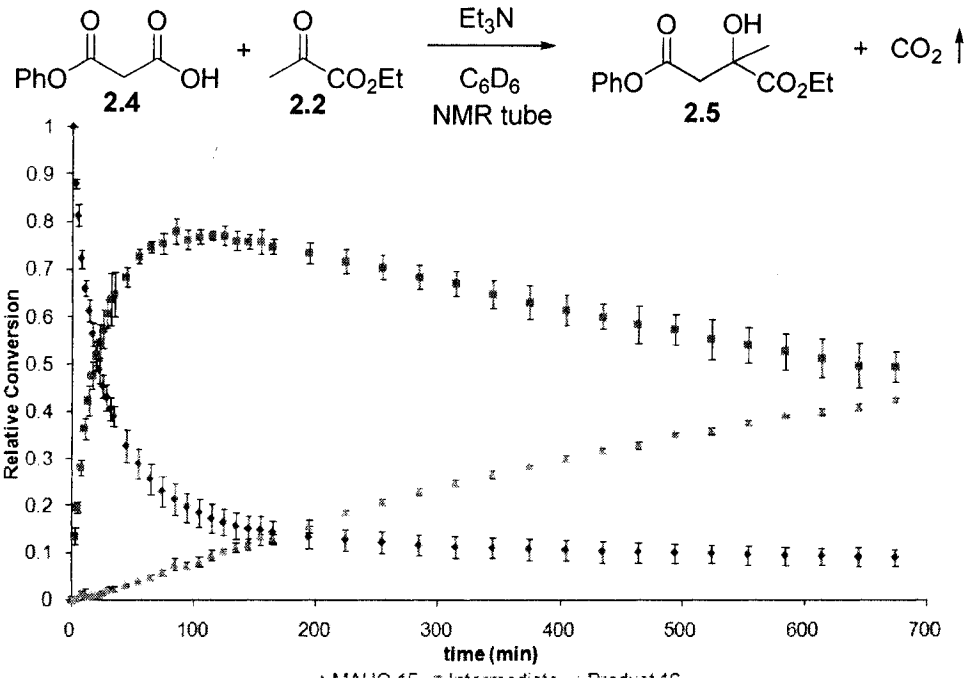

Figure 2.3 **Relative concentration of MAHO 2.4 (blue), intermediate (green) and β-hydroxyester 2.5 (red) over 12 hours analyzed by ^{1}H NMR. Data points represent the mean of 3 trials, and error bars represent the standard deviation. Integrations were measured relative to an internal standard (pentachlorobenzene).**

This accumulation of the intermediate, combined with its longer lifetime, allowed for analysis of the reaction mixture with DOSY NMR (Diffusion-Ordered Spectroscopy).[36] DOSY is a two dimensional spectroscopic method of 'separating' components in a mixture according to diffusion constants which depend on variations in size and charge. One dimension contains the ^{1}H spectrum of the reaction mixture, and the other contains the spectrum of the diffusion coefficients (Figure 2.4). As a type of 'NMR chromatography', this method is ideal for the characterization of our postulated intermediate which is unstable to isolation procedures. In these experiments, deuterated Et_3N was used to minimize peak overlap in the spectrum.

[36] Morris, K. F.; Johnson Jr., C. S. *J. Am. Chem. Soc.*, **1993**, *115*, 4291.

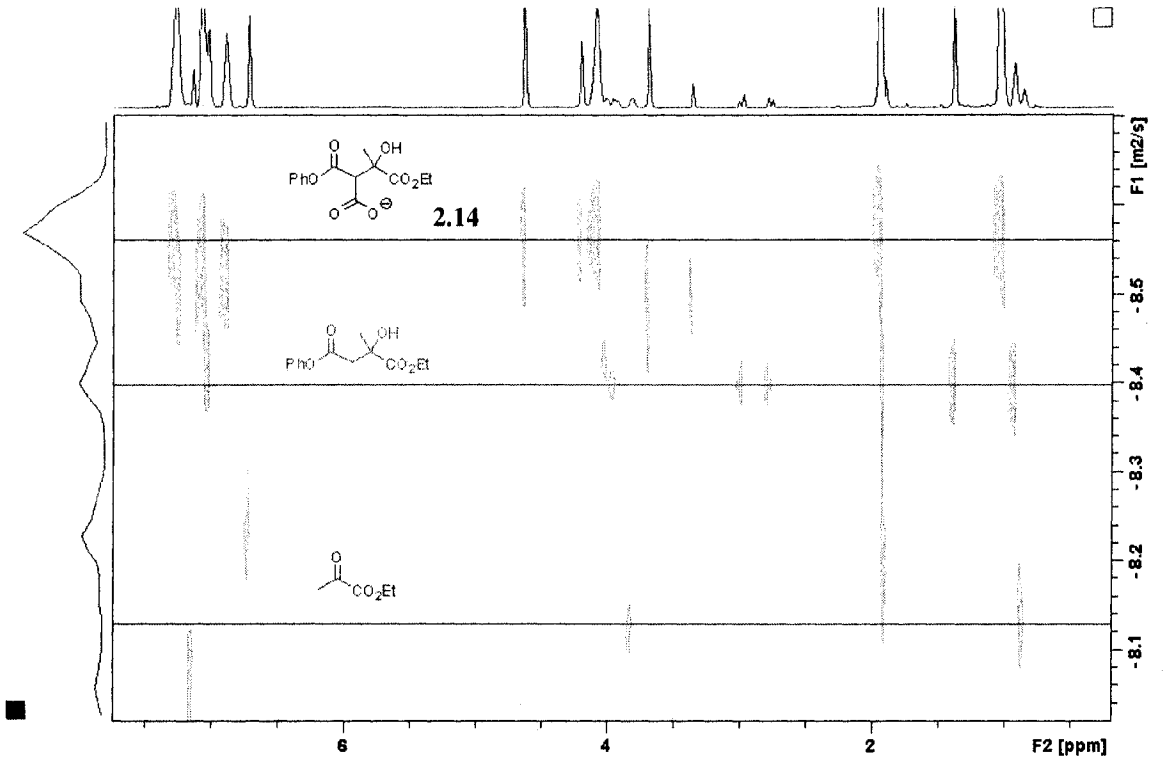

Figure 2.4 **DOSY spectrum of reaction mixture and extracted ^{1}H NMR spectra of reaction components.**

The clean ^{1}H spectrum of each compound is apparent by extracting horizontal traces from points along the diffusion axis corresponding to the reaction components. As shown in Figure 2.5, the spots highest on the y-axis correspond to the ^{1}H spectrum of the relatively large and charged species **2.14**, confirming that the reaction indeed follows a pathway involving a post-addition, pre-decarboxylation intermediate (Mechanism 2, Scheme 2.5).

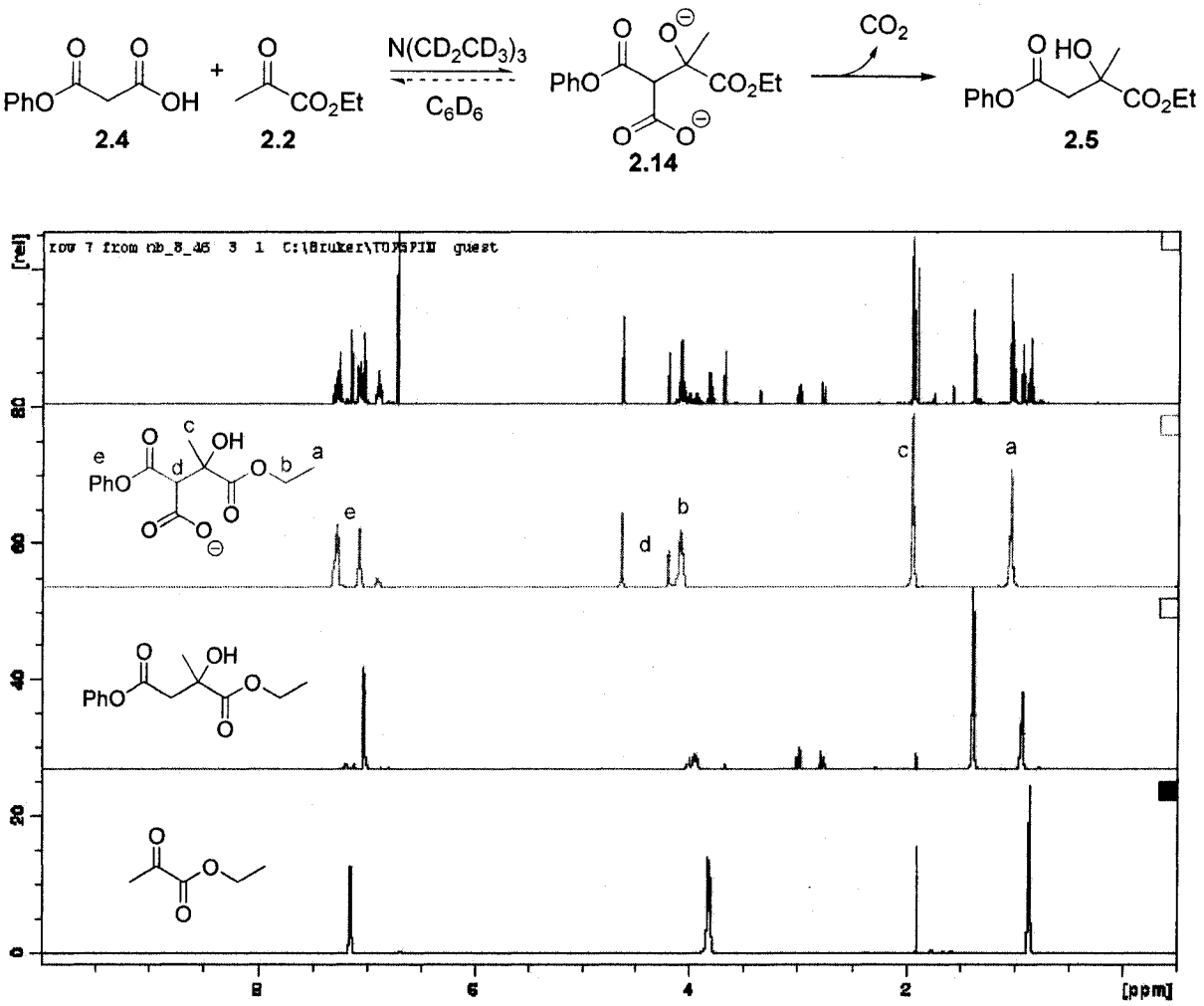

Figure 2.5 **Extracted ^{1}H NMR spectra of ethyl pyruvate, β-hydroxyester 2.5 and intermediate 2.14 from the DOSY experiment.**

This is the first direct detection of the existence of such an intermediate. Additional spectroscopic evidence was collected to further confirm the existence of this intermediate (^{13}C, HMBC and COSY).[37]

In order to prove that the corresponding reaction with MAHTs follows the same mechanism as the MAHO, we attempted to slow down the reaction sufficiently to be analyzed spectroscopically. A low temperature DOSY experiment (0 °C) was run in deuterated toluene to slow the reaction of the MAHT starting material. The same type of post-addition pre-

[37] See supporting information.

decarboxylation intermediate was detected, supporting a common mechanism for both thioester and ester nucleophiles (Figure 2.6).

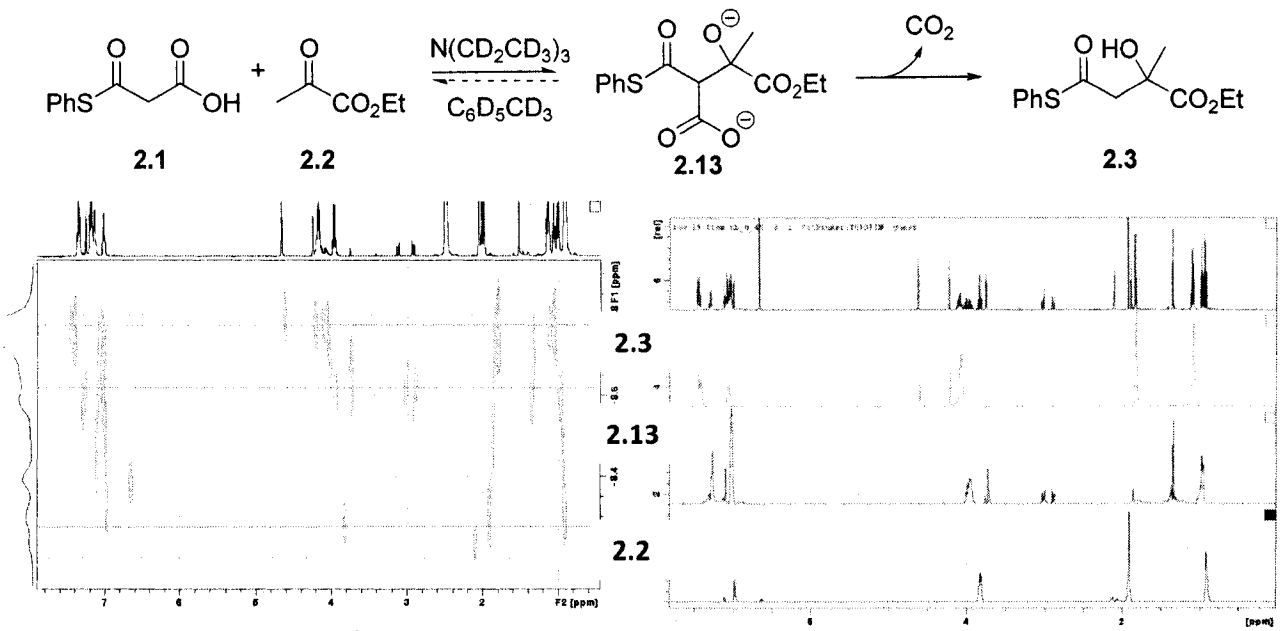

Figure 2.6 **DOSY and extracted ^{1}H NMR spectra of the reaction of MAHT 2.1 and ethyl pyruvate 2.2.**

2.2.2 Reversibility of Intermediate Formation

In order to probe the reversibility of the first step in our proposed mechanism, both kinetic and experimental investigations were performed. We propose that reversible formation of intermediates **2.13** and **2.14** in a retro-aldol type mechanism could explain the lower yields obtained with certain substrates when subsequent decarboxylation is slow.

When devising a strategy for this experiment, we supposed that if the first step, addition of MAHO **2.4** to ethyl pyruvate, is reversible, and a second electrophile was added partway through the reaction at maximal conversion to intermediate, one should see products arising from addition to both electrophiles.[38] Ethyl trifluoropyruvate (**2.15**) was chosen as it is structurally very similar to ethyl pyruvate, and also reacts very quickly with the MAHO under normal reaction conditions (Figure 2.7). As can be seen in the figure below, the starting material disappears completely when the first spectrum is taken of the reaction between MAHO **2.4** and **2.15**, and the product appearance and intermediate decay are rapid.

[38] This work was done in collaboration with Honours student Daniel Shore.

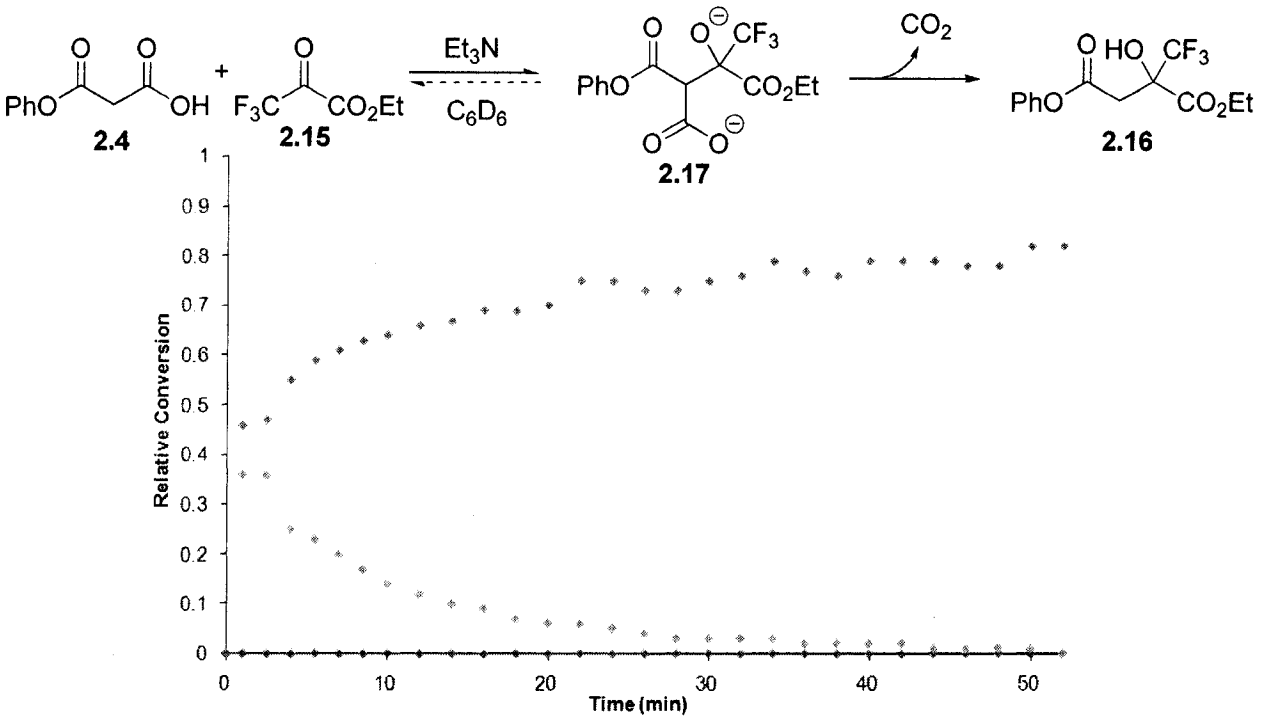

Figure 2.7 **Relative concentration of MAHO 2.4 (blue), intermediate 2.17 (green) and β-hydroxyester 2.16 (red) over 12 hours analyzed by ^{1}H NMR. Integrations were measured relative to an internal standard (pentachlorobenzene).**

Also, the ^{1}H NMR spectrum of the reaction mixture of ethyl trifluoropyruvate **2.15** and MAHO **2.4** is clearly distinguishable from the ethyl pyruvate reaction spectrum, meaning accurate integrations can be collected for both products (Figure 2.8).[39]

[39] Shore, D. G. **2007**, Honours thesis: Ottawa, University of Ottawa.

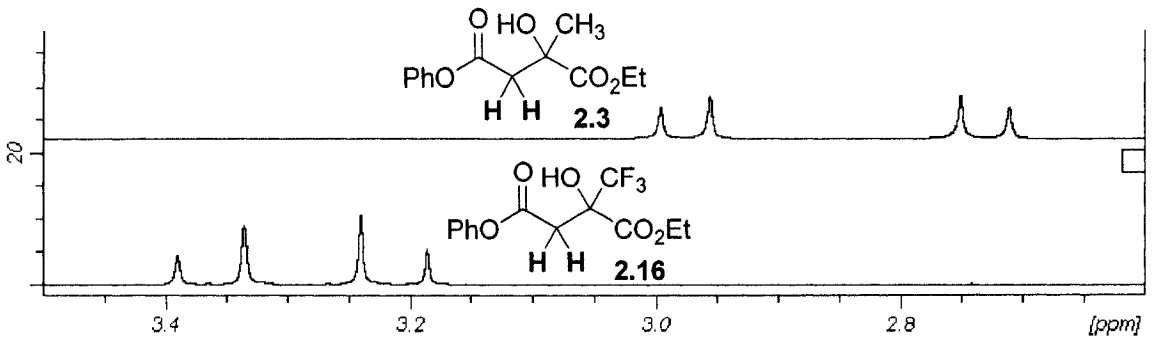

Figure 2.8 **Product peaks of ethyl pyruvate 2.2 and ethyl trifluoropyruvate 2.15 addition products, 2.3 and 2.16. Peaks shown are hydrogens in bold.**

At 75 % conversion to intermediate **2.14**, 130 minutes into the reaction, the ethyl trifluoropyruvate was added to the reaction mixture and the results observed by ^{1}H NMR. At this point a significant deviation from the behavior of the baseline reaction with ethyl pyruvate was observed. There was an immediate decrease in concentration of intermediate **2.14**, as well as total depletion of the MAHO starting material (Figure 2.9). The appearance of product was also significantly retarded.

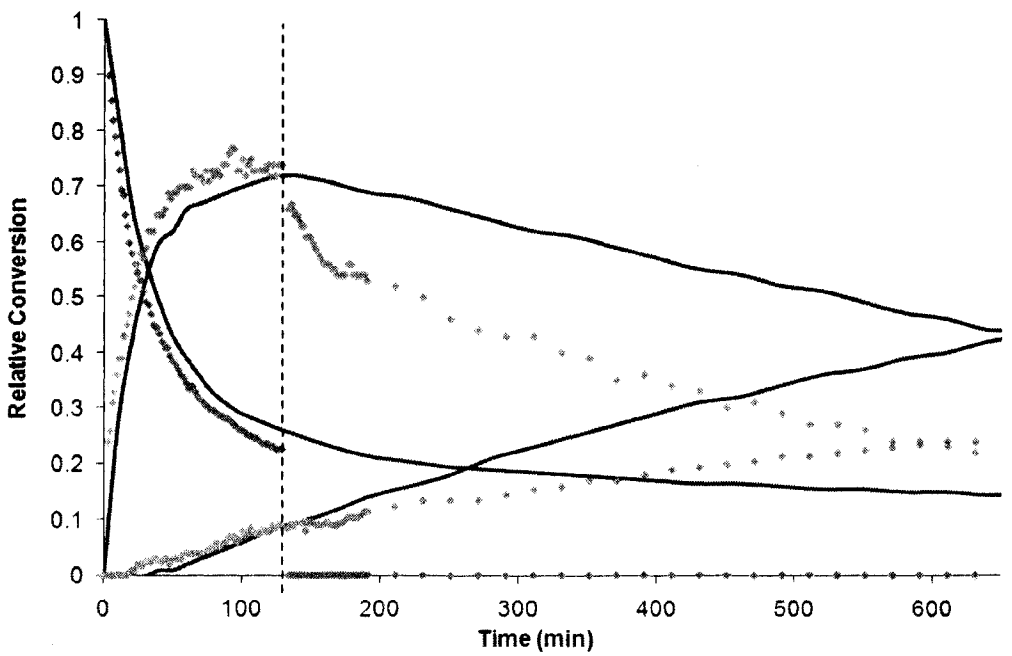

Figure 2.9 **Comparison of the relative concentration of MAHO 2.4, intermediate 2.14, and product 2.5 under standard conditions (solid black lines) with the relative concentrations of the same compounds (blue, green and red data points, respectively) when ethyl trifluoropyruvate 2.15 is added partway through the reaction. The dashed line represents the addition of ethyl trifluoropyruvate.**

In an irreversible reaction, the intermediate already formed at the point of addition of the second electrophile (ethyl trifluoropyruvate) would be expected to be committed to product formation. We could, however, still expect a maximum of 15 % of the product resulting from reaction with the ethyl trifluoropyruvate to occur, given that not all starting material was converted to intermediate at this point (Scheme 2.6). In actual fact, we observed almost 41 % conversion to the fluorinated product **2.16**, indicating a necessary reversion to starting material from the first intermediate **2.14** for reaction with ethyl trifluoropyruvate to occur (Scheme 2.6).

Scheme 2.6 **Competition experiment between ethyl pyruvate and ethyl trifluoropyruvate electrophiles monitored by ^{1}H NMR to determine the reversibility of intermediate formation.**

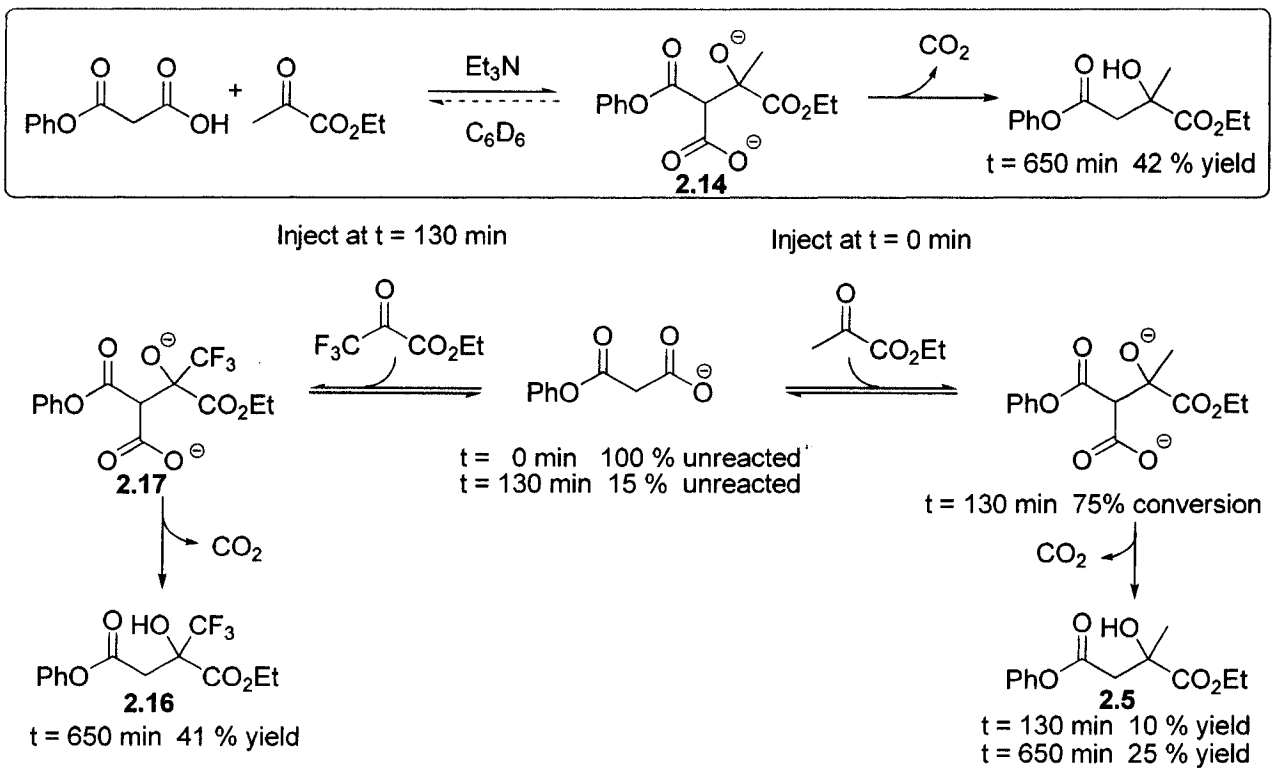

This reversibility is further demonstrated by the significant decrease in concentration of intermediate **2.14** at the point of addition (Figure 2.9). This can be explained by the decrease in effective concentration of starting material due to its immediate reaction with the ethyl trifluoropyruvate electrophile.

2.2.3 Kinetic Studies

2.2.3.1 Analysis with Excel Using Simplified Models

With the aim of evaluating the mechanism kinetically, multiple ^{1}H NMR spectra of the reaction mixture were collected over time and analyzed for variations in concentration of starting materials, intermediates and products. When evaluating potential kinetic models for the acquired curves, the steady-state approximation is not an accurate means of analysis because of the significant buildup of intermediate prior to product appearance. Instead, the fully integrated rate laws of simplified model systems for both reversible and irreversible intermediate formation were employed (equations 1 and 2). In both models, the second step (decarboxylation) is assumed to be irreversible since CO_2 can bubble out of the reaction. The concentration of CO_2 remaining in the reaction mixture is assumed to be too low to significantly influence the kinetics of the reaction. A reversible second step would also severely complicate the integrated rate equations since the steady-state approximation cannot be used.

Irreversible Reaction: $A \xrightarrow{k_1} I \xrightarrow{k_2} P$ (1)

Reversible Reaction: $A \underset{k_{-1}}{\overset{k_1}{\rightleftharpoons}} I \xrightarrow{k_2} P$ (2)

Where A = MAHO **2.4**, I = Intermediate **2.14**, and P = product **2.5**.

These integrated rate equations for both models were then fit to the experimental data obtained by ^{1}H NMR analysis and compared for smallest error. The overall rate laws and rate equations are shown below.

For an irreversible first step (equation 1), the rate laws are:

$$-\frac{d[A]}{dt} = k_1[A] \qquad \frac{d[I]}{dt} = k_1[A] - k_2[I] \qquad \frac{d[P]}{dt} = k_2[I]$$

The integrated rate equations used for comparison with experimental data are:

$$[A]_t=[A]_0\exp(-k_1t) \qquad [I]_t = \frac{k_1[A]_0}{k_2-k_1}[\exp(-k_1t)-\exp(-k_2t)]$$

$$[P]_t = [A]_0\{1-\frac{1}{k_2-k_1}[k_2\exp(-k_1t)-k_1\exp(-k_2t)]\}$$

These equations were fitted to the experimental data collected in both C_6D_6 and THF-d_8;[40] however, as is apparent from the dashed lines in (Figure 2.10) (THF-d_8) and (Figure 2.11) (C_6D_6), an irreversible first step would predict a much quicker drop off of starting material than is observed, as well as a larger intermediate buildup prior to decarboxylation.

For a *reversible* first step (equation 1), the rate laws are:

$$-\frac{d[A]}{dt} = k_1[A]-k_{-1}[I] \qquad \frac{d[I]}{dt} = k_1[A]-k_{-1}[I]-k_2[I] \qquad \frac{d[P]}{dt} = k_2[I]$$

The integrated rate equations used for comparison with experimental data are:

$$[A]=\frac{k_1[A]_0}{x_2-x_3}\{\frac{x_2-k_2}{x_2}\exp(-x_2t)-\frac{x_3-k_2}{x_3}\exp(-x_3t)\} \qquad [I]_t = \frac{k_1[A]_0}{x_2-x_3}[\exp(-x_3t)-\exp(-x_2t)]$$

$$[P]_t = [A]_0\{1+\frac{x_3}{x_2-x_3}\exp(-x_2t)-\frac{x_2}{x_2-x_3}\exp(-x_3t)\}$$

where $x_2 = 0.5(p+q)$, $x_3 = 0.5(p-q)$, $p = k_1+ k_{-1}+ k_2$, and $q = (p^2-4\,k_1k_2)^{1/2}$.

The best fit to the experimental data obtained with these equations is represented by solid lines (Figure 2.10 and Figure 2.11). In this case, it is clear that the reversible first step provides a much better fit and more accurate description of the reaction kinetics. This remained true regardless of the solvent being used. The slight deviation of the theoretical starting material line from the experimental data towards the end of the reaction can be explained by side reactions happening with the starting material, such as decarboxylation of MAHO **2.4,** resulting in a lower concentration of MAHO than predicted.

[40] See supporting information for additional details.

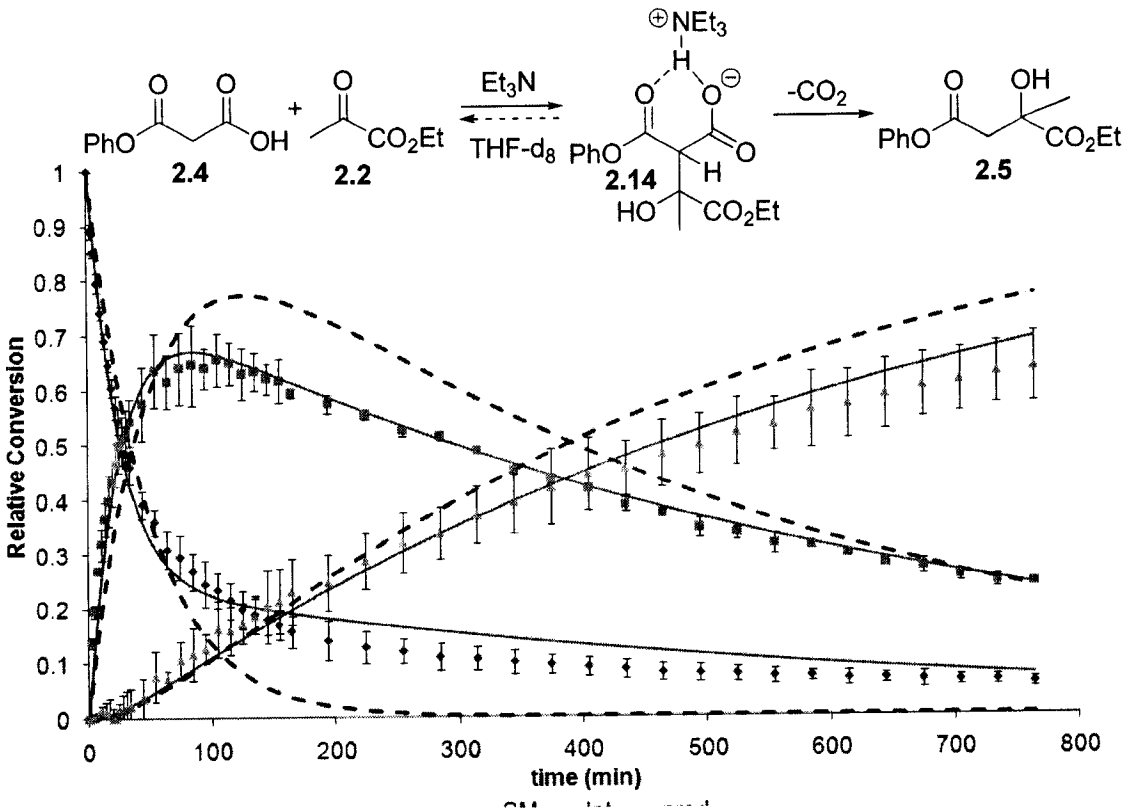

Figure 2.10 **Relative concentration of MAHO 2.4 (blue), intermediate (green) and β-hydroxyester 2.5 (red) over 12 hours analyzed by ^{1}H NMR in THF-d_8 overlapped with the theoretical curves obtained from the irreversible (dashed lines) and reversible (solid lines) integrated rate equations. Data points represent the mean of 3 trials, and error bars represent the standard deviation. Integrations were measured relative to an internal standard (pentachlorobenzene).**

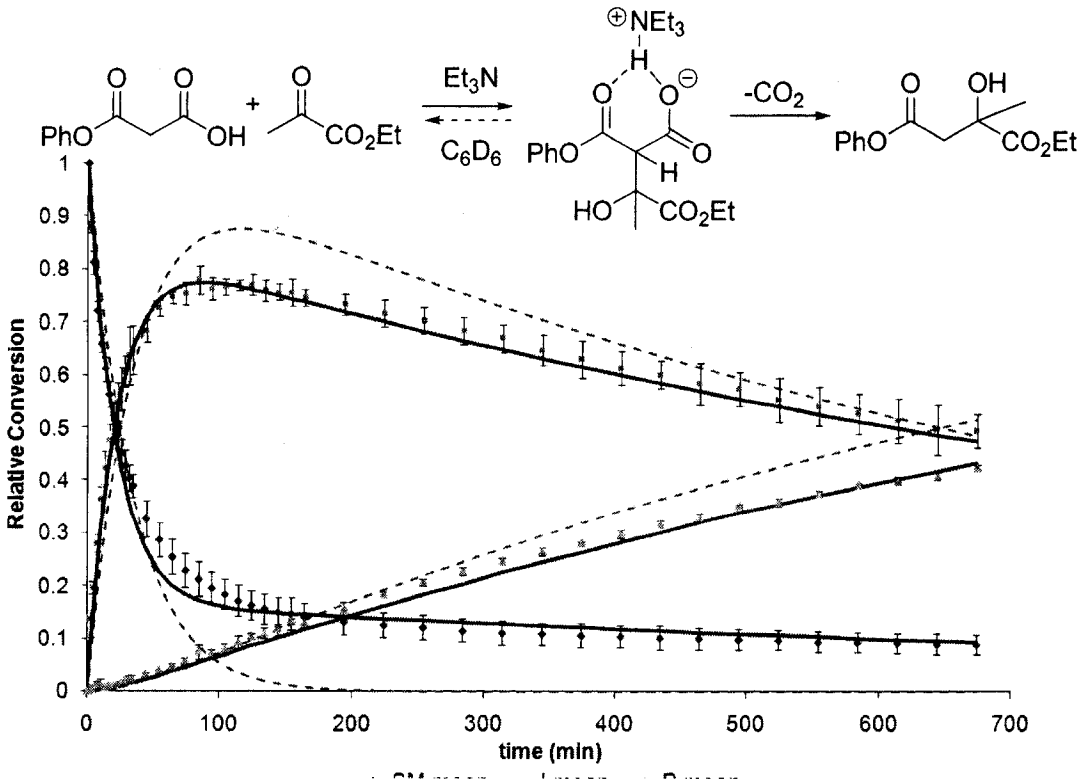

Figure 2.11 **Relative concentration of MAHO 2.4 (blue), intermediate (green) and β-hydroxyester 2.5 (red) over 12 hours analyzed by ^{1}H NMR in C_6D_6 overlapped with the theoretical curves obtained from the irreversible (dashed lines) and reversible (solid lines) integrated rate equations. Data points represent the mean of 3 trials, and error bars represent the standard deviation. Integrations were measured relative to an internal standard (pentachlorobenzene).**

It should also be noted that the lines were fit to various time periods in the experiment (700, 400 and 200 minutes), to ensure that the fit is representative of the actual reaction and not altered by the different, more constant chemical environment at the end. The goodness of fit of each model was quantitatively measured with the chi square statistic x^2, a statistic used to evaluate the error between an experimental and theoretical curve. The fit error did indeed get smaller as the reaction time being compared was decreased, indicating that our model is an accurate kinetic description of the initial transformation, where the largest changes in conversion occur.[41] The chi square values were calculated for reactions run in deuterated benzene, THF and acetone (Table 2.4). In the case of acetone, the error values were larger due to the increased amount of

[41] See supporting information for values.

side reactions (decarboxylation, etc.) that occur in more polar solvents; however, the reversible model still provided a better fit of predicted and experimental values.

Table 2.4 **Chi square values for reversible and irreversible model fits to experimental data.**

	Reversible	Irreversible	critical chi square value
Benzene	0.751	4940627	26.5
THF	0.839	40758	28.9
Acetone	8.624	1488.5	27.3

Solving these theoretical equations also allowed us to calculate the rate constants for the reaction in each solvent. The results are shown in Table 2.5.

Table 2.5 **Rate constants for the reversible addition model calculated by excel.**

Solvent	k_1 (1/s)	k_{-1} (1/s)	k_2 (1/s)
Benzene-d_6 (MAHO)	0.0388	0.00743	0.00104
Benzene-d_6 (MAHT)	0.367	0.150	0.519
THF-d_8	0.0308	0.00899	0.00207
Acetone-d_6	0.0248	0.00871	0.00280

2.2.3.2: Evaluation of Kinetic Models using COPASI.

We initially employed these simplified models because at this point in the project we were not aware of any kinetic programs capable of analyzing our data. It was later brought to our attention that a kinetics analysis software, COPASI (**Co**mplex **Pa**thway **Si**mulator),[42] could be used to process and analyze complex kinetic information. Using this software, we could more

[42] Hoops, S.; Sahle, S.; Gauges, R.; Lee, C.; Pahle, J.; Simus, N.; Singhal, M.; Xu, L.; Mendes, P.; Kummer, U. *Bioinformatics*, **2006**, *22*, 3067.

accurately analyze our data by using the actual equations in which two molecules of starting material are present: A + B ↔ I → P instead of one. This type of model, with a second order rate constant for intermediate formation, was too complex to be analyzed manually. Using COPASI, our experimental data could be imported into this program and we rapidly obtained more precise fits of theoretical equations to our data. Once again, we saw that a reversible first step provided a better fit to our experimental data and a smaller error (Figure 2.12 and Figure 2.13, solid lines). In this case, the predicted lines of best fit for the irreversible model were closer than those predicted by excel with the simplified model, but still not as accurate as the reversible model (Figure 2.12 and Figure 2.13, dashed lines).

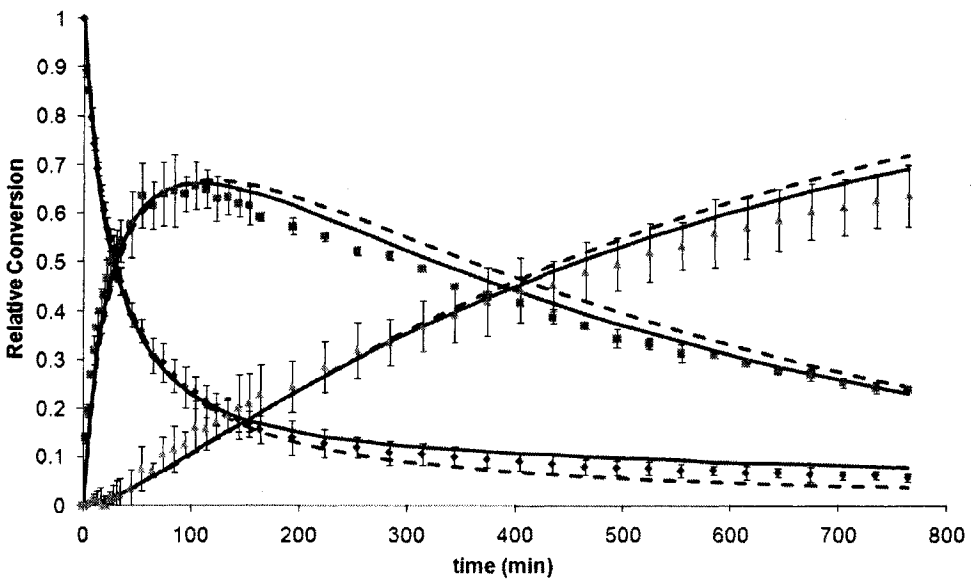

Figure 2.12 **Relative concentration of MAHO 2.4 (blue), intermediate (green) and β-hydroxyester 2.5 (red) over 12 hours analyzed by ^{1}H NMR in THF-d_8 overlapped with the theoretical curves obtained from the irreversible (dashed lines) and reversible (solid lines) integrated rate equations predicted by COPASI. Data points represent the mean of 3 trials, and error bars represent the standard deviation. Integrations were measured relative to an internal standard (pentachlorobenzene).**

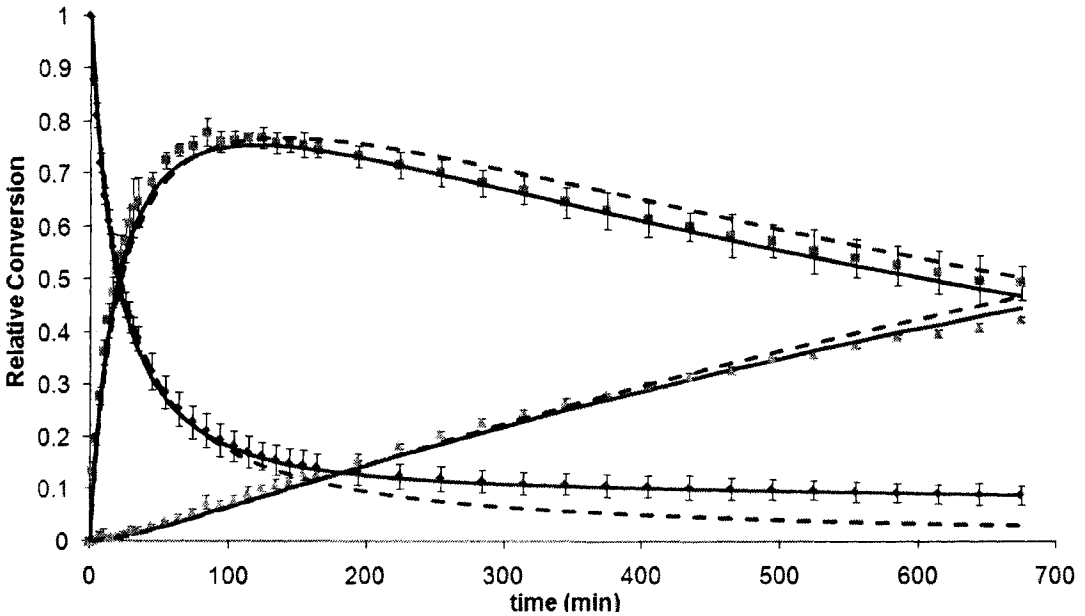

Figure 2.13 **Relative concentration of MAHO 2.4 (blue), intermediate (green) and β-hydroxyester 2.5 (red) over 12 hours analyzed by ^{1}H NMR in C_6D_6 overlapped with the theoretical curves obtained from the irreversible (dashed lines) and reversible (solid lines) integrated rate equations predicted by COPASI. Data points represent the mean of 3 trials, and error bars represent the standard deviation. Integrations were measured relative to an internal standard (pentachlorobenzene).**

The rate constants for the reversible model were calculated and are listed in Table 2.6. The relative speed of the decarboxylative reaction of MAHTs relative to MAHOs is demonstrated by the significantly larger rate constants. This is consistent with the shorter reaction times observed with MAHT nucleophiles. It is also revealed that the decarboxylation step is generally slow relative to intermediate formation.

Table 2.6 **Rate constants for the reversible addition model predicted by COPASI.**

Solvent	k_1 (L/mol·s)	k_{-1} (1/s)	k_2 (1/s)
Benzene-d_6 (MAHO)	0.0519	0.000788	0.00107
Benzene-d_6 (MAHT)	1.234	0.279	0.132
THF-d_8	0.185	0.000680	0.00203
Acetone-d_6	0.151	0.000455	0.00274

The goodness of fit of each model was quantitatively measured with the chi square statistic (Table 2.7). In each case the chi square value was smaller for the reversible model than the irreversible model; however, as the polarity of the solvent increased, the difference between the reversible and irreversible values became smaller. This correlates with the calculated rate constants. As the polarity of the solvent increases, the ratio of k_1 to k_{-1} becomes larger, and k_2 becomes larger as well, diminishing the reversible character of the reaction (if $k_1 >> k_{-1}$, $k_{obs} \approx k_1$) (Table 2.6). Even though the first step is reversible, the reaction gains more and more irreversible character as the polarity of the medium increases.

Table 2.7 **Chi square values for each solvent.**

Solvent	Reversible model	Irreversible Model	critical chi square value
Benzene-d_6	0.48	3.00	23.6
THF-d_8	0.14	0.23	25.9
Acetone-d_6	1.54	1.58	22.2

In this case, the chi square values for the reversible and irreversible models are both below the critical chi square value at the 0.99 level of significance. This indicates that although both

models are valid, the reversible first step provides a slightly better fit to the experimental data. Again, the fact that the equilibrium lies toward the intermediate in the first step gives some irreversible character to the reaction, explaining the low chi square values.

Although this kinetic data alone does not prove the reversibility of the first step, this information combined with the experimental evidence strongly suggests a reversible formation of the post-addition, pre-decarboxylation intermediate.

2.3 Conclusion

In conclusion, a variety of MAHO nucleophiles have been shown to undergo decarboxylative nucleophilic addition reactions with ketone and aldehyde electrophiles under exceptionally mild conditions. These reactions are run in THF open to air in the presence of Et_3N; however, a variety of solvents and amine bases are compatible with this transformation, and catalytic amounts of base will also induce product formation over longer reaction times.

It was also demonstrated that the decarboxylative aldol reaction of both MAHT and MAHO nucleophiles proceeds through a post-addition, pre-decarboxylation intermediate. This species was analyzed spectroscopically and identified with DOSY NMR.

The formation of this intermediate was shown to be reversible using both experimental and kinetic means of analysis. The rate constants for intermediate formation and decomposition to product were calculated for both MAHT and MAHO nucleophiles in different solvents. It was observed that increasing the solvent polarity gave the reaction more irreversible character by increasing the rate of formation of the intermediate relative to its reversion to starting materials, as well as by increasing the rate of decarboxylation. This information provides an insight into the limitations of this methodology. The success of product formation is dependent on the rate constants for intermediate formation and decarboxylation. Too much reversible character will result in low yields as the decarboxylation step is generally rate-limiting and therefore slower than the formation of starting materials from the intermediate.

Chapter 3

Introduction

3.1 Introduction

Over the last few years, increased attention has been focused on alternative fuel sources due to dwindling fossil fuel supplies and the deteriorating effects of their combustion products on our environment. With the accelerating industrialization of developing nations and over 65 % of our refined petroleum products being dedicated to the transport of people and goods, the need for sustainable, clean and transportable fuel is at an all-time high.

A hydrogen economy has been touted as one of the possible solutions in the effort to decrease our dependence on fossil fuels. With water as the only oxidation product, theoretically, hydrogen has all the qualifications necessary for a sustainable source of energy; however, vast amounts of chemical and engineering research and innovation remain necessary to make this a reality. Assuming an efficient process for the extraction of hydrogen from water can be developed, there remains the obstacle of safely storing and transporting it in an energy-efficient manner.

3.2 Hydrogen Storage Methods

Current on-board hydrogen storage methods include pressurized and liquid hydrogen tanks. However, even if one disregards the energy-intensive processes necessary to store the gas in such a manner, the fact remains that the energy density of these systems is quite poor, especially when compared to hydrocarbons. The highest energy density achievable by pure hydrogen is in the liquid form ($\leq$ 20 Kelvin), and even this does not meet the energy requirements for an efficient transportation system.[43]

[43] Amos, W. A. *Costs of Storing and Transporting Hydrogen*; National Renewable Energy Laboratory, U.S. Department of Energy: Golden, Colorado. 1998.

The U.S. Department of Energy (DOE) has set specific targets for the capabilities of on-board hydrogen storage systems. By 2010, the entire hydrogen storage and delivery system must have a gravimetric density of 6 wt % and a volumetric density of 0.045 kg H_2/L. By 2015, these numbers change to 9 wt % and 0.081 kg H_2/L respectively.[44] These are challenging goals; and, if hydrogen is to be used in its elemental form, there is little room left for adding much else to the system.

Materials-based hydrogen storage systems are an area of intense research as they have the potential to significantly increase the energy density achievable for on-board storage. Metal-organic frameworks, carbon nanotubes, aerogels and nanofibers can all reversibly store hydrogen by adsorbing the gas molecules onto a chemical surface, decreasing the volume of the system and therefore improving the energy density.[45] These systems, although an improvement on compressed gas and cryogenic liquid hydrogen tanks, have yet to achieve practical energy densities.

3.3 Chemical Hydrogen Storage

Chemical hydrogen storage is another promising area of research as the covalent modification of hydrogen allows one to potentially store it as a liquid or a solid, an immediate and drastic improvement on the volumetric density previously achievable by compressed gas. Metal hydrides are being explored as possible hydrogen delivery systems, although gravimetric densities and unfavourable thermodynamics for hydrogen release have, until recently, limited their applicability.[46,47] Regeneration of waste products in an efficient manner also still poses a problem; however, this is an active area of investigation and researchers are optimistic about the potential of metal hydrides.

---

[44] *Targets for On-Board Hydrogen Storage Systems*; Hydrogen, Fuel Cells & Infrastructure Technologies Program, U.S. Department of Energy, Energy Efficiency and Renewable Energy. http://www1.eere.energy.gov/hydrogenandfuelcells/storage/pdfs/targets_onboard_hydro_storage.pdf. 2006.

[45] U.S. Department of Energy. (2007). *2007 Annual Progress Report* (Part IV. Hydrogen Storage). Washington, D.C.

[46] Grochala, W.; Edwards, P. P. *Chem Rev.* **2004**, *104*, 1283.

[47] Yang, J.; Sudik, A.; Siegel, D. J.; Halliday, D.; Drews, A.; Carter III, R. O.; Wolverton, C.; Lewis, G. J.; Sachtler, J. W. A.; Low, J. J.; Faheem, S. A.; Lesch, D. A.; Ozolins, V. *Angew. Chem. Int. Ed.* **2008**, *47*, 882.

3.4 Ammonia-Borane as a Hydrogen Storage Chemical

Ammonia-borane **3.1** (AB) has recently been gathering much attention as a potential storage system due to its high hydrogen content by weight (19.6 wt %). AB exists as an air-stable solid at room temperature and has the important characteristic of containing both protic and hydridic hydrogens within the same chemical structure (Scheme 3.1).

Scheme 3.1 **Structure of ammonia-borane.**

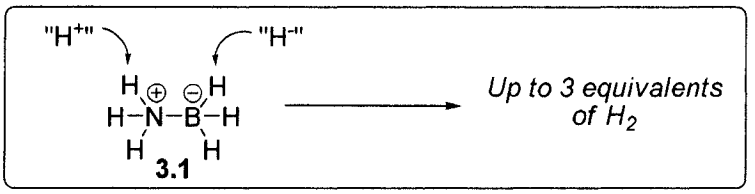

One can easily picture these protons and hydrides combining to evolve up to 3 equivalents of hydrogen from one molecule of AB under the right conditions.

Hydrolytic conditions for the dehydrogenation of AB have been reported;[48] however, although hydrogen release is rapid, the borate compounds produced as a result are essentially a thermodynamic dead end when considering the reversibility of products to starting materials. For this reason, hydrolysis of AB compounds is generally not considered a viable strategy for hydrogen storage.

3.4.1 Thermal Hydrogen Release from Ammonia-Borane

Simply heating ammonia-borane in the solid state[49] has shown the release of up to 13 wt % H_2 over 3 distinct stages defined by temperature ranges of 85-100 °C, 105-150 °C, and over 200 °C; however, these high temperatures indicate that a significant energy input is necessary for the amount of energy output attainable. Rapid heating of AB at 500 °C releases 16.5 wt % H_2 in

[48] (a) Yan, J.-M.; Zhang, X.-B.; Han, S.; Shioyama, H.; Xu, Q. *Angew. Chem. Int. Ed.* **2008**, *47*, 2287; (b) Chandra, M.; Xu, Q. *J. Power Sources* **2006**, *159*, 855.

[49] (a) Hu, M. G.; Geanangel, R. A.; Wendlandt, W. W. *Thermochim. Acta,* **1978**, *23*, 249. (b) Sit, V.; Geanangel, R. A.; Wendlandt, W. W. *Thermochim. Acta.* **1987**, *113*, 379. (c) Wolf, G.; Baumann, J.; Baitalow, F.; Hoffmann, F. P. *Thermochim. Acta,* **2000**, *343*, 19. (d) Baitalow, F.; Baumann, J.; Wolf, G.; Jaenicke-Rößler, K.; Leitner, G. *Thermochim. Acta,* **2002**, *391*, 159. (e) Damle, A.. U.S. DOE Hydrogen Program *2007 Annual Progress Report*, Section IV.B.4, **2007**, 460.

less than 30 seconds, showing that near exhaustive dehydrogenation of AB is possible, albeit at a significant energetic cost. Borazine **3.2** ($(NHBH)_3$, see structure below), a volatile compound known to poison fuel cells, is also a common undesirable product in the thermal decomposition of AB.

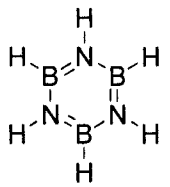

3.2
Borazine

3.4.1.1 Heating in Ionic Liquids

More recently, it has been demonstrated that in an ionic liquid medium (bmimCl, **3.3**), ammonia-borane can release up to 1.5 equivalents of H_2 (5.4 wt %) under milder thermal conditions (95 °C) over the course of 3 hours (Scheme 3.2).[50] In a subsequent report to the DOE, the authors reported an enhancement of H_2 release in other ionic liquids, albeit over a longer time period of up to 24 hours.[51]

Scheme 3.2 **H_2 evolution from ammonia-borane in ionic liquids.**

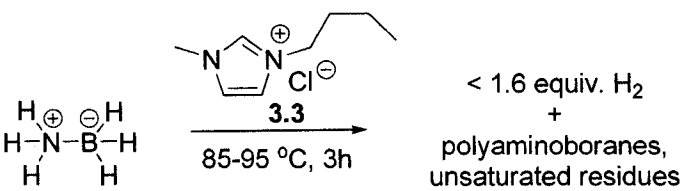

3.4.1.2 Acid-Catalyzed Dehydrogenation

Acidic conditions have also been shown to catalyze H_2 evolution from AB under milder conditions, with catalytic amounts of both BrØnsted and Lewis acids showing reactivity (Scheme 3.3).[52] 0.5 mol % of $B(C_6F_5)_3$, $HOSO_2CF_3$ and HCl can induce release of 1.1 to 1.3 equivalents H_2 in 18 – 24 hours at 60 °C. The authors postulate that non-volatile acids such as solid-supports

[50] Bluhm, M. E.; Bradley, M. G.; Butterick III, R.; Kusari, U.; Sneddon, L. G. *J. Am. Chem. Soc.* **2006**, *128*, 7748.
[51] Sneddon, L.G. U.S. DOE Hydrogen Program *2007 Annual Progress Report*, Section IV.B.5e, **2007**, 488.
[52] Stephens, F. H.; Baker, R. T.; Matus, M. H.; Grant, D. J.; Dixon, D. A. *Angew. Chem. Int. Ed.* **2007**, *46*, 746.

or polyphosphoric acid could catalyze AB dehydrogenation as well, but do not report results from any such experiments. The reaction was found to produce acyclic aminoborane oligomers in the first dehydrogenation process, followed by cyclic compounds upon heating. The reaction is thought to be initiated by abstraction of a hydride from AB to form cationic **3.4** followed by coordination of another molecule of AB for dehydrogenation (Scheme 3.3).

Scheme 3.3 **Proposed mechanism for the acid-catalyzed ammonia-borane dehydrogenation.**

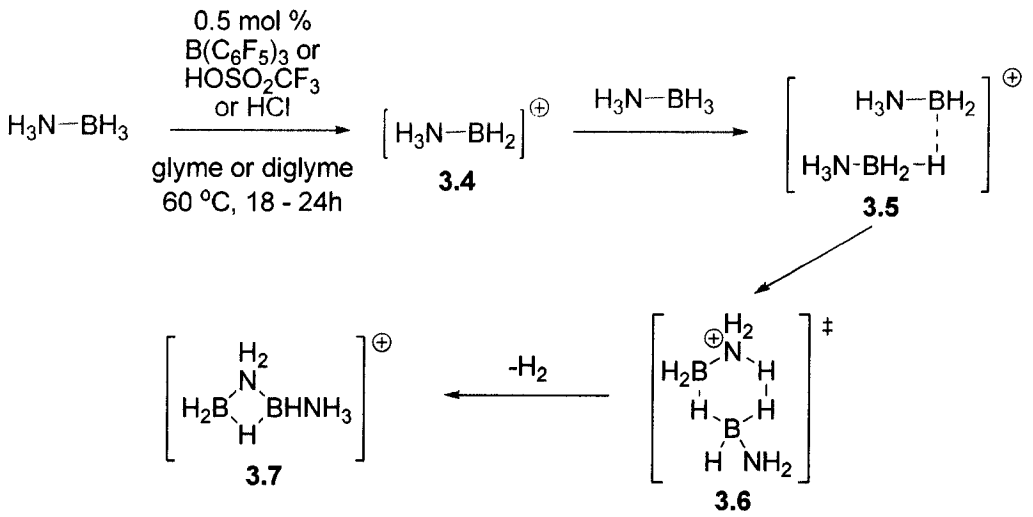

For these acid-catalyzed systems, no overall system weight percentage of hydrogen release is reported.

3.4.2. Transition Metal Catalyzed AB Dehydrogenation

A multitude of transition metal catalysts have also been explored for their potential dehydrogenation activity. With the initial purpose of synthesizing new amine-borane compounds, Manners and co-workers have developed several dehydrogenation catalysts. This group has made use of AB, substituted ammonia-boranes, and phosphine-borane adducts as dehydrocoupling precursors.[53] As the first to report the catalytic dehydrocoupling of AB, the group described a rhodium catalyst capable of fully converting the starting material to oligomeric and polymeric B-N compounds over 48-84 hours.[54] When 0.6 mol % of $[Rh(1,5\text{-cod})(\mu\text{-Cl})]_2$ (**3.8**) was added to a solution of AB in diglyme or tetraglyme at 45 °C, two intermediate products

[53] Clark, T. J.; Lee, K.; Manners, I. *Chem. Eur. J.* **2006**, *12*, 8634.
[54] Jaska, C. A.; Temple, K.; Lough, A. J.; Manners, I. *J. Am. Chem. Soc.* **2003**, *125*, 9424.

were observed by ^{11}B NMR. Although these compounds could not be isolated due to the rapid formation of the polymeric species, they could still be characterized as cyclic trimers **3.9** and **3.10** (Scheme 3.4).

Scheme 3.4 **Rhodium catalyzed AB dehydrocoupling.**

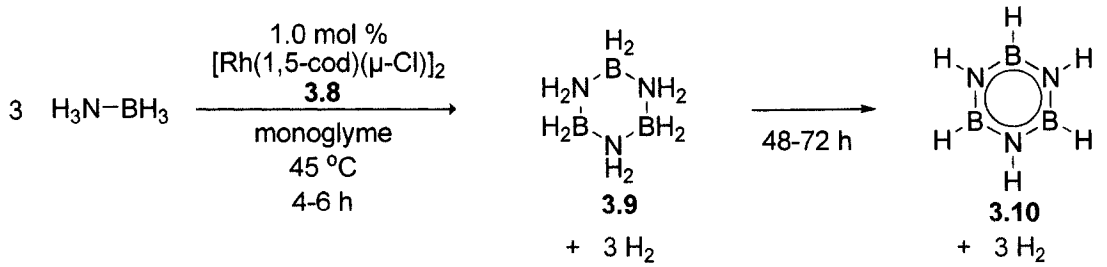

No gravimetric density was reported for this methodology, as the goal was the synthesis of new amine-borane compounds, and not hydrogen storage. It also follows that hydrogen release was not monitored for these reactions. The Manners group has also pioneered transition-metal catalyzed dehydrogenation of alkylamine-boranes (*vide infra*).

The most recent reports of transition-metal catalyzed ammonia-borane dehydrogenation came from the laboratories of Baker, Heinekey, and Goldberg. Goldberg and co-workers have reported an iridium-pincer catalyst capable of dehydrogenating AB at unprecedented rates (Scheme 3.5).[55] On the notion that AB and ethane are isoelectronic compounds, these authors examined catalysts traditionally used for alkane dehydrogenation. They found that 0.5 mol % of catalyst **3.11** was capable of releasing up to 1 equivalent of H_2 in less than 15 minutes, corresponding to an overall system weight of 0.1 % H_2.

Scheme 3.5 **Iridium-catalyzed dehydrogenation of ammonia-borane.**

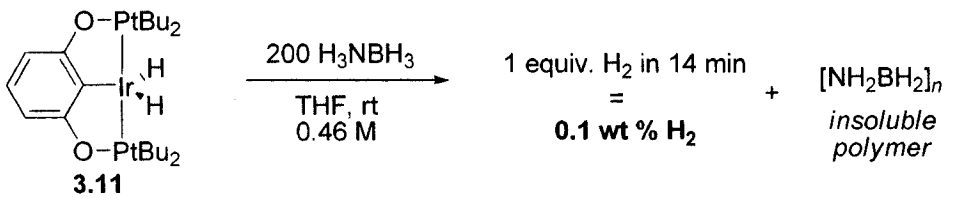

Mercury poisoning experiments revealed that the reaction was likely proceeding through homogeneous catalysis. The authors also noted that a dormant form of their catalyst was formed throughout the reaction; however, it could be regenerated by applying H_2 pressure. In later

[55] Denney, M. C.; Pons, V.; Hebden, T. J.; Heinekey, D. M.; Goldberg, K. I. *J. Am. Chem. Soc.* **2006**, *128*, 12048

reports to the Department of Energy, the authors revealed an improvement in conditions that led to the release of 1 equivalent of H_2 in 4 minutes as well as the dehydrogenation of AB/Methylammonia-borane mixtures. Although very rapid rates of H_2 release are observed, this methodology is run in fairly dilute conditions, meaning that the overall system weight of H_2 is significantly reduced from a potential 11 wt % to 0.4 wt %. Also, the AB systems can only release a maximum of 1 equivalent H_2, most likely due to an insoluble precipitate formed following the first dehydrogenation step. This insoluble solid was characterized as a cycloborazane pentamer by solid state ^{11}B NMR. There are, however, some doubts about the cyclical nature of the oligomer in the literature; it has also been suggested that a linear polymer is a likely structure for this insoluble precipitate.[56]

Until recently, it was commonly thought that AB dehydrogenation occurred through a mechanism involving oxidative insertion into the B-H bond followed by β-hydride elimination of the N-H. Mechanistic studies published by a separate group of researchers revealed that although this Ir-pincer catalyst is active in the dehydrogenation of both alkanes and ammonia-borane, a completely separate mechanism is responsible for each of these processes.[57] While oxidative addition to a C-H bond is common in alkane dehydrogenation, computational results predicted no such analogous process for AB. Instead, a pathway involving the coordination of a B-H hydride to the iridium center to form **3.12** followed by deprotonation and coordination of the N-H hydrogen to the Ir-H and Ir center in a concerted fashion to form **3.14** was predicted. At this point, a rate-limiting dissociation of H_2 from **3.15** from the iridium center occurs to regenerate the starting catalyst (Scheme 3.6). In this mechanism, the ligand never directly participates in any chemical transformations.

[56] Staubitz, A.; Presa Soto, A.; Manners, I. *Angew. Chem. In. Ed.* **2008**, *47*, Early View.
[57] Ankan, P.; Musgrave, C. B. *Angew. Chem. Int. Ed.* **2007**, *46*, 8153.

Scheme 3.6 **Computationally predicted mechanism for the iridium catalyzed AB dehydrogenation reaction.**

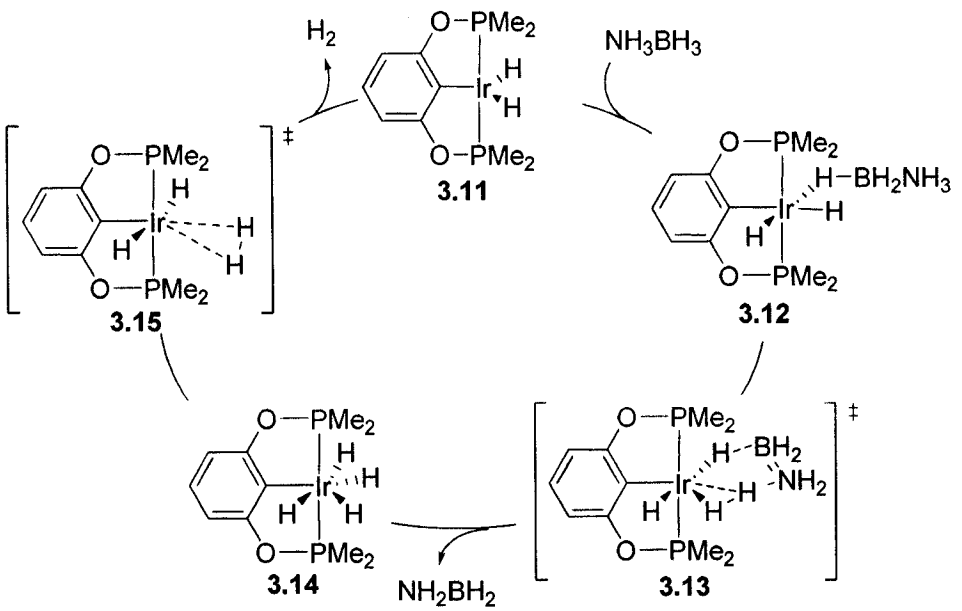

The authors of this mechanistic paper also suggest that the formation of the insoluble cycloborazane pentamer is not induced by the catalyst, but is formed as a result of the THF solvent initiating polymerization.

The only transition-metal catalyst reported to date to release > 1 equivalent of H_2 from AB was described by Baker and co-workers.[58] Although many metals were tested (Ni, Rh, Ru), the most reactive catalyst was found to be a Nickel-carbene complex (Scheme 3.7), which could release up to 2.5 equivalents H_2 in 3 hours at 60 °C.

Scheme 3.7 **Nickel-carbene catalyzed dehydrogenation of AB.**

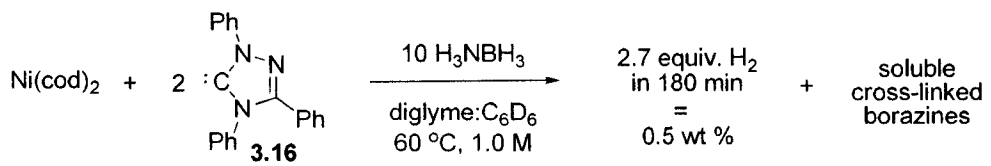

Despite its unprecedented ability to almost exhaustively dehydrogenate AB, this catalyst system is required in a 10 mol % loading, which due to the high molecular weight of the ligands represents a significant portion of the overall system weight. Taking into consideration the

[58] Keaton, R. J.; Blacquiere, J. M.; Baker, R. T. *J. Am. Chem. Soc.* **2007**, *129*, 1844.

catalyst loading combined with the relatively dilute conditions (1.0 M in diglyme), the gravimetric density is reduced to 0.5 system wt % H_2.

The authors also performed isotopic labeling experiments and found a kinetic isotope effect of 2.3 when the nitrogen is deuterated, 1.7 when the boron is deuterated and 2.0 when the entire AB molecule is deuterated. From this information, they proposed a mechanism involving either a concerted H_2 release from AB, or two similarly kinetically significant steps involving B-H insertion and β-hydride elimination from N-H.

Computational studies later published by Yang and Hall suggested a different mechanism, in which there is no insertion to the B-H bond but rather a series of hydrogen and hydride transfer steps involving participation of the carbene ligands.[59] The NH_3 is first deprotonated by the carbene ligand, which then transfers the H to the nickel center. Following another H transfer from the boron to the Ni, H_2 can be released in a concerted fashion. Due to the apparent necessity for these high molecular weight carbene ligands, the overall catalyst loadings must be diminished in order to meet the standards for overall gravimetric density of the hydrogen storage and delivery system.

3.5 Substituted Ammonia-Boranes

3.5.1. Transition Metal Catalyzed Dehydrogenation of Substituted Ammonia-Boranes.

Substituted ammonia-boranes are also an area of interest in chemical hydrogen storage. The overall hydrogen density is reduced in these systems due to the increase in molecular weight and decrease in hydrogen content (a maximum of 2 equivalents of H_2 is possible instead of 3); however, these compounds can potentially behave differently than unsubstituted AB. Manners and co-workers first reported the rhodium-catalyzed dehydrocoupling of primary and secondary aminoboranes with the intention of synthesizing new aminoborane and borazine compounds. They found that although dimethylaminoborane (Me_2NHBH_3, **3.17**) can be dehydrogenated thermally at temperatures above 130 °C, the same process can be carried out in the presence of

[59] Yang, X.; Hall, M. B. *J. Am. Chem. Soc.* **2008**, *130*, 1798.

0.5 mol % [Rh(1,5-cod)(μ-Cl)]$_2$ (**3.18**) at 25 °C to afford full conversion to dimer **3.19** in 8 hours (Scheme 3.8).

Scheme 3.8 **Rhodium catalyzed dehydrocoupling of dimethylaminoborane.**

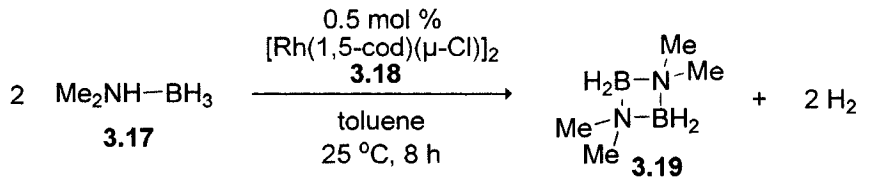

Heating these solutions accelerates the rate of formation of **3.19**. Neutral and cationic rhodium complexes as well as Rh(III) salts were also catalytically active, although none as effective as **3.18**. Other late transition-metal catalysts were also investigated ([Ir(1,5-cod)(μ-Cl)]$_2$, trans-$RuMe_2(PMe_3)_4$, Pd/C); however, these all showed increased reaction times, spanning from 16 to 136 hours. A later report described the use of 2 mol % of Cp_2Ti which fully converted dimethylaminoborane to **3.19** in a significantly decreased reaction time of 4 hours.[60] In terms of hydrogen storage capacity, these compounds are not considered efficient due to the fact that they can release only one equivalent of H_2. In this case, the lighter-weight ammonia-borane is a better option.

Other disubstituted aminoboranes were investigated (pyrrolidine-borane, $PhCH_2(Me)NHBH_3$), although longer reaction times and lower yields were observed. When the substituents were sufficiently bulky (iPr$_2$NHBH$_3$), formation of the unsaturated monomer (iPr$_2$NBH$_2$) was observed instead of dimer formation.

When primary aminoboranes were subjected to these reaction conditions, the formation of borazines (unsaturated trimers) and their dehydrocoupled analogues was almost exclusive (Scheme 3.9). In the presence of 1.0 mol % [Rh(1,5-cod)(μ-Cl)]$_2$ at 45 °C, full conversion of methylammonia-borane (MeAB, **3.20**) to trimer **3.21** was observed over 4-6 hours, translating to the loss of 1 equivalent of H_2. The release of a second equivalent of H_2 to form *N,N,N*-trimethylborazine **3.22** was a much slower process, occurring over 48-72 hours at the same temperature.

[60] Clark, T. J.; Russell, C. A.; Manners, I. *J. Am. Chem. Soc.* **2006**, *128*, 9582.

Scheme 3.9 **Rhodium catalyzed dehydrocoupling of methylammonia-borane.**

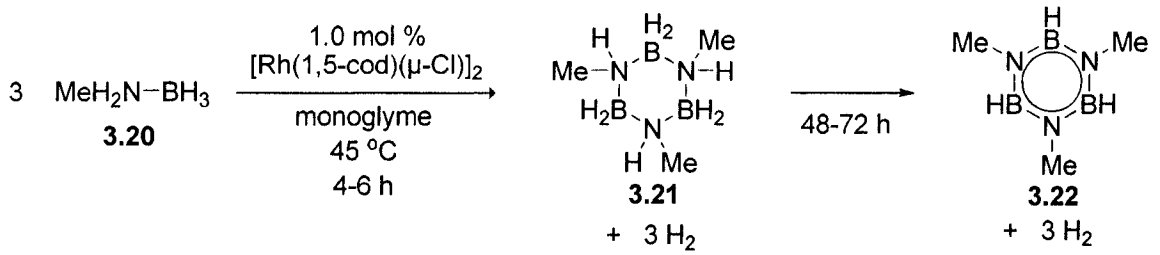

Thermally, the analogous uncatalyzed process requires temperatures up to 200 °C for 2 equivalents of H_2 to be released. Phenylaminoborane was found to be dehydrogenated more rapidly than methylaminoborane (16 h); however, more by-products were observed in this case.

3.6. A New Strategy for Transition-Metal Catalyzed Ammonia-Borane Dehydrogenation.

When considering strategies for dehydrogenation, AB is often compared to ethane. Hence, the catalysts described to date were all chosen for their similarity to known alkane dehydrogenation catalysts. However, as was discussed in previous sections, computational predictions provide little mechanistic support for this analogy. In terms of local dipoles and reactivity, AB may better be compared to methanol (Scheme 3.10). As several catalysts have been developed for alcohol redox processes, we decided to investigate the plausibility of this analogy.

Scheme 3.10 **Dehydrogenation of ammonia borane and methanol.**

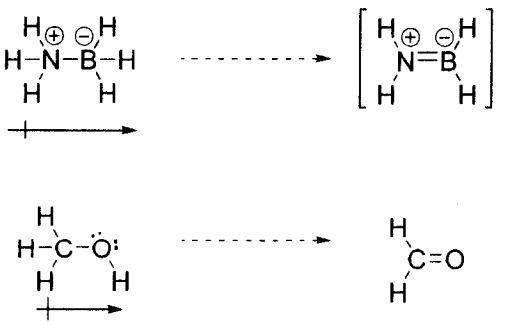

Noyori and co-workers have developed very efficient ruthenium-based catalysts designed for asymmetric transfer hydrogenation reactions.[61] These catalysts generally contain diamine or P-N ligands which participate directly in the transfer hydrogenation process through an outer sphere mechanism (Scheme 3.11).[62] The amide ligand deprotonates an alcohol (**3.24**), which also transfers a hydride to the Ru center through a 6-membered transition state (**3.25**). This 'Ru-hydride' (**3.27**) form of the catalyst can then reduce carbonyls and imines stereoselectively.

Scheme 3.11 **Computed mechanism for the transfer hydrogenation reaction with Ru catalysts.**

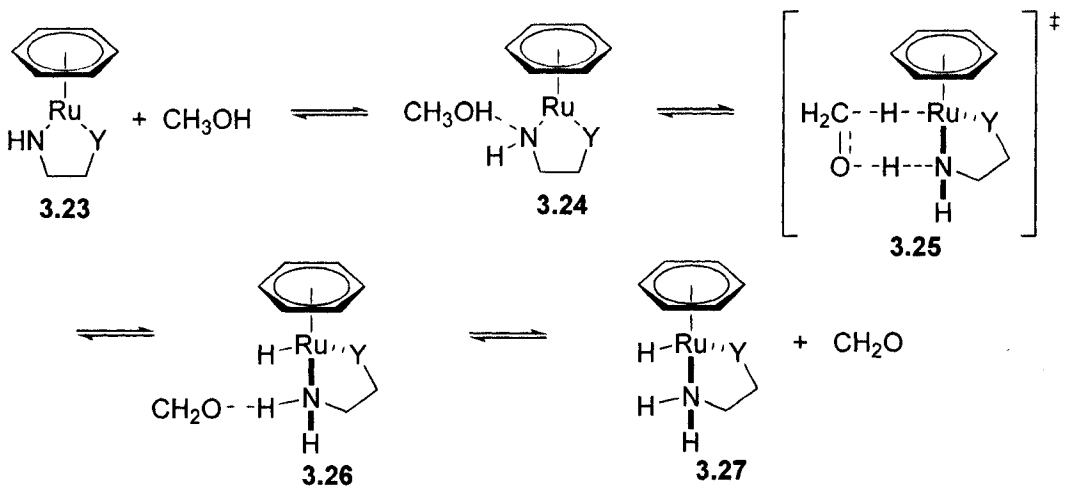

In an analogous process, the 'Ru-hydride' catalyst **3.28** could potentially be formed from ammonia-borane compounds (Scheme 3.12). Once formed, this catalyst could have the potential to release hydrogen gas. Although the mechanism is unknown, some known Ru-hydride catalysts are known to be unstable, even in inert atmospheres, and lose H_2 over time.[63]

---

[61] (a) Ikariya, T.; Blacker, A. J. *Acc. Chem. Res.* **2007**, *40*, 1300. (b) Noyori, R.; Hashiguchi, S. *Acc. Chem. Res.* **1997**, *30*, 97.

[62] a) Noyori, R.; Yamakawa, M.; Hashiguchi, S. *J. Org. Chem.* **2001**, *66*, 7931. (b) Sandoval, C.A.; Ohkuma, T.; Muñiz, K.; Noyori, R. *J. Am. Chem. Soc.* **2003**, *125*, 13490. (c) Noyori, R.; Ohkuma, T. *Angew. Chem. Int. Ed.* **2001**, *40*, 40. (d) Haack, K.-J.; Hashiguchi, S.; Fujii, A.; Ikariya, T.; Noyori, R. *Angew, Chem, Int. Ed. Eng.* **1997**, *36*, 285.

[63] Abdur-Rashid, K.; Clapham, S. E.; Hadzovic, A.; Harvey, J. N.; Lough, A. J.; Morris, R. H. *J. Am. Chem. Soc.* **2002**, *124*, 15104.

Scheme 3.12 **Possible mechanism for the catalytic dehydrogenation of ammonia-borane.**

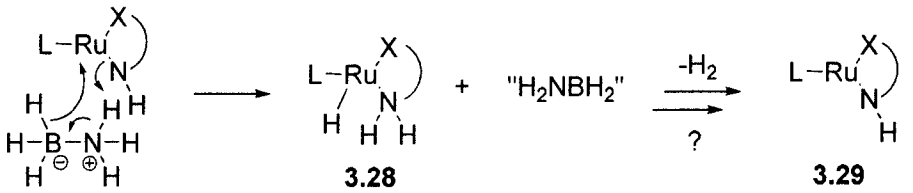

3.7 Transfer Hydrogenation Using Amine-Boranes as a Source of Hydrogen.[64]

Another potential application of these systems is the transfer hydrogenation of unsaturated compounds using AB or analogues as a source of H_2.[65] Many transfer hydrogenation reactions require either high H_2 pressures or protic solvents; this could present an alternative, solid source of H_2 for these reductions.

The catalyzed transfer hydrogenation reaction using AB derivatives for the reduction of alkenes and alkynes has been demonstrated by Manners and co-workers.[66] Using 2 mol % [{Rh(μ-Cl)(1,5-cod)}$_2$] and Me_2NHBH_3 as a source of hydrogen, quantitative reduction of cyclohexene **3.30** and 1-methyl-1-cyclohexene **3.31** was observed (Scheme 3.13).

Scheme 3.13 **Rhodium-catalyzed transfer hydrogenation of alkenes using Me_2NHBH_3.**

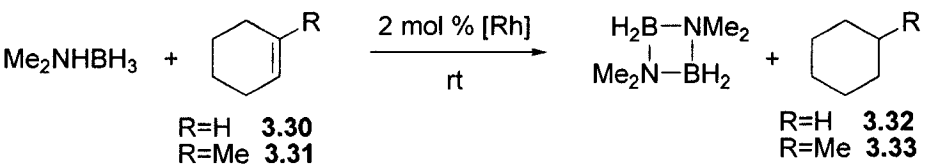

This process can also be catalyzed by Re(I) complexes.[67]

---

[64] This work was done in collaboration with Dr. Daniel Black.

[65] For uncatalyzed reductions using amine-boranes see: (a) Uyeda, C.; Biscoe, M.; LePlae, P.; Breslow, R. *Tet. Lett.* **2006**, *47*, 127. (b) Allwood, B. L.; Shahriari-Zavareh, H.; Stoddart, J. F.; Williams, D. J. *Chem. Commun.* **1984**, *22*, 1461.

[66] Clark, T. J.; Lee, K.; Manners, I. *Chem. Eur. J.* **2006**, *12*, 8634.

[67] Jiang, Y.; Berke, H. *Chem. Commun.* **2007**, 3571.

3.8 Project Goals

The goal of this project was to apply the use of traditional transfer hydrogenation catalysts to the dehydrogenation of ammonia-borane and substituted amine-boranes with the aim of decreasing the overall catalyst loadings and increasing the system weight percentage of H_2 obtainable. We also aimed to evaluate the mechanism at hand for hydrogen release as well as to identify any active catalytic species during the course of the reaction. Finally, the use of AB derivatives in conjunction with ruthenium transfer hydrogenation catalysts was evaluated for the reduction of ketones and Schiff bases.

Chapter 4

Results and Discussion

4.1 Investigation of Catalyst Reactivity

4.1.1 Initial Results

Initially, we decided to investigate a commonly used transfer hydrogenation catalyst **4.1** (Scheme 4.1). This catalyst was treated with KOH to yield the deprotonated amido catalyst **4.2**, which is the active catalytic species in transfer hydrogenation reactions. When this catalyst was added to a 0.5 M solution of AB in THF, no hydrogen release was observed whatsoever (Table 4.1). Catalyst **4.3**, after being deprotonated by 2 equivalents of KO*t*Bu to form **4.4**, was also evaluated under the same conditions but in a higher loading of 5 mol %, and still no evolution of hydrogen was observed. However, when increasing the catalyst loading to 10 mol %, vigorous bubbling was observed and approximately one equivalent of H_2 was evolved over the course of 35 minutes. With this proof of concept in hand, we proceeded to attempt to lower the catalyst loading, as 10 mol % **4.3** accounts for a significant portion of the overall system weight of the reaction. Since such a drastic change in reactivity was observed between 5 and 10 mol % **4.3**, we hypothesized that the concentration of catalyst, rather than the actual loading, could have an effect on hydrogen evolution. We decreased the amount of catalyst to 1.0 mol % but increased the overall concentration of catalyst to be equivalent to what it was in entry 3 at 10.0 mol % (0.05 M). Gratifyingly, we observed 0.76 equivalents of hydrogen being evolved under these conditions. This not only allows us to use low catalyst loadings, but the high concentration necessary for reaction also lowers the overall system weight for the hydrogen delivery system.

Scheme 4.1 **Activation of catalysts 4.1 and 4.3 for AB dehydrogenation.**

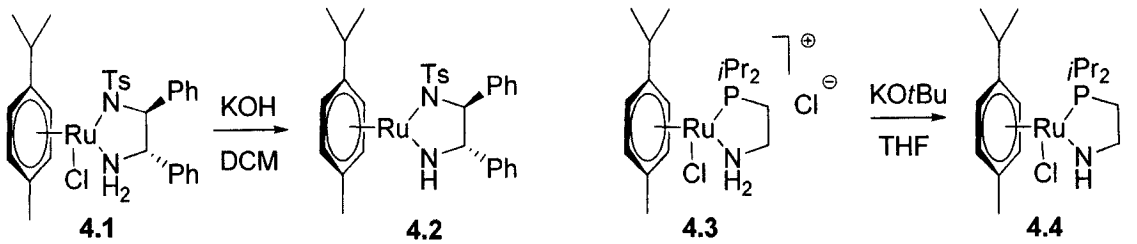

4.1 **4.2** **4.3** **4.4**

Table 4.1 **Evolution of hydrogen with respect to catalyst loading and concentration.**

$NH_3BH_3 \xrightarrow[THF]{\text{catalyst}} H_2 + [NH_2BH_2]_n$

Entry	Catalyst	Loading (mol %)	[catalyst] (mol/L)	[AB] (mol/L)	Time (min)	H_2 equiv.
1	**4.2**	1.0	0.005	0.5	30	0
2	**4.3**	5.0	0.02	0.4	35	0
3	**4.3**	10.0	0.04	0.4	35	> 0.9
4	**4.3**	1.0	0.05	5.0	30	0.8
5	**4.3**	0	0	0.4	35	0

*Timing was started upon injection of the activated catalyst solution to the AB solution. Conditions: AB (1 equiv.) and catalyst in THF at room temperature under N_2.

4.1.2 Active Dehydrogenation Catalysts

A preliminary qualitative investigation of other similar catalytic complexes analogous to known transfer hydrogenation catalysts[68] was performed. 1.0 mol % of catalysts **4.5-4.9** (Scheme 4.2) were activated with 2 equivalents of KO*t*Bu (2.0 mol %) and injected into 5.0 M solutions of AB (Table 4.2). It was observed that catalysts **4.5-4.9** with bis-PN ligand systems were the most reactive, resulting in > 0.9 equivalents of H_2 in less than 10 minutes. Of these, **4.5** is the most reactive, and, as an additional benefit, is the most lightweight.

[68] (a) Tianshu, L.; Churlaud, R.; Lough, A. J.; Abdur-Rashid, K.; Morris, R. H. *Organometallics*, **2004**, *23*, 6239. (b) Abdur-Rashid, K.; Clapham, S. E.; Hadzovic, A.; Harvey, J. N.; Lough, A. J.; Morris, R. H. *J. Am. Chem. Soc.* **2002**, *124*, 15104. (c) Clapham, S. E.; Hadzovic, A.; Morris, R. H. *Coord. Chem. Rev.* **2004**, *248*, 2201.

Scheme 4.2 **Initial precatalysts investigated for AB dehydrogenation**

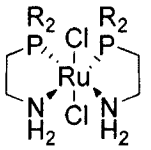

R = iPr **4.5**
R = tBu **4.6**
R = Ph **4.7**

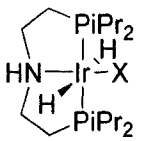

X = Cl **4.8**
X = H **4.9**

Table 4.2 **AB dehydrogenation with 1.0 mol % 4.4-4.9.**

NH_3BH_3 —(1.0 mol % catalyst, THF, 5.0 M)→ H_2 + $[NH_2BH_2]_n$

Entry	Catalyst	Time (min)	H_2 equiv.
1	**4.4**	30	0.8
2	**4.5**	< 5	> 0.9
3	**4.6**	< 10	> 0.9
4	**4.7**	25	0.9
5	**4.8**	180	0.33
6	**4.9**[a]	180	0.4

[a] Catalyst **4.9** was not deprotonated prior to addition to the AB solution. Timing was started upon injection of the activated catalyst solution to the AB solution. Conditions: AB (1 equiv.), catalyst (1.0 mol %) in THF (5.0 M) at room temperature under N_2.

With this information in hand, we attempted to lower the catalyst loading below 1.0 mol %. Due to the low molecular weight of AB (30.87 g/mol) and the high molecular weight of **4.5** (494.43 g/mol), 1.0 mol % **4.5** still accounts for 14 % of the mass of both substances combined. As can be seen in Figure 4.1, 0.5 mol % **4.5** still induces almost instantaneous (< 30 seconds) release of > 0.9 equivalents of H_2; however, at lower catalyst loadings, a peculiar observation was noted. An 'activation period' was observed in which very little H_2 was released until about 18 minutes into the reaction, at which point a large amount of H_2 was released in very little time (Figure 4.1, A). Keeping the concentration of catalyst constant while lowering the loading had no effect on this activation period (Figure 4.1, B). In fact, the length of this activation period and the amount of H_2 evolved thereafter was difficult to reproduce.

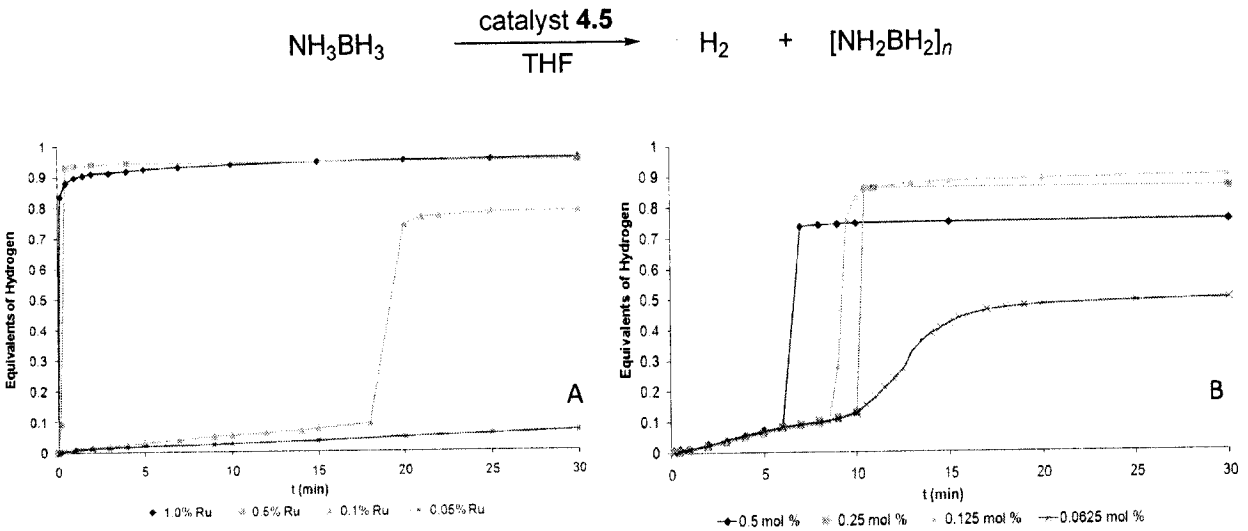

Figure 4.1 **Hydrogen Evolution as a function of time and catalyst loading. (A): [AB] = 5.0 M. (B): [4.5] = 0.025 M.**

Due to these reproducibility issues, we then attempted to isolate the factors responsible for the activation period.

4.1.3 Investigation of Reproducibility

One possible explanation for this observation is that the reaction is thermally activated. The first equivalent of H_2 released from AB is an exothermic reaction (-6.3 to -9.0 kcal/mol);[69] therefore, it is possible that once a sufficient amount of heat is generated *in situ*, the reaction is accelerated and the 'burst phase' occurs. Heating the reaction to 50 °C generally did eliminate or shorten the activation period (*vide infra*); however, reproducibility was still an issue.

It also occurred to us that the catalyst activation step may have an influence on the reaction outcome. Using only 1 or 2 equivalents of KO*t*Bu may not completely deprotonate the catalyst, especially when considering that the base is not entirely soluble in THF. This decreases the effective amount of active catalyst being injected into the reaction mixture, explaining the variation in outcome. Indeed, we found that using an excess of base to deprotonate the catalyst prior to injection into the AB solution (Scheme 4.3) shortened the activation period. Control reactions run with AB and 10 mol % KO*t*Bu in the absence of catalyst eliminated the possibility of base-enabled dehydrogenation.

[69] Arduengo III, A. J.; Dixon, D. A. U.S. DOE Hydrogen Program *2007 Annual Progress Report*, Section IV.B.5k, **2007**, 514.

Scheme 4.3 **Base activation trials.**

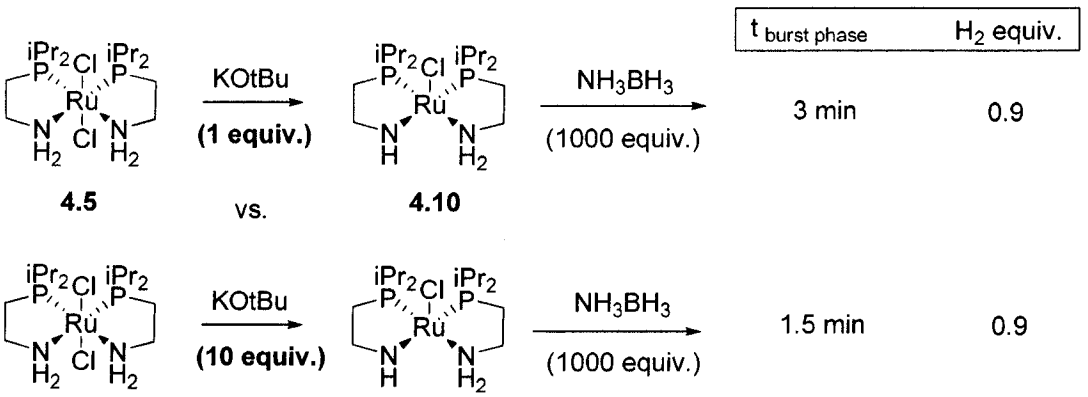

We also became aware that the quality of AB varied depending on the preparation method used. Two different methods, A and B (Scheme 4.4), were evaluated.

Scheme 4.4 **Two methods used for the synthesis of AB.**

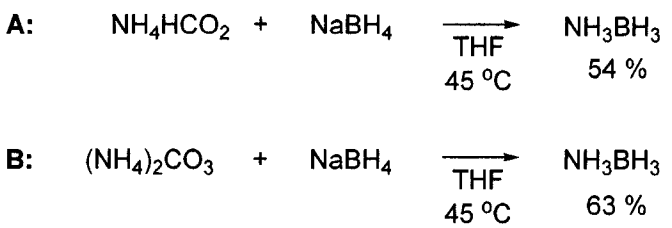

Although they both appeared pure by ^{1}H NMR, the physical appearance of the different batches were slightly different: method B yielded a finer powder than method A. Comparing hydrogen evolution from the different AB batches for several catalysts confirmed that using ammonium carbonate as the ammonia source (method B) resulted in higher quality AB and, therefore, higher yields of H_2 evolution (Figure 4.2).

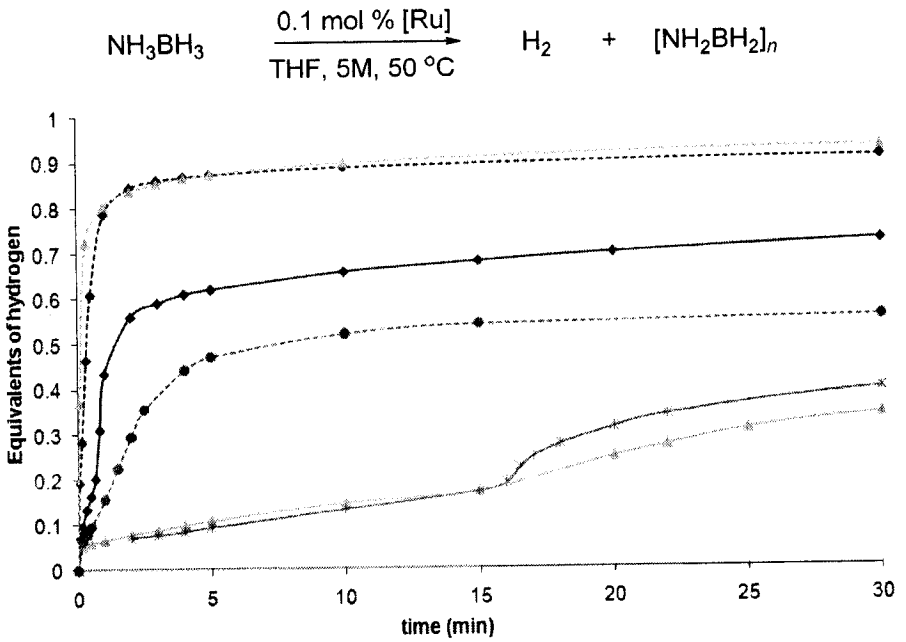

Figure 4.2 **Hydrogen evolution from different AB sources using 0.1 mol % Ru in THF at 50 °C. Solid lines represent dehydrogenation of AB prepared by method A. Dashed lines represent dehydrogenation of AB prepared by method B. Blue = 4.5, Orange = 4.6 and Purple = 4.7.**

To summarize these findings, the rate and yields of dehydrogenation of AB are affected by many factors. High catalyst concentration is vital to the success of the reaction. Accordingly, to ensure full deprotonation of the pre-catalysts, a large excess of KO*t*Bu with respect to catalyst is required; a 30:1 ratio of KO*t*Bu:Ru was found to be optimal and provided the most reproducible results. Care must be taken to avoid all exposure of these activated catalysts to air, as they are highly unstable and decompose rapidly. Heat was also found to accelerate the reaction, although for the most reactive catalysts **4.5** and **4.6**, hydrogen evolution is almost instantaneous at room temperature providing that the reaction is highly concentrated, a large excess of base is used and the AB is prepared from $(NH_4)_2CO_3$ and not NH_4HCO_2.

Section 4.1.4 Optimization of Conditions

With these technical conditions resolved, we evaluated the optimal concentration and catalyst loading for these conditions. High [AB] was found to be most successful, with 5.0 M being the optimal concentration (Figure 4.3). Once again, activation periods were observed at lower concentrations.

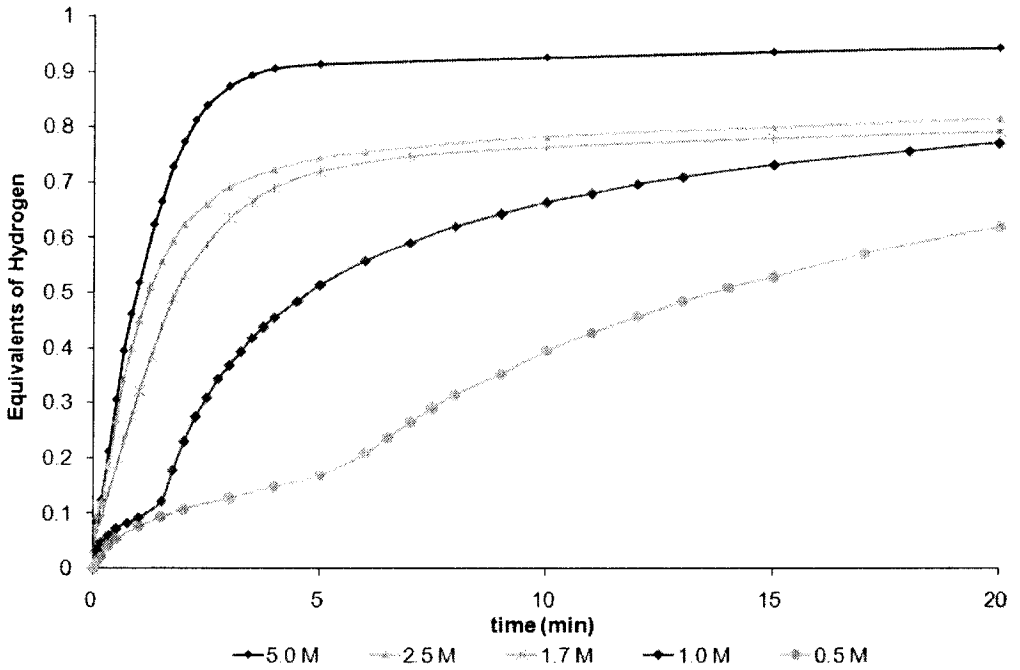

Figure 4.3 **Hydrogen evolved as a function of time and [AB].**

Increasing the concentration any further resulted in irreproducible and poor yields. This is most likely due to an insoluble precipitate that is formed as the major decomposition product of AB dehydrogenation over the course of the reaction. As this solid is formed, the stirring is either slowed or stopped, and this is more likely to happen when there is minimal solvent in the reaction, bringing H_2 evolution to a halt. Goldberg and co-workers have observed a similar precipitate, which they have defined as a cyclic borazane pentamer;[45] however, as previously mentioned, this could also be a linear polymer.[55]

Scheme 4.4 **Polymeric or cyclic pentamer product formed from the first dehydrogenation reaction of AB.**

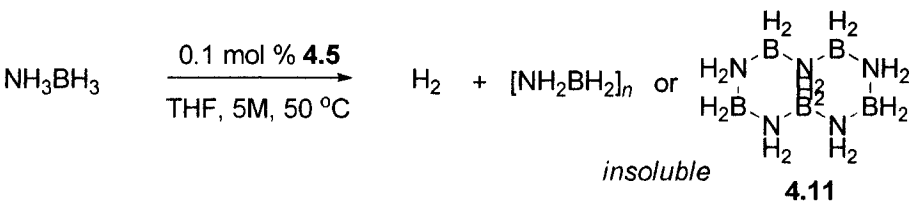

We found that decreasing the catalyst loading below 0.1 mol % resulted in longer reaction times and lower H_2 yields (Figure 4.4). However, the loading can be decreased to 0.03 mol % before seeing a significant drop in H_2 evolution, with only slightly longer reaction times (10 minutes for 1 equiv. H_2 versus < 4 minutes for 1 equiv. with 0.1 mol % **4.5**).

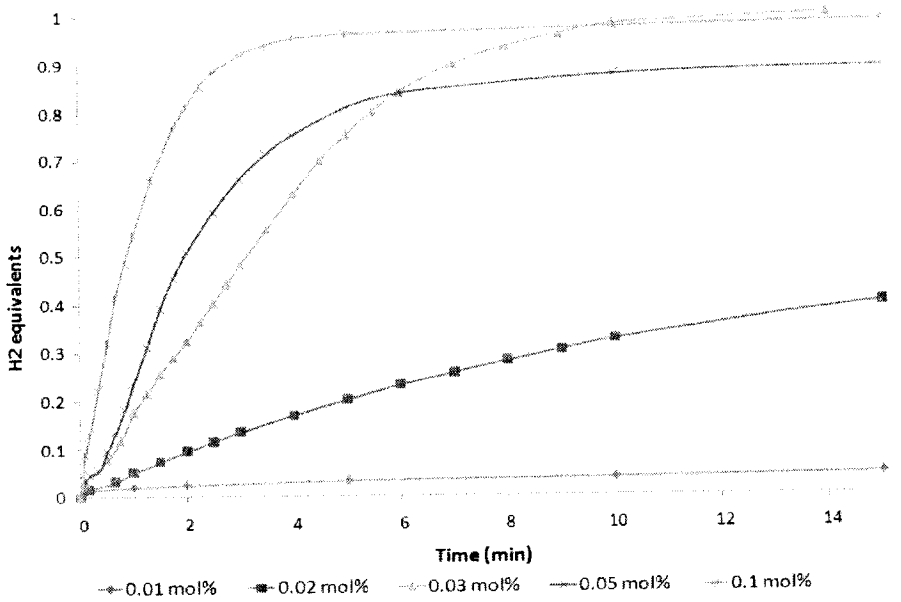

Figure 4.4 **Hydrogen evolution as a function of time and catalyst loading.**

Dehydrogenation of AB by deprotonated catalysts **4.4-4.8** and **4.12** (Scheme 4.5) was monitored under the optimal conditions, and the results are summarized in Figure 4.5.

Scheme 4.5 **Precatalysts evaluated for AB dehydrogenation.**

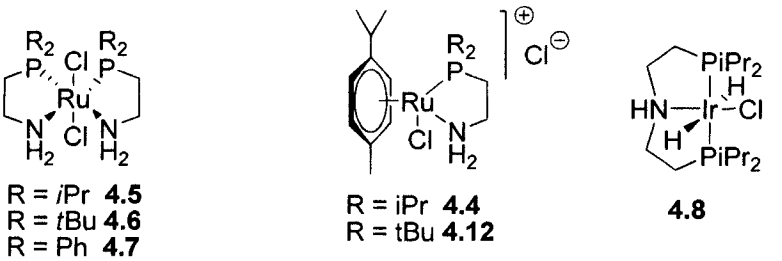

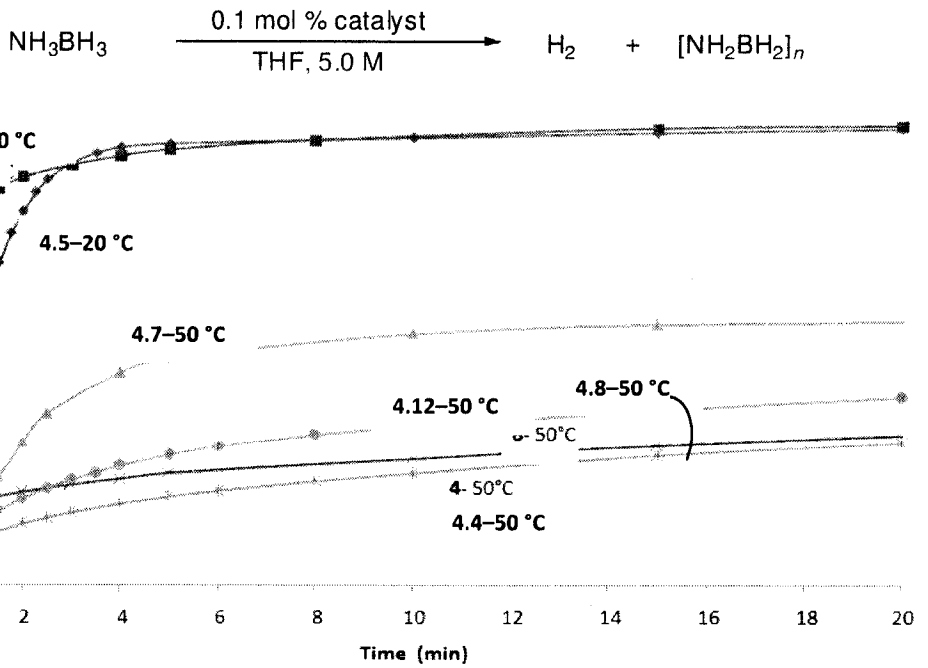

Figure 4.5 **Evolution of Hydrogen over time catalyzed by 4.4-4.8 and 4.12 at room temperature or 50 °C. Precatalysts were deprotonated with 30 equivalents KO*t*Bu prior to use.**

Catalysts **4.5** and **4.6** remain the most reactive under optimized conditions, releasing > 0.9 equiv. H_2 in less than 4 minutes. Iridium catalyst **4.8** did show some dehydrogenation, albeit at lower yields and longer reaction times. In general, most ruthenium-centered transfer hydrogenation catalysts with similar ligand systems seem to show some activity; however, **4.5** and **4.6** are by far the most reactive that we have evaluated.

4.2 Mechanistic Studies

4.2.1 Experimental Investigation of the Active Catalytic Species

In order to identify the active catalytic species in the dehydrogenation of AB, we considered mechanisms in which either a Ru-hydride **4.14** or Ru-borohydride[70] **4.13** species is formed in the presence of AB. These catalysts were synthesized independently (Scheme 4.6) and the rate of H_2 evolution was compared to the rate of H_2 evolution catalyzed by **4.10** (Figure 4.6).

Scheme 4.6 **Synthesis and structures of catalysts mimicking potential reactive intermediates.**

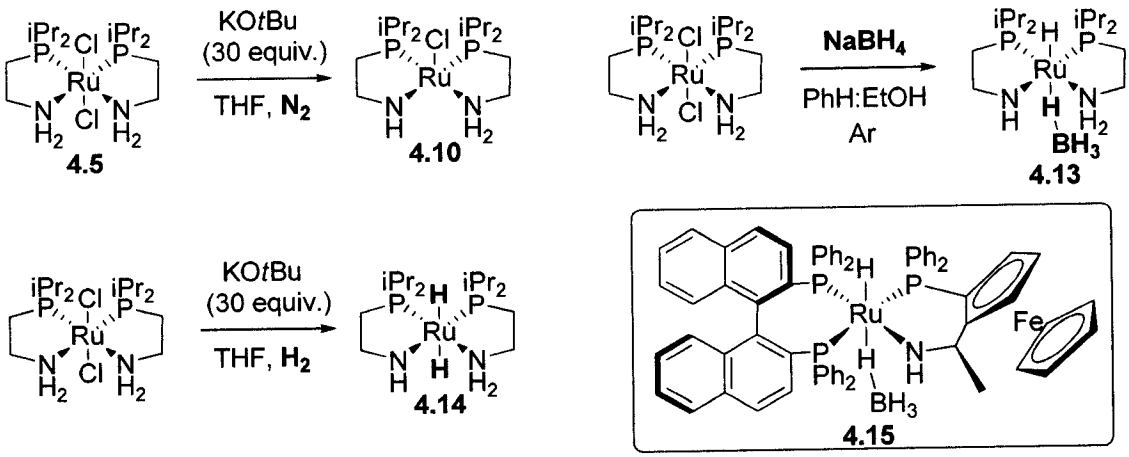

[70] Analogues were prepared according to the procedures by: Guo, R.; Morris, R. H.; Song, D. *J. Am. Chem. Soc.* **2005**, *127*, 516.

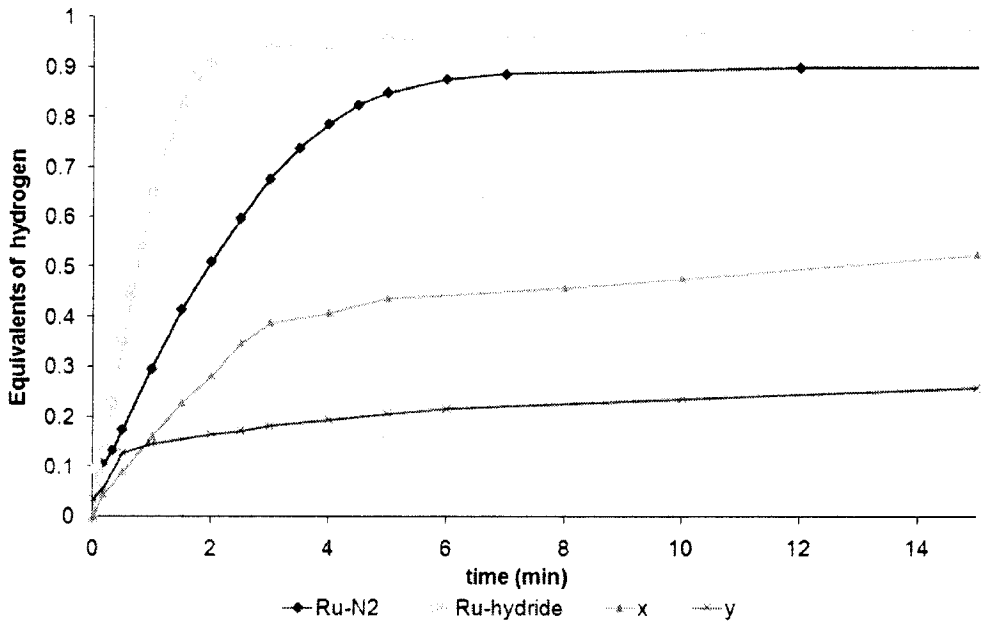

Figure 4.6 **Rate of hydrogen evolution from AB catalyzed by different catalytic species 4.10, 4.13, 4.14 and 4.15.**

These results suggest that the Ru-hydride species **4.14** is an active catalytic species in the reaction as it catalyzes the release of > 0.9 equiv. H_2 in less than 2 minutes; the shortest time period observed thus far. The borohydride species **4.13** and **4.15** were less reactive, suggesting there is no formation of such an intermediate *in situ*.

4.2.2 Computational Studies

These conclusions were supported by density functional theory calculations at the B3LYP level performed by Dr. Serge Gorelsky.[71] Starting from the deprotonated Ru-hydride **4.16**, the generation of **4.17** is predicted to occur by the energetically favorable deprotonation and coordination of AB to the Ru center (Scheme 4.7). Oxidation of AB and formation of the dihydride **4.18** is slightly energetically uphill; however, a reaction coordinate scan in forward and reverse directions revealed that this step does not have a kinetic barrier in gas phase calculations. Dissociation of molecular dihydrogen from **4.18** through transition state **4.19** was

[71] See supporting information for computational details.

found to be the most energetically demanding step with a kinetic barrier of 21.8 kcal/mol in THF. This step regenerates our initial active catalyst **4.16**.

Scheme 4.7 **Catalytic cycle for dehydrogenation of AB with the Ru catalyst in THF and gas phase from DFT calculations. Black and blue lines indicate different conformers of the P,N ligands of the Ru species. Values are shown in kcal/mol.**

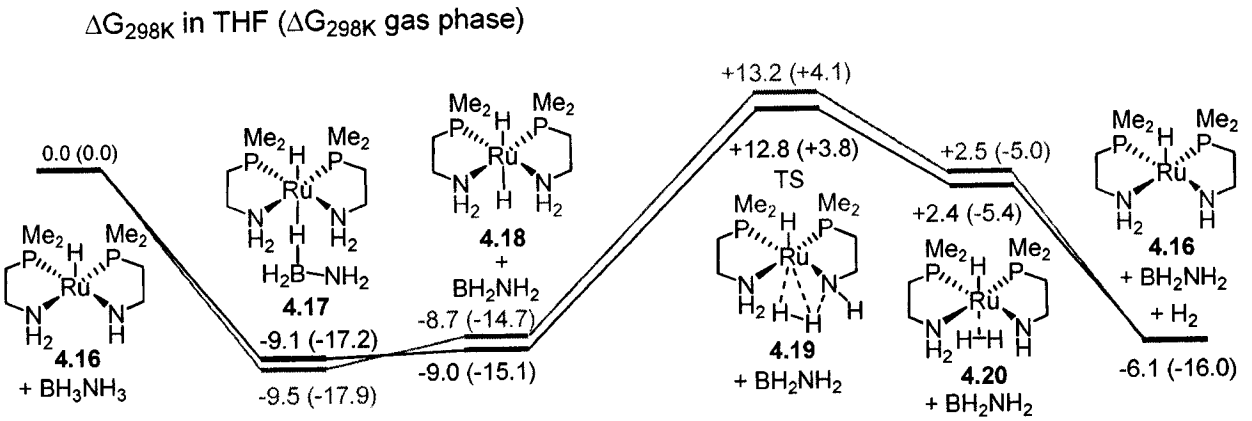

Although species **4.17** closely resembles the borohydride transfer hydrogenation precatalyst **4.13** evaluated previously (Scheme 4.6), the poor reactivity of the latter species could be explained by its inability to dissociate and form a dihydride species of type **4.18**.

4.3 AB/MeAB Mixtures

With the aim of surpassing the 1.0 equivalent H_2 barrier observed with AB, alternative ammonia-borane analogues were explored. It is known that mixtures of AB and methylammonia-borane (MeAB) exhibit lower melting points than the corresponding isolated compounds (mp = 35 – 50 °C).[72] This presents an opportunity for solvent-free reactions, which could significantly boost the overall gravimetric density of H_2 delivered by the overall system.

4.3.1 50:50 Mixture of AB:MeAB

We first evaluated 1:1 mixtures of AB:MeAB (Scheme 4.8). In the first trial (Figure 4.7), a minimal amount of THF was used because deprotonation of the catalyst was carried out in a

[72] Lane, C. F. U.S. DOE Hydrogen Program *2007 Annual Progress Report*, Section IV.B.5j, 2007.

separate flask; solvent was necessary to stir the catalyst and base together, as well as for transfer of the active catalyst into the AB/MeAB mixture. In the second trial, the precatalyst and base were added directly to the AB/MeAB, and activation of the catalyst was carried out *in situ*. Although hydrogen evolution was observed for both these trials, a maximum of about 0.8 equivalents of H_2 was obtained over significantly longer reaction times (100 minutes) than AB alone. This represents an overall system gravimetric density of 3.0 % for the first trial and 3.6 % for the second trial, compared to 1.0 system wt % for AB dehydrogenation under our standard conditions.

Scheme 4.8 **Ruthenium catalyzed dehydrogenation of AB/MeAB mixtures.**

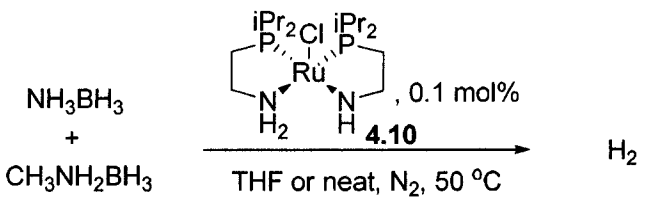

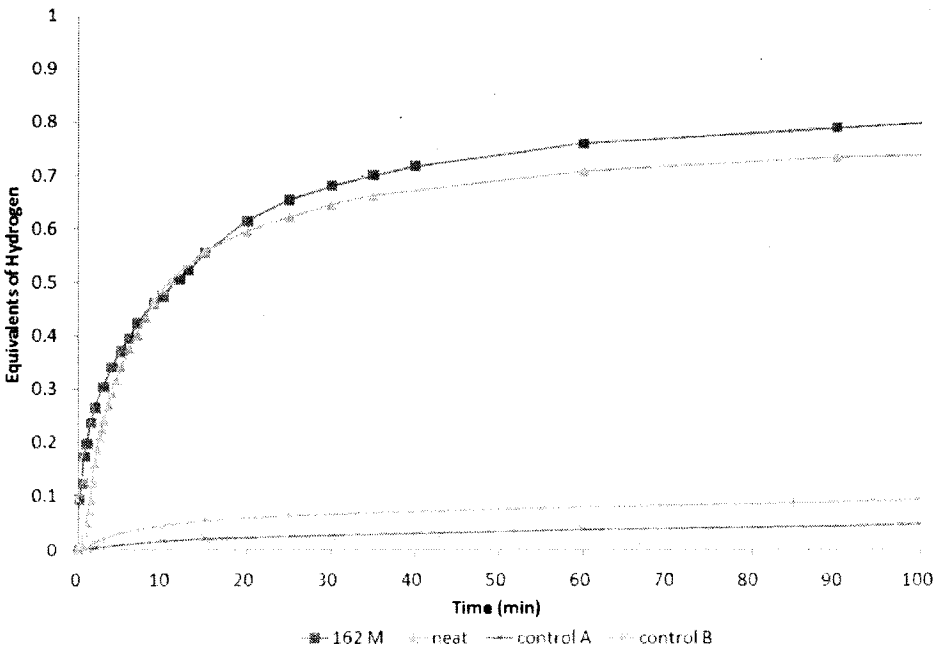

Figure 4.7 Evolution of hydrogen from a 1:1 AB:MeAB mixture as a function of time. Control A was run in the absence of catalyst and base, and control B was run in the absence of catalyst.

Control reactions were also run in which the AB/MeAB mixtures were heated in the absence of catalysts. Control A contained only AB and MeAB, and control B also contained 10 mol %

KO*t*Bu. In both cases, less than 0.1 equivalent of H_2 was evolved over the course of several hours.

4.3.2 35:65 Mixture of AB:MeAB

We then evaluated a 35:65 AB:MeAB mixture which is known to have a lower melting point than the 1:1 mixture. When all the reagents were mixed together with no solvent, such as in Figure 4.8 (orange line), irreproducible results and poor yields (< 0.7 equiv. H_2) were obtained. Better results were obtained when the catalyst was activated in a separate flask; therefore, a minimal amount of THF was necessary for transfer. Once again, hydrogen evolution was observed, albeit over the same time scale as previous trials with AB/MeAB mixtures. Technical issues seemed to dominate the factors affecting yields and gravimetric densities obtainable in these systems. For example, on a small scale, the AB/MeAB mixtures would occupy a very small volume. Therefore stirring was limited, and the reaction mixture tended to stick to the sides of the vial minimizing contact of the overall reaction medium. Also, we were limited as to how little THF could be used for activation of the catalyst; below a certain concentration (11 M), little or no stirring was possible and more rapid decomposition of the active catalyst was observed. Therefore, the only strategy to improve stirring and therefore gravimetric density was to increase the scale of the reaction. As the amount of AB/MeAB increases, the volume of THF remains the same, therefore better gravimetric density can be obtained. As is shown in Figure 4.8, the best results were obtained on the largest scale tested (100 mg), resulting in > 0.9 equivalents and 3.0 wt % H_2.

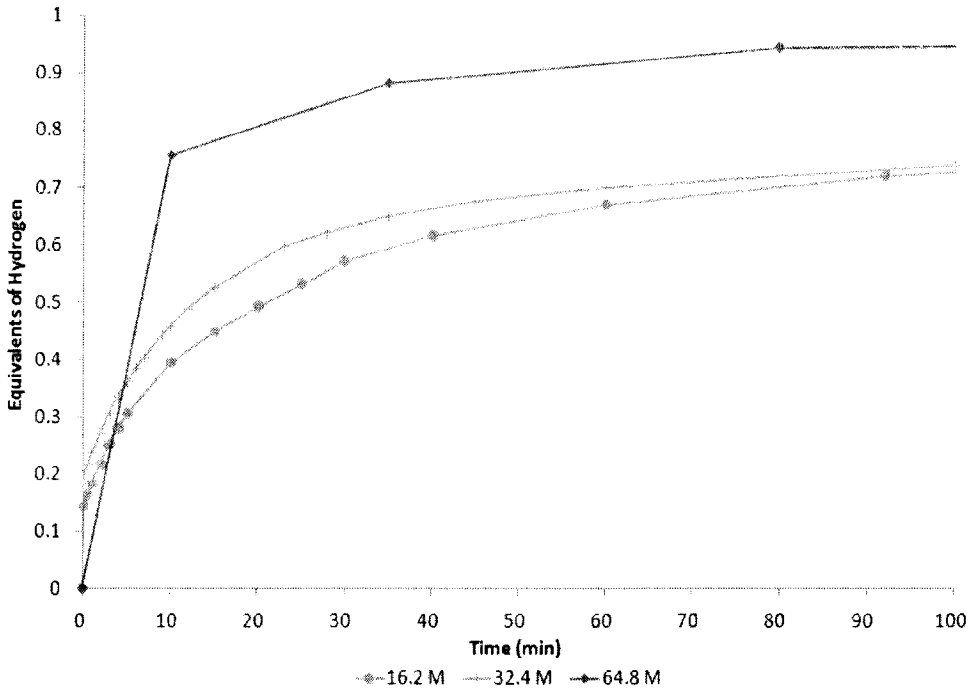

Figure 4.8 **Evolution of hydrogen from a 35:65 AB:MeAB mixture as a function of time and concentration.**

A larger reaction scale was not attempted due to safety and measurement issues.

4.4 Dehydrogenation of Methylammonia-Borane

With the ultimate goal of achieving > 1 equivalent H_2 release, pure MeAB was evaluated as a hydrogen storage material. If our proposed mechanism is correct, the dehydrogenation of ammonia-borane analogues beyond one equivalent should be possible as long as the products remain in solution. MeAB was evaluated as a source of H_2 in the hopes of circumventing the insoluble powder formed in the AB dehydrogenation reaction. Gratifyingly, we saw exceptionally fast dehydrogenation of MeAB to release 1 equivalent of H_2 in the presence of catalyst **4.5** under our standard conditions (Figure 4.9). At 0.1 mol % catalyst loading, it was difficult to surpass one equivalent, even when heating the reaction to 50 °C; however, no insoluble by-products were observed in this case, suggesting that it would be possible to keep the reaction going.

Increasing the catalyst loading had a positive effect on H_2 release, with 0.3 mol % **4.5** liberating up to 1.6 equivalents H_2 at room temperature and up to 1.8 equivalents at 50 °C. The optimal catalyst loading was found to be 0.5 mol % at 50 °C, affording > 1.9 equivalents of H_2 in approximately 2 hours (Figure 4.9).

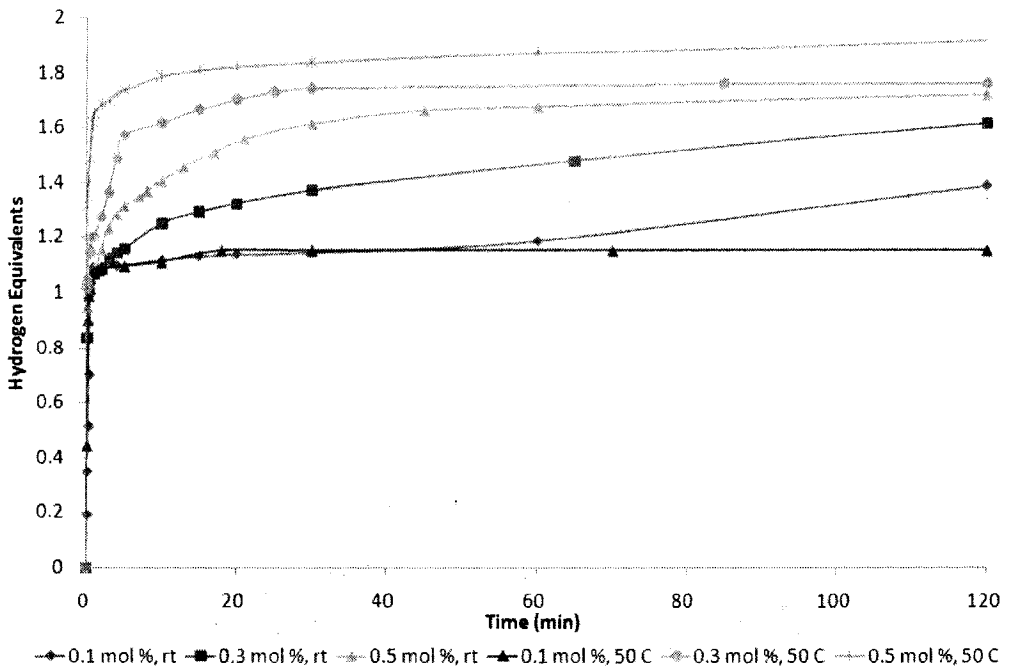

Figure 4.9 **Hydrogen evolution from MeAB as a function of time and catalyst loading. [MeAB] = 1.0 M.**

These trials were run at 1.0 M, but due to the higher molecular weight of MeAB, very high concentrations are required before one can reach a practical gravimetric density. We then evaluated how much the concentration could be increased before compromising stirring and yields. We found that concentrations up to 11.0 M were tolerated, and even afforded quicker release of > 1.9 equivalents of H_2 (Figure 4.10). This concentration corresponds to a gravimetric density of approximately 3 wt % H_2.

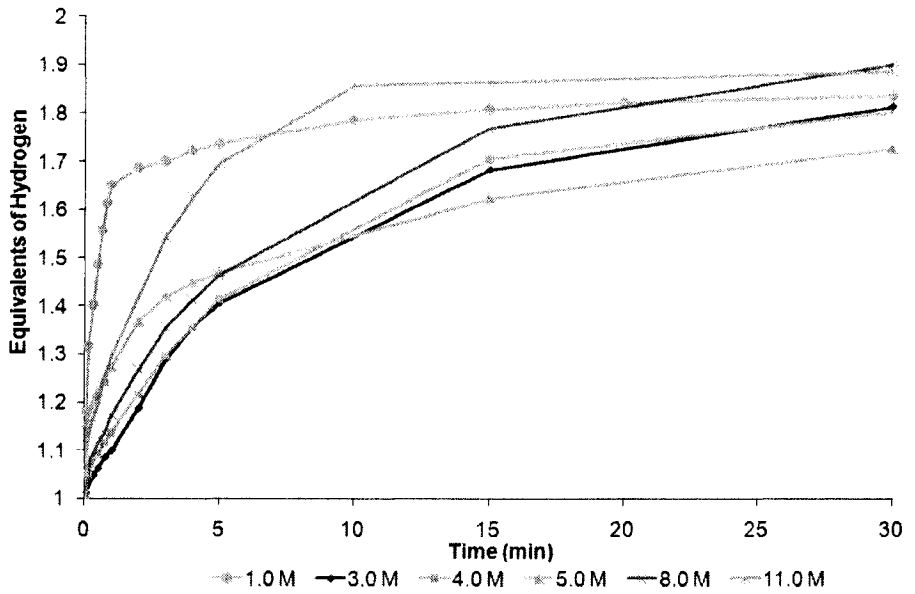

Figure 4.10 **Evolution of the second equivalent of hydrogen from MeAB as a function of time and concentration. [Ru] = 0.5 mol %, 50 °C.**

Concentration did not have a significant effect on the release of the first equivalent of H_2, as it is nearly instantaneous (< 10 seconds) in every case (Figure 4.11).

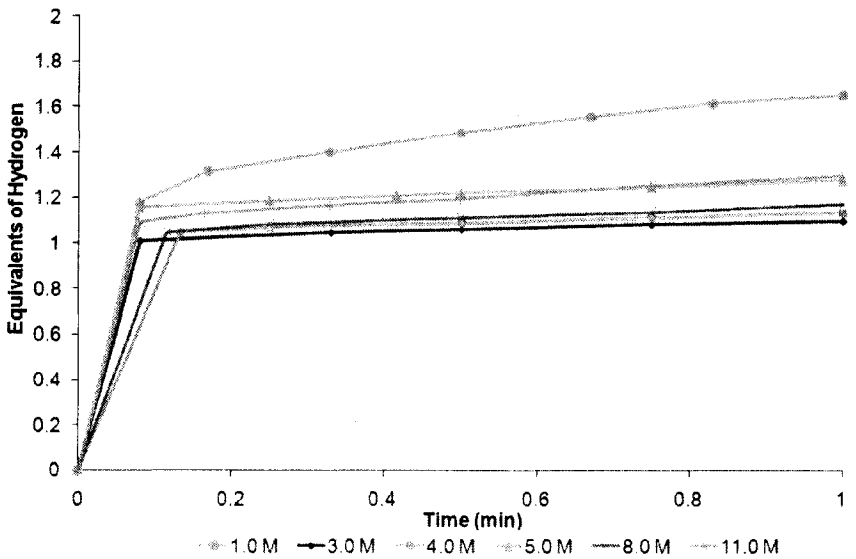

Figure 4.11 **Evolution of the first equivalent of hydrogen from MeAB as a function of time and concentration. [Ru] = 0.5 mol %, 50 °C.**

4.5 Characterization of hydrogen

In order to unquestionably prove that hydrogen was the gas being evolved from the mixture, a sample was subjected to mass spectrometry. With the help of Dr. A. A. Mommers, Dr. C. W. Kazakoff and Dr. P. M. Mayer from the Mass Spectrometry Center, we were able to determine that the gas evolved from AB dehydrogenation is predominantly H_2. By comparing the reference signal given by a pure sample of H_2 (1.1 V) with the signal obtained from the gas evolved from our reaction mixture (0.9 V), it became clear that the majority of the gas was H_2. Small signals were observed for the masses of ammonia and borazine (a volatile fuel cell poison); however, these were negligible compared to the hydrogen signal.[73]

4.6 Transfer Hydrogenation Using Ammonia-Boranes as a Source of Hydrogen.

Since our mechanistic studies indicated the formation of a dihydride species **4.14** (Scheme 4.6), we inferred that these catalysts could potentially make use of AB and its derivatives as a H_2 source for transfer hydrogenation reactions. We decided to evaluate the reduction of acetophenone (**4.21**) in the presence of AB in THF catalyzed by our most reactive dehydrogenation catalyst **4.5** (Scheme 4.9). We also ran a control reaction in the absence of catalyst to measure the background reduction of acetophenone by AB alone.

Scheme 4.9 **Transfer hydrogenation of acetophenone by AB.**

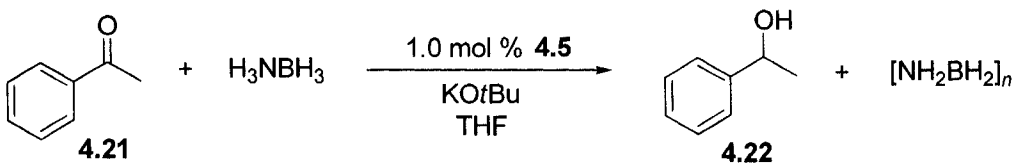

The control reaction showed full conversion to the reduced product 1-phenylethanol **4.22** overnight by AB alone. However, in the presence of catalyst **4.5**, full conversion was observed within one hour, at which point very little of the control reaction had reacted. From this, we

[73] Small amounts of nitrogen and oxygen were also noted in the spectrum; most likely due to some exposure to air during the transportation of the sample to the mass spectrometry laboratory.

could conclude that, although there is a significant background reaction, the transfer hydrogenation *can* be catalyzed by these ruthenium compounds.

The transfer of stereochemical information was then monitored. Chiral catalysts **4.1** and **4.23** (Scheme 4.10) were activated and placed in the presence of AB and acetophenone in various loadings and time periods (Table 4.3). In general, the *ee*'s varied and were low; as a rule, higher catalyst loadings afforded higher *ee*'s. However, as the reaction time increased, there was a general decrease in *ee* suggesting that the background reaction eventually took over and was too rapid to allow efficient transfer of stereochemical information from the chiral catalysts.

Scheme 4.10 **Catalysts used for the transfer hydrogenation of acetophenone with AB.**

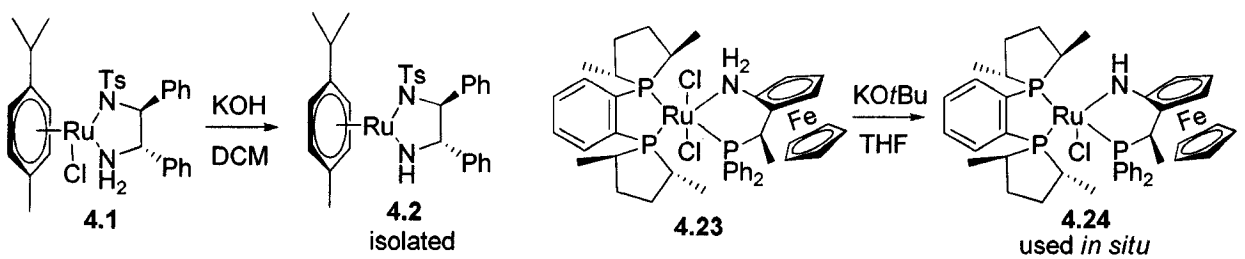

Table 4.3 **Transfer hydrogenation of acetophenone by catalysts 4.2 and 4.24.**

Entry	Catalyst	Loading (mol %)	Time (h)	*ee* (%)
1	**4.2**	10.0	16	10
2	**4.2**	1.0	20	2
3	**4.2**	1.0	6	20
4	**4.24**	5.0	16	0
5	**4.24**	10.0	16	20

Conditions: AB (1 equiv.), acetophenone (1.0 equiv.) and catalyst in THF at room temperature under N_2.

Acyclic imines were found to be generally unreactive in both the control reaction and catalytic reactions. Left stirring overnight, mainly starting material was reisolated from the mixture.

This project was then taken over by Dr. Daniel Black, who found that in the presence of 1.5 mol % **4.7**, a slightly less reactive dehydrogenation catalyst (Scheme 4.5), and 3 equivalents of pyrrolidine-borane (PyrAB, **4.25**), the reduction of some representative ketones and cyclic

imines could be accomplished in a controlled fashion (Scheme 4.11). No background reductions were observed with PyrAB. However, asymmetric transfer hydrogenation remains a challenge as *ee*'s above approximately 76 % were not attainable under all attempted reaction conditions. Nevertheless, this methodology remains an alternative to transfer hydrogenation reactions requiring high H_2 pressures or protic solvents.

Scheme 4.11 **Reduction of ketones and imines using PyrAB as the source of H_2.**

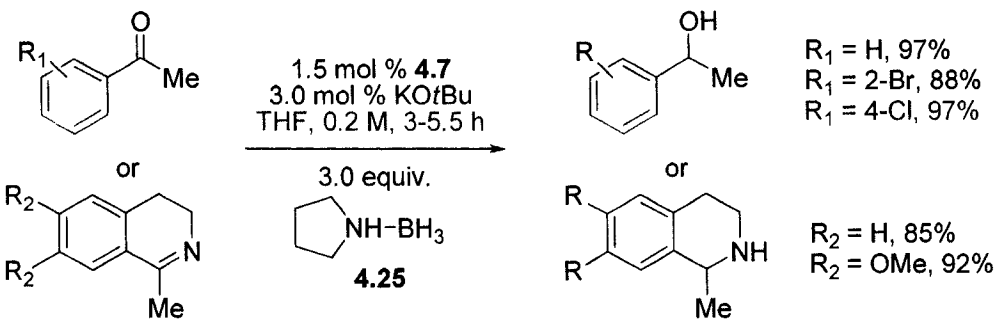

4.7 Conclusion

Several ruthenium transfer hydrogenation catalysts have been successfully employed to catalyze the release of up to 1 equivalent of hydrogen from AB and up to 2 equivalents of hydrogen from MeAB with unprecedented speed and catalyst loading. Hydrogen system weights up to 3.6 % were obtained from mixtures of AB and MeAB. Computational and experimental data indicated that the catalytic cycle is similar to known transfer hydrogenation mechanisms which go through an active Ru-hydride species. Significant challenges remain in the development of this dehydrogenation methodology. The full potential of AB as a hydrogen-storage material can only be attained by increasing the amount of H_2 released to well over 1.0 equivalent, as well as by solving the important problem of regenerating AB from the waste products;[74] however, the exceptionally low catalyst loadings and high concentration achievable by this system present a new strategy for approaching the important goals set by the DOE.

[74] For theoretical studies on the properties of AB and its decomposition products, see: Caetano, M. R.; Gerbrand, C. *J. Chem. Phys.* **2007**, *126*, 184703. (b) For studies on regeneration of AB: Hausdorf, S.; Baitalow, F.; Wolf, G.; Mertens, F. O. R. L. *Int. J. Hydr. Energy*, **2008**, *33*, 608. (c) Sneddon, L. G. U.S. DOE Hydrogen Program *2007 Annual Progress Report*, Section IV.B.5e, 2007.

Chapter 5

Supporting Information- Decarboxylative Aldol Reaction

5.1 General Methods

All experiments were carried out open to air, unless otherwise indicated. ^{1}H and ^{13}C NMR were recorded in $CDCl_3$ solutions using a Bruker AVANCE 300 or Bruker Avance 400 spectrometer with Me_4Si as an internal standard. High-resolution mass spectra were obtained on a Kratos Concept IIH. Infra-Red analysis was performed with a Bruker EQUINOX 55. HPLC Grade THF, Et_2O, benzene, toluene and CH_2Cl_2 are dried and purified via MBraun SP Series solvent purification system. Ethyl glyoxylate was purchased from Fluka as a 50% solution in toluene and was distilled before use.[75] Unless otherwise specified, all reagents and solvents were used as is from commercial sources.

5.2 Kinetic Experiments

5.2.1 Experimental Methods

The malonic acid half ester (0.139 mmol) and deuterated triethylamine (1.0 equiv.) were dissolved in 0.7 ml of THF-d_8, C_6D_6 or acetone-d_6 and added to an NMR tube. Directly prior to taking the first spectrum, ethyl pyruvate (1.0 equiv) was added to the NMR tube and shaken. A small hole was pierced in the cap in order to allow the release of carbon dioxide. Using a timed kinetic program in Bruker XWIN NMR, ^{1}H NMR spectra were collected every 3 minutes for 30 minutes, followed by every 10 minutes for 2 hours, and finally every 30 minutes overnight. The spectra were analyzed and integrated using TOPSPIN.

[75] Evans, D. A.; Burgey, C. S.; Paras, N. A.; Vojkovosky, T.; Tregay, S. W. *J. Am. Chem. Soc.* **1998**, *120*, 5824.

5.2.2 Analysis Using Excel Solver

The data from the multiple NMR experiments was then exported into Microsoft Excel and put into graph format using the time scale in minutes for the x axis and adjusted integration (corrected to relative molar conversion) for the y axis. The following equations[76] were used to represent the lines of best fit for the irreversible first step in the model system: A → I → P:

The rate law for each species is:

$$-\frac{d[A]}{dt} = k_1[A] \qquad \frac{d[I]}{dt} = k_1[A] - k_2[I] \qquad \frac{d[P]}{dt} = k_2[I]$$

And the integrated rate equations are:

$$[A]=[A]_0\exp(-k_1 t)$$

$$[I]_t = \frac{k_1[A]_0}{k_2-k_1}[\exp(-k_1 t)-\exp(-k_2 t)]$$

$$[P]_t = [A]_0\{1-\frac{1}{k_2-k_1}[k_2\exp(-k_1 t)-k_1\exp(-k_2 t)]\}$$

The following equations were used to represent the lines of best fit for the reversible first step in the model system: A<-> I → P:

[76] Espenson, James. H. Chemical Kinetics and Reaction Mechanisms, Second Edition. New York: McGraw-Hill, Inc., 1995.

The rate law for each species is:

$$-\frac{d[A]}{dt} = k_1[A]-k_{-1}[I] \qquad \frac{d[I]}{dt} = k_1[A]-k_{-1}[I]-k_2[I] \qquad \frac{d[P]}{dt} = k_2[I]$$

And the integrated rate equations are:

$$[A]= \frac{k_1[A]_0}{x_2-x_3}\left\{\frac{x_2-k_2}{x_2}\exp(-x_2t) - \frac{x_3-k_2}{x_3}\exp(-x_3t)\right\}$$

$$[I]_t = \frac{k_1[A]_0}{x_2-x_3}[\exp(-x_3t)-\exp(-x_2t)]$$

$$[P]_t = [A]_0\left\{1+\frac{x_3}{x_2-x_3}\exp(-x_2t) - \frac{x_2}{x_2-x_3}\exp(-x_3t)\right\}$$

where:

$x_2 = 0.5(p+q)$
$x_3 = 0.5(p-q)$
$p = k_1+k_{-1}+k_2$
$q = (p^2-4k_1k_2)^{1/2}$

These lines were simultaneously fit to the experimental data using the Solver program in Microsoft excel, by minimizing the sum of squares of the differences between the experimental and calculated data.

The following graphs illustrate the fit of the reversible vs. irreversible equations in acetone-d_6. Each graph was constructed using the mean values of three experimental trials. The error bars represent the standard deviation of each data point.

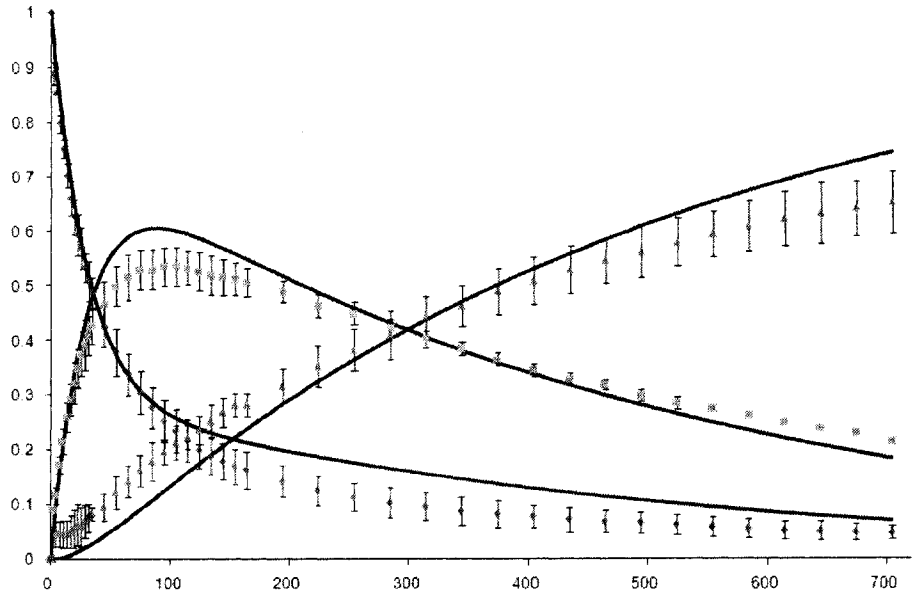

Figure 5.6 **Relative concentration of MAHO 2.4 (blue), intermediate 2.14 (green) and β-hydroxyester 2.5 (red) over 12 hours analyzed by ^{1}H NMR in Acetone-D_6 overlapped with the theoretical curves obtained from the reversible (solid lines) integrated rate equations. Data points represent the mean of 3 trials, and error bars represent the standard deviation. Integrations were measured relative to an internal standard (pentachlorobenzene).**

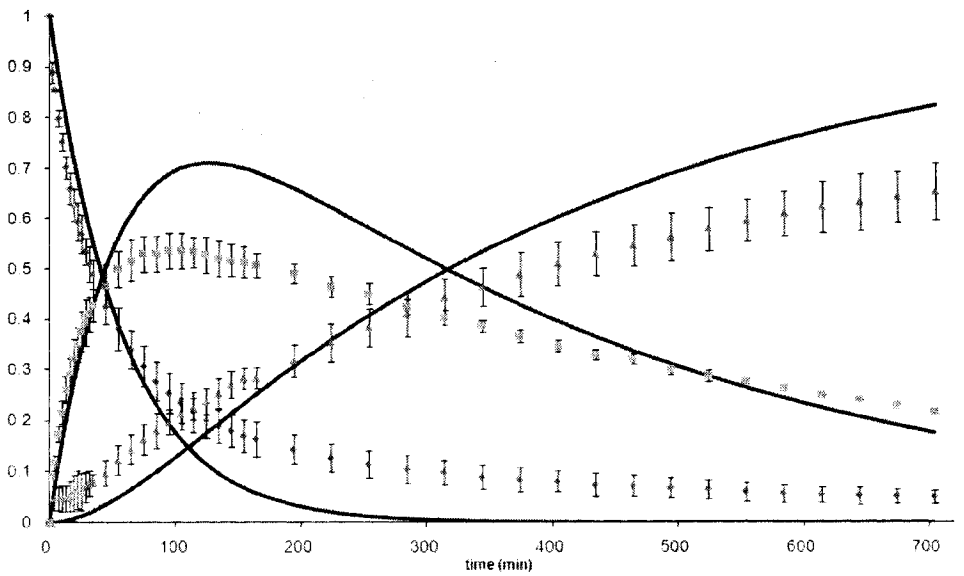

Figure 5.7 **Relative concentration of MAHO 2.4 (blue), intermediate 2.14 (green) and β-hydroxyester 2.5 (red) over 12 hours analyzed by ^{1}H NMR in Acetone-D_6 overlapped with the theoretical curves obtained from the irreversible (solid lines) integrated rate equations. Data points represent the mean of 3 trials, and error bars represent the standard deviation. Integrations were measured relative to an internal standard (pentachlorobenzene).**

5.3 Characterization of the Reaction Intermediate 2.14

Scheme 5.1 **Reaction being monitored by NMR.**

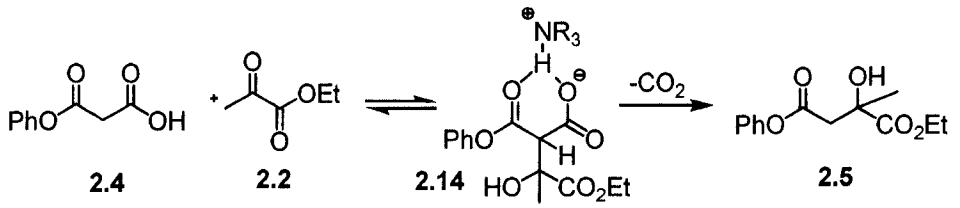

In addition to the DOSY, a COSY, ^{13}C, and HMBC spectrum were collected of the reaction mixture. Shown below are the spectra and relevant expansions of the carbonyl regions, showing the expected number of peaks accounting for starting materials, diastereomeric intermediates and products. Also shown are overlaps of the clean ^{13}C spectra of starting materials and products, showing the location of the intermediate peaks by elimination.

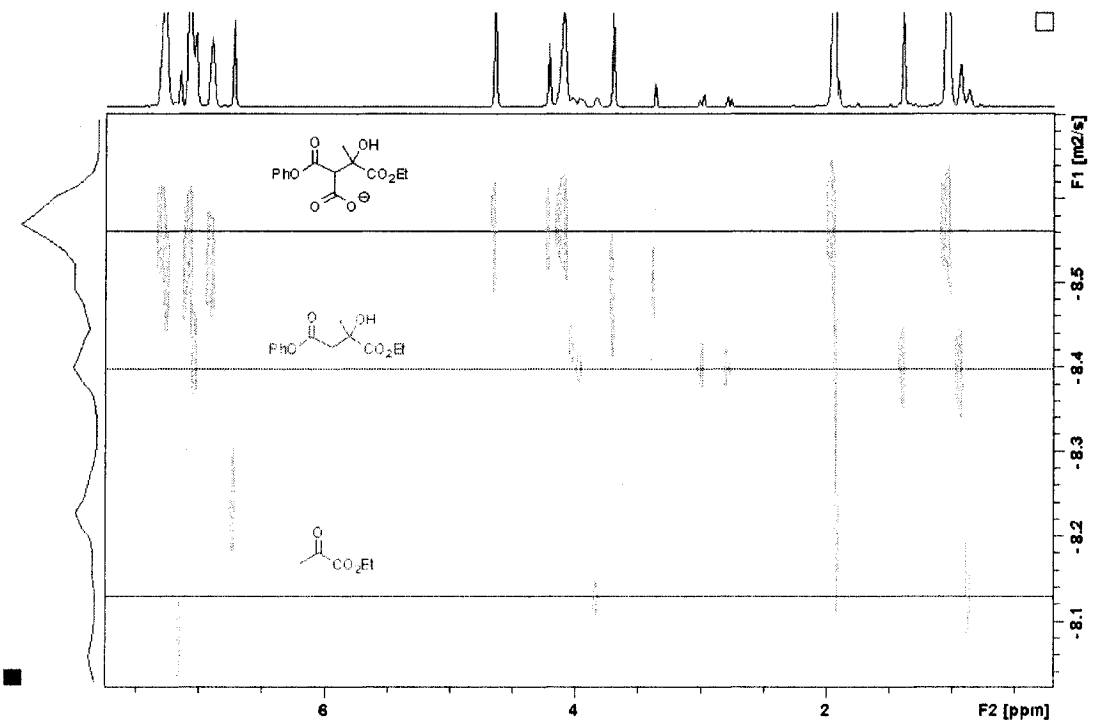

Figure 5.3 **DOSY spectrum of reaction mixture for the reaction shown in scheme 5.1 (above), with horizontal lines and chemical structures added.**

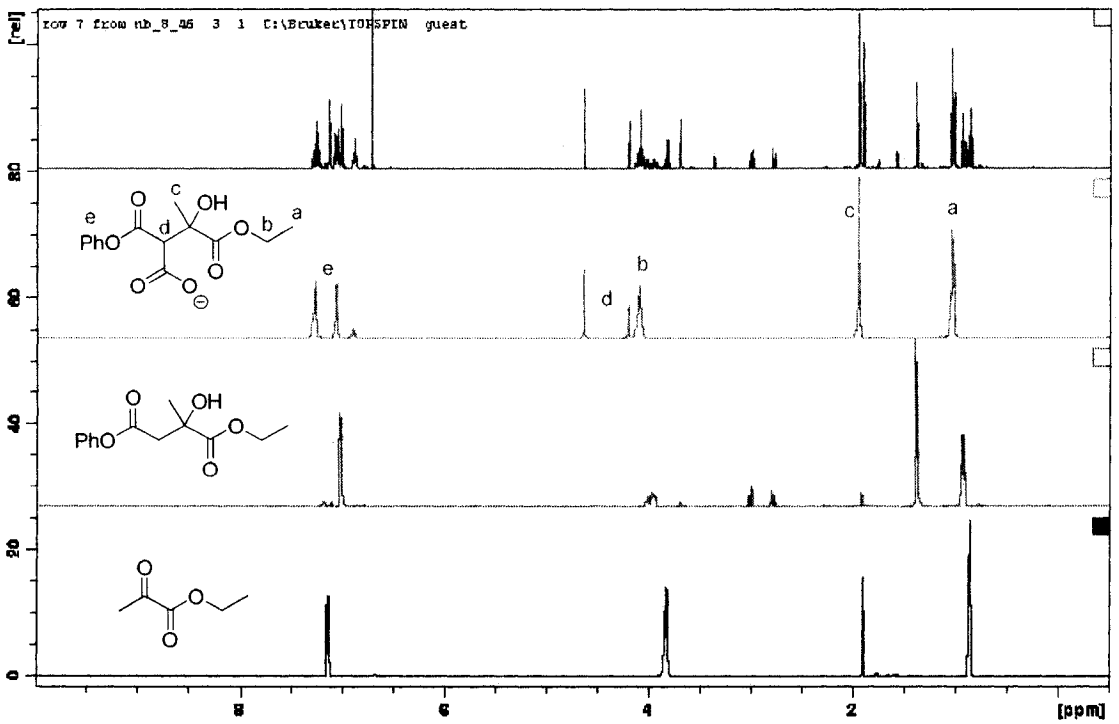

Figure 5.4 **Extracted ^{1}H spectra from the DOSY spectrum of reaction mixture for the reaction shown in scheme 5.1 (above), with chemical structures added and peaks assigned for the intermediate.**

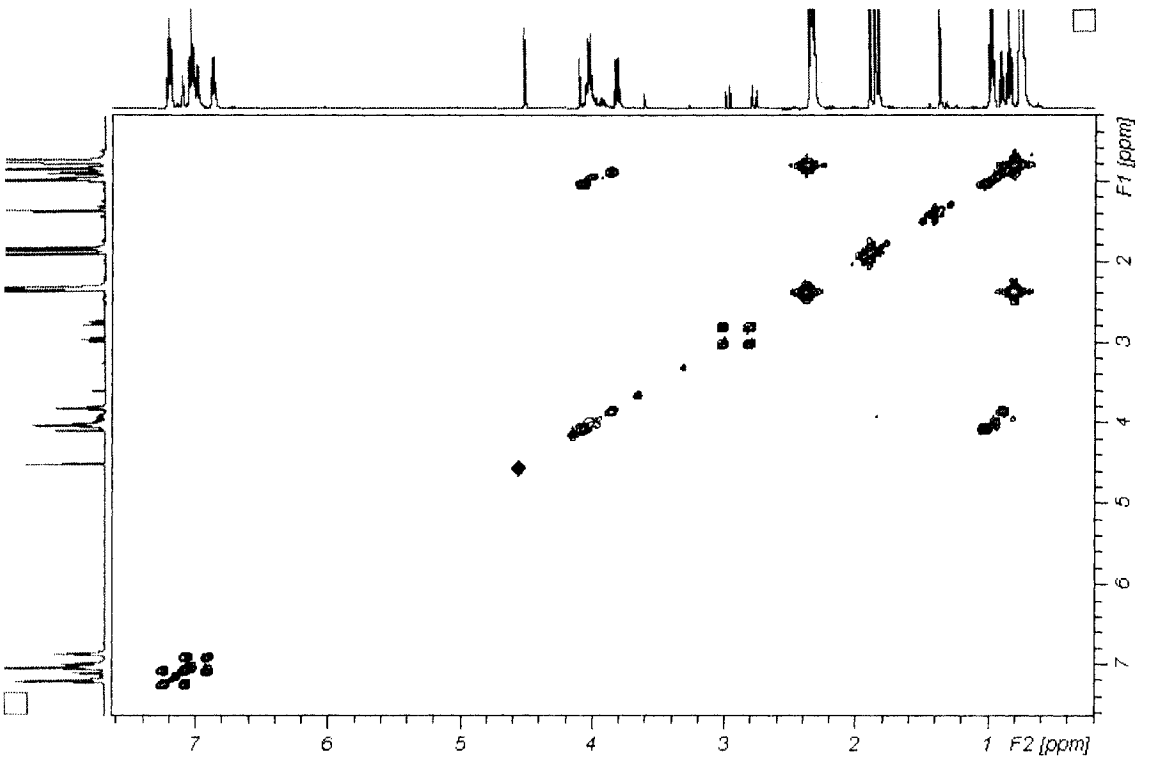

Figure 5.5 **COSY spectrum of reaction mixture for the reaction shown in scheme 5.1 (above).**

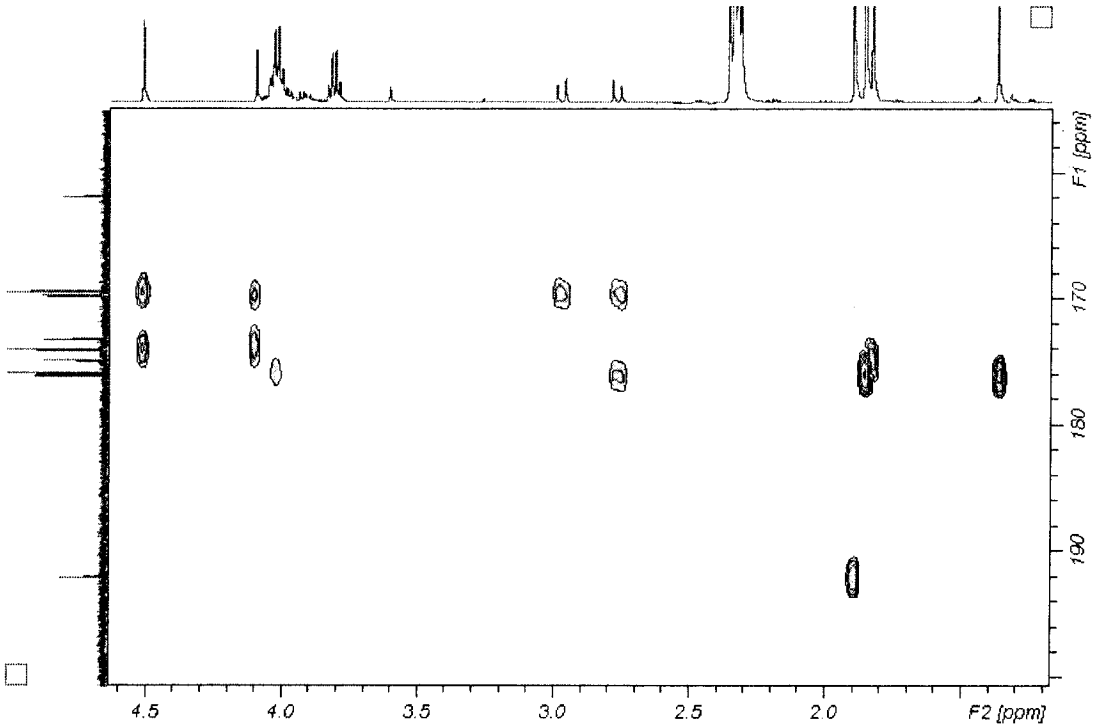

Figure 5.6 **Expanded HMBC spectrum of the carbonyl region of reaction mixture for scheme 5.1 (above).**

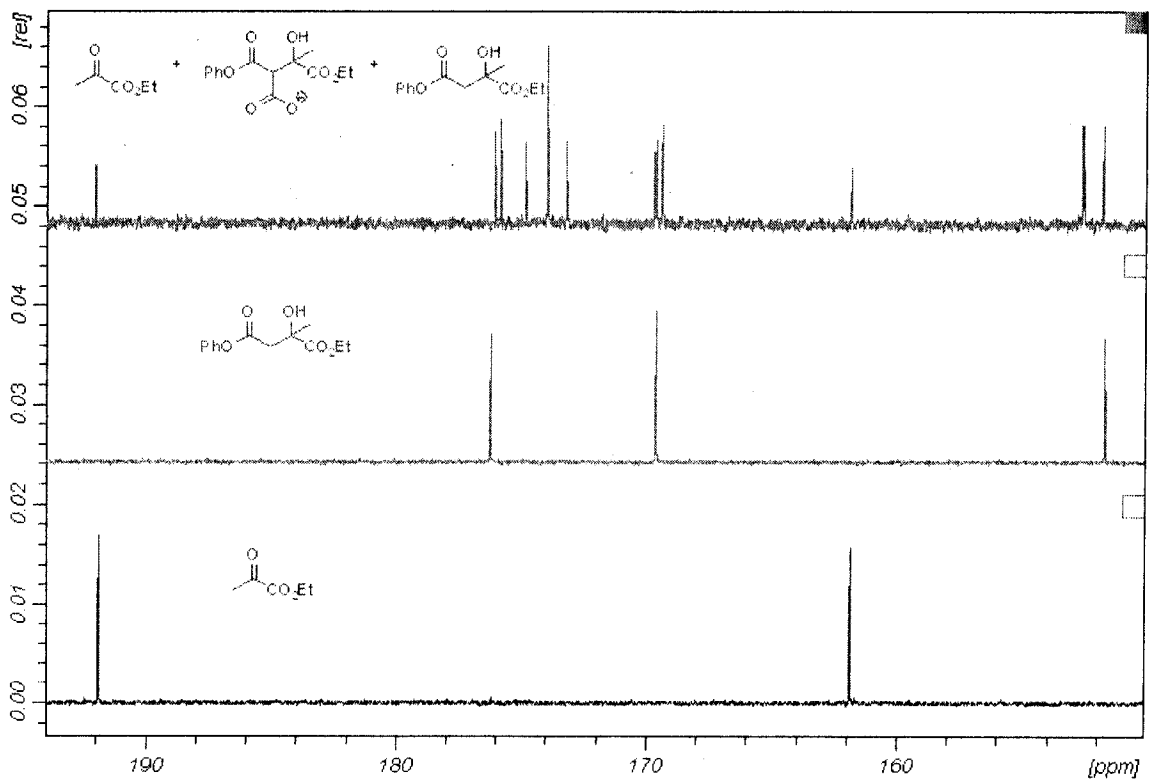

Figure 5.7 **Expanded ^{13}C spectrum of the carbonyl region of reaction mixture for scheme 5.1 (above).**

5.4 General procedure for ^{1}H NMR-monitored competition experiments

MAHO **2.4** (30 mg, 1.0 equiv.), and internal standard pentachlorobenzene (41.7 mg, 1.0 equiv.) were weighed into a disposable glass vial. The vial was then charged with 0.75 mL, (0.22 M) of C_6D_6. The reaction mixture was then stirred until homogeneous and the entire solution was transferred by pipette into a clean, oven-dried NMR tube. A baseline ^{1}H NMR spectrum was obtained. All NMR spectra were taken with sample spinning enabled to ensure that the reaction mixture was sufficiently mixed. Et_3N (23 µL, 1.0 equiv.), was then added to the NMR tube via syringe, the cap was replaced and the tube was inverted several times to ensure adequate mixing. A ^{1}H NMR spectrum was then taken to ensure the starting material had been completely deprotonated. Ethyl pyruvate **2.2** (1.0 equiv.) was added via syringe, the time was noted, the tube was inverted to mix and a ^{1}H NMR spectrum was obtained. Maximum intermediate concentration is observed at around t = 130 min. As such, the NMR tube cap was replaced with one in which a hole had been pierced to allow the escape of CO_2 gas and 10 ^{1}H NMR spectra were taken at 1.5 min intervals. Once this program was complete, ^{1}H NMR spectra were taken at 2 min intervals until t = 130 min. At this point, the second electrophile ethyl trifluoropyruvate **2.15** (1.0 equiv.) was added via syringe, the tube was inverted and a starting point ^{1}H NMR spectrum was obtained. 10 ^{1}H NMR spectra were then taken at 1.5 min intervals. Once this program was complete, 20 ^{1}H NMR spectra were taken at 2 min intervals. Upon completion of these spectral scans, spectra were then taken at 20-30 min intervals as the sample reacted overnight (8-18 hours).

5.5 Starting Material Synthesis

General procedure for the preparation of malonic acid half thioesters[77,78] To a solution of ethyl polyphosphate (PPE) (10.4g) in $CHCl_3$ (60 mL) and THF (10 mL) was added malonic acid (100 mmol, 4.0 equiv) and the benzyl mercaptan or benzene thiol (25 mmol, 1.0 equiv) via syringe. The reaction was stirred at 25°C for 40 hr, diluted with Et_2O, and extracted with saturated aq. $NaHCO_3$ (3X). The aqueous extracts were acidified with 10% HCl to a pH=1-2 and then extracted with $CHCl_3$ (2X). The organic layer is then dried over $MgSO_4$, filtered and evaporated under reduced pressure to afford a yellow oil, which was purified via silica gel chromatography (60:40 EtOAc/hexane).

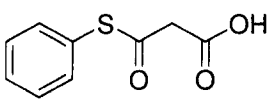

***S*-phenyl malonic acid half thioesters 2.1**

Obtained as a clear oil in 74% yield. **^{1}H NMR (300MHz, $CDCl_3$, 293K, TMS):** 3.71 (2H, s), 7.41-7.46 (5H, m), 10.61 (1H, b);

Exhibited spectral data identical to previous reports: Imamoto, T.; Kodera, M.; Yokoyama, M. *Bull. Chem. Soc. Jpn.* **1982**, *55*, 2303.

General procedure for the preparation of phenyl malonic acid: A neat solution of 2,2-dimethyl-1,3-dioxane-4,6-dione (1.0 equiv.) and phenol (1.0 equiv.) was refluxed at 120°C for 2 hours, and then cooled to room temperature. The reaction mixture was

[77] Lalic, G.; Aloise, A.D.; Shair, M.D.; *J. Am. Chem. Soc.* **2003**, *125*, 2852.
[78] Imamoto, T.; Kodera, M.; Yokoyama, M. *Bull. Chem. Soc. Jpn.* **1982**, *55*, 2303.

placed under reduced pressure, and loaded directly on a silica gel column (30% EtOAc in hexanes) for purification.

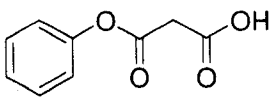

Monophenyl malonate 2.4

Obtained as a white solid in 75% yield. **^{1}H NMR (300MHz, $CDCl_3$, 293K, TMS):** 3.66 (2H, s), 7.11-7.14 (2H, m), 7.22-7.27 (1H, m), 7.35-7.41 (2H, m), 8.85 (1H, b);

Exhibited spectra data identical to previous reports: Ryu, Y; Scott, A.I.; *Tetrahedron Letters,* **2003**, *44*, 7499.

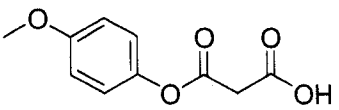

Malonic acid mono-(4-methoxy-phenyl) ester

Obtained as a beige solid in 81% yield. Rf = 0.09 on silica gel (30% EtOAc in Hexanes); Melting point = 88-90 °C **^{1}H NMR (300MHz, $CDCl_3$, 293K, TMS):** 3.68 (2H, s), 3.81 (3H, s), 6.87-6.93 (2H, m), 7.03-7.08 (2H, m), 8.40 (1H, b); **^{13}C NMR (100MHz, $CDCl_3$, 293K, TMS) :** 41.0 (CH_2), 55.6 (CH_3), 114.6 (CH), 122.1 (CH), 143.8 (C), 157.6 (C), 165.4 (C), 171.4 (C); **IR *(vmax* /cm^{-1})**: 3113, 3056, 2988, 2962, 2951, 2839, 1751, 1715, 1515, 1436, 1277, 1186, 1100, 1033, 845, 657; **HRMS calculated for $C_{10}H_{10}O_5$ (M+)** 210.0528; Found : 210.0511.

Exhibited spectra data identical to previous reports: Commercially available – CAS # 58303-20-1

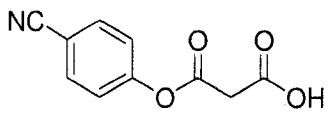

Malonic acid mono-(4-cyano-phenyl) ester

Obtained as a white solid in 27% yield. Rf = 0.06 on silica gel (30% EtOAc in Hexanes); Melting point=76-80 °C **^{1}H NMR (400MHz, $CDCl_3$, 293K, TMS):** 3.72 (2H, s), 7.26-7.31 (2H, m), 7.71-7.74 (2H, m), 9.15 (1H, b); **^{13}C NMR (400MHz, $CDCl_3$, 293K, TMS) :** 41.05, 110.41, 117.97, 122.56, 133.84, 153.38, 163.78, 171.09; **IR *(vmax* /cm^{-1})**: 3004 (m), 2900 (b), 2229 (s), 1773 (l), 1708 (l), 1205 (m), 1142 (m), 866 (s); **HRMS calculated for $C_{10}H_7N_1O_4$ (M+)** 205.0375; Found : 205.0376.

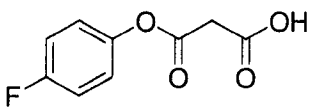

2-((4-fluorophenoxy)carbonyl acetic acid

Chromatography on silica gel (40% EtOAc in hexanes) afforded the product as a white solid in 73% yield. Rf = 0.14 on silica gel (30% EtOAc in Hexanes); Melting point = 68-70 °C **^{1}H NMR (300MHz, $CDCl_3$, 293K, TMS):** 3.66 (2H, s), 7.01-7.10 (4H, m), 11.25 (1H, b); **^{13}C NMR (100MHz, $CDCl_3$, 293K, TMS) :** 40.9 (CH_2), 116.3 (d, *J*=23.6 Hz) (CH), 122.8 (d, *J*=8.6 Hz) (CH), 146.1 (d, *J*=2.9 Hz) (C), 161.8 (C), 162.1 (d, *J*=558.7 Hz) (C), 171.2 (C); **IR *(vmax* /cm^{-1})**: 3173, 3124, 3079, 2990, 2948, 1750, 1715, 1512, 1437, 1340, 1278, 1183, 1162, 851; **HRMS calculated for $C_9H_7O_4F$ (M+)** 198.0328; Found : 198.0324

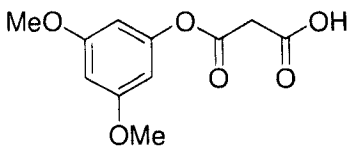

Malonic acid mono-(3,5-dimethoxy-phenyl) ester

Chromatography on silica gel (40% EtOAc in hexanes) afforded the product as a beige solid in 66% yield. Rf = 0.05 on silica gel (40% EtOAc in Hexanes); Melting point = 78-80 °C **^{1}H NMR (300MHz, $CDCl_3$, 293K):** 3.67 (2H, s), 3.78 (6H, s), 6.30 (2H, d, J=1.8Hz), 6.36 (1H, t, J=2.3Hz); **^{13}C NMR (75MHz, $CDCl_3$, 293K):** 40.80, 55.53, 98.71, 99.86, 151.63, 161.16, 164.98, 170.30; **IR *(vmax* /cm^{-1})**:3082, 2978, 2942, 2841, 2576, 1750, 1718, 1592, 1350, 1213, 1154, 931, 835; **HRMS calculated for $C_{11}H_{12}O_6$ (M+)**: 240.0634; Found : 240.0629;

5.6 Product Synthesis

General procedure for the decarboxylative addition of malonic acid half esters to electrophiles: The malonic acid half ester (1.0 equiv.) was weighed into a dry screw-cap vial equipped with a magnetic stir bar. The solvent (0.5 M), triethylamine (1.0 equiv.) and electrophile (1.0 equiv.) were added via syringe. The resulting mixture was stirred at room temperature for 4 hours, with a hole pierced in the septum to allow release of built up pressure. Upon completion, the solvent was evaporated in vacuo and the reaction mixture was loaded directly on a silica gel column for purification.

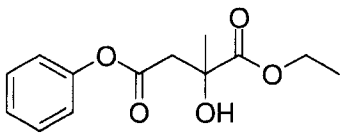

2-Hydroxy-2-methyl-succinic acid 1-ethyl ester 4-phenyl ester (table 2.3, entry 1)

Chromatography on silica gel (20% EtOAc in hexanes) afforded the product as a clear oil in 81% yield. R_f = 0.40 on silica gel (20% EtOAc in hexanes); **^{1}H NMR (400MHz, $CDCl_3$, 293K, TMS):** 1.30 (3H, t, *J*=7.5Hz), 1.52 (3H, s), 2.93 (1H, d, *J*=16.0Hz), 3.22 (1H, d, *J*=16.6Hz), 3.77 (1H, b), 4.22-4.33 (2H, m), 7.05-7.09 (2H, m), 7.20-7.26 (1H, m), 7.35-7.39 (2H, m); **^{13}C NMR (400MHz, $CDCl_3$, 293K, TMS) :** 14.14 (CH_3), 26.51 (CH_3), 44.37 (CH_2), 62.25 (CH_2), 72.54 (C), 121.46 (CH), 126.06 (CH), 129.46 (CH), 150.29 (C), 169.35 (C), 175.40 (C); **IR (*vmax* /cm^{-1})**: 3192 (b), 3075 (s), 2936 (m), 1755 (l), 1742 (l), 1592 (m), 1459 (m), 1195 (l), 1115 (m), 759 (s). **HRMS calculated for $C_{13}H_{16}O_5$ (M+)** 252.0998; Found: 252.0984

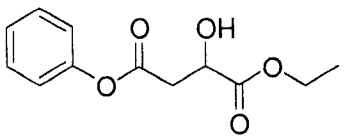

1-ethyl 4-phenyl 2-hydroxysuccinate (table 2.3, entry 4)

Chromatography on silica gel (20% EtOAc in hexanes) afforded the product as a clear oil in 65% yield. R_f = 0.18 on silica gel (20% EtOAc in hexanes); **^{1}H NMR (400MHz, $CDCl_3$, 293K, TMS):** 1.32 (3H, t, *J*=7.1Hz), 3.05 (1H, dd, *J*=16.3, 5.9 Hz), 3.11 (1H, dd, *J*=16.3, 4.7 Hz), 3.27 (1H, bd, *J*=4.4 Hz), 4.24-4.36 (2H, m), 4.58-4.62 (1H, m), 7.08-7.11 (2H, m), 7.21-7.26 (1H, m), 7.35-7.40 (2H, m); **^{13}C NMR (100MHz, $CDCl_3$, 293K, TMS) :** 14.1 (CH_3), 38.9 (CH_2), 62.3 (CH_2), 67.2 (CH), 121.4 (CH), 126.0 (CH), 129.4 (CH), 150.3 (C), 168.9 (C), 173.1 (C); **IR *(vmax* /cm^{-1})**: 3494, 3069, 2984, 2939, 2907, 1760, 1735, 1592, 1493, 1368, 1195, 1104, 1023, 931, 752, 691; **HRMS calculated for $C_{13}H_{16}O_5$ (M+)** 238.0841; Found: 238.0838

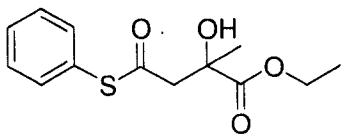

2-Hydroxy-2-methyl-succinic acid 1-ethyl ester 4-phenyl thioester 2.3

Chromatography on silica gel (20% EtOAc in hexanes) afforded the product as a clear oil in 70% yield. R_f = 0.45 on silica gel (30% EtOAc in hexanes); **^{1}H NMR (400MHz, $CDCl_3$, 293K, TMS):** 1.28 (3H, t, *J*=7.1Hz), 1.45 (3H, s), 3.05 (1H, d, *J*=16.1Hz), 3.27 (1H, d, *J*=16.1Hz), 4.18-4.29 (2H, m), 7.38-7.42 (5H, m); **^{13}C NMR (75MHz, $CDCl_3$, 293K, TMS) :** 14.1 (CH_3), 26.3 (CH_3), 52.3 (CH_2), 62.1 (CH_2), 72.8 (C), 127.0 (C), 129.2 (CH), 129.6 (CH), 134.4 (CH), 175.1 (C), 195.5 (C); **IR *(vmax* /cm^{-1})**:3506 (br), 3060, 2982, 2935, 1734, 1708, 1477, 1443, 1269, 1210, 1114, 1013, 748, 690. **HRMS calculated for $C_{13}H_{16}O_4S$ (M+)** 268.0769; Found: 268.0734.

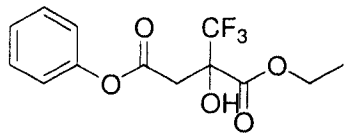

1-ethyl 4-phenyl 2-(trifluoromethyl)-2-hydroxysuccinate (table 2.3, entry 2)

Chromatography on silica gel (10:90 Et_2O:hexanes) afforded the product as a white solid in 84% yield. R_f = 0.40 on silica gel (20% Et_2O in hexanes); **mp:** 54-56ºC; **^{1}H NMR (400MHz, $CDCl_3$, 293K, TMS):** 1.30 (3H, t, *J*= 7.1Hz), 3.20 (1H, d, *J*= 16.6Hz) 3.43 (1H, d, *J*= 16.6Hz), 4.32 (1H, br), 4.37 (2H, q, *J*=7.1), 7.01-7.11 (2H, m), 7.19-7.26 (1H, m), 7.32-7.41 (2H, m); **^{13}C NMR (100MHz, $CDCl_3$, 293K, TMS) :** 13.81, 37.21, 64.12, 75.23 (q, J_F= 30.0Hz), 121.23, 122.9 (q, J_F= 286.5Hz), 126.27, 129.50, 150.05, 166.96, 168.16; **IR (*vmax* /cm^{-1})**: 3475 (br), 2988 (m), 1765 (s), 1593 (m), 1493 (m), 1378 (m), 1239 (s), 1138 (s), 1198 (s), 1074 (m), 1011 (m), 935 (m), 755 (m), 689 (s). **HRMS calculated for $C_{13}H_{13}O_5F_3$ (M+)** 306.0715; Found : 306.0732.

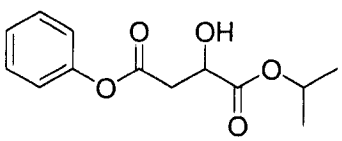

1-isopropyl 4-phenyl 2-hydroxysuccinate (table 2.3, entry 5)

Chromatography on silica gel (25:75 EtOAc:hexanes) afforded the product as a pale yellow oil in 46% yield. R_f = 0.32 on silica gel (30% EtOAc in hexanes); **^{1}H NMR (400MHz, $CDCl_3$, 293K, TMS):** 1.28 (3H, d, *J*= 6.7Hz), 1.30 (3H, d, *J*= 6.7Hz), 3.03 (1H, dd, J_{AB}= 16.3Hz, J_{AX}= 5.8Hz), 3.09 (1H, dd, J_{BA}= 16.3Hz, J_{BX}= 4.7Hz), 3.28 (1H, b), 4.60-4.52 (1H, m), 5.15 (1H, s, *J*= 6.3Hz), 7.06-7.42 (5H, m); **^{13}C NMR (100MHz, $CDCl_3$, 293K, TMS) :** 21.70, 38.93, 67.26, 70.25, 121.41, 125.99, 129.42, 150.36, 168.84, 172.71; **IR (*vmax* /cm^{-1})**: 3511 (s) 2923 (m), 2852 (m), 1759 (s), 1735 (s), 1489 (m), 1375 (m), 1195 (s), 1164 (s), 1104 (s), 748 (m), 690 (m). **HRMS calculated for $C_{13}H_{16}O_5$ (M+)** 252.0998; Found : 252.1024.

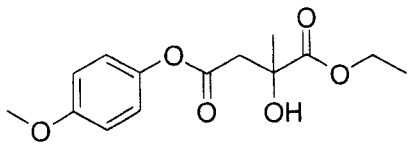

2-Hydroxy-2-methyl-succinic acid 1-ethyl ester 4-(4-methoxy-phenyl) ester (table 2.3, entry 11)

Chromatography on silica gel (20% EtOAc in hexanes) afforded the product as clear oil in 73% yield. R_f = 0.41 on silica gel (20% EtOAc in hexanes); **^{1}H NMR (400MHz, $CDCl_3$, 293K, TMS):** 1.29 (3H, t, *J*=7.1Hz), 1.50 (3H, s), 2.90 (1H, d, *J*=16.3Hz), 3.19 (1H, d, *J*=16.3Hz), 3.77 (3H, s), 3.82 (1H, b), 4.19-4.32 (2H, m), 6.84-6.88 (2H, m), 6.96-7.00 (2H, m); **^{13}C NMR (400MHz, $CDCl_3$, 293K, TMS) :** 14.14, 26.51, 44.37, 62.25, 72.54, 121.46, 126.06, 129.46, 150.29, 169.35, 175.40; **IR (*vmax* /cm^{-1})**: 3503 (b), 2983 (m), 2938 (m), 2838 (s), 1756 (l), 1507 (m), 1195 (l), 1031 (m), 840 (m). **HRMS calculated for $C_{14}H_{18}O_6$ (M+)** 282.1103; Found: 282.1085.

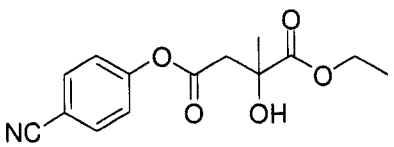

2-Hydroxy-2-methyl-succinic acid 4-(4-cyano-phenyl) ester 1-ethyl ester (table 2.3, entry 7)

Chromatography on silica gel (20% EtOAc in hexanes) afforded the product as a clear oil in 42% yield. R_f = 0.45 on silica gel (20% EtOAc in hexanes); **^{1}H NMR (400MHz, $CDCl_3$, 293K, TMS):** 1.30 (3H, t, *J*=7.1Hz), 1.52 (3H, s), 2.96 (1H, d, *J*=16.2Hz), 3.23 (1H, d, *J*=16.2Hz), 3.69 (1H, b), 4.29 (2H, qd, *J*=2.0Hz, 7.1Hz), 7.21-7.24 (2H, m), 7.66-7.70 (2H, m); **^{13}C NMR (400MHz, $CDCl_3$, 293K, TMS) :** 14.13, 26.65, 44.27, 62.44, 72.48, 110.01, 118.13, 122.67, 133.69, 153.51, 168.29, 175.28; **IR (*vmax* /cm^{-1})**: 3484 (br), 2985, 2945, 2231, 1761, 1735, 1604, 1502, 1207, 1170, 1141, 1014, 858; **HRMS calculated for $C_{14}H_{15}NO_5$ (M+)** 277.0950; Found: 277.1001.

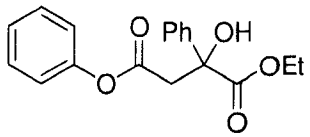

1-ethyl 4-phenyl 2-hydroxy-2-phenylsuccinate (table 2.3, entry 3)

Chromatography on silica gel (15% EtOAc in hexanes) afforded the product as an off-white solid in 46% yield. Rf = 0.30 on silica gel (15% EtOAc in Hexanes); Melting point = 94-96 °C **^{1}H NMR (400MHz, $CDCl_3$, 293K):** 1.27 (3H, t, J=7.2Hz), 3.16 (1H, d, J=16.4Hz), 3.70 (1H, d, J=16.4Hz), 4.23-4.33 (2H, m), 4.32 (1H, b), 7.07-7.10 (2H, m), 7.22-7.26 (1H, m), 7.32-7.42 (5H, m), 7.63-7.66 (2H, m); **^{13}C NMR (75MHz, $CDCl_3$, 293K):** 14.00, 44.76, 62.74, 76.17, 121.44, 125.13, 126.07, 128.28, 128.54, 129.46, 140.20, 150.30, 169.39, 173.54; **IR (*vmax* /cm^{-1})**: 3487, 3062, 2991, 2939, 1750, 1728, 1589, 1490, 1185, 1121, 726, 693; HRMS calculated for $C_{18}H_{18}O_5$ (M-93) 314.1154; Found : 314.1103.

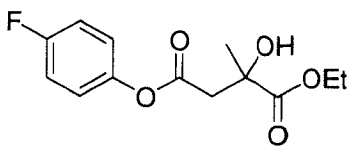

1-ethyl 4-(4-fluorophenyl) 2-hydroxy-2-methylsuccinate (table 2.3, entry 8)

Chromatography on silica gel (20% EtOAc in hexanes) afforded the product as a pale yellow oil in 70% yield. Rf = 0.28 on silica gel (20% EtOAc in Hexanes); **^{1}H NMR (400MHz, $CDCl_3$, 293K):** 1.29 (3H, t, J=7.2Hz), 1.51 (3H, s) 2.92 (1H, d, J=16.0Hz), 3.20 (1H, d, J=16.0Hz), 3.73 (1H, b), 4.23-4.31 (2H, m), 7.03-7.05 (4H, m); **^{13}C NMR (75MHz, $CDCl_3$, 293K):** 14.09, 26.51, 44.23, 62.27, 72.49, 116.07 (d, J=23.5Hz), 122.85 (d, J=8.6Hz), 146.07 (d, J=2.9Hz), 160.30 (d, J=244.5Hz), 169.28, 175.35; **IR (*vmax* /cm^{-1})**: 3508, 3082, 2984, 2938, 1760, 1738, 1598, 1504, 1452, 1360, 1281, 1187, 1144, 1091, 1014, 844, 774; HRMS calculated for $C_{13}H_{15}FO_5$ (M+) 270.0904; Found : 270.0887.

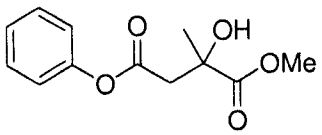

1-methyl 4-phenyl 2-hydroxy-2-methylsuccinate (table 2.3, entry 6)

Chromatography on silica gel (25% EtOAc in hexanes) afforded the product as pale yellow oil in 47% yield. Rf = 0.20 on silica gel (20% EtOAc in Hexanes); **^{1}H NMR (400MHz, $CDCl_3$, 293K):** 1.52 (3H, s), 2.93 (1H, d, J=16.4), 3.22 (1H, d, J=16.4Hz), 3.77 (1H, b), 3.81 (3H, s), 7.05-7.09 (2H, m), 7.20-7.25 (1H, m), 7.34-7.39 (2H, m); **^{13}C NMR (75MHz, $CDCl_3$, 293K)** :26.5 (CH_3), 44.4 (CH_2), 53.1 (CH_3), 72.7 (C), 121.4 (CH), 126.1 (CH), 129.5 (CH), 150.3 (C), 169.4 (C), 175.9 (C); **IR (*vmax* /cm^{-1})**: 3507, 2990, 1957, 1757, 1741, 1592, 1492, 1348, 1278, 1194, 1163, 689; **HRMS calculated for $C_{13}H_{15}FO_5$ (M+)**: 238.0804; Found : 238.0787.

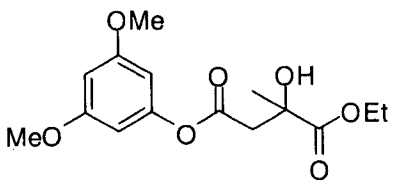

4-(3,5-dimethoxyphenyl) 1-methyl 2-hydroxy-2-methylsuccinate (table 2.3, entry 10)

Chromatography on silica gel (25% EtOAc in hexanes) afforded the product as clear oil in 50% yield. Rf = 0.23 on silica gel (30% EtOAc in Hexanes); ^{1}H NMR (400MHz, $CDCl_3$, 293K): 1.30 (3H, t, *J*=7.1Hz), 1.51 (3H, s) 2.91 (1H, d, *J*=16.3Hz), 3.20 (1H, d, J=16.3Hz), 3.76 (6H, s), 4.21-4.33 (2H, m), 6.24 (2H, d, *J*=2.2Hz), 6.33 (1H, t, *J*=2.2Hz); ^{13}C NMR (100MHz, $CDCl_3$, 293K,): 14.1 (CH_3), 26.5 (CH_3), 44.3 (CH_2), 55.5 (CH_3), 62.2 (CH_2), 72.5 (C), 98.4 (CH), 100.1 (CH), 151.8 (C), 161.1 (C), 169.1 (C), 175.4 (C); **IR (*vmax* /cm^{-1})**: 3521 (b), 2980 (m), 2938 (m), 2836 (s), 1760 (l), 1510 (m), 1195 (l), 1030 (m), 842 (m). HRMS calculated for $C_{13}H_{15}FO_5$ (M+) 312.1204; Found : 312.1187.

Chapter 6

Supporting Information- Ammonia-Borane Dehydrogenation

6.1 General Methods

All experiments were carried out under an atmosphere of nitrogen or hydrogen. ^{1}H and ^{13}C NMR were recorded in $CDCl_3$ solutions using a Bruker AVANCE 300 or 400 spectrometer. High-resolution mass spectra were obtained on a Kratos Concept IIH. Infrared (IR) spectra were obtained as neat films on a sodium chloride cell. Chemical shifts are reported downfield from tetramethylsilane (δ scale) in ppm. HPLC Grade THF was dried and purified via an MBraun SP Series solvent purification system and degassed with nitrogen prior to use. Dioxane was freshly distilled from CaH_2 before every use. Precatalysts **4.4-4.9 and 4.12** were obtained from KCT Chemical Company. All other reagents and solvents were used as is from commercial sources. Hydrogen was detected using a VG-ZAB-2F double-focussing mass spectrometer.

6.2 Synthesis of Ammonia-borane:[79]

To a solution of $(NH_4)_2CO_3$ (1.0 equivalent, 100 mmol) in dioxane was added $NaBH_4$ (1.0 equivalent, 100 mmol). The reaction was stirred at 40-45℃ for 24 hours, then cooled to room temperature. The solid was filtered off and the filtrate concentrated *in vacuo.* The white solid was then dissolved in a minimum amount of THF and recrystallized in 10% dicholoromethane/hexane to obtain a white solid (1.93 g, 63% yield).

This compound has been previously prepared by Geanangel *et. al.* (ref: Hu, M. G.; Van Paasschen, J. M.; Geanangel, R. A. *J. Inorg. Nucl. Chem.* **1977**, *39*, 2147) and exhibited identical spectral data.

^{1}H NMR (400MHz, $CDCl_3$, 293K, TMS): 3.40 (3H, t, br), 1.61 (3H, q, br).

[79] Hu, M. G.; Van Paasschen, J. M.; Geanangel, R. A. *J. Inorg. Nucl. Chem.* **1977**, *39*, 2147.

6.3 Synthesis of Methylammonia-borane:[54]

To a 2.0 M solution of methylamine in THF (1.0 equivalent, 66.8 mmol) cooled to -78°C was added a 1.0M solution of BH_3·THF in THF (1.0 equivalent, 66.8 mmol). The reaction was warmed to room temperature and stirred overnight. The reaction mixture was concentrated *in vacuo*, redissolved in THF, and filtered. The filtrate was then concentrated and $MeNH_2BH_3$ was precipitated with hexanes to obtain a white solid (2g, 67% yield).

This compound has been previously prepared by Manners *et. al.* (ref: Jaska, C. A.; Temple, K.; Lough, A. J.; Manners, I. *J. Am. Chem. Soc.* **2003**, *125*, 9424) and exhibited identical spectral data.

^{1}H NMR (400MHz, $CDCl_3$, 293K, TMS): 3.83 (2H, br), 2.55 (3H, t, *J*=6.3 Hz), 2.0-1.0 (3H, q, br).

6.4 General Procedure for AB dehydrogenation:

The precatalyst **1** (0.8 mg, 0.1 mol %) and KO^{t}Bu (5.4 mg, 3.0 mol %)[80] were added to a small oven-dried vial equipped with a Teflon stir-bar. The vial and its contents were put under vacuum and refilled with nitrogen 3 times. Degassed THF (0.32 mL) was added to the mixture and the reaction was stirred for approximately 10 minutes. The mixture was then transferred by syringe to a vial containing 50 mg of ammonia-borane under a nitrogen atmosphere and containing a Teflon stir-bar. The vial was connected to a water-filled eudiometer via a needle piercing the septum and attached to PVC tubing. Timing was started upon addition of the catalyst solution to the vial containing AB. CAUTION: Hydrogen evolution can be very rapid. Rapid formation of an insoluble white powder was also observed. 1.0 equivalent of hydrogen occupies a volume of 39.7 mL at atmospheric pressure. Hydrogen gas was detected using mass spectrometry (VG-ZAB-2F double-focussing mass spectrometer).

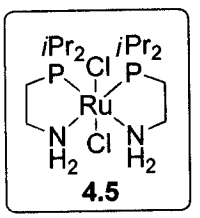

4.5

[80] A 1:30 Ru:KOtBu ratio was always employed for catalyst activation regardless of catalyst loading.

Volumes were measured at atmospheric pressure and corrected for water vapor pressure at 20 °C.

Note: Catalysts are extremely air-sensitive once deprotonated, and reaction rates are very sensitive to variations in the conditions employed. Also, stock solutions of the catalyst/base mixtures were often prepared for ease of weighing and transfer.

The infrared spectrum of the insoluble solid formed during the reaction revealed its identity as the same polymeric compound obtained by both Goldberg[54] and Manners[55] (*figure 6.1*).

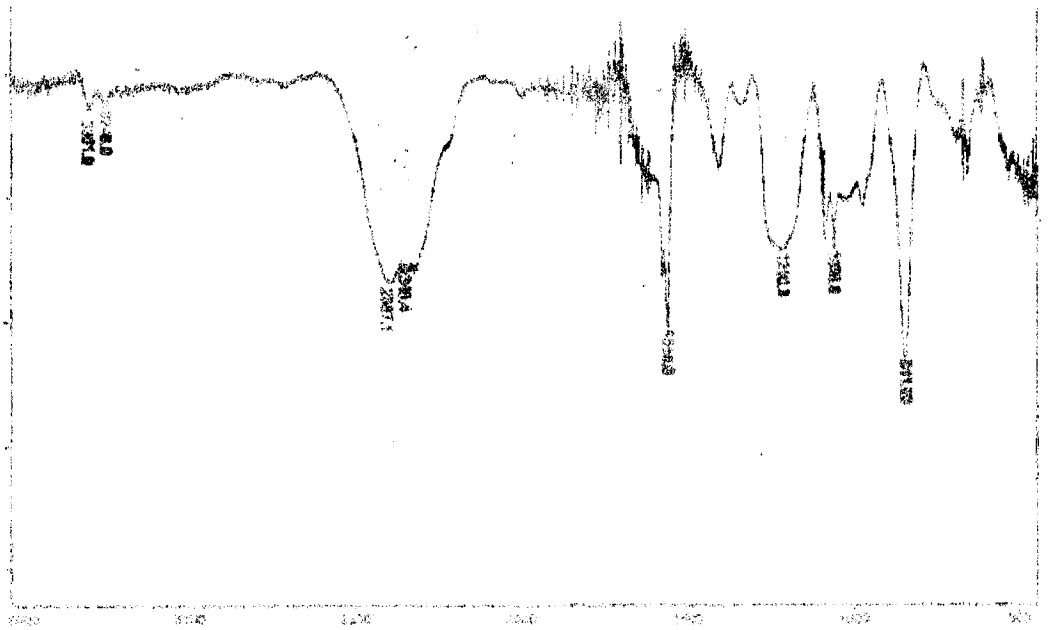

Figure 6.8 **Infrared spectrum of insoluble solid obtained from AB dehydrogenation.**

6.5 General Procedure for MeAB dehydrogenation:

The precatalyst **1** (1.4 mg, 0.5 mol %) and KO^{t}Bu (9.4 mg, 15.0 mol %) were added to a small oven-dried vial equipped with a Teflon stir-bar. The vial and its contents were put under vacuum and refilled with nitrogen 3 times. Degassed THF (0.56 mL, 1.0M) was added to the mixture and the reaction was stirred for approximately 10 minutes. The mixture was then transferred by syringe to a vial containing 25 mg of methylammonia-

borane under a nitrogen atmosphere and containing a Teflon stir-bar. The vial was connected to a water-filled eudiometer via a needle piercing the septum and attached to PVC tubing. Timing was started upon addition of the catalyst solution to the vial containing MeAB. **CAUTION:** Hydrogen evolution is rapid. 1.0 equivalent of hydrogen occupies a volume of 13.7 mL at atmospheric pressure, 2.0 equivalents yield 27.4 mL.

^{1}H and ^{11}B NMR confirmed that the product obtained following the release of one equivalent of H_2 is a poly(*N*-methylaminoborane) species previously characterized by Manners (figure 6.2).[55]

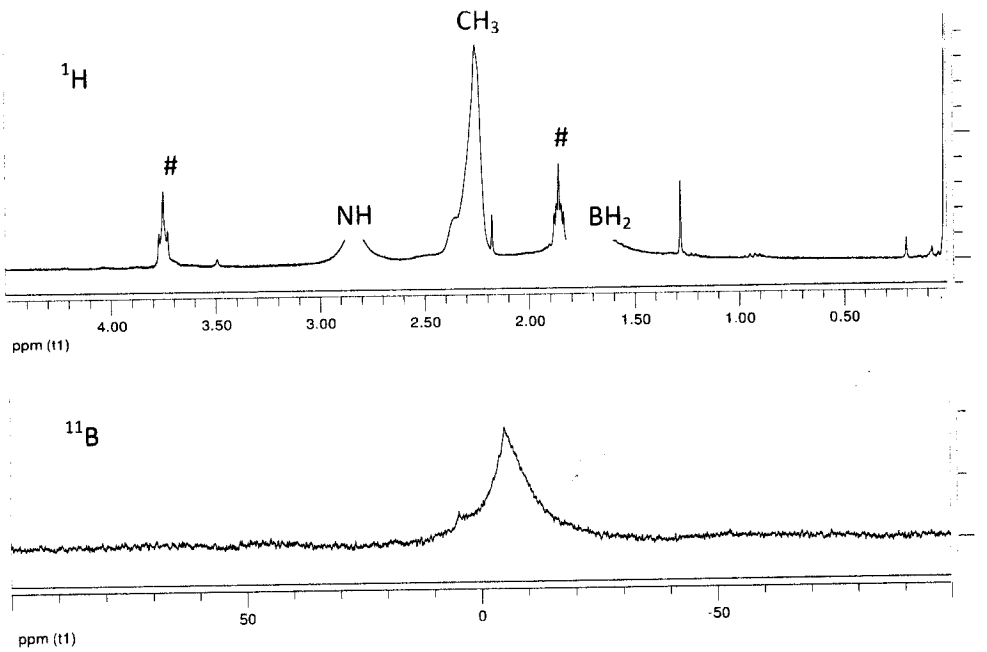

Figure 6.9 **^{1}H and ^{11}B NMR in $CDCl_3$ of poly(*N*-methylaminoborane) obtained after the release of 1 equivalent of H_2 from MeAB. # symbol represents residual THF peaks.**

Spectra obtained from the dehydrogenation products of poly(*N*-methylaminoborane) (2 equiv. H_2) are included below. Spectra were taken in both $CDCl_3$ and C_6D_6, and in both cases multiplets are present in the 3.1-2.4 ppm and 1.5-1.1 ppm range. Characteristic peaks corresponding to *N,N,N*-trimethylborazine are not observed.[2] Representative spectra are shown in *figure 6.3*.

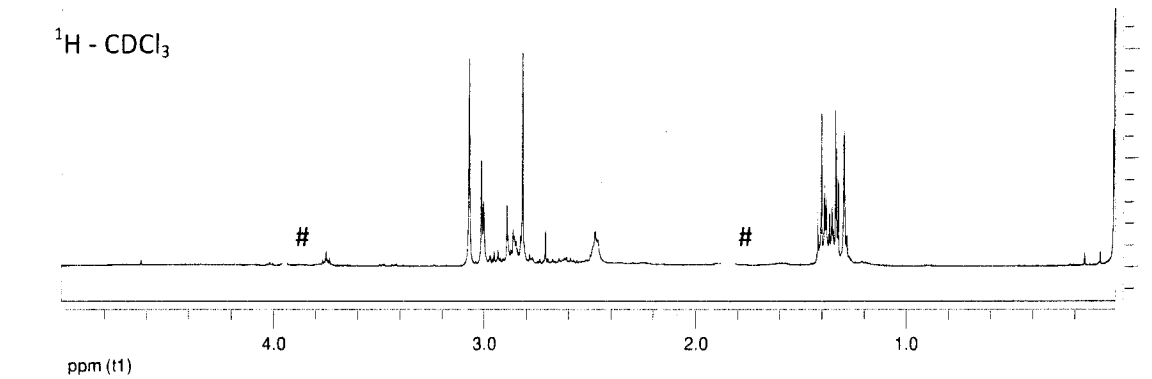
^{1}H - $CDCl_3$
#
#
4.0
3.0
2.0
1.0
ppm (t1)

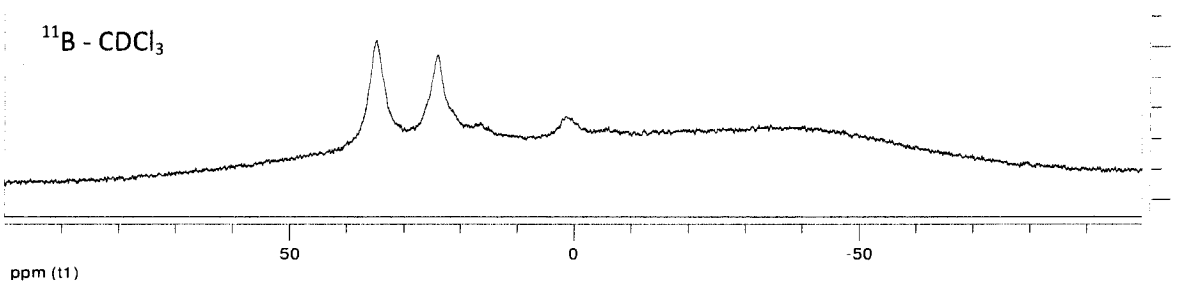
^{11}B - $CDCl_3$
50
0
-50
ppm (t1)

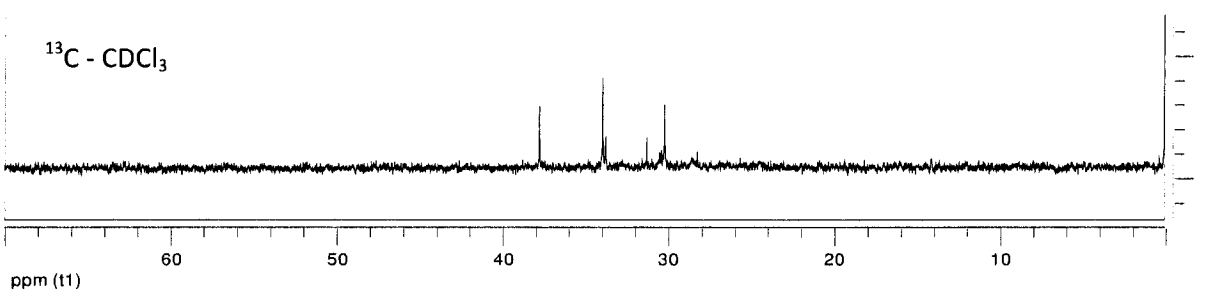
^{13}C - $CDCl_3$
60
50
40
30
20
10
ppm (t1)

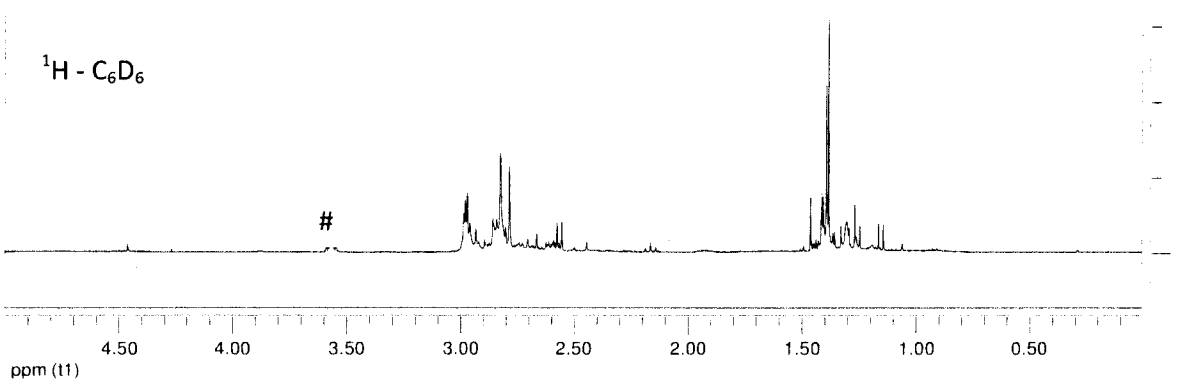
^{1}H - C_6D_6
#
4.50
4.00
3.50
3.00
2.50
2.00
1.50
1.00
0.50
ppm (t1)

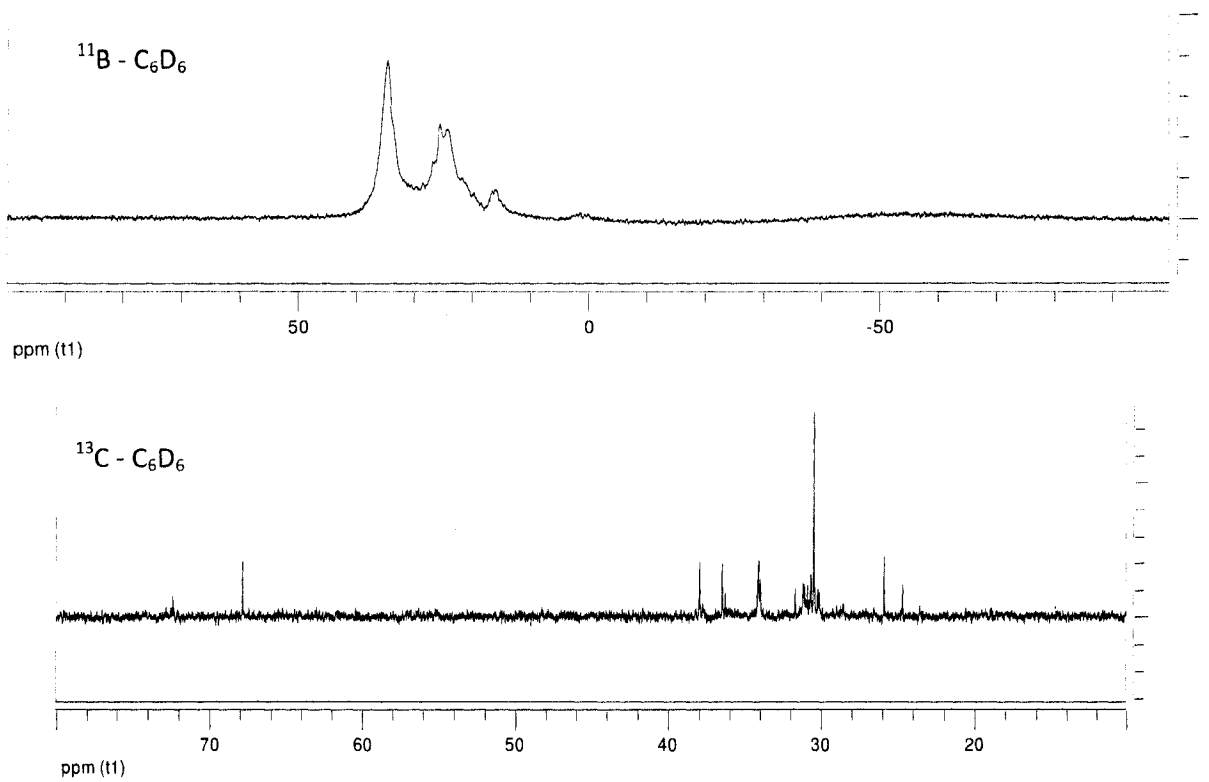

Figure 6.10 **^{1}H, ^{11}B, and ^{13}C NMR spectra of the products arising from the release of 2 equiv. H_2 from MeAB in $CDCl_3$ and C_6D_6.**

6.6 Ammonia-borane/Methylammonia-borane dehydrogenation:

The precatalyst **1** (0.8 mg, 0.1 mol %) and KO^{t}Bu (5.4 mg, 3.0 mol %) were added to a small oven-dried vial equipped with a Teflon stir-bar. The vial and its contents were put under vacuum and refilled with nitrogen 3 times. Degassed THF (10 µL) was added to the mixture and the reaction was stirred for approximately 10 minutes. The mixture was then transferred by syringe to a vial containing ammonia-borane (25.0 mg, 0.81 mmol) and methylammonia-borane (36.4 mg, 0.81 mmol) under a nitrogen atmosphere and containing a Teflon stir-bar. The vial was connected to a water-filled eudiometer via a needle piercing the septum and attached to PVC tubing. Timing was started upon addition of the catalyst solution to the vial containing AB/MeAB. CAUTION: Hydrogen evolution can be very rapid. 1.0 equivalent of hydrogen occupies a volume of 39.7 mL at atmospheric pressure. In the case of solvent-free reactions, all solids were added to the same vial and timing was started upon heating of the mixture.

^{1}H, ^{11}B and ^{13}C spectra of the products obtained following the release of 1 equiv. H_2 are shown below (*figure 6.4*). Since the spectra do not exhibit peaks analogous to those observed after one and two equivalents of hydrogen loss from MeAB alone, this supports the claim that the product is comprised of an analogous polymeric mixture as that observed for AB and for MeAB alone, except with incorporation of both AB and MeAB into the polymeric structure.

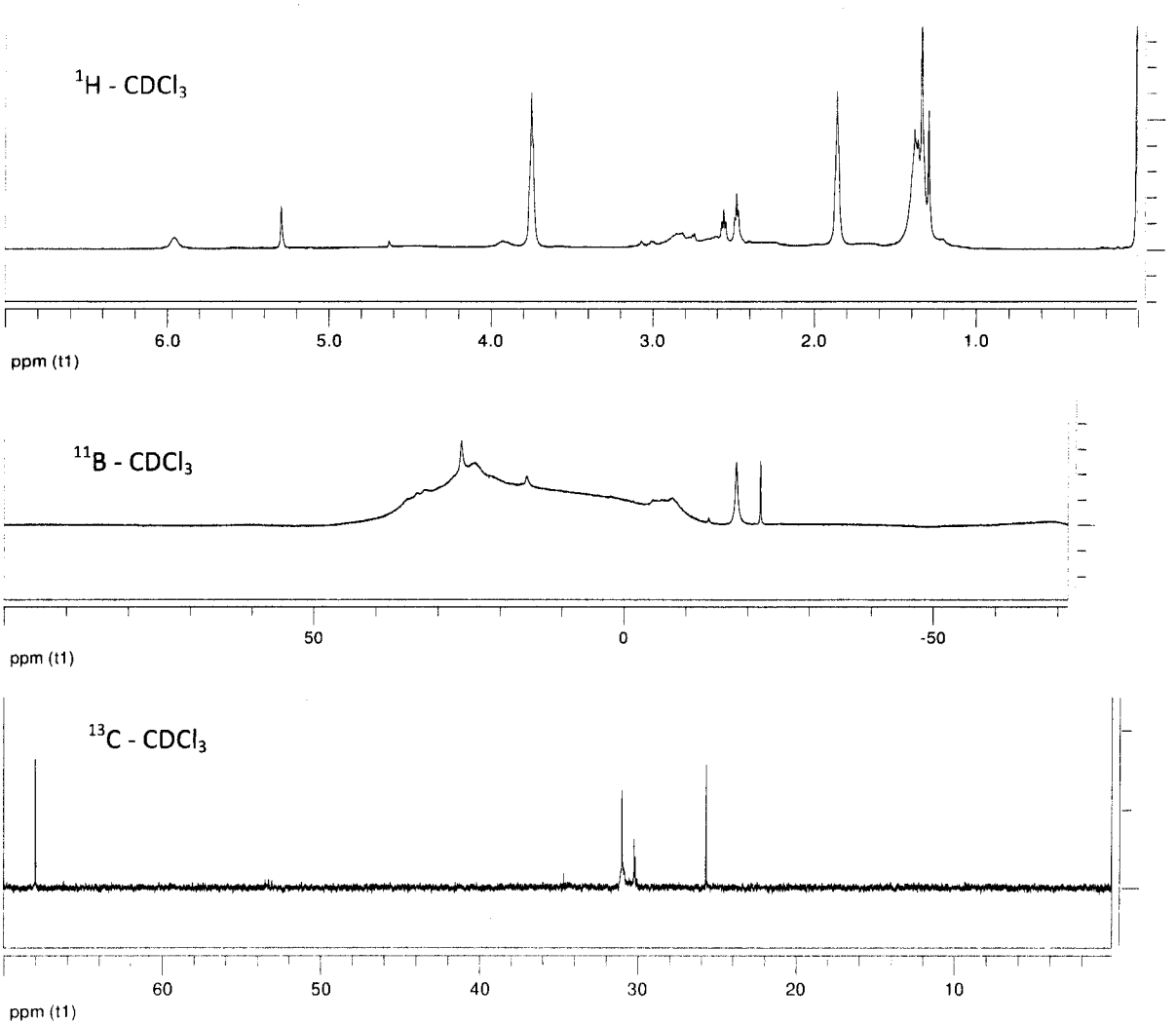

Figure 6.4 **^{1}H, ^{11}B, and ^{13}C NMR spectra of the products arising from the release of 1 equiv. H_2 from a 1:1 mixture of MeAB:AB in $CDCl_3$.**

6.7 General Procedure for Amine-Borane Transfer Hydrogenation of Imines and Ketones:

All reactions were performed on a 0.3 mmol scale. To an oven-dried 2 mL septum-capped vial was added pyrrolidine-borane (3.0 equiv.) and a stir bar. This was placed under an Ar atmosphere by purging with an Ar-filled balloon. In a separate vial purged with Ar equipped with a stir bar, was placed pyrAB **4.25** (0.015 equiv.) and dry KO^{t}Bu (0.03 equiv.). To this was added 0.5 mL of dry THF, and this solution was stirred for 5 minutes (turns purple). This solution was subsequently added via a syringe to the vial containing the amine-borane. Then, the imine or ketone (1.0 equiv.) was dissolved in 1 mL of dry THF, and this solution was added dropwise via a syringe to the septum-capped vial. Concentration of the substrate was 0.2 M. This orange solution was stirred for 3 hours at RT (imines) or 5.5 hours at RT (ketones). The reaction was subsequently concentrated in vacuo, and the crude mixture was subjected to column chromtography using 5% MeOH in DCM for the imine substrates or 5 to 10% EtOAc in Hexanes for the ketone substrates, providing the pure amine or alcohol products.

Structural Assignment of Pyrrolidine-Borane

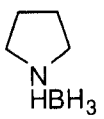

This compound has been previously prepared by Manners et. al. (ref: Jaska, C. A.; Temple, K.; Lough, A. J.; Manners, I., *J. Am. Chem. Soc.*, **2003**, *125*, 9424.) and exhibited identical spectral data (^{1}H, ^{13}C, and ^{11}B NMR reported).

IR *(vmax* /cm-1): 3214.5, 2971.6, 2310.1, 2265.2, 1459.1, 1164, 930.7.

HRMS calculated for C4H12NB (M+) 85.1063; Found: 85.1012.

6.8 Structural Assignments of Products

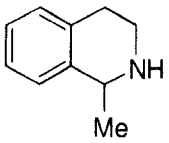

Isolated Yield : 85%.

This compound has been previously prepared by Moody et. al. (ref: Pitts, M. R.; Harrison, J. R.; Moody, C. J., *J. Chem. Soc., Perkin Trans. 1*, **2001**, *9*, 955.) and exhibited identical spectral data. CAS # 4965-09-7. Commercially available.

^{1}H NMR (400MHz, $CDCl_3$, 293K, TMS): 7.17 (4 H, m), 4.12 (1 H, q, *J*=7.2Hz), 3.39–2.61 (4 H, m), 1.82 (1 H, br s), 1.51 (3 H, d, *J*=7.2Hz).

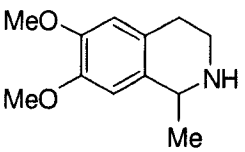

Isolated Yield : 92%.

This compound has been previously prepared by Moody et. al. (ref: Pitts, M. R.; Harrison, J. R.; Moody, C. J., *J. Chem. Soc., Perkin Trans. 1*, **2001**, *9*, 955.) and exhibited identical spectral data. CAS # 493-48-1. Commercially available.

^{1}H NMR (400MHz, $CDCl_3$, 293K, TMS): 6.62 (1 H, s), 6.57 (1 H, s), 4.04 (1 H, q, *J*=6.6Hz), 3.86 (3 H, s), 3.85 (3 H, s), 3.25 (1 H, m), 3.00 (1 H, m), 2.79 (1 H, m), 2.64 (1 H, m), 1.68 (1 H, br s), 1.44 (3 H, d, *J*=6.6Hz).

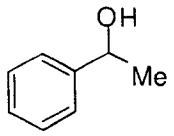

Isolated Yield : 97%.

This compound is commercially available. CAS # 98-85-1.

^{1}H NMR (400MHz, $CDCl_3$, 293K, TMS): 7.34 (4 H, m), 7.27 (1 H, m), 4.82 (1 H, q, *J*=6.8Hz), 2.74 (1 H, br s), 1.46 (3 H, d, *J*=6.8Hz).

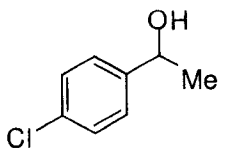

Isolated Yield : 97%.

This compound is commercially available. CAS # 3391-10-4.

^{1}H NMR (400MHz, $CDCl_3$, 293K, TMS): 7.24 (4 H, m), 4.77 (1 H, q, *J*=6.4Hz), 2.72 (1 H, br s), 1.40 (3 H, d, *J*=6.4Hz).

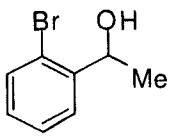

Isolated Yield : 88%.

This compound is commercially available. CAS # 5411-56-3.

^{1}H NMR (400MHz, $CDCl_3$, 293K, TMS): 7.54 (1 H, dd, *J*=8.0Hz, 2.0Hz), 7.47 (1 H, dd, *J*=8.0Hz, 2.0Hz), 7.30 (1 H, td, *J*=8.0Hz, 1.6Hz), 7.09 (1 H, td, *J*=8.0Hz, 1.6Hz), 5.18 (1 H, q, *J*=6.4Hz), 2.65 (1 H, br s), 1.43 (3 H, d, *J*=6.4Hz).

6.9 Computational Details

Density Functional Theory (DFT) calculations have been performed using the *Gaussian 03* program.[81] In all calculations, the spin-restricted method was employed. Wave function stability calculations were performed to confirm that the calculated wave functions corresponded to the electronic ground state. The structures of all species (*scheme 6.1*) were optimized using the B3LYP exchange-correlation functional[82,83] with the mixed basis set (DZVP[84] on Ru and TZVP[85] on all other atoms). Tight SCF convergence criteria (10^{-8} a.u.) were used for all calculations. Harmonic frequency calculations with the analytic evaluation of force constants (the *Opt=CalcAll* keyword) were used to determine the nature of the stationary points. Intrinsic reaction coordinate (IRC)[86],[87] calculations were used to confirm the reaction pathways. Free energies of species were evaluated at 298K and 1 atm.

Solvent effects were evaluated at the single-point calculations of the solvation energies using the gas-phase geometries. Solvation energies in THF were calculated using the PCM model[88] with the UFF atomic radii. Gibbs free energies in the solution were estimated by addition of the solvation energy ΔG_{solv} to gas-phase Gibbs free energies.

---

[81] Frisch, M. J.; Trucks, G. W.; Schlegel, H. B.; Scuseria, G. E.; Robb, M. A.; Cheeseman, J. R.; Montgomery, J., J. A.; Vreven, T.; Kudin, K. N.; Burant, J. C.; Millam, J. M.; Lyengar, S. S.; Tomasi, J.; Barone, V.; Mennucci, B.; Cossi, M.; Scalmani, G.; Rega, N.; Petersson, G. A.; Nakatsuji, H.; Hada, M.; Ehara, M.; Toyota, K.; Fukuda, R.; Hasegawa, J.; Ishida, M.; Nakajima, T.; Honda, Y.; Kitao, O.; Nakai, H.; Klene, M.; Li, X.; Knox, J. E.; Hratchian, H. P.; Cross, J. B.; Adamo, C.; Jaramillo, J.; Gomperts, R.; Stratmann, R. E.; Yazyev, O.; Austin, A. J.; Cammi, R.; Pomelli, C.; Ochterski, J. W.; Ayala, P. Y.; Morokuma, K.; Voth, G. A.; Salvador, P.; Dannenberg, J. J.; Zakrzewski, V. G.; Dapprich, S.; Daniels, A. D.; Strain, M. C.; Farkas, O.; Malick, D. K.; Rabuck, A. D.; Raghavachari, K.; Foresman, J. B.; Ortiz, J. V.; Cui, Q.; Baboul, A. G.; Clifford, S.; Cioslowski, J.; Stefanov, B. B.; Liu, G.; Liashenko, A.; Piskorz, P.; Komaromi, I.; Martin, R. L.; Fox, D. J.; Keith, T.; Al-Laham, M. A.; Peng, C. Y.; Nanayakkara, A.; Challacombe, M.; Gill, P. M. W.; Johnson, B.; Chen, W.; Wong, M. W.; Gonzalez, C.; Pople, J. A. *Gaussian 03, Revision C.01*, Gaussian, Inc.: 2003.

[82] Becke, A. D., *J. Chem. Phys.* **1993**, 98, 5648.

[83] Lee, C.; Yang, W.; Parr, R. G., *Phys. Rev.* **1988**, B37, 785.

[84] Godbout, N.; Salahub, D. R.; Andzelm, J.; Wimmer, E., *Can. J. Chem.* **1992**, 70, 560-571.

[85] Schafer, A.; Huber, C.; Ahlrichs, R., *J. Chem. Phys.* **1994**, 100, 5829-5835.

[86] Gonzalez, C.; Schlegel, H. B., *J. Chem. Phys.* **1989**, 90, 2154.

[87] Gonzalez, C.; Schlegel, H. B., *J. Phys. Chem.* **1990**, 94, 5523.

[88] Barone, V.; Cossi, M.; Tomasi, J., *J. Comput. Chem.* **1998**, 19, 404-417.

Alternative mechanisms were not evaluated in this study. However, the energy values and experimental evidence lend support to this type of transfer hydrogenation mechanism taking place for the dehydrogenation of ammonia-boranes.

Scheme 6.1 **The reaction cycle for AB dehydrogenation. The H-H distances are shown in red.**

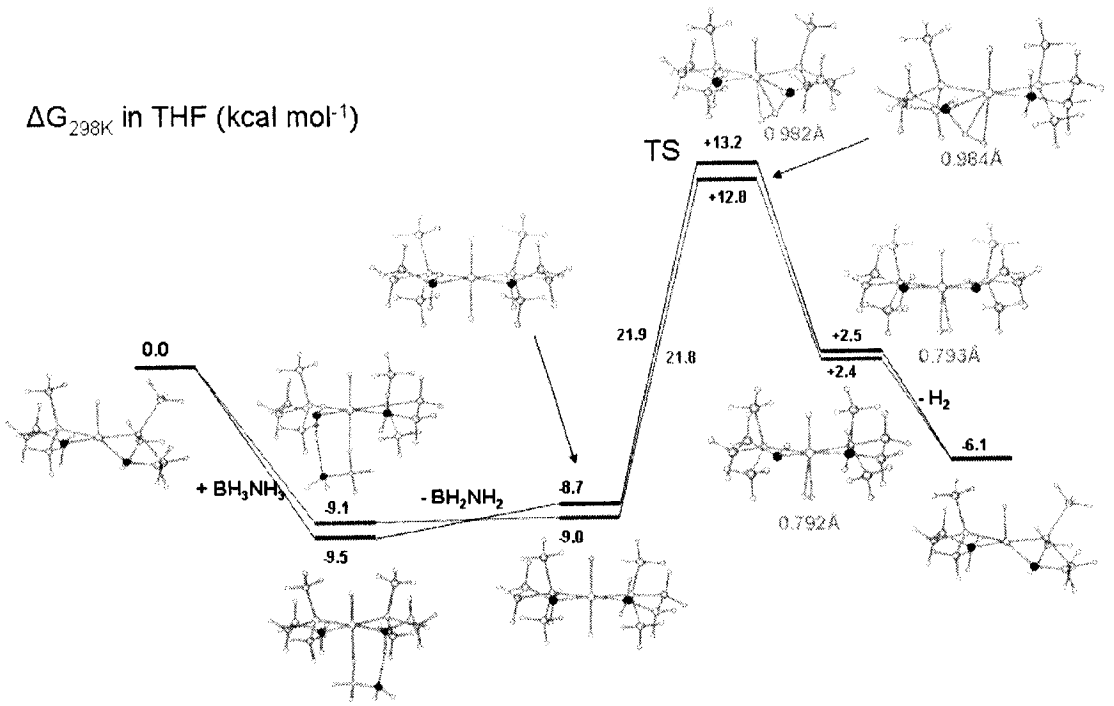

XYZ Atomic coordinates (Å), total electronic energies E(SCF), Gibbs free energies G (at 298K and 1 atm.) and the orbital energies of the highest occupied molecular orbital (HOMO) and the lowest unoccupied molecular orbital (LUMO) for Ru species in Scheme 4.7.

Structure 7

E(SCF)= -5554.586058 G= -5554.314431 a.u.

E(HOMO)= -4.045 eV, E(LUMO)= -0.004 eV, Gap= 4.041 eV

Ru	0.018641	-0.553045	0.105059
P	-1.786489	0.852493	-0.129825
C	-2.034078	1.946241	-1.620766
C	-2.431691	1.998088	1.195788
C	-3.224690	-0.354947	-0.327619
C	-2.928885	-1.626750	0.461014
N	-1.581025	-2.144452	0.117169
H	-3.057504	2.323250	-1.691691
H	-1.350905	2.794717	-1.557941
H	-1.790621	1.383260	-2.522226
H	-3.386401	2.455591	0.925209
H	-2.542873	1.438654	2.124813
H	-1.696889	2.785805	1.370828
H	-4.174081	0.082280	-0.008124
H	-3.314535	-0.587925	-1.392804
H	-2.917110	-1.407393	1.529427
H	-3.704395	-2.380927	0.282380
H	-1.290938	-2.847344	0.788355
H	-1.591088	-2.588183	-0.796997
P	1.876578	0.771531	0.123188
C	2.687941	1.125308	1.757940
C	2.049431	2.427869	-0.706315
C	3.139254	-0.276231	-0.774701

C	2.834974	-1.744343	-0.468104
N	1.389152	-1.951138	-0.472579
H	2.812489	0.187773	2.299278
H	3.660096	1.607934	1.634185
H	2.036219	1.769258	2.349433
H	1.679517	2.359038	-1.729474
H	1.448975	3.165887	-0.171812
H	3.088903	2.764620	-0.721061
H	2.985040	-0.087442	-1.840327
H	4.166000	0.000741	-0.519024
H	3.332006	-2.375679	-1.219392
H	3.294745	-2.007085	0.500374
H	1.188374	-2.945819	-0.424169
H	-0.256993	-0.219678	1.652184

Structure 8

E(SCF)= -5637.891969 G= -5637.550472 a.u.

E(HOMO)= -4.809 eV, E(LUMO)= 0.182 eV, Gap= 4.991 eV

Ru	-0.029869	-0.268014	-0.377174
P	-1.955449	0.830466	0.174076
C	-2.401084	2.519706	-0.454450
C	-2.508186	0.954690	1.944947
C	-3.291110	-0.239922	-0.596975
C	-2.852295	-1.698257	-0.510925
N	-1.474856	-1.868736	-1.042628
H	-3.448533	2.762397	-0.261607
H	-1.773803	3.266361	0.035395
H	-2.205083	2.559377	-1.525552
H	-3.533634	1.321143	2.031506
H	-2.423454	-0.025351	2.414530

H	-1.841299	1.632943	2.479084
H	-4.262443	-0.099090	-0.115761
H	-3.388985	0.067050	-1.642015
H	-2.823428	-2.023898	0.529632
H	-3.560354	-2.346644	-1.038650
H	-1.091721	-2.735814	-0.674511
H	-1.485567	-1.914717	-2.055538
P	1.586577	1.248634	0.154453
C	1.822618	1.933400	1.864923
C	1.839444	2.777583	-0.871022
C	3.183960	0.301251	-0.114460
C	2.976258	-0.720070	-1.230108
N	1.737429	-1.493130	-0.984623
H	1.757094	1.117046	2.583849
H	2.783807	2.441553	1.971241
H	1.024040	2.644247	2.083422
H	1.915724	2.491096	-1.919509
H	0.971342	3.429507	-0.767402
H	2.736052	3.324342	-0.570667
H	4.022989	0.964623	-0.338770
H	3.408466	-0.216403	0.821287
H	2.876990	-0.210911	-2.191271
H	3.847644	-1.383076	-1.294345
H	1.550008	-2.081257	-1.790022
H	1.856505	-2.115353	-0.147496
H	-0.114796	0.442967	-1.852656
H	0.094520	-1.098065	1.299399
N	1.611576	-2.864520	1.514405
H	2.296004	-2.588842	2.210495
H	1.609777	-3.877910	1.514516

B	0.202818	-2.290054	1.801551
H	-0.651636	-3.005440	1.295067
H	-0.049657	-2.071098	2.974637

Structure 8b

E(SCF)= -5637.892949 G= -5637.551597 a.u.

E(HOMO)= -4.816 eV, E(LUMO)= 0.158 eV, Gap= 4.974 eV

Ru	-0.028042	0.281143	-0.351992
P	-1.957794	-0.794858	0.243590
C	-2.295081	-1.381951	1.972308
C	-2.637028	-2.209104	-0.752884
C	-3.273982	0.531319	0.031293
C	-2.863366	1.474750	-1.094569
N	-1.463260	1.923120	-0.899094
H	-3.347856	-1.632705	2.121134
H	-1.690266	-2.266281	2.178167
H	-2.000237	-0.599042	2.670965
H	-3.635178	-2.503673	-0.420861
H	-2.667638	-1.918871	-1.802832
H	-1.965641	-3.064530	-0.664969
H	-4.261451	0.104314	-0.160244
H	-3.327086	1.081160	0.974705
H	-2.907280	0.958357	-2.054996
H	-3.549256	2.328518	-1.142823
H	-1.157819	2.446238	-1.712381
H	-1.388313	2.538049	-0.086088
P	1.588866	-1.264699	0.090060
C	1.819837	-2.746249	-1.007539
C	1.856490	-2.026606	1.763078
C	3.183524	-0.306154	-0.159117

C	2.965410	0.757456	-1.232240
N	1.727115	1.519155	-0.949799
H	1.871852	-2.414611	-2.044085
H	2.721876	-3.306983	-0.752450
H	0.952974	-3.401445	-0.912403
H	1.803236	-1.244289	2.519877
H	1.063756	-2.748963	1.963817
H	2.820466	-2.536435	1.827835
H	3.417266	0.173748	0.794476
H	4.020472	-0.959847	-0.417318
H	3.835378	1.423655	-1.279487
H	2.858055	0.284519	-2.210886
H	1.526168	2.124385	-1.739072
H	-0.150394	-0.366364	-1.851728
N	1.582333	2.864863	1.575155
H	1.847411	2.125326	-0.102186
H	1.501117	3.874494	1.559537
H	2.323999	2.655531	2.234028
B	0.245711	2.180241	1.945308
H	0.129765	1.858649	3.115212
H	0.140645	1.029732	1.357529
H	-0.704950	2.868497	1.588065

Structure 9

E(SCF)= -5555.785500 G= -5555.494074 a.u.

E(HOMO)= -4.240 eV, E(LUMO)= 0.125 eV, Gap= 4.365 eV

Ru	0.000010	-0.579576	0.000226
P	1.755139	0.842385	0.072571
C	2.045482	2.069039	1.442696
C	2.247980	1.879389	-1.395616

C	3.248188	-0.289785	0.273945
C	2.945689	-1.634889	-0.375674
N	1.639833	-2.149065	0.103823
H	3.055367	2.486218	1.417556
H	1.327944	2.886332	1.351670
H	1.871137	1.570840	2.395732
H	3.209158	2.378702	-1.248527
H	2.289695	1.237878	-2.275164
H	1.479937	2.633704	-1.574258
H	4.155162	0.148206	-0.150011
H	3.415377	-0.420622	1.347011
H	2.856718	-1.517914	-1.456606
H	3.754326	-2.348714	-0.174828
H	1.387443	-2.975784	-0.425874
H	1.698805	-2.409764	1.082392
P	-1.755089	0.842427	-0.072521
C	-2.044703	2.069426	-1.442476
C	-2.248746	1.879025	1.395698
C	-3.248002	-0.289675	-0.274967
C	-2.945988	-1.634749	0.374941
N	-1.639877	-2.149082	-0.103759
H	-1.869816	1.571509	-2.395559
H	-3.054635	2.486528	-1.417781
H	-1.327305	2.886774	-1.350834
H	-2.290926	1.237236	2.275020
H	-1.480793	2.633275	1.574986
H	-3.209848	2.378376	1.248244
H	-4.155292	0.148336	0.148297
H	-3.414364	-0.420573	-1.348150
H	-2.857655	-1.517697	1.455921

H	-3.754556	-2.348535	0.173705
H	-1.387727	-2.975566	0.426419
H	-1.698440	-2.410224	-1.082236
H	-0.093563	-0.654710	1.729088
H	0.093598	-0.654294	-1.728642

Structure 9b

E(SCF)= -5555.785449 G= -5555.493434 a.u.

E(HOMO)= -4.240 eV, E(LUMO)= 0.111 eV, Gap= 4.351 eV

Ru	0.000000	-0.576042	-0.085731
P	-1.756451	0.843514	-0.000336
C	-2.107999	2.133069	-1.295794
C	-2.181043	1.807211	1.537490
C	-3.257262	-0.280240	-0.189243
C	-2.926307	-1.654647	0.379871
N	-1.643974	-2.142667	-0.183914
H	-3.116661	2.544634	-1.207827
H	-1.388273	2.947437	-1.198103
H	-1.973424	1.680043	-2.277370
H	-3.148439	2.310074	1.459768
H	-2.180818	1.124992	2.386890
H	-1.406295	2.555012	1.714952
H	-4.144564	0.134954	0.294949
H	-3.471211	-0.359363	-1.259066
H	-2.787965	-1.590382	1.460053
H	-3.743565	-2.359301	0.181659
H	-1.369742	-2.994287	0.292940
H	-1.749242	-2.357556	-1.169697
P	1.756450	0.843514	-0.000334
C	2.181039	1.807209	1.537494

C	2.107998	2.133073	-1.295789
C	3.257263	-0.280237	-0.189243
C	2.926309	-1.654646	0.379866
N	1.643976	-2.142665	-0.183920
H	2.180814	1.124988	2.386892
H	3.148435	2.310072	1.459774
H	1.406290	2.555009	1.714957
H	1.973424	1.680048	-2.277366
H	1.388270	2.947439	-1.198097
H	3.116658	2.544639	-1.207820
H	3.471213	-0.359357	-1.259066
H	4.144564	0.134957	0.294951
H	3.743568	-2.359299	0.181651
H	2.787969	-1.590385	1.460048
H	1.749242	-2.357549	-1.169704
H	1.369745	-2.994289	0.292930
H	-0.000001	-0.553291	-1.823671
H	0.000002	-0.746248	1.634525

Structure 10

Transition state (one imaginary mode at -1202.6 cm^{-1})

E(SCF)= -5555.750166 G= -5555.464033 a.u.

E(HOMO)= -4.439 eV, E(LUMO)= 0.135 eV, Gap= 4.574 eV

Ru	0.008577	-0.560259	-0.011704
P	1.820387	0.834459	0.008250
C	2.056137	2.193375	1.254854
C	2.342485	1.692853	-1.552437
C	3.253875	-0.310540	0.383555
C	2.931313	-1.699196	-0.175807
N	1.603042	-2.107312	0.249921

H	3.071363	2.596229	1.229905
H	1.352064	3.002269	1.052058
H	1.846520	1.798774	2.249055
H	3.299626	2.205936	-1.433293
H	2.417311	0.953193	-2.348552
H	1.578497	2.416699	-1.839108
H	4.196577	0.076619	-0.011220
H	3.337427	-0.362457	1.472415
H	3.017035	-1.659573	-1.275284
H	3.703602	-2.401517	0.174251
P	-1.790822	0.853201	0.000148
C	-2.040113	2.234777	-1.217633
C	-2.398424	1.674197	1.560978
C	-3.229602	-0.285842	-0.424266
C	-2.957716	-1.673559	0.148943
N	-1.601805	-2.135712	-0.241772
H	-1.814138	1.863554	-2.216680
H	-3.057275	2.632606	-1.191495
H	-1.342540	3.042446	-0.989617
H	-2.459571	0.929757	2.355314
H	-1.673668	2.428461	1.871276
H	-3.372969	2.150787	1.429132
H	-4.184713	0.100479	-0.059556
H	-3.288344	-0.337640	-1.515101
H	-2.980363	-1.640125	1.239772
H	-3.728853	-2.381598	-0.176351
H	-1.361933	-2.978797	0.268641
H	-1.574385	-2.361908	-1.230426
H	-0.020917	-0.396011	-1.655432
H	1.369972	-3.028237	-0.100040

H	0.877768	-1.562058	1.347329
H	0.214635	-1.006608	1.815863

Structure 10b

Transition state (one imaginary mode at -1194.8 cm^{-1})

E(SCF)= -5555.749872 G= -5555.463478 a.u.

E(HOMO)= -4.437 eV, E(LUMO)= 0.109 eV, Gap= 4.546 eV

Ru	0.009614	-0.560131	-0.074273
P	-1.804948	0.838172	-0.072871
C	-2.253784	1.975061	-1.478691
C	-2.211660	1.934014	1.375196
C	-3.265544	-0.355487	-0.098986
C	-2.863413	-1.666352	0.569928
N	-1.581873	-2.159481	0.005727
H	-3.272320	2.361162	-1.390909
H	-1.559461	2.816499	-1.496642
H	-2.148364	1.431841	-2.417985
H	-3.194448	2.401410	1.278876
H	-2.170451	1.341843	2.288850
H	-1.453696	2.715284	1.452162
H	-4.151008	0.066740	0.382690
H	-3.519776	-0.534266	-1.148094
H	-2.694162	-1.506194	1.635022
H	-3.659616	-2.412369	0.462044
H	-1.214796	-2.909544	0.581287
H	-1.727338	-2.537136	-0.925596
P	1.808510	0.845404	0.066237
C	2.243057	1.618431	1.697219
C	2.102641	2.275134	-1.086261
C	3.269932	-0.267859	-0.297415

C	2.931246	-1.689002	0.161207
N	1.629916	-2.075607	-0.357536
H	2.281993	0.836297	2.454358
H	3.201081	2.141864	1.655692
H	1.460362	2.322259	1.983708
H	1.962275	1.938145	-2.113333
H	1.376970	3.064355	-0.882671
H	3.109101	2.684824	-0.973118
H	3.411226	-0.255579	-1.381510
H	4.186509	0.101684	0.169118
H	3.725731	-2.365239	-0.190175
H	2.960137	-1.715195	1.264098
H	1.395954	-3.027617	-0.104008
H	-0.082384	-0.496254	1.569786
H	0.949786	-1.470452	-1.456559
H	0.299106	-0.900255	-1.920077

Structure 11

E(SCF)= -5555.765671 G= -5555.478526 a.u.

E(HOMO)= -3.799 eV, E(LUMO)= 0.086 eV, Gap= 3.885 eV

Ru	-0.028241	-0.534012	-0.127800
P	-1.892249	0.804052	-0.070656
C	-2.308666	2.038723	-1.396371
C	-2.267727	1.792678	1.455217
C	-3.295493	-0.422997	-0.158093
C	-2.802176	-1.707880	0.507845
N	-1.531333	-2.098289	-0.090541
H	-3.321236	2.431629	-1.278438
H	-1.599804	2.867477	-1.360234
H	-2.223372	1.557937	-2.371256

H	-3.258664	2.249140	1.402554
H	-2.215571	1.132680	2.320299
H	-1.519429	2.576451	1.580241
H	-4.211516	-0.031993	0.293302
H	-3.484706	-0.614856	-1.217891
H	-2.755013	-1.529256	1.599773
H	-3.566849	-2.488489	0.360814
P	1.823940	0.866763	0.059799
C	2.000919	2.135059	1.408275
C	2.631771	1.793461	-1.348027
C	3.186490	-0.350865	0.528742
C	2.936902	-1.689242	-0.161459
N	1.546974	-2.142565	0.088433
H	1.667561	1.697509	2.348877
H	3.030195	2.487152	1.509926
H	1.358962	2.988491	1.184664
H	2.780734	1.116123	-2.190191
H	1.964257	2.590916	-1.678436
H	3.592337	2.230063	-1.062949
H	4.181591	0.028316	0.282620
H	3.142354	-0.480487	1.613836
H	3.050350	-1.581170	-1.242397
H	3.667664	-2.435557	0.171321
H	1.311903	-2.935018	-0.500356
H	1.439704	-2.444486	1.051030
H	-0.084557	-0.466190	1.490942
H	-1.176058	-2.872803	0.466934
H	-0.246953	-1.084865	-1.946566
H	0.141776	-0.402036	-2.044394

Structure 11b

E(SCF)= -5555.765032 G= -5555.477959 a.u.

E(HOMO)= -3.792 eV, E(LUMO)= 0.048 eV, Gap= 3.839 eV

Ru	0.031989	-0.534136	-0.210215
P	-1.829449	0.855321	-0.006082
C	-2.441400	2.133393	-1.220461
C	-2.152147	1.763433	1.587229
C	-3.260620	-0.372092	-0.049576
C	-2.806115	-1.711752	0.521732
N	-1.548613	-2.153042	-0.133105
H	-3.447158	2.488515	-0.981855
H	-1.758376	2.984347	-1.216596
H	-2.439105	1.705977	-2.223934
H	-3.164564	2.171643	1.630747
H	-1.991877	1.083032	2.423006
H	-1.436913	2.581737	1.684096
H	-4.137694	-0.002815	0.488109
H	-3.549268	-0.494146	-1.098193
H	-2.587513	-1.609976	1.585272
H	-3.596734	-2.463247	0.413135
H	-1.126397	-2.910558	0.392604
H	-1.741840	-2.513230	-1.062792
P	1.875432	0.817570	0.005814
C	2.147161	1.748249	1.588838
C	2.344971	2.110854	-1.244652
C	3.301479	-0.385384	-0.050928
C	2.780165	-1.716931	0.491337
N	1.562487	-2.071119	-0.225505
H	2.063450	1.051253	2.421841
H	3.129003	2.226228	1.608888

H	1.375891	2.510973	1.705060
H	2.327552	1.665773	-2.239901
H	1.617858	2.924110	-1.221124
H	3.340394	2.517497	-1.051584
H	3.573778	-0.507315	-1.102752
H	4.173276	-0.012976	0.493758
H	3.563062	-2.479267	0.345302
H	2.653548	-1.614093	1.586835
H	1.204006	-2.922126	0.204298
H	0.035219	-0.575506	1.407718
H	0.335692	-0.955561	-2.048683
H	-0.090632	-0.291119	-2.120608

Appendix

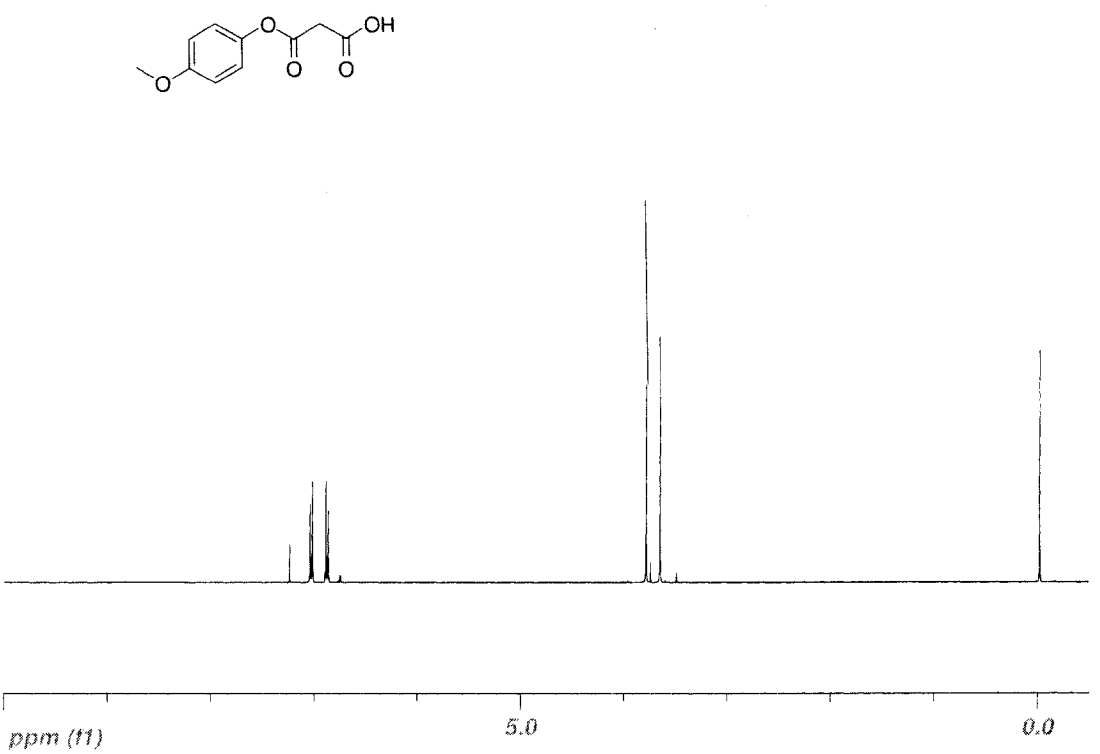
OH
O
O
O
O
ppm (f1)
5.0
0.0

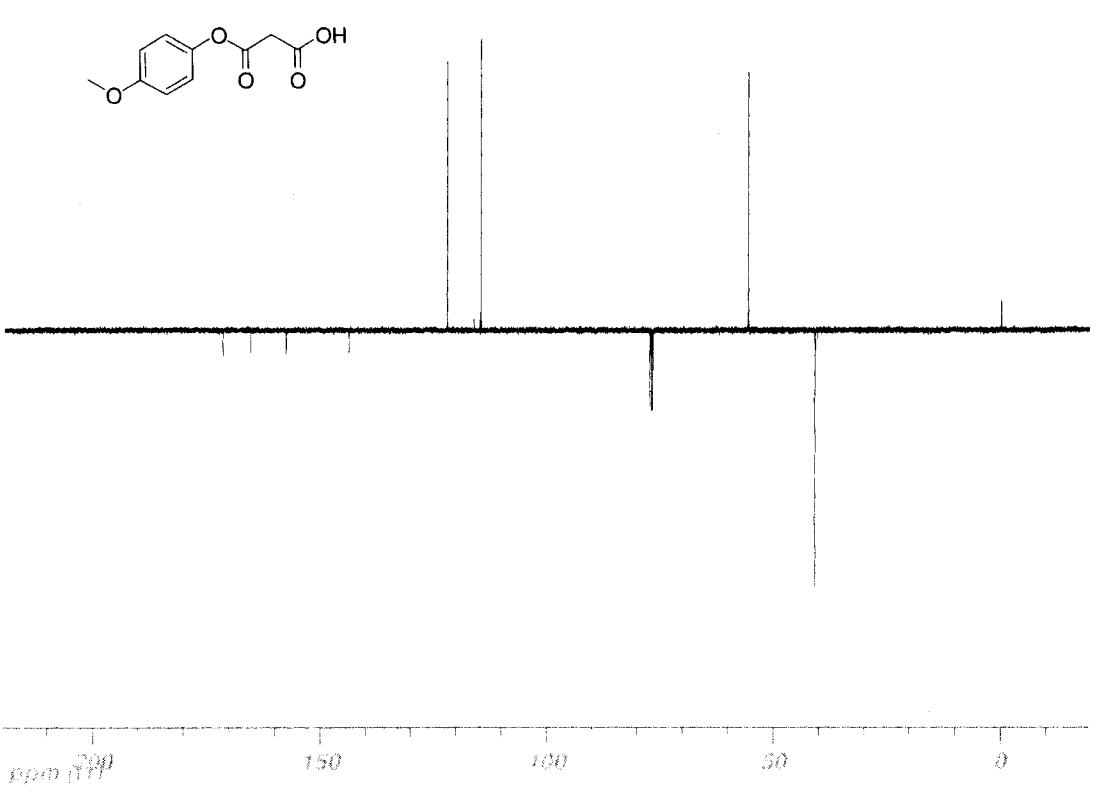
OH
O
O
O
O
200
150
100
50
0

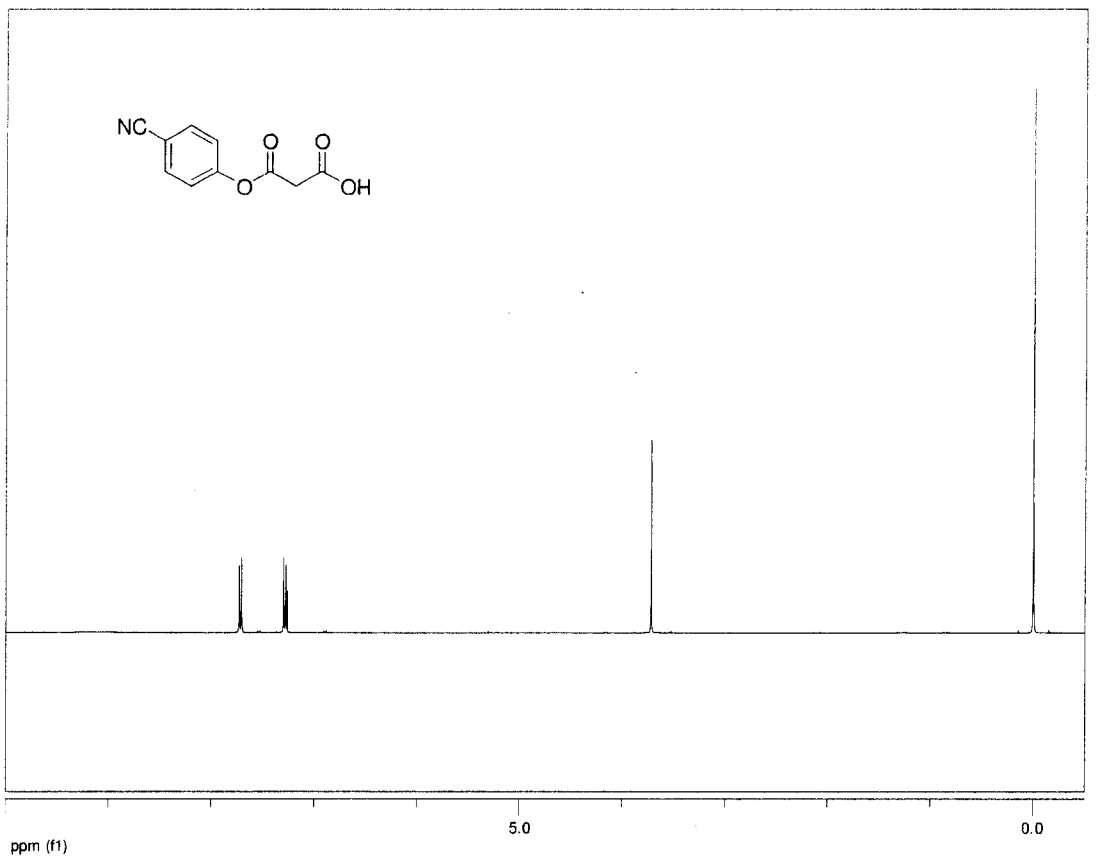
NC
O
O
O
OH
5.0
0.0
ppm (f1)

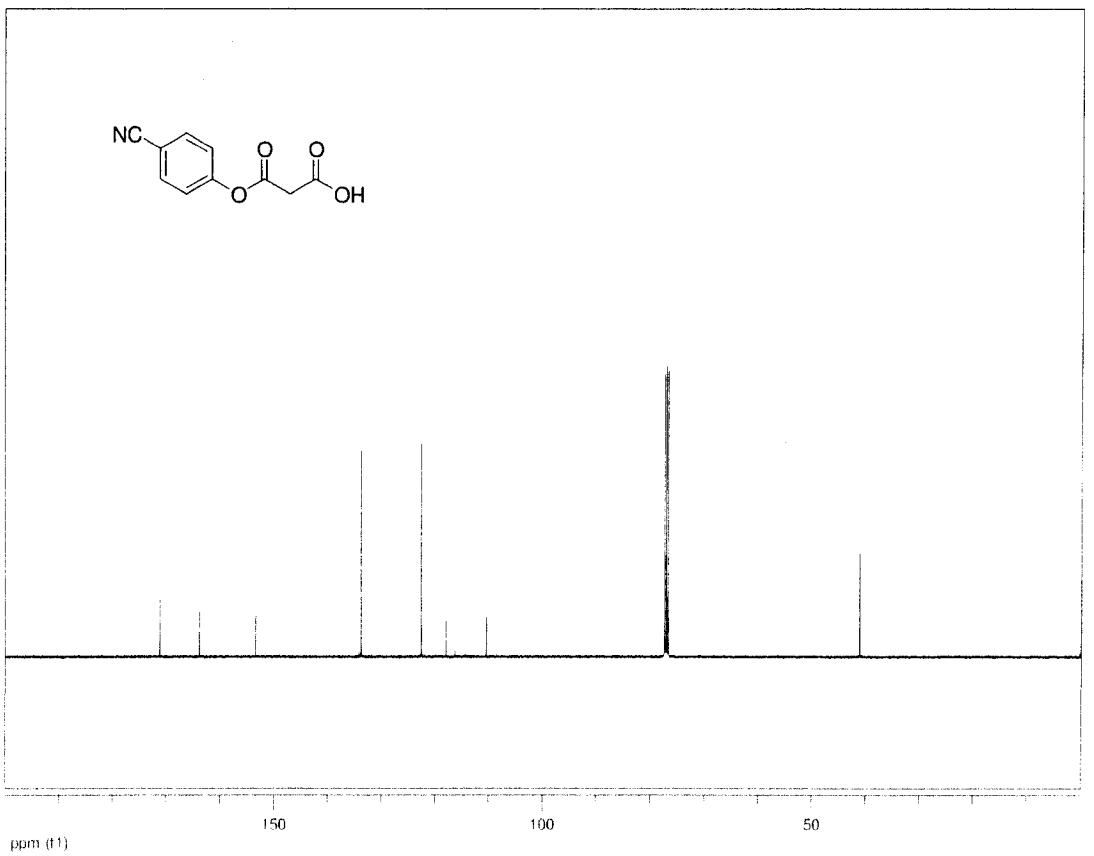
NC
O
O
O
OH
150
100
50
ppm (f1)

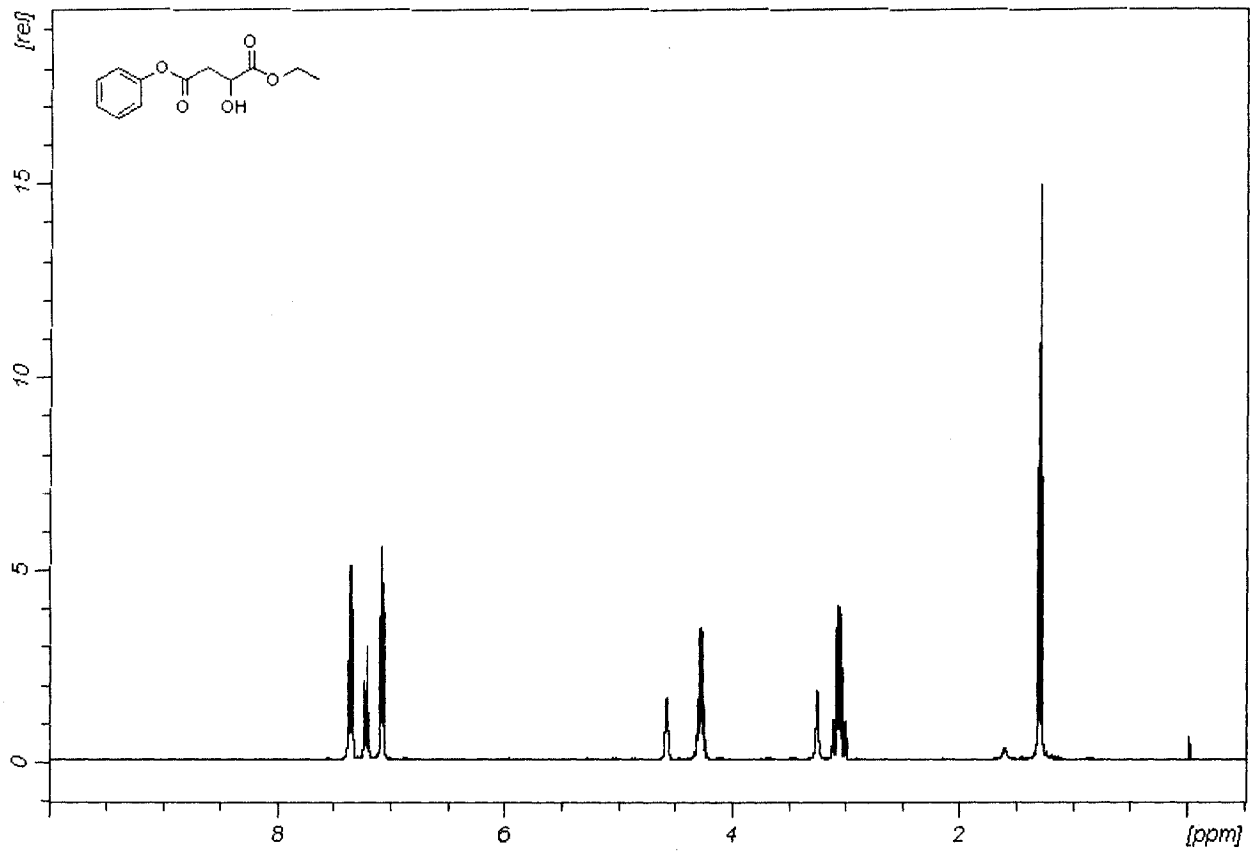
[rel]
15
10
5
0
8
6
4
2
[ppm]
O
O
O
O
OH

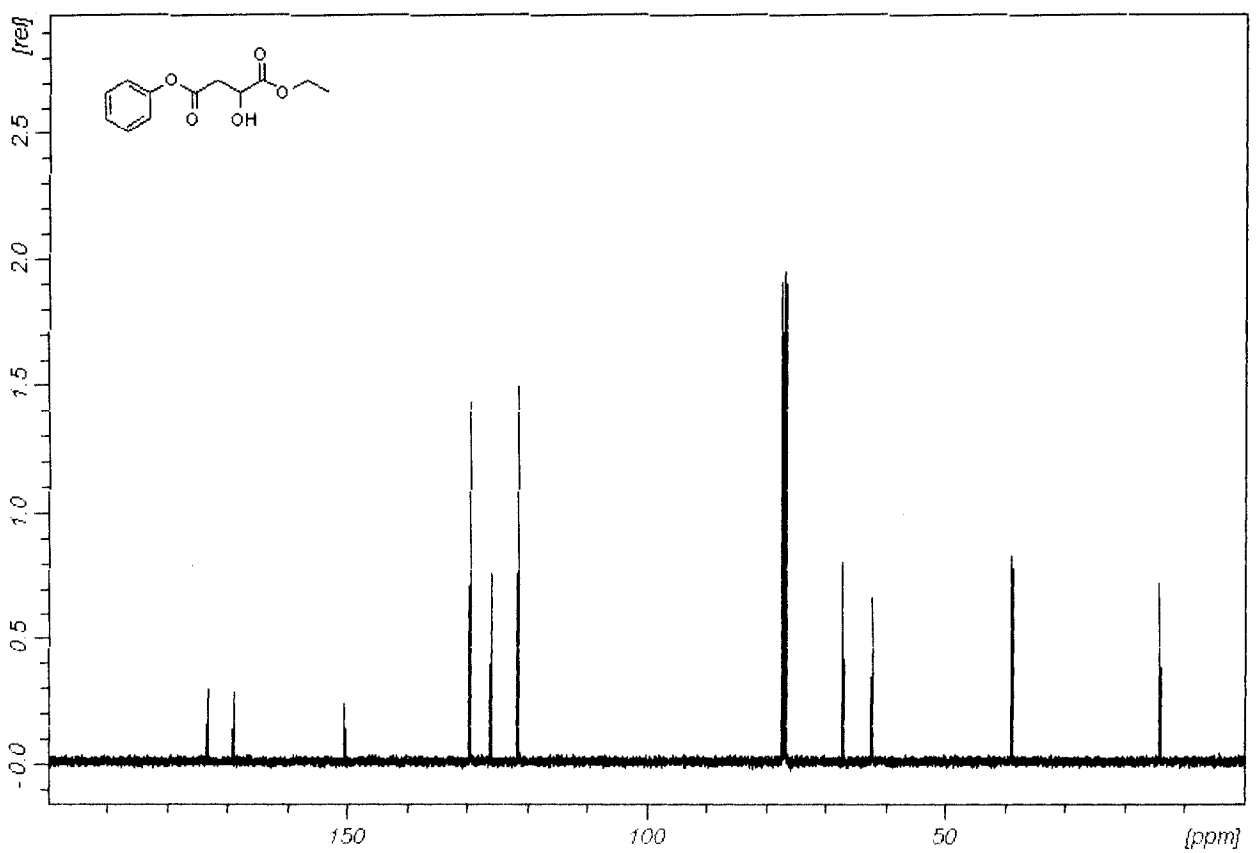
[rel]
2.5
2.0
1.5
1.0
0.5
-0.0
150
100
50
[ppm]
O
O
O
O
OH

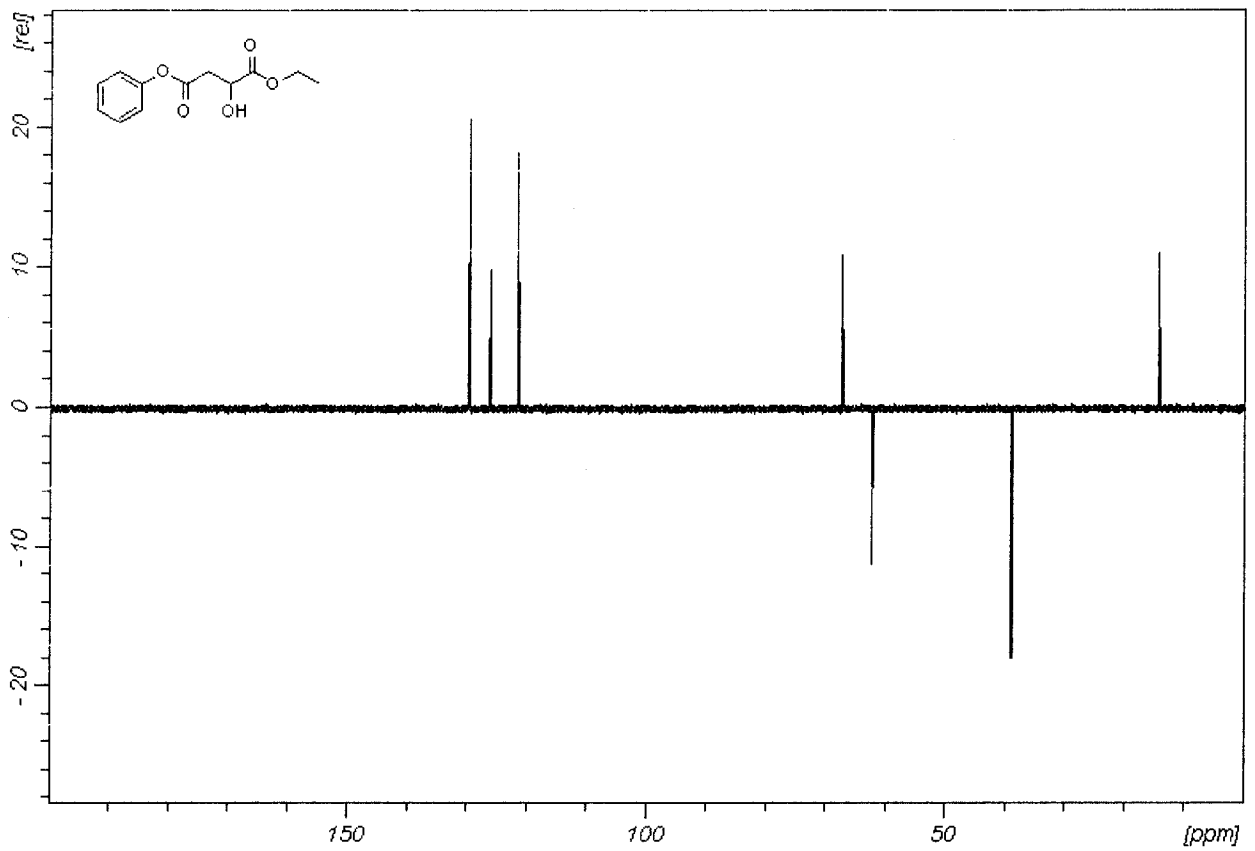
[rel]
20
10
0
-10
-20
150
100
50
[ppm]
O
O
O
O
OH

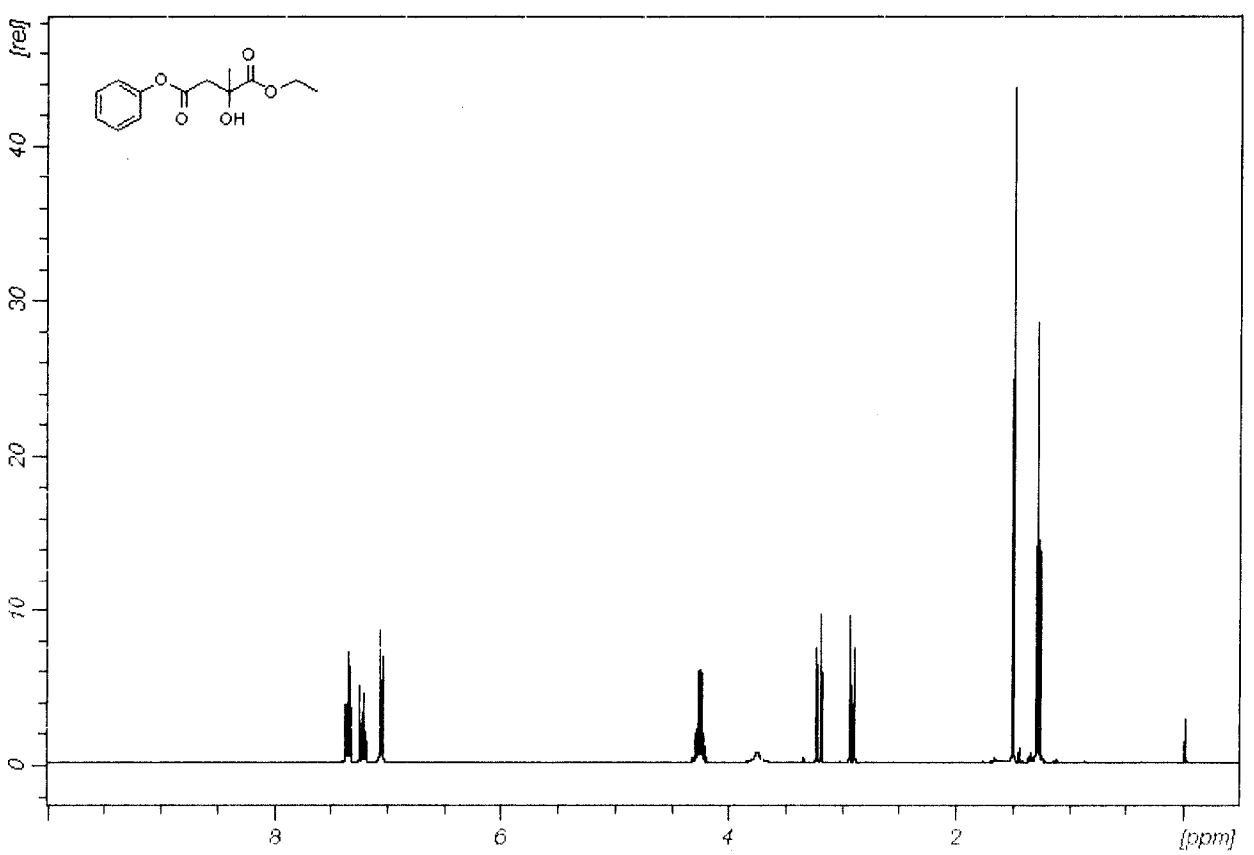
[rel]
40
30
20
10
0
8
6
4
2
[ppm]
O
O
O
O
OH

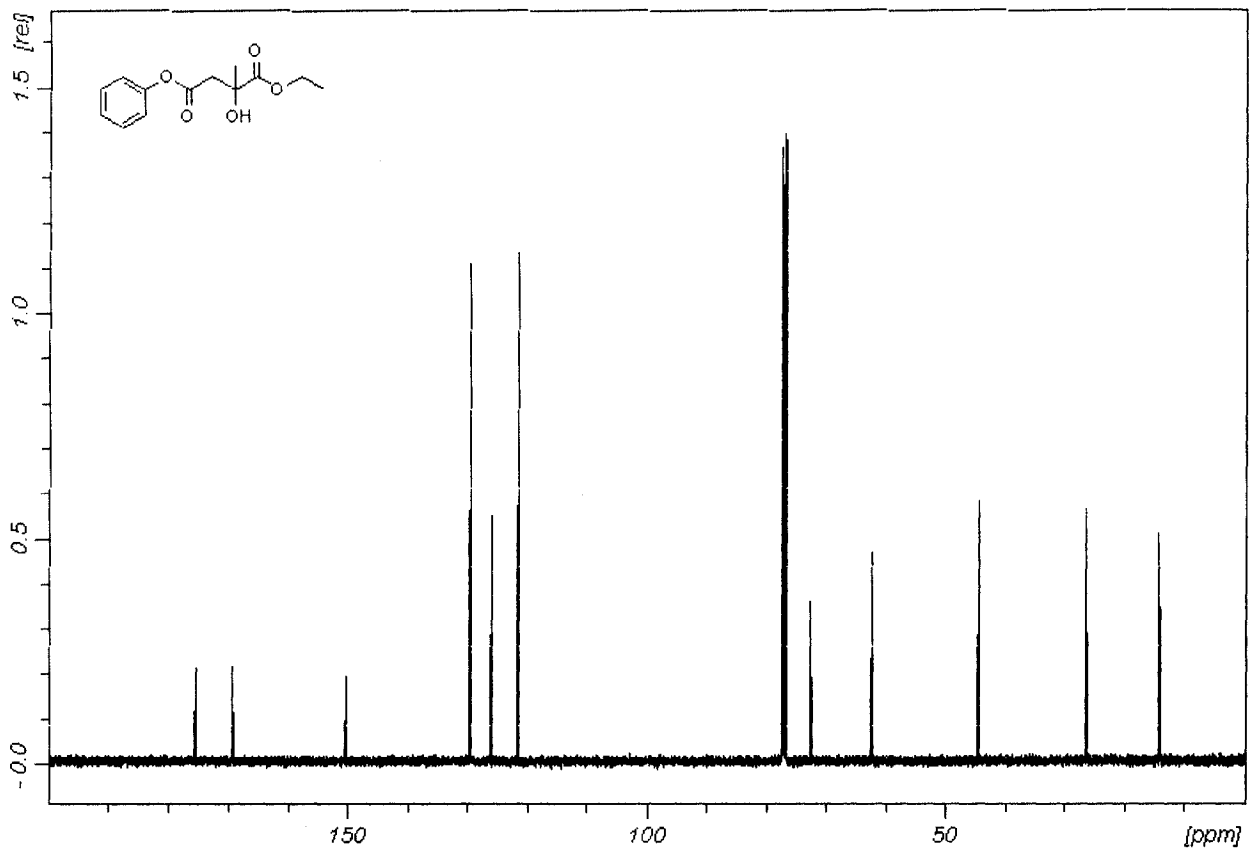
1.5 [rel]
1.0
0.5
-0.0
150
100
50
[ppm]
O
O
O
O
OH

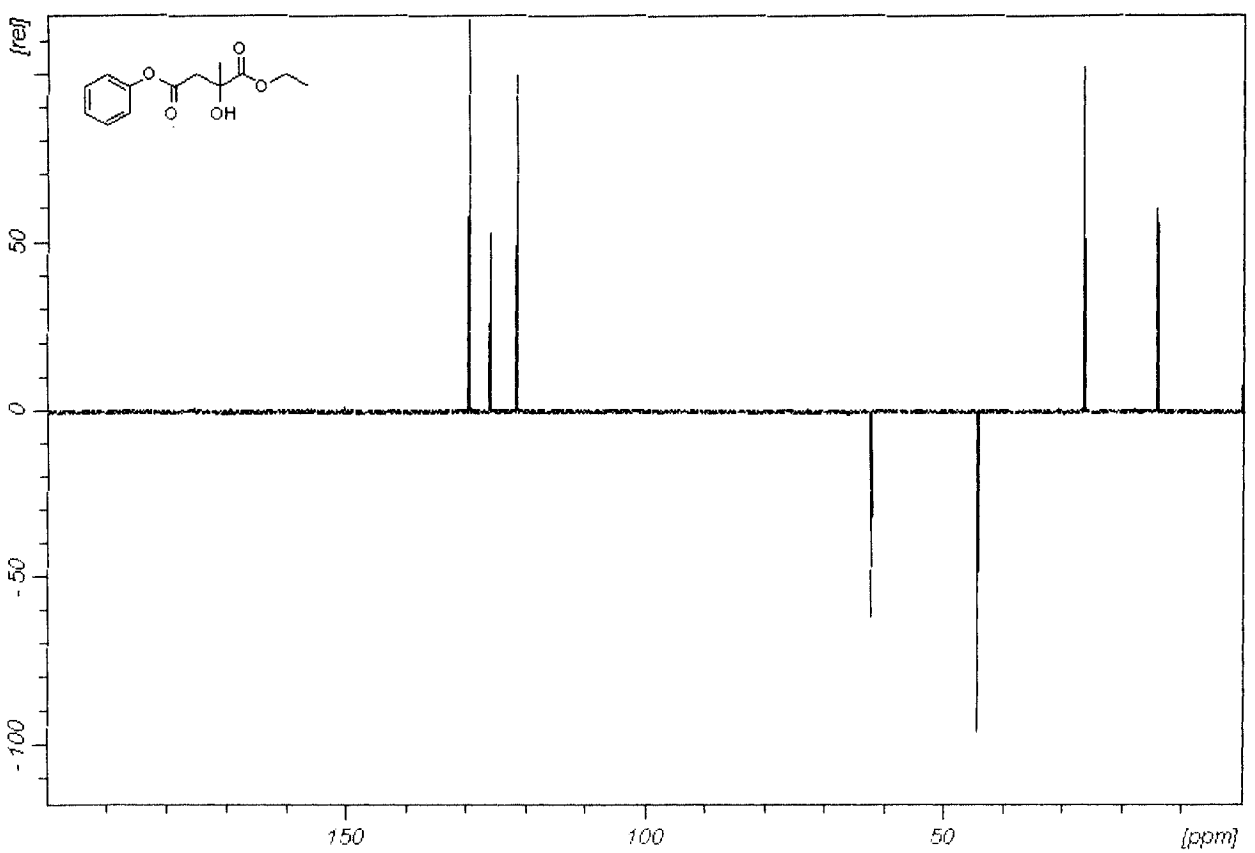
[rel]
50
0
-50
-100
150
100
50
[ppm]
O
O
O
O
OH

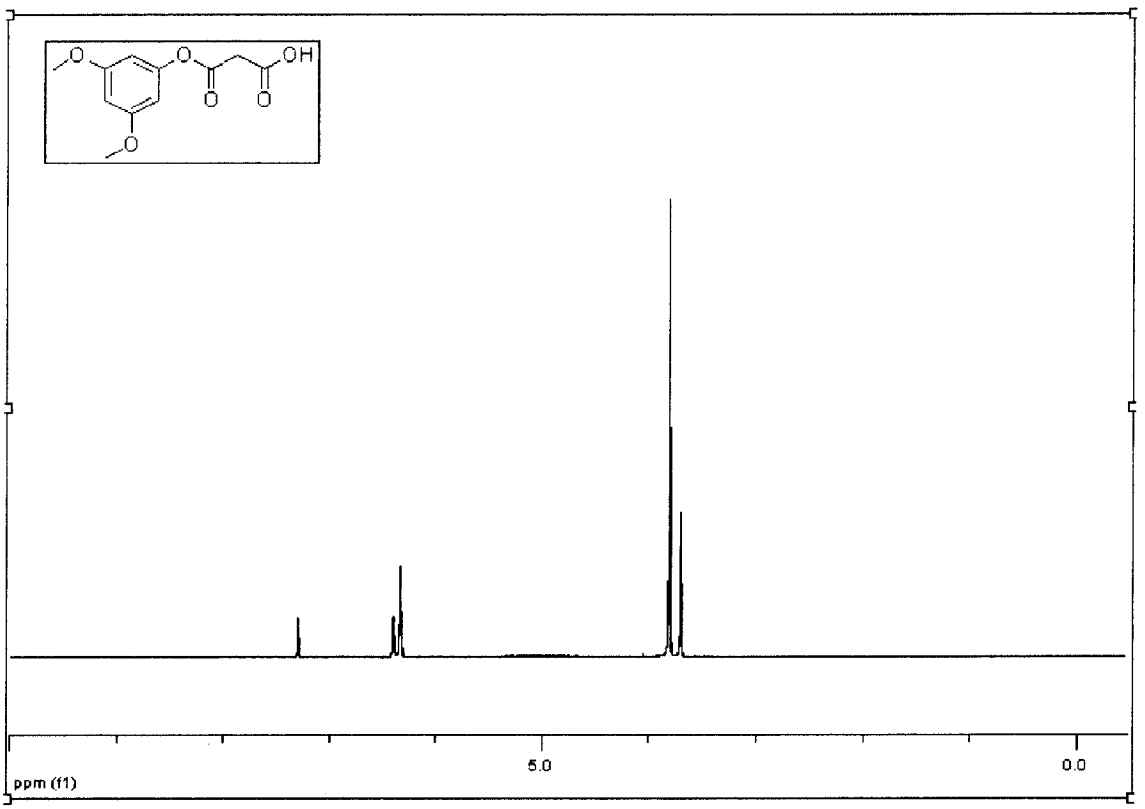
O
O
OH
O
O
O
5.0
0.0
ppm (f1)

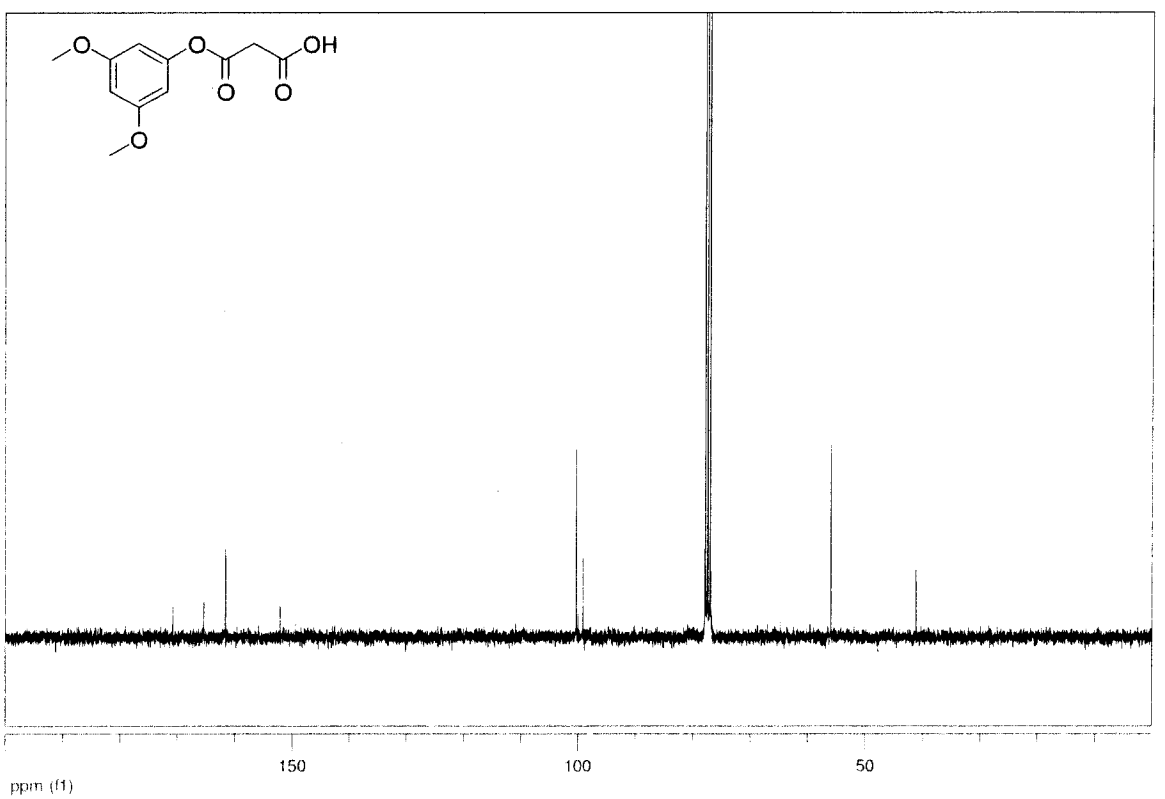
O
O
OH
O
O
O
150
100
50
ppm (f1)

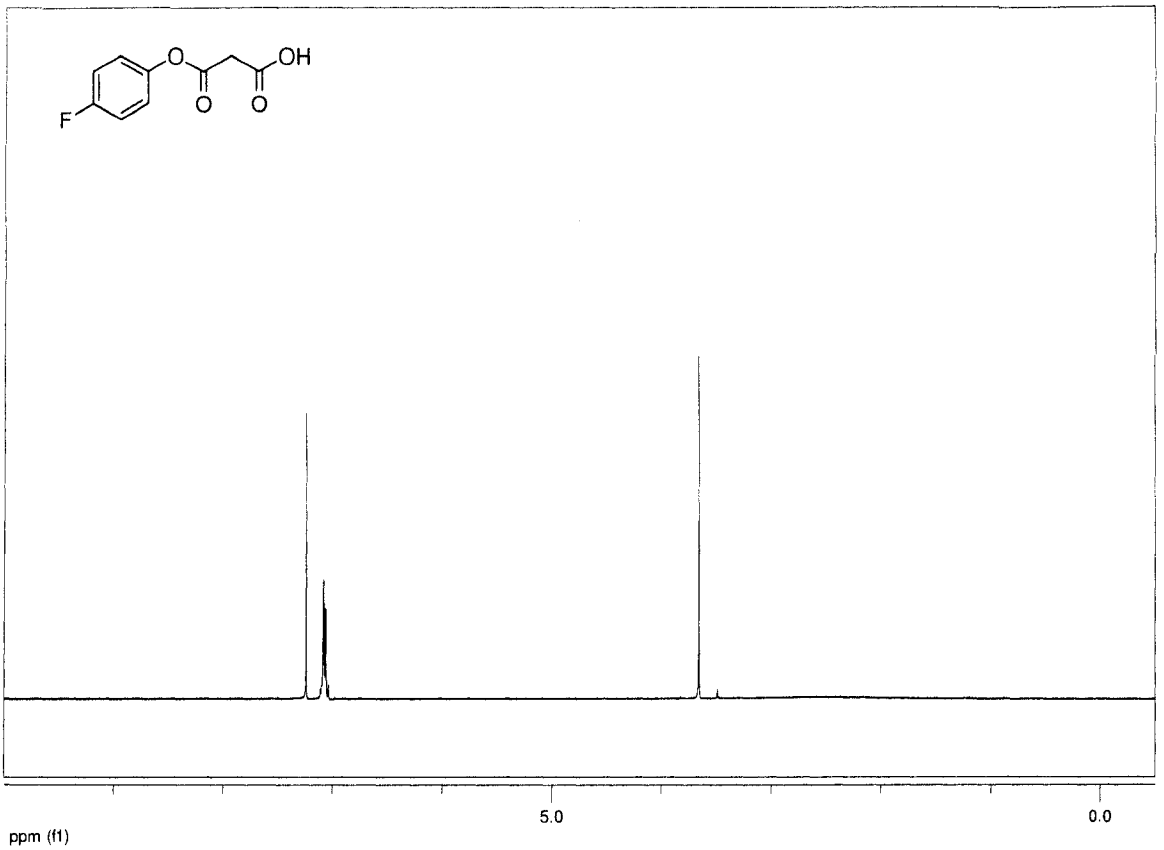
O
OH
F
O
O
5.0
0.0
ppm (f1)

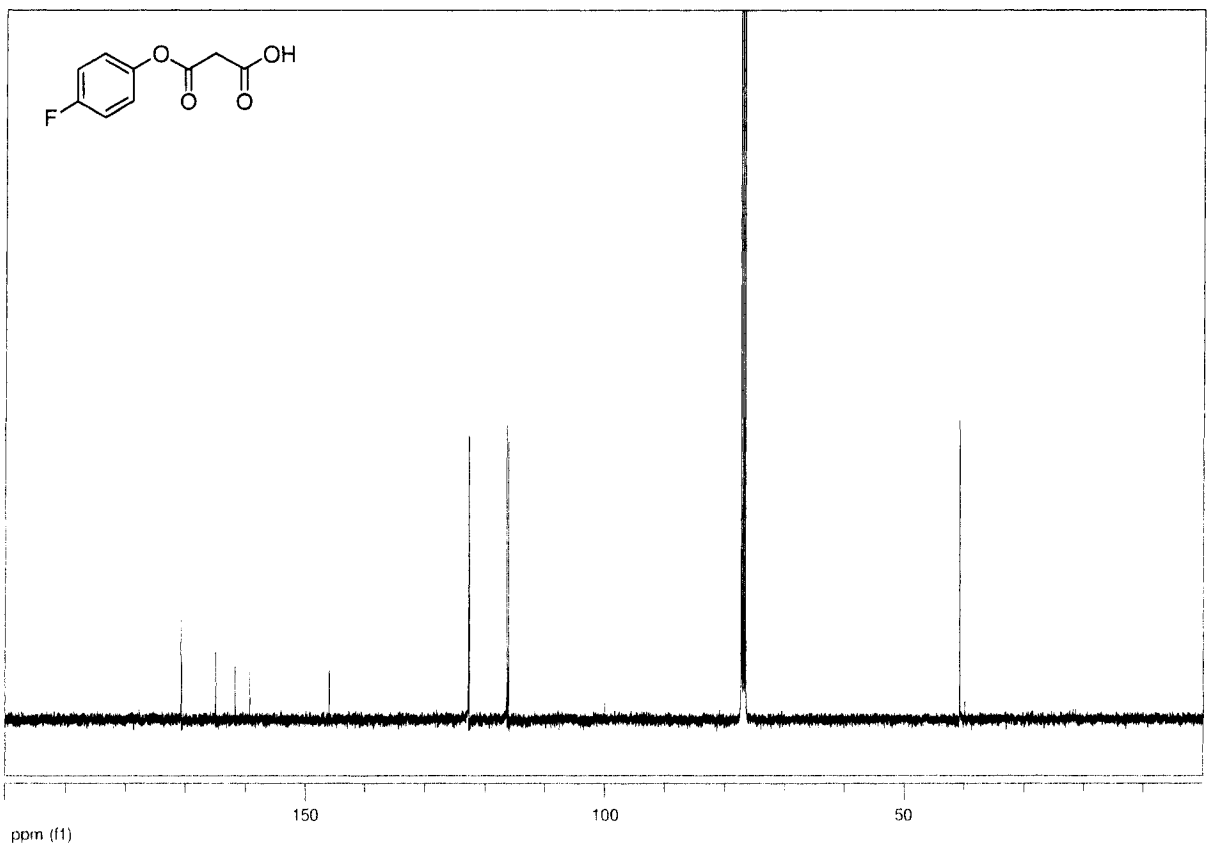
O
OH
F
O
O
150
100
50
ppm (f1)

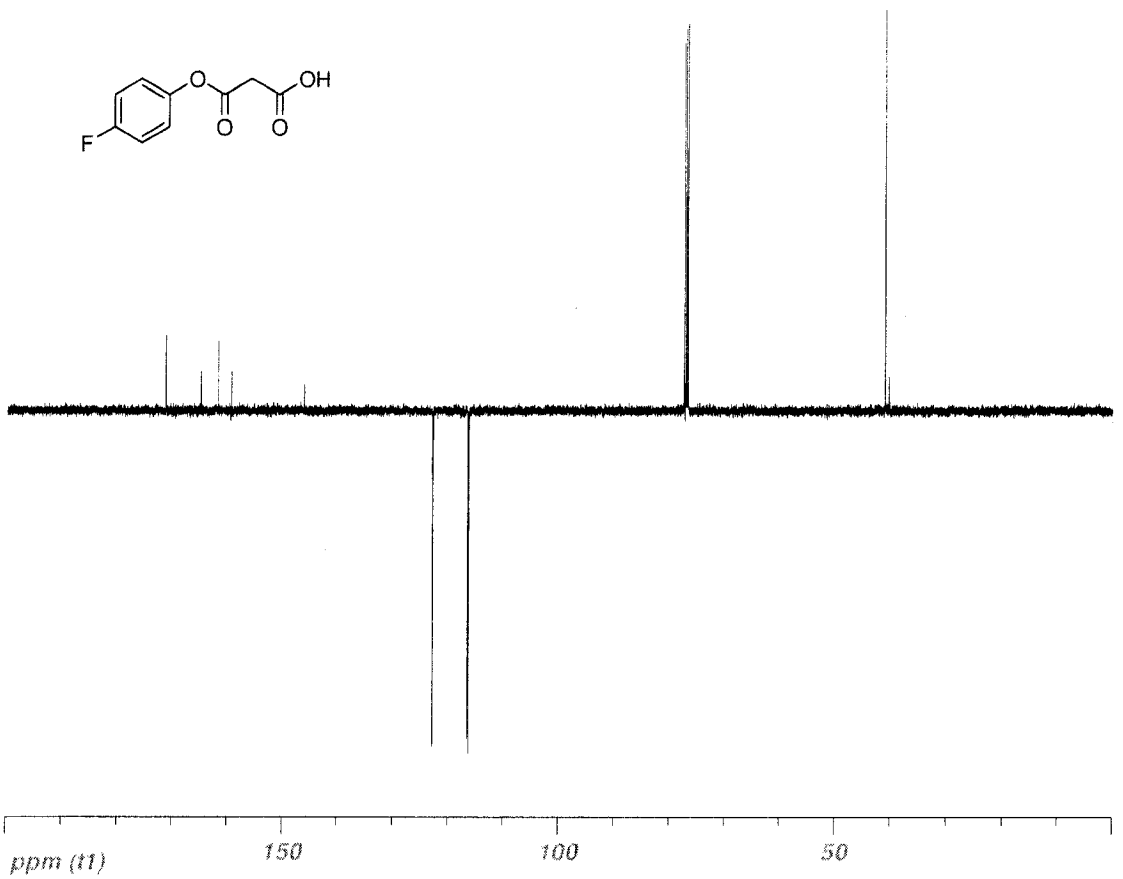
F
O
O
O
OH
ppm (t1)
150
100
50

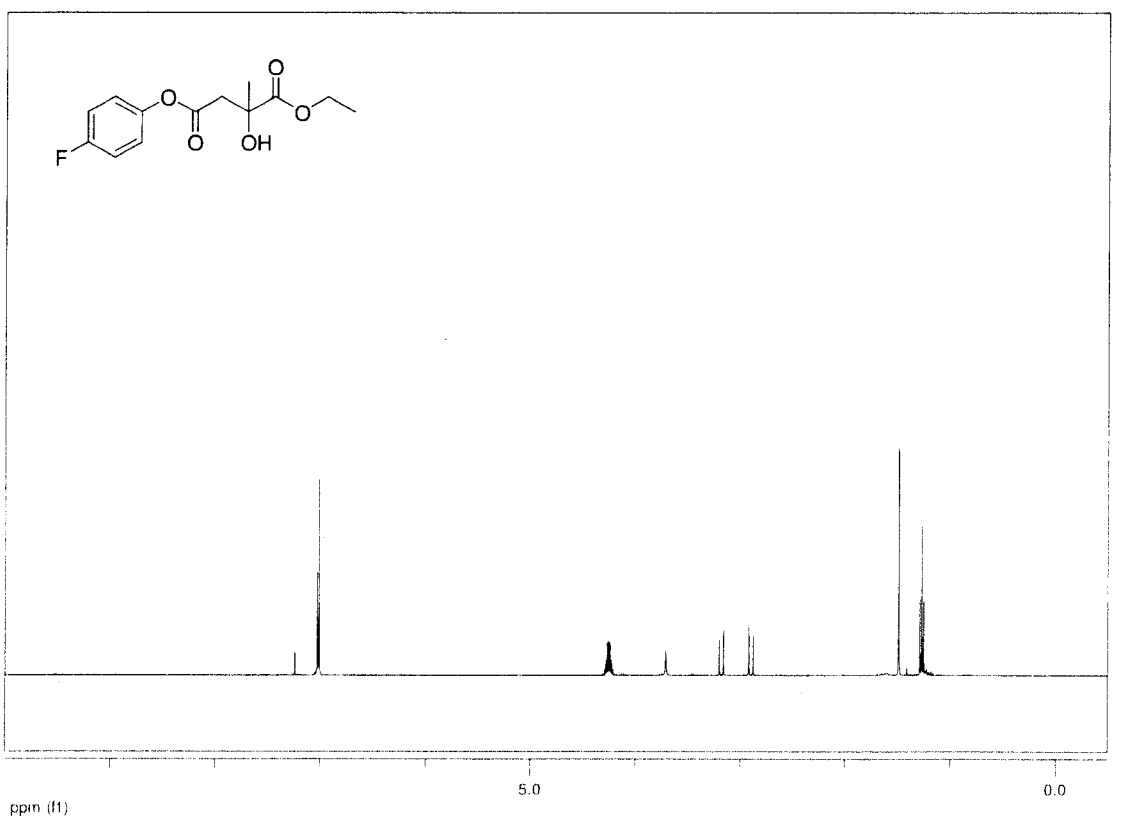
F
O
O
O
OH
O
O
5.0
0.0
ppm (f1)

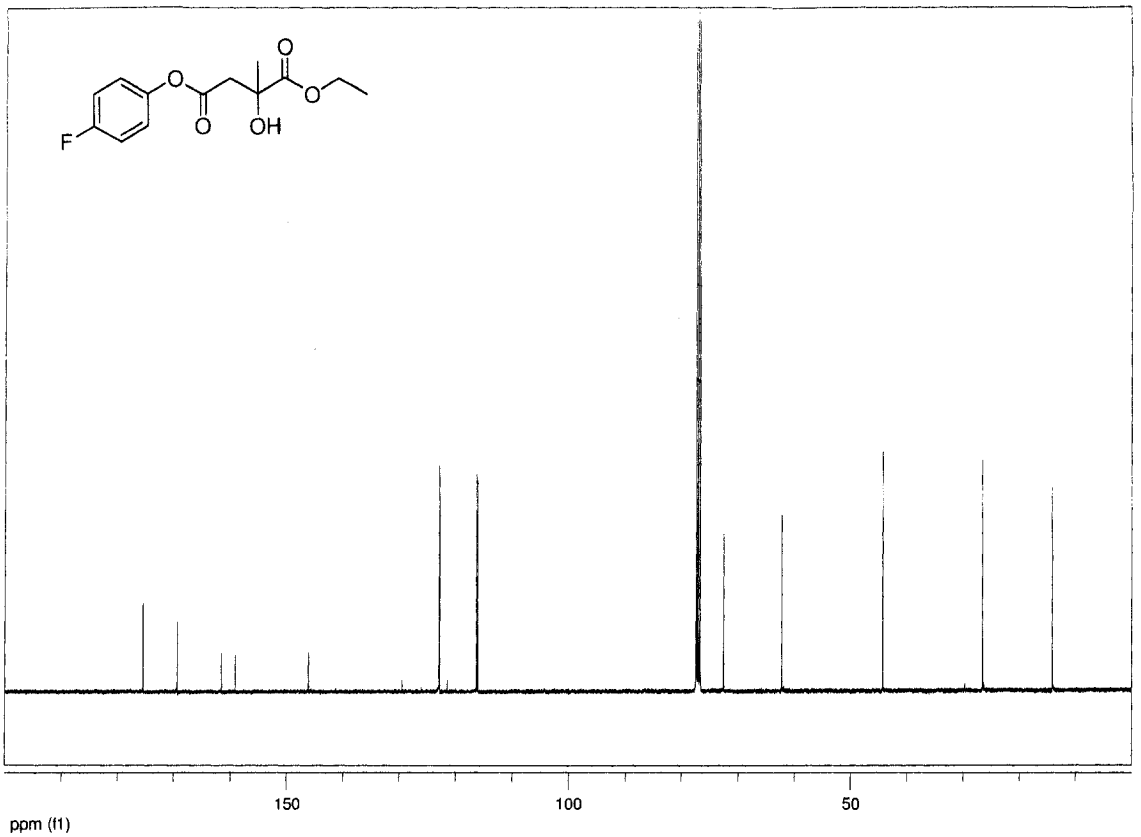
F
O
O
O
O
OH
150
100
50
ppm (f1)

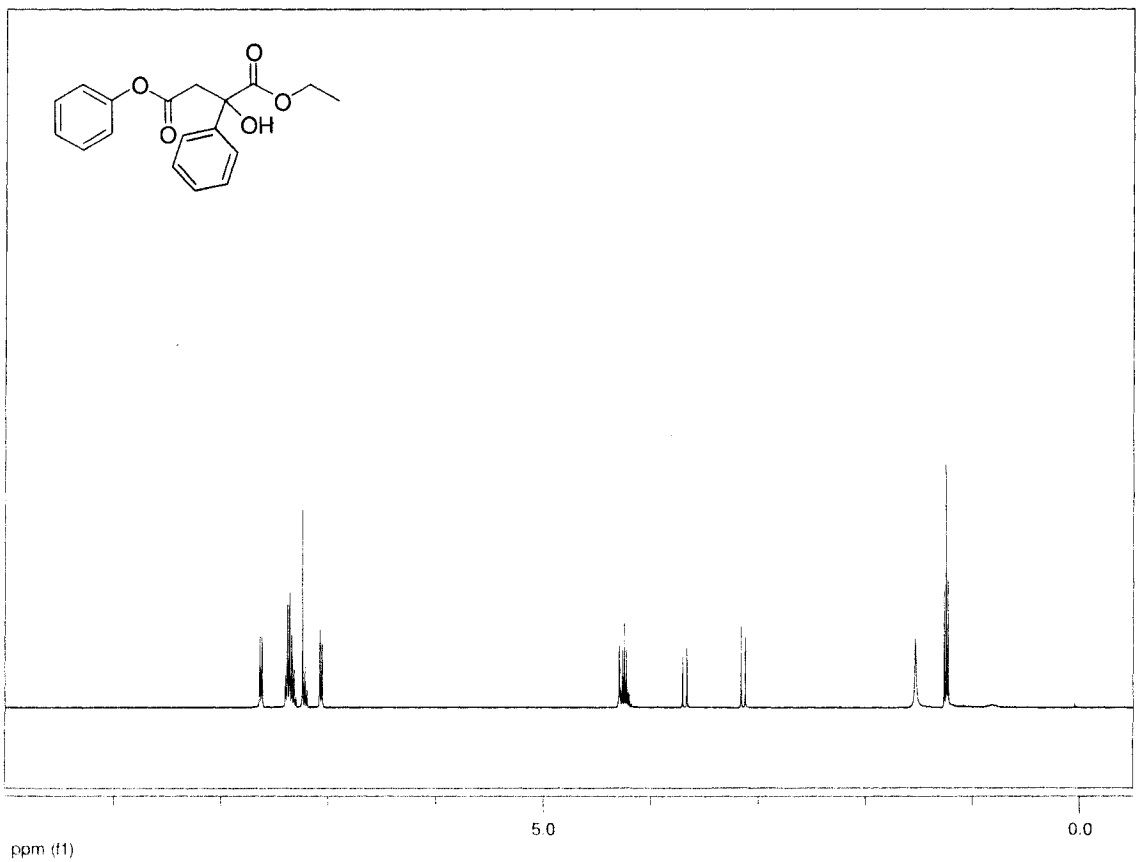
O
O
O
O
OH
5.0
0.0
ppm (f1)

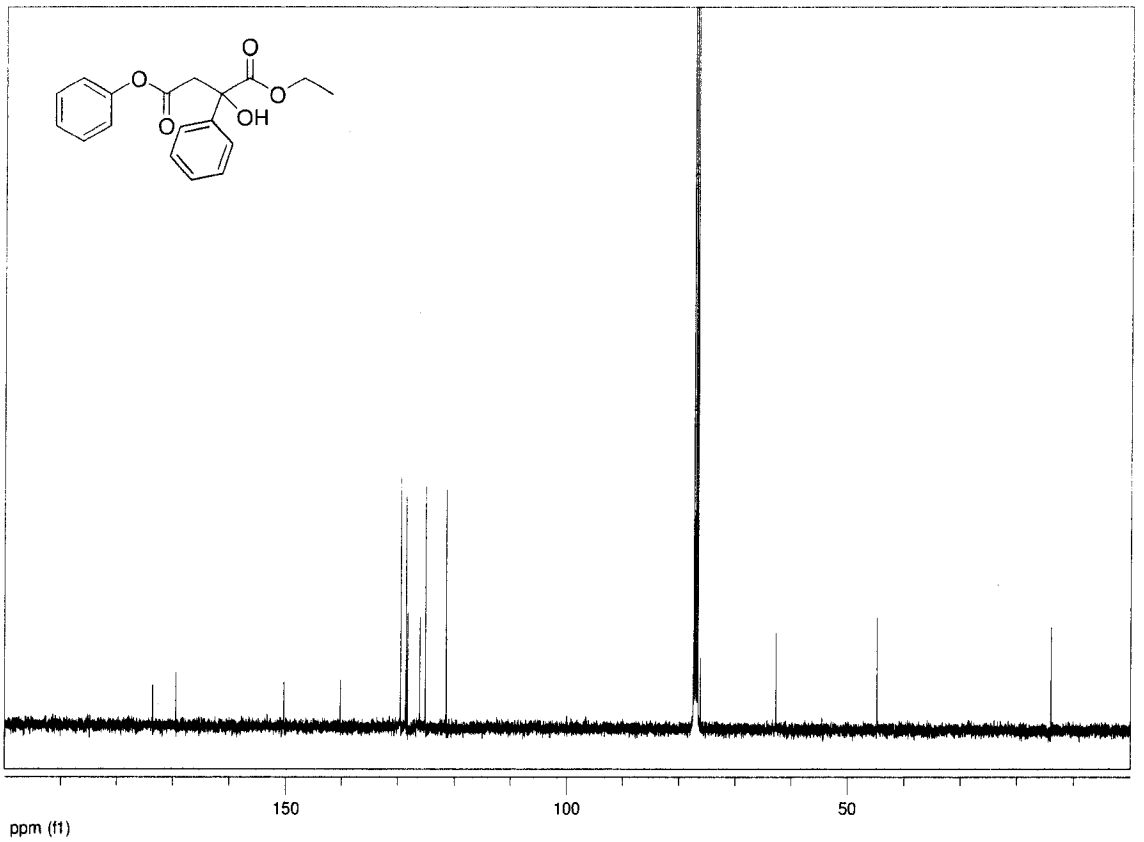
O
O
O
O
OH
150
100
50
ppm (f1)

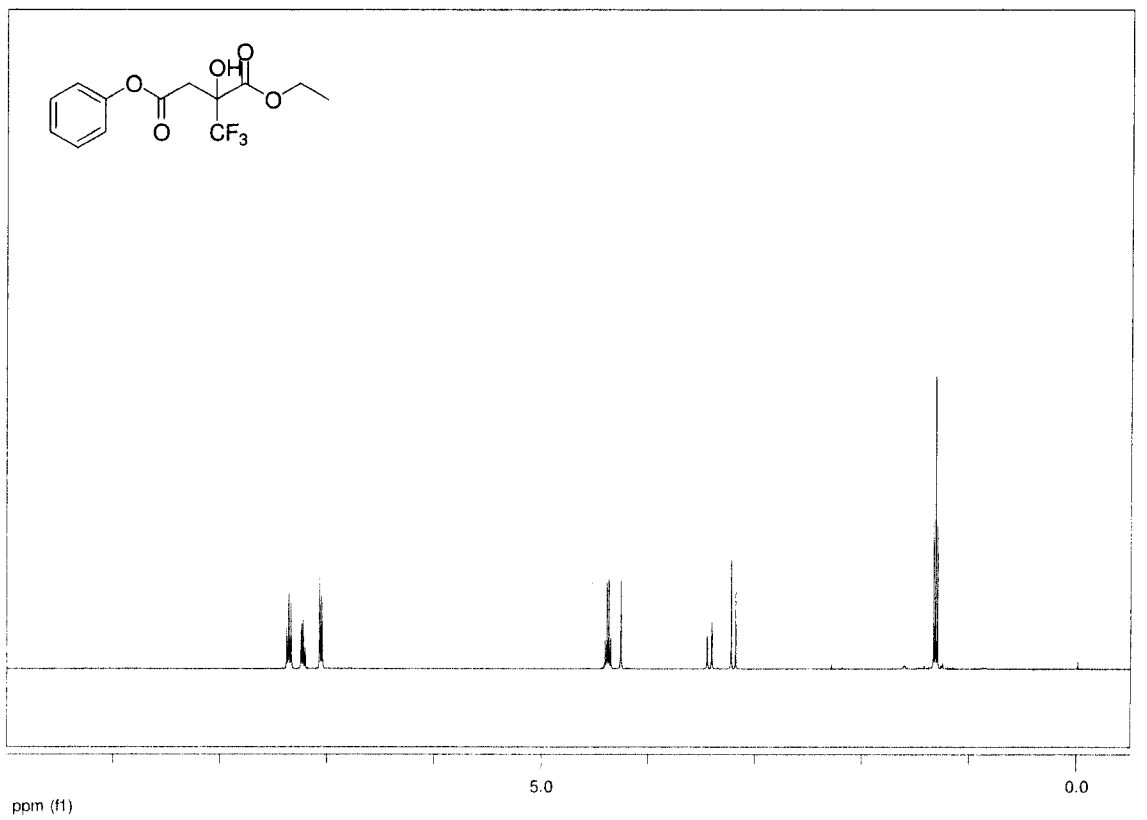
OH
O
O
O
CF3
5.0
0.0
ppm (f1)

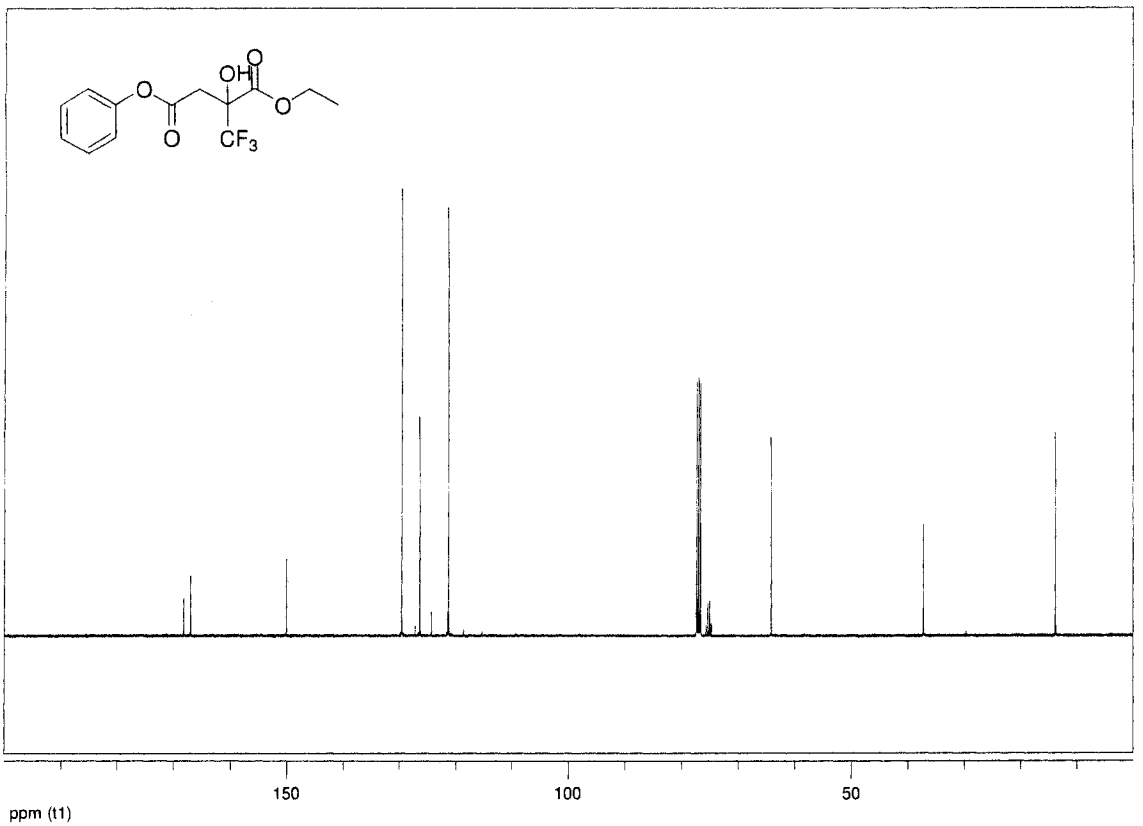
OH
O
O
O
O
CF_3
150
100
50
ppm (t1)

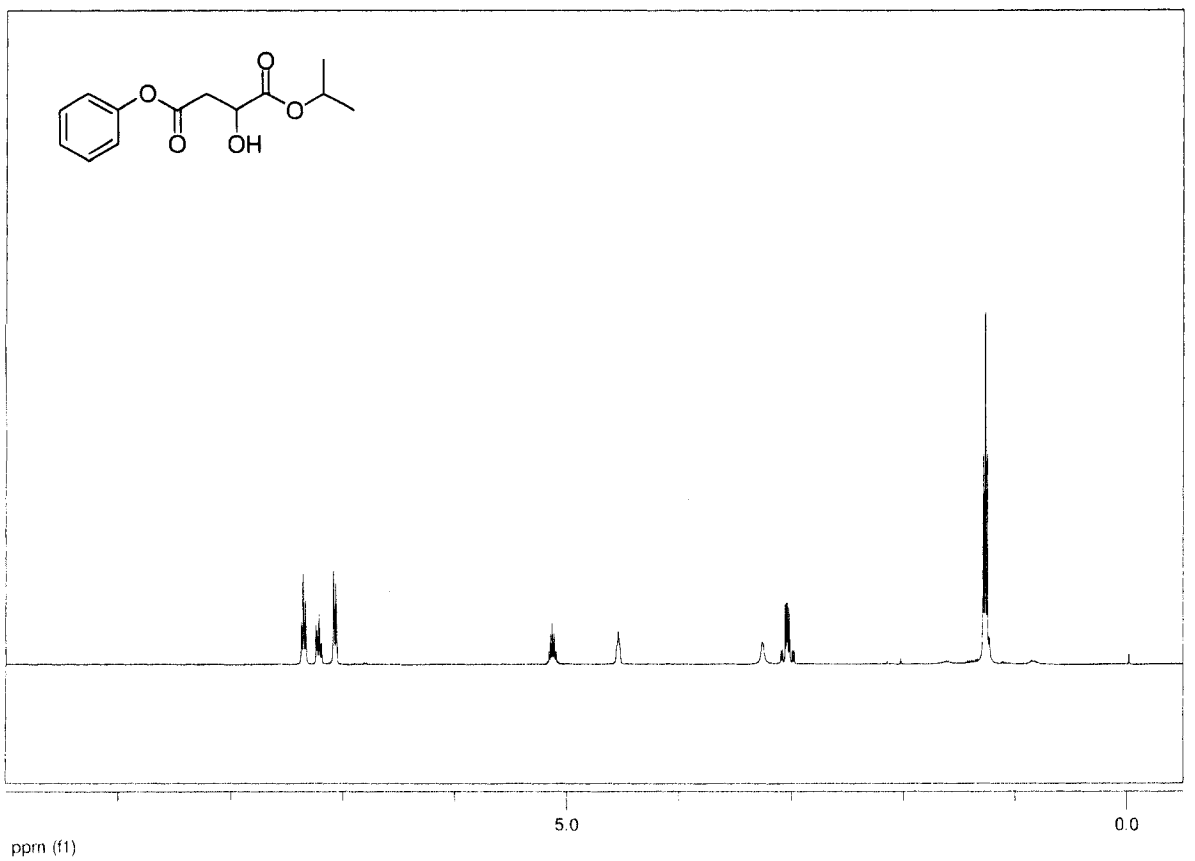
O
O
O
O
OH
5.0
0.0
ppm (f1)

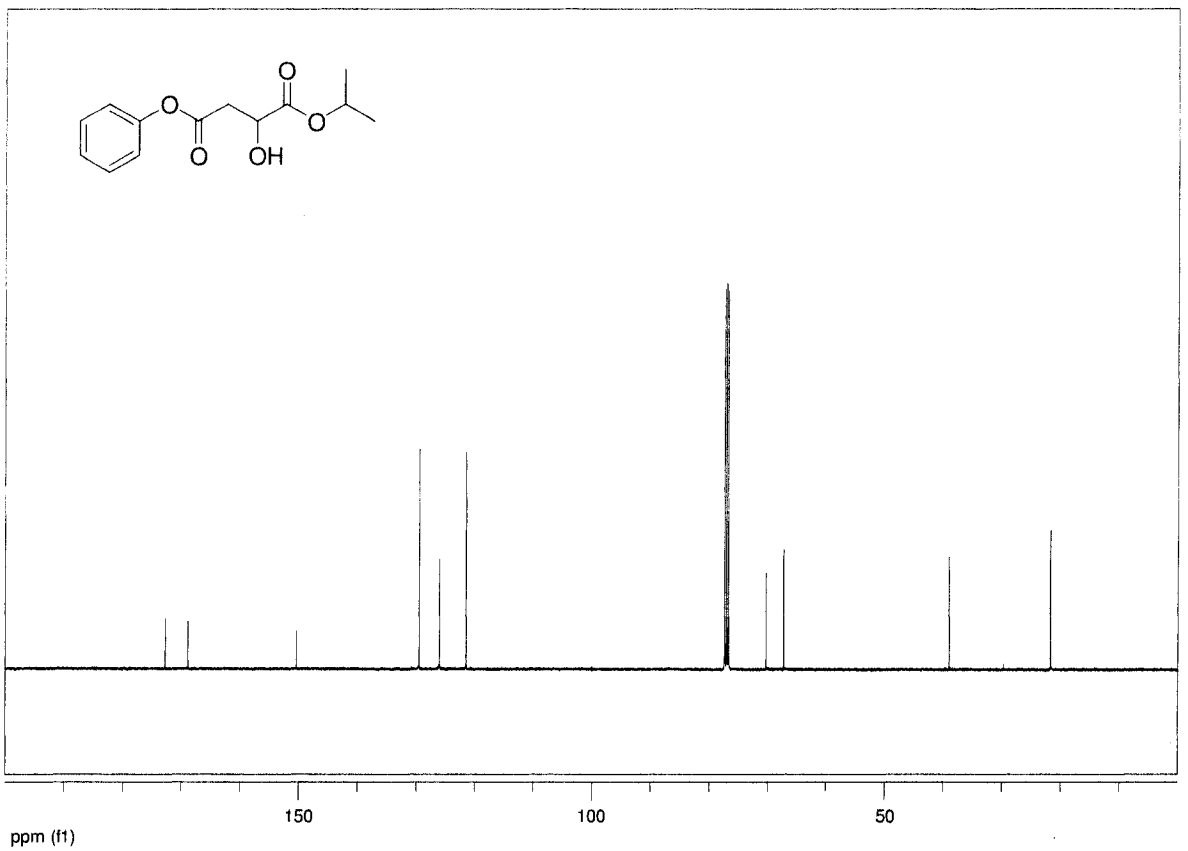
O
O
O
O
OH
150
100
50
ppm (f1)

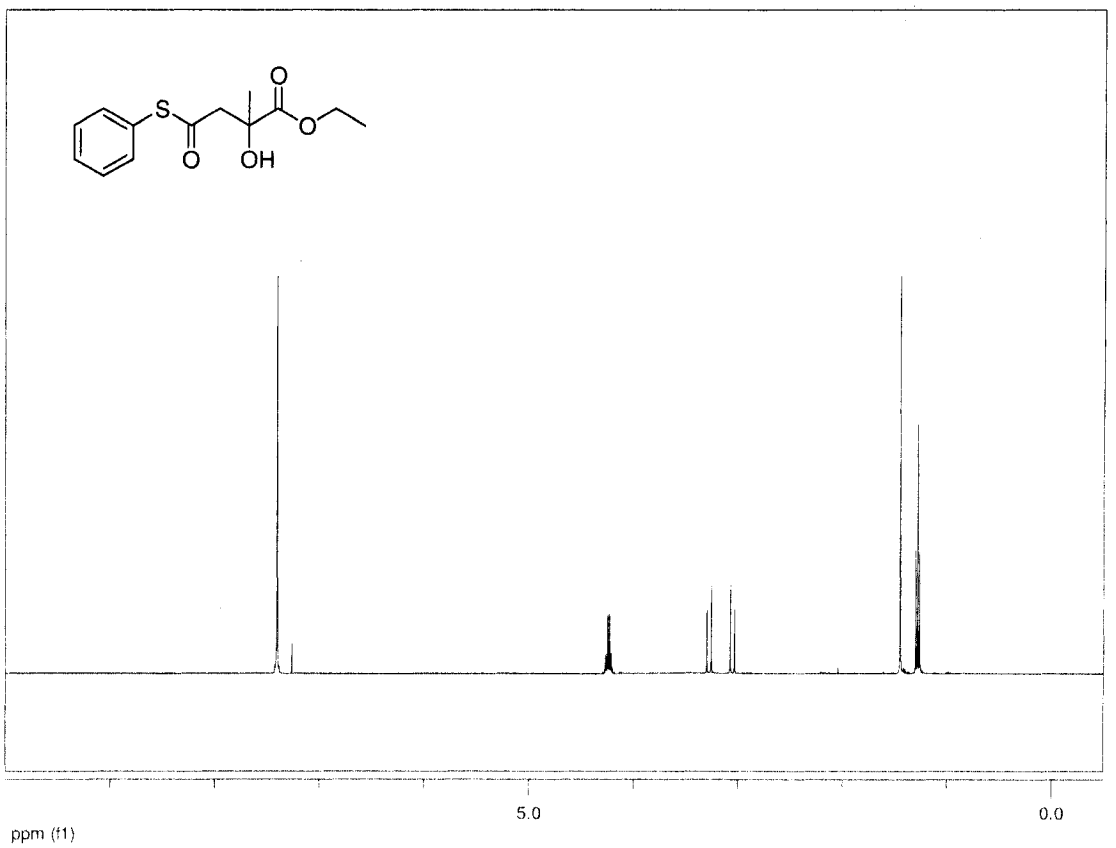
O
S
O
O
OH
5.0
0.0
ppm (f1)

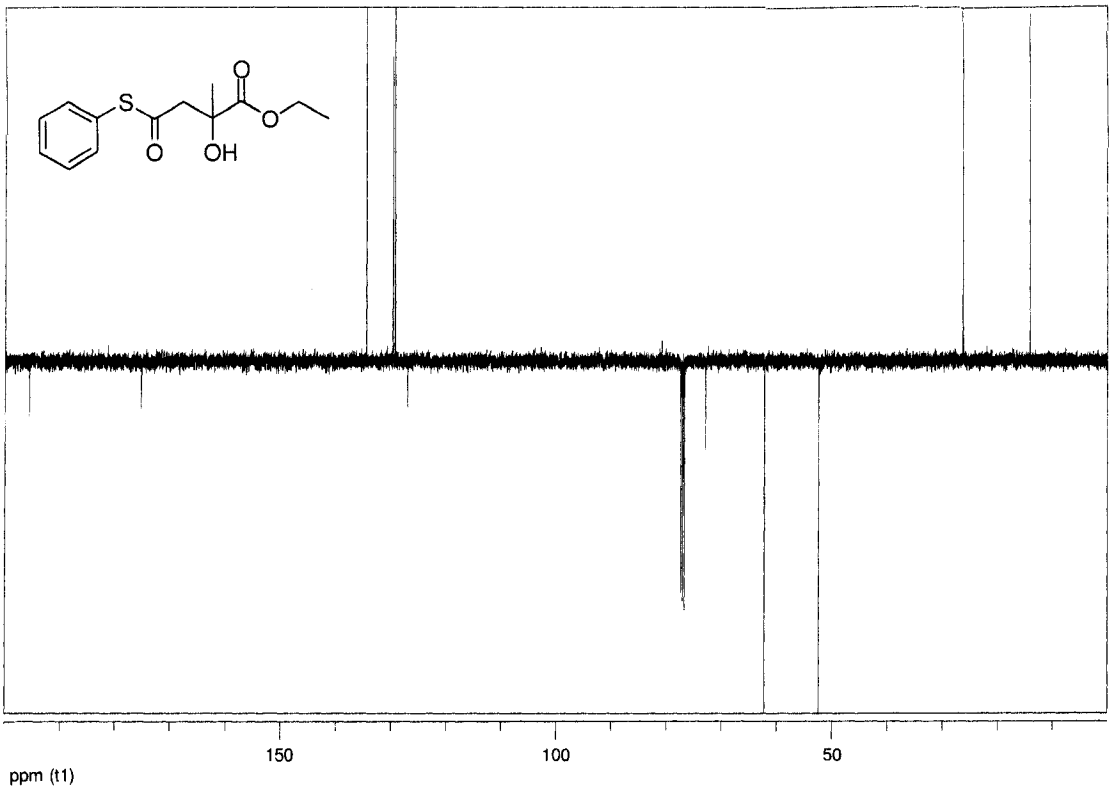
S
O
O
OH
O
150
100
50
ppm (t1)

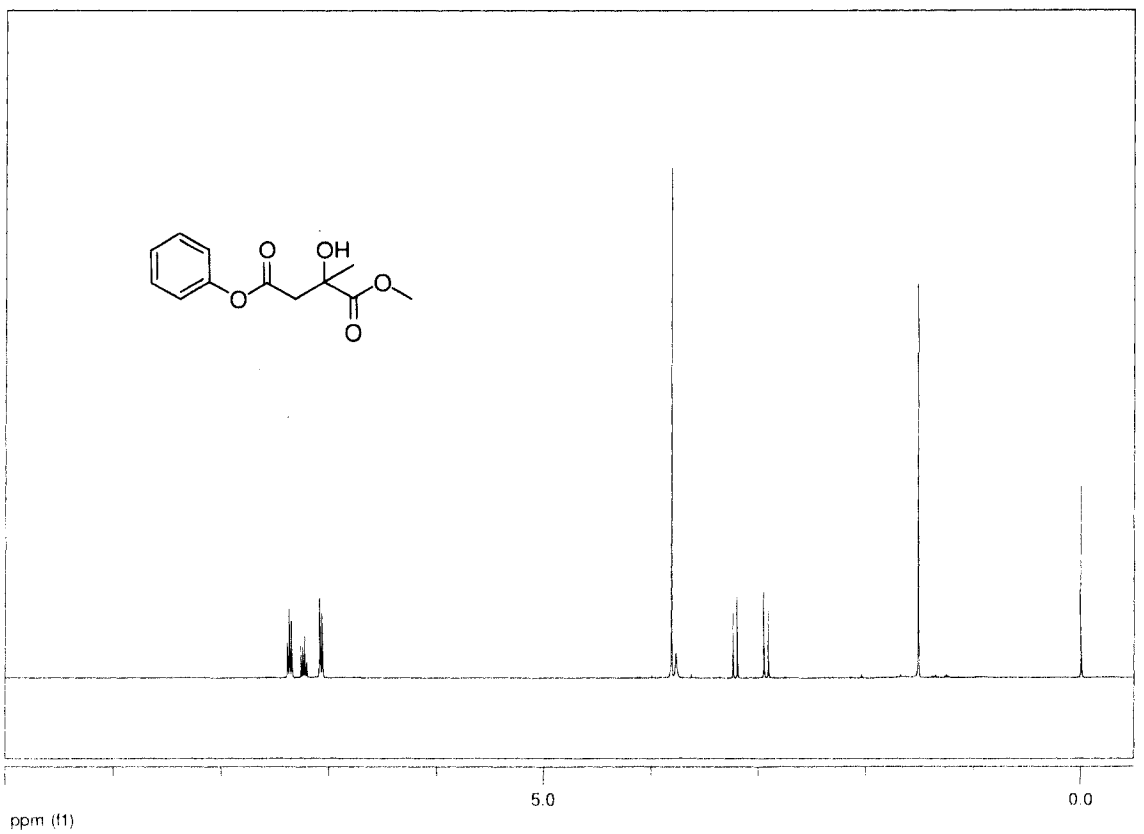
O
OH
O
O
O
5.0
0.0
ppm (t1)

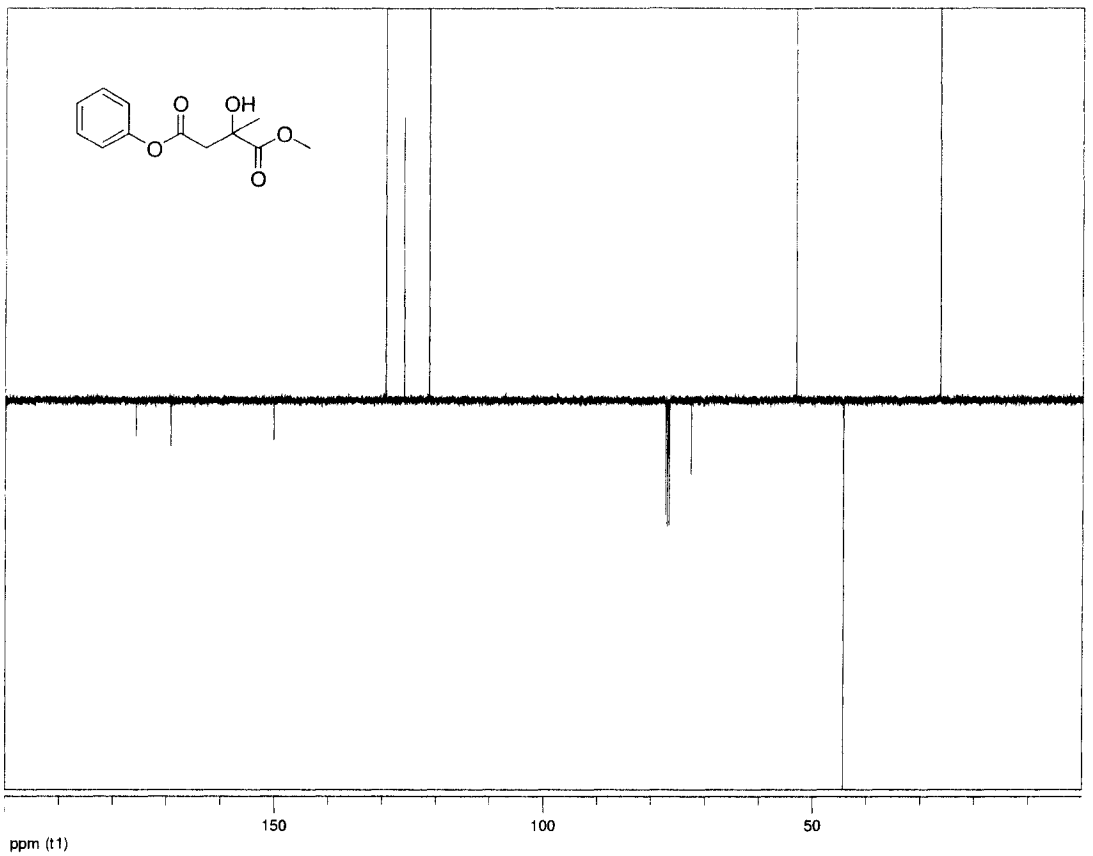
O
OH
O
O
O
150
100
50
ppm (t1)

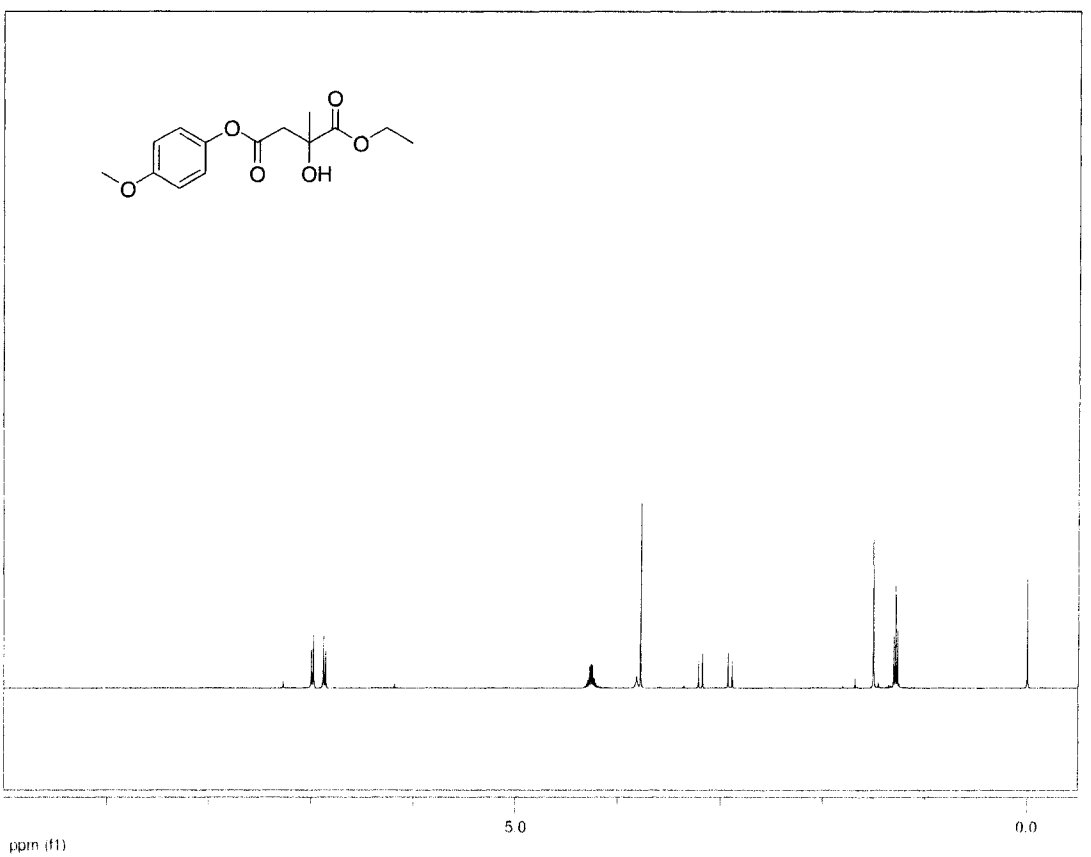
O
O
O
O
OH
O
5.0
0.0
ppm (f1)

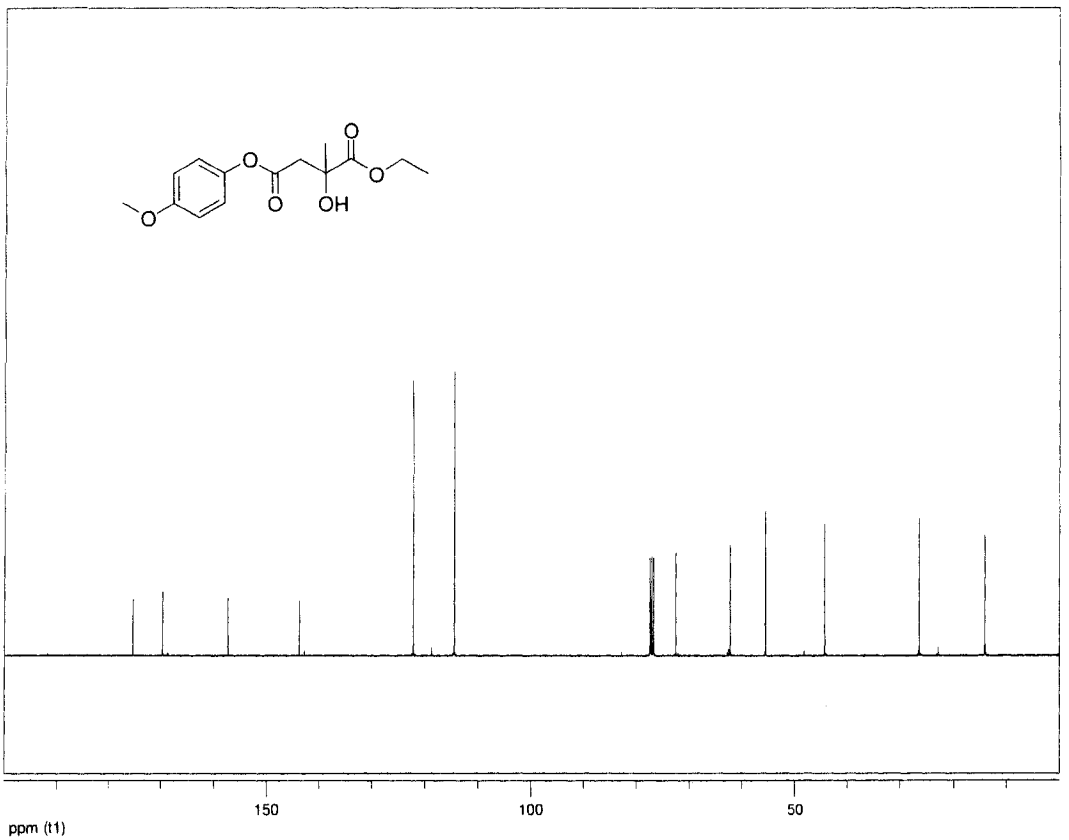
O
O
O
O
O
OH
150
100
50
ppm (t1)

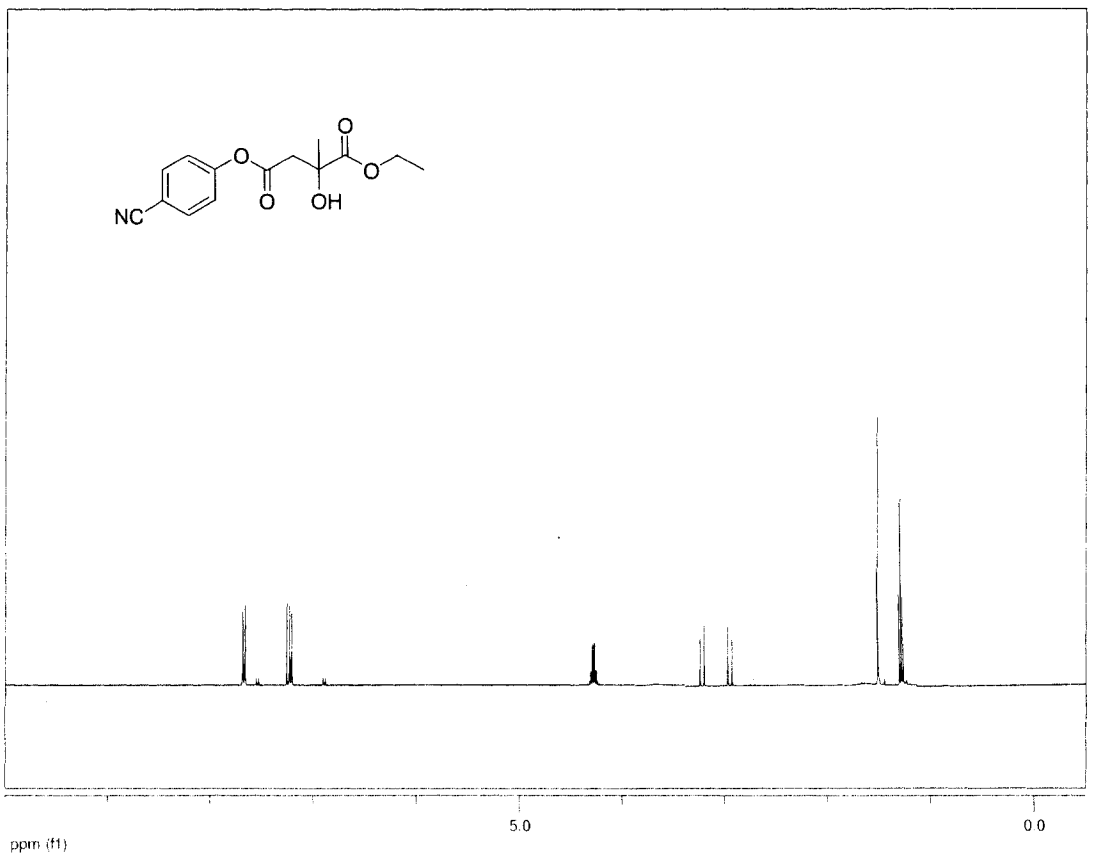
O
O
O
O
NC
OH
5.0
0.0
ppm (t1)

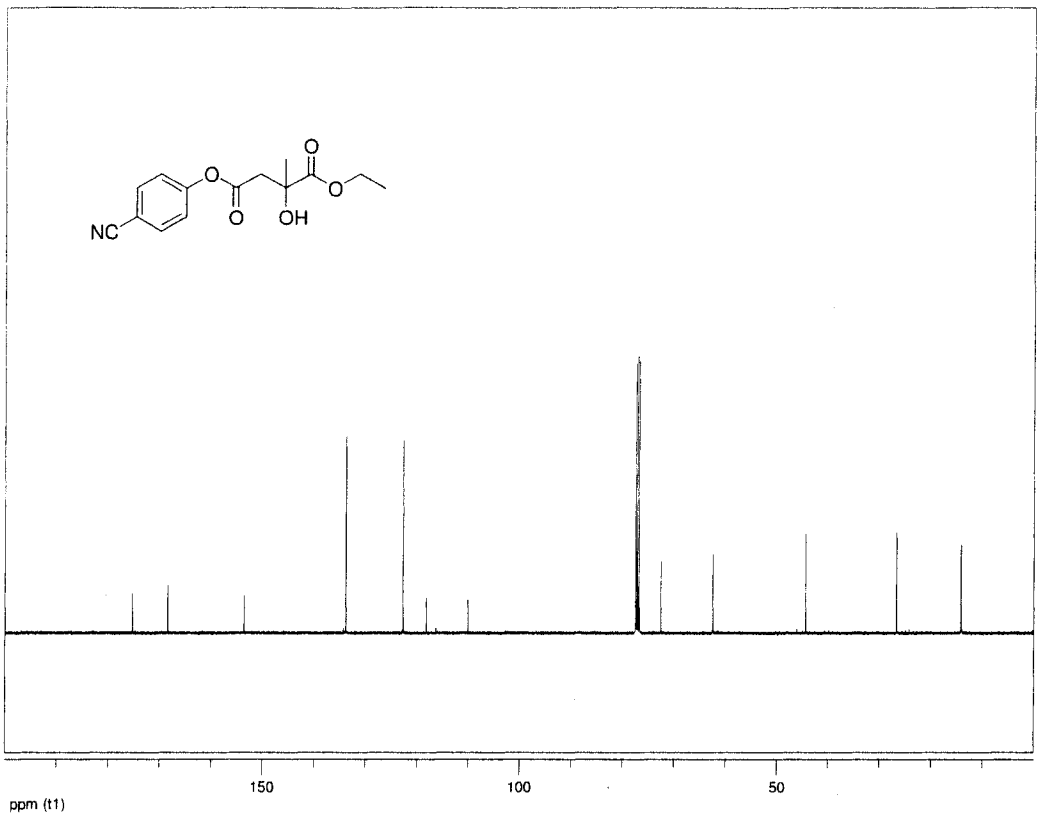
NC
O
O
O
O
OH
150
100
50
ppm (t1)

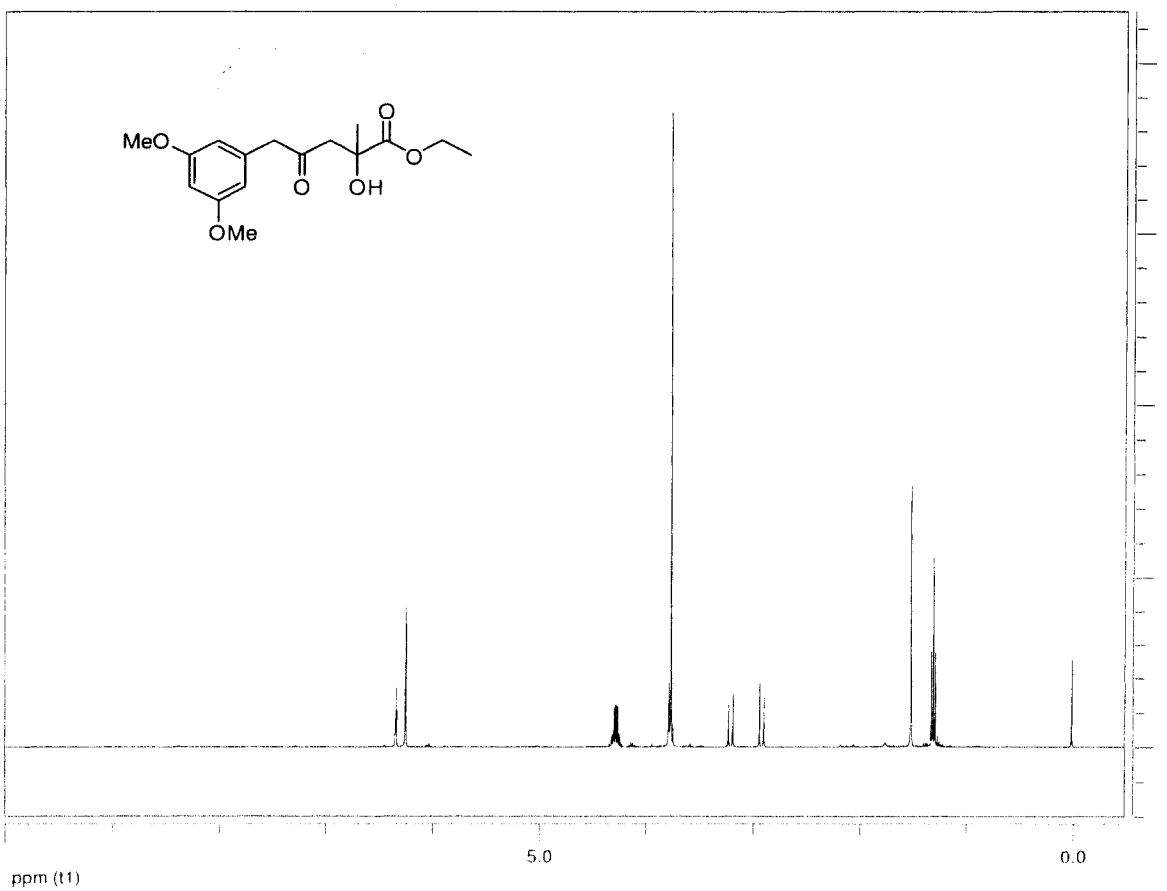
MeO
OMe
O
O
O
OH
5.0
0.0
ppm (t1)

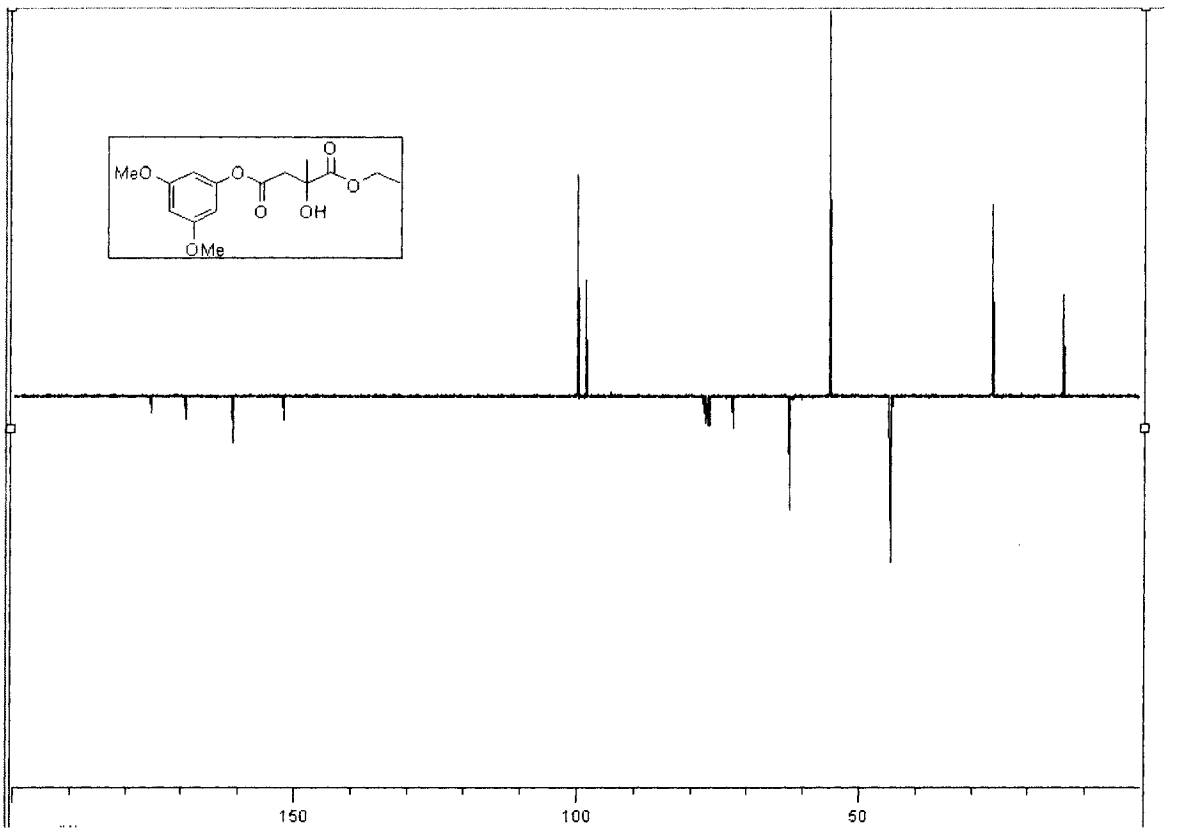
MeO
O
O
O
O
OH
OMe
150
100
50

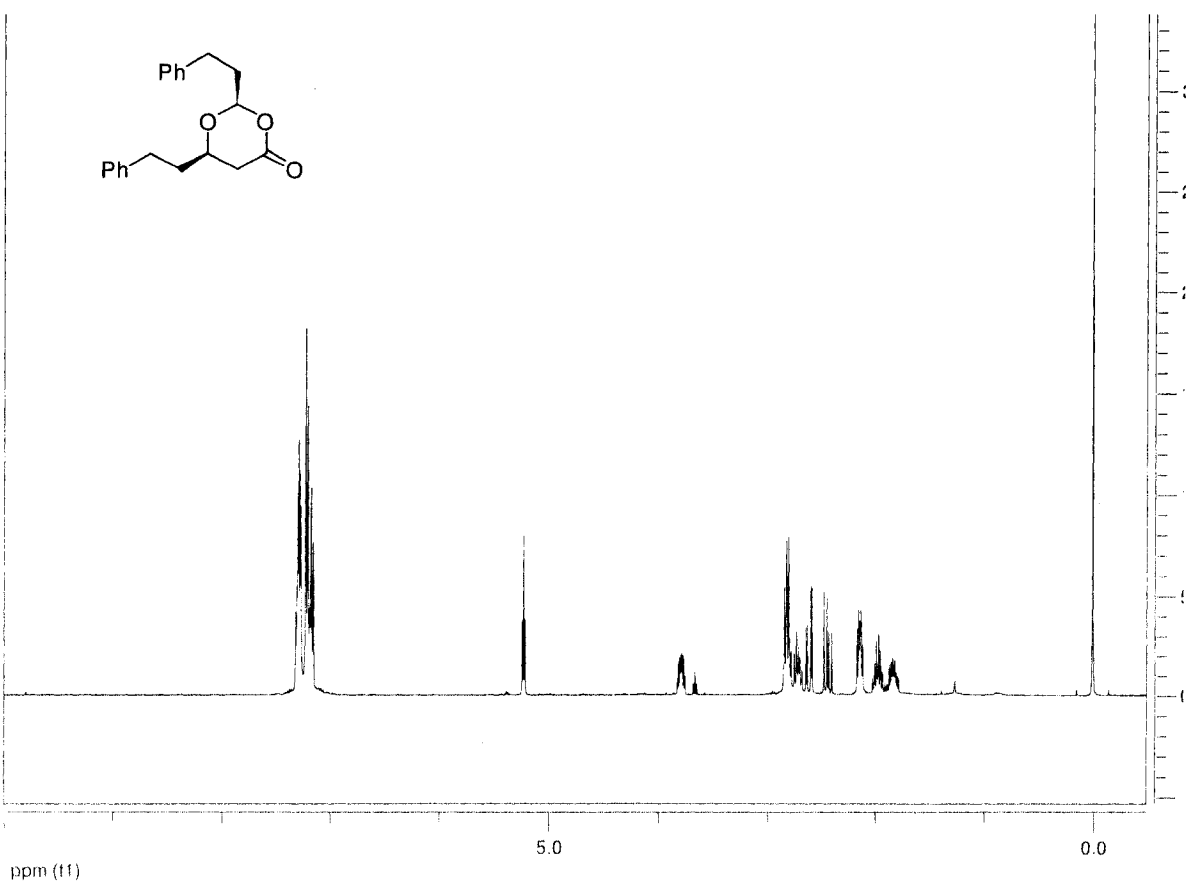
Ph
O
O
Ph
O
5.0
0.0
ppm (f1)

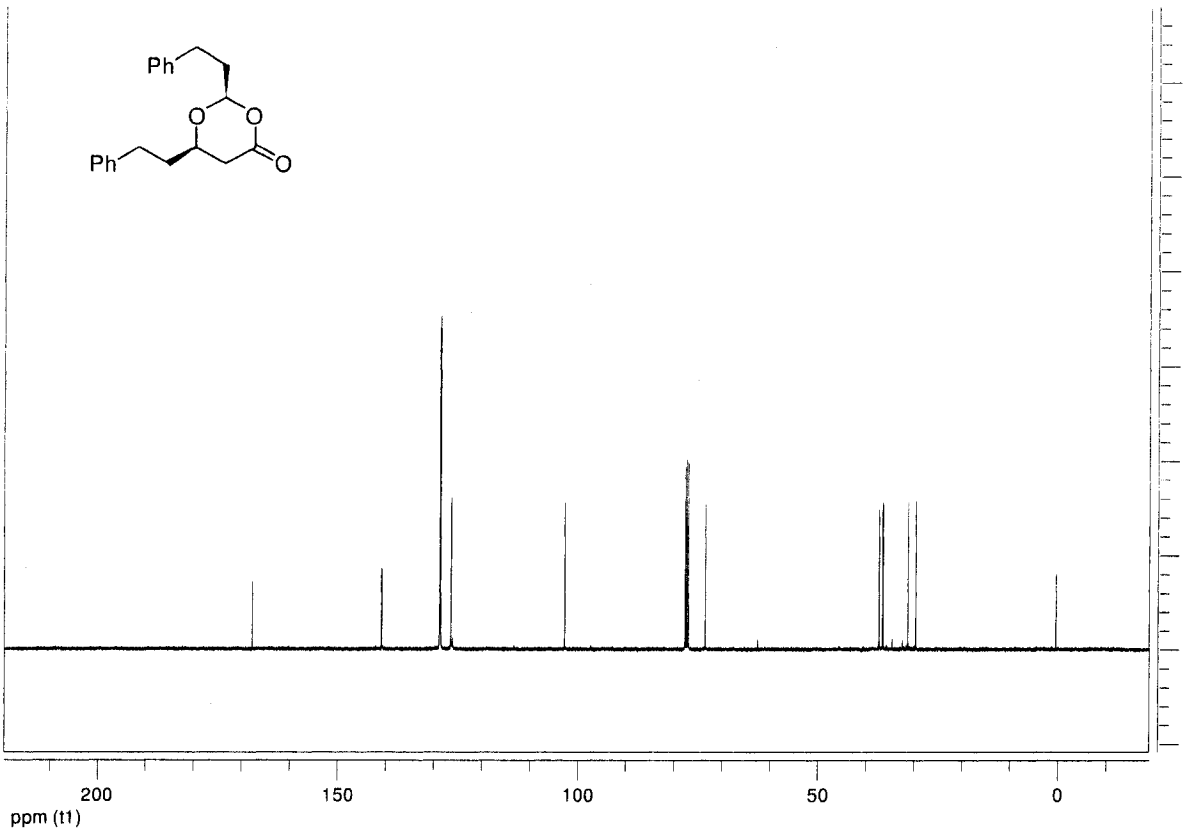
Ph
O
O
Ph
O
200
150
100
50
0
ppm (t1)

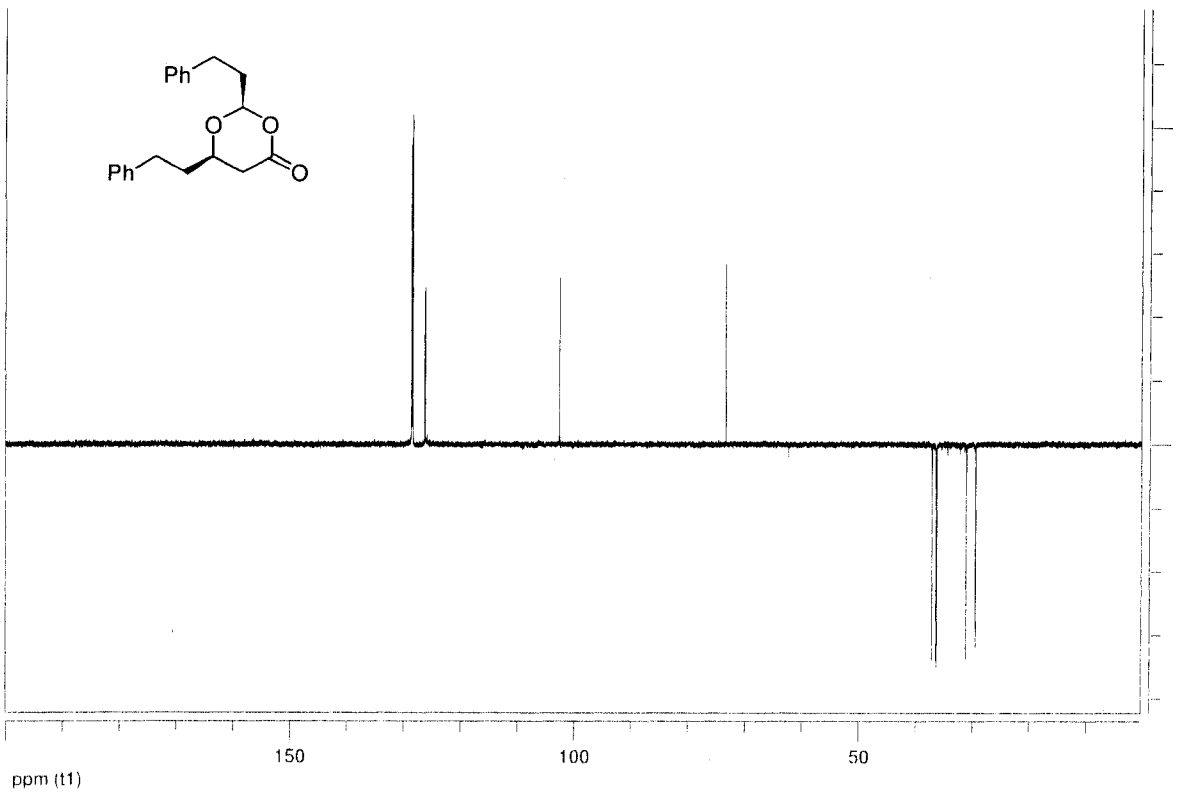
Ph
O
O
Ph
O
150
100
50
ppm (t1)

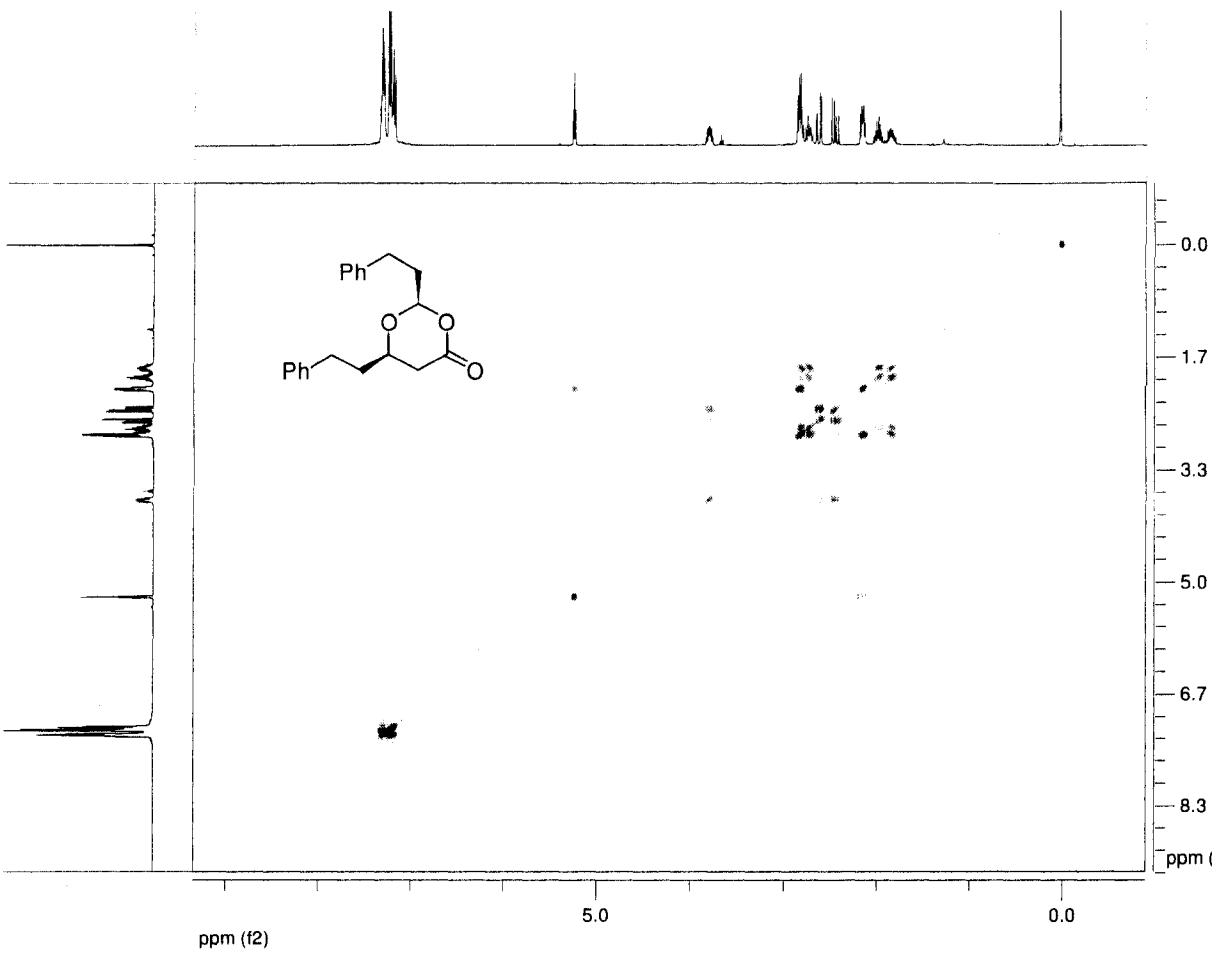
Ph
O
O
Ph
O
0.0
1.7
3.3
5.0
6.7
8.3
ppm (
5.0
0.0
ppm (f2)